Study of the redox and acid-base properties of soda-lime silicate glass: application to the high temperature corrosion of Ni-based alloys and ceramic materials

Tuti Katrina Abdullah

Faculté des Sciences et Technologies

U.F.R. : Sciences et Techniques

Ecole doctorale : S.E.S.A.M.E.S

Formation doctorale : Chimie et Physique Moléculaire

THESE

Présentée pour l'obtention de grade de

Docteur de l'Université de Lorraine

En Chimie et Physique Moléculaire

Par

Tuti Katrina ABDULLAH

Study of the redox and acid-base properties of soda-lime silicate glass: application to the high temperature corrosion of nickel-based alloys and ceramic materials

Etude des propriétés acido-basiques et oxydo-réductrices de verres sodo-calciques: application à la corrosion à haute température d'alliages base nickel et de matériaux céramiques

Soutenue publiquement le 15 Novembre 2013 à l'Université Sains Malaysia

Membres de jury:

M. Farook ADAM	Professeur des Universités, USM
M. Azizan AZIZ	Professeur des Universités, USM
Mme. Céline CABET	Ingénieur de Recherche, CEA
M. Mohd Jain Noordin MOHD KASSIM	Professeur des Universités, USM
M. Pierre-Jean PANTEIX	Ingénieur de Recherche, CEA
M. Michel VILASI	Professeur des Universités, UL

ACKNOWLEDGEMENTS

Foremost, I would like to thank to my supervisors and co-supervisors from Université de Lorraine (UL) and Universiti Sains Malaysia (USM), Prof. Michel Vilasi (UL), Prof. Christophe Rapin (UL), Assoc. Prof. Dr. Zuhailawati Hussain (USM) and Assoc. Prof. Dr. Afidah Abdul Rahim (USM) for their continuous guidance, patience, motivation and support throughout this study.

My sincere gratitude to Ministry of Education (Malaysia) and USM for granting me the scholarship through Academic Staff Training Scheme (ASTS). My sincere appreciation also goes to Institut Jean Lamour (France) for the financial support during the last few months of my stay in France.

I offer my sincerest gratitude to Dr. Pierre-Jean Panteix and Dr. Carine Petitjean who has supported me throughout this research with their knowledge and patience. All their encouragements and supports help me a lot to complete my study.

I would like to express my gratitude to my fellow lab mates in Corrosion and Thermodynamic Department for the stimulating discussions and for all the time that we had spent for the last four years. A lot of thanks to Lionel and Thierry for always trying to solve my problems.

Last but not least special thanks goes to my family for trusting and allowing me to go abroad for doing my research. I would like to thank to my husband, Annuar Fakry and my daughter, Iman for their encouragement and spiritually support.

TABLE OF CONTENTS

LIST OF TABLES

LIST OF FIGURES

LIST OF SYMBOLS

Symbols	Descriptions
E_a	Activation energy
a	Activity
β_a	Anodic kinetics constant
β_c	Cathodic kinetics constant
I_{corr}	Corrosion current density
E_{corr}	Corrosion potential
$V_{thickness\ loss}$	Corrosion rate (thickness loss)
V_{corr}	Corrosion rate (Stern-Geary)
ρ	Density
Ø	Diameter
k'_l	Linear constant
D*	Network oxygen diffusion coefficient
D	Oxygen diffusion coefficient
fO_2	Oxygen fugacity

k'_p	Parabolic constant
Rp	Polarisation resistance
S	Surface area
T	Temperature
t	Time
Λ_{th}	Theoretical optical basicity
η	Viscosity

LIST OF ABBREVIATIONS

BSE	Backscattered electron
DTA	Differential thermal analysis
EPMA	Electron probe micro-analysis
SEM	Scanning electron microscope
SE	Secondary electron
NCxS	Na_2O-CaO-xSiO_2 (Soda-lime silicate)
NxS	Na_2O-xSiO_2 (Soda silicate)
TGA	Thermogravimetric analysis
UV-Vis	Ultaviolet-visible spectroscopy
XRD	X-ray diffraction analysis

KAJIAN SIFAT-SIFAT REDOKS DAN ASID-BES KACA SODA-KAPUR SILIKAT: APLIKASI UNTUK KAKISAN BERSUHU TINGGI ALOI BERASASKAN NIKEL DAN BAHAN-BAHAN SERAMIK

ABSTRAK

Sifat kakisan aloi-aloi pembentuk kromia (Cr_2O_3) dan alumina (Al_2O_3) dalam leburan soda-kapur silikat dikaji dengan menggunakan teknik 'rendaman' yang disertakan dengan pengukuran elektrokimia. Gabungan kedua-dua teknik tersebut membawa kepada penentuan aspek-aspek umum kakisan oleh kaca terlebur serta tindakbalas redoks dan kinetik yang mengawal proses kakisan. Keputusan eksperimen mendedahkan bahawa Al_2O_3 tidak dapat memberikan perlindungan terhadap kakisan oleh kaca terlebur oleh kerana ia mempunyai keterlarutan yang tinggi di dalam leburan tersebut. Walau bagaimanapun, aloi pembentuk Cr_2O_3 dapat menahan terhadap kakisan oleh kaca terlebur jika aloi tersebut telah dilakukan rawatan pra-pengoksidaan dalam udara sebelum rendaman. Oleh kerana ketahanan lapisan Cr_2O_3 berkait dengan persaingan antara pembentukan oksida dan keterlarutannya dalam leburan, maka ciri-ciri fizikokimia Cr_2O_3 dalam kaca leburan seterusnya dikaji dengan mendalam bagi memahami pengaruh parameter yang berbeza terhadap had keterlarutan Cr_2O_3. Kajian telah dijalankan dengan mengambil kira pengaruh suhu (T), fugasiti oksigen (fO_2) dan komposisi kaca terhadap kebolehlarutan Cr_2O_3 dalam leburan. Kajian awal kinetik mendedahkan bahawa masa untuk mencapai keseimbangan berbeza bagi parameter tersebut. Walau bagaimanapun, masa keseimbangan kompromi dipilih untuk memuaskan semua masalah yang dihadapi. Kajian termodinamik menunjukkan bahawa pengaruh T dan fO_2 terhadap keterlarutan Cr_2O_3 dalam leburan soda-kapur silikat ternari (Na_2O-CaO-

$xSiO_2$) kelihatan koheren dengan leburan binari (Na_2O-$xSiO_2$). Walau bagaimanapun, keterlarutan Cr_2O_3 dalam leburan ternari adalah lebih rendah daripada leburan binari. Nilai keterlarutan Cr dalam Na_2O-CaO-$xSiO_2$ (x = 3, 4, 5 and 6) untuk suhu yang berbeza (T = 1200^oC, 1300^oC and 1350^oC) dan fugasiti oksigen yang berbeza ($-12 \leq \log fO_2 \leq -0.6$) berada antara 0.23 at.% hingga 1.09 at.%. Pengaruh kebesan dikaji terhadap leburan ternari dan binari dengan mengambil kira kebesan optik teori (Λ_{th}) dan aktiviti Na_2O. Nisbah redoks (Cr^{II}/Cr^{III} and Cr^{VI}/Cr^{III}) ditentukan melalui penghalusan matematik. Perbandingan dengan keputusan yang telah diperoleh dalam leburan binari dan penyimpangan dari nilai teori yang dijangkakan apabila melibatkan spesies kromium, menimbulkan andaian mengenai peranan yang dimainkan oleh CaO dalam mempengaruhi tindak balas yang melibatkan spesies daripada pasangan O^{2-}/O_2.

STUDY OF THE REDOX AND ACID-BASE PROPERTIES OF SODA-LIME SILICATE GLASS: APPLICATION TO THE HIGH TEMPERATURE CORROSION OF NICKEL-BASED ALLOYS AND CERAMIC MATERIALS

ABSTRACT

The corrosion behaviour of chromia (Cr_2O_3) and alumina (Al_2O_3) forming alloys in soda-lime silicate melts was studied by using 'raw immersion' technique which was coupled with electrochemical measurements. The combination of both techniques leads to the determination of the general aspects of the corrosion by the molten glass as well as the redox reactions and the kinetics that rule the corrosion process. The results revealed that Al_2O_3 is not able to provide protection against corrosion by molten glass since it has a high dissolution in the melt. However Cr_2O_3 forming alloy could resist against corrosion by molten glass if the alloy was subjected to a preoxidation treatment in air before the immersion. As the durability of the Cr_2O_3 layer is linked to the competition between the oxide growth and its dissolution in the melt, the physicochemical properties of Cr_2O_3 in molten glasses were then thoroughly studied in order to understand the influence of different parameters on the limit of Cr_2O_3 solubility. The works were conducted by taking into account the influence of temperatures (T), oxygen fugacities (fO_2) and the glass compositions on the solubility of Cr_2O_3 in the melts. The preliminary kinetics study revealed that the time to reach equilibrium varies with the parameters (T, fO_2 and glass compositions). However, a compromising equilibrium time was chosen in order to satisfy all the problems encountered. The thermodynamic study showed that the influence of T and fO_2 on the Cr_2O_3 solubility in ternary soda-lime silicate melts (Na_2O-CaO-xSiO_2) seems to be in coherence with the results in binary melts (Na_2O-

$xSiO_2$). Nevertheless, the Cr_2O_3 solubility in ternary melts is lower than in binary melts. The Cr solubility values in Na_2O-CaO-$xSiO_2$ (x = 3, 4, 5 and 6) for different temperatures (T = 1200°C, 1300°C and 1350°C) and different oxygen fugacity ($-12 \leq \log fO_2 \leq -0.6$) lie between 0.23 at.% to 1.09 at.%. The influence of basicity was studied in these ternary and binary melts by taking into account the theoretical optical basicity (Λ_{th}) and the activity of Na_2O (aNa_2O). The redox ratios (Cr^{II}/Cr^{III} and Cr^{VI}/Cr^{III}) were determined through a mathematical refinement. The comparison with the results obtained in binary melts and the deviation from the theoretical values expected when speciation of Cr is involved, induce the assumption of the role played by CaO in influencing the reactions involving species from O^{2-}/O_2 couple.

ETUDE DES PROPRIÉTÉS ACIDO-BASIQUES ET OXYDO-RÉDUCTRICES DE VERRES SODO-CALCIQUES: APPLICATION À LA CORROSION À HAUTE TEMPÉRATURES D'ALLIAGES BASE NICKEL ET DE MATÉRIAUX CÉRAMIQUES

RÉSUMÉ

Le comportement en corrosion d'alliage chromine (Cr_2O_3) et alumine (Al_2O_3) formeurs dans des verres sodo-calciques à haute température a été étudié en couplant des techniques électrochimiques avec la caractérisation post-mortem des matériaux immergés dans le milieu fondu. Les mécanismes réactionnels de la corrosion par ce type de milieu ont ainsi pu être abordés, de même que les aspects cinétiques. Les résultats ont montré que l'alumine n'était pas capable de protéger les alliages contre la corrosion, dans la mesure où sa solubilité dans le verre est particulièrement importante. Cependant, les alliages chromine formeurs ont montré de bonne propriété de résistance à la corrosion, dans la mesure où ceux-ci ont préalablement subi un traitement de pré-oxydation. Lors de l'immersion, une compétition entre la croissance de la couche de chromine et sa dissolution dans le verre s'installe, régissant ainsi la durée de vie de la couche d'oxyde protectrice. En conséquence, une attention particulière a été portée sur la physico-chimie de la chromine en milieu verre fondu. La solubilité de la chromine a donc étudiée afin de comprendre l'influence des paramètres température (T), fugacité en oxygène (fO_2) et composition du verre. Une étude cinétique préliminaire a permis de mettre en évidence l'influence de ses paramètres sur les mécanismes et le temps de mise à l'équilibre. D'un point de vue thermodynamique, l'influence des paramètres T et fO_2 sur la solubilité du chrome dans des verres ternaires Na_2O-CaO-xSiO_2 est cohérente avec les études antérieurement menées sur des verres binaires Na_2O-xSiO_2. Néanmoins, la solubilité

de la chromine est nettement plus faible dans le cas des verres ternaires. Les valeurs de la solubilité de Cr dans Na_2O-CaO-xSiO_2 (x = 3, 4, 5 and 6) pour différentes températures (T = 1200°C, 1300°C and 1350°C) et différente fugacité en oxygène ($-12 \leq \log fO_2 \leq -0.6$) se situent entre 0.23 at.% à 1.09 at.%. L'influence de la basicité a été parallèlement étudiée dans les verres binaires et ternaires, en prenant en compte la basicité optique théorique (Λ_{th}) et l'activité en oxyde de sodium (aNa_2O). Les rapports redox (Cr^{II}/Cr^{III} et (Cr^{VI}/Cr^{III}) ont été déterminées suite à un affinement mathématique. La comparaison avec les résultats obtenus dans le cas des verres binaires ainsi que de grandes différences observées par rapport aux résultats théoriques dans le cas où la spéciation du chrome intervient laissent penser que l'oxyde de calcium CaO a une influence dans les réactions impliquant les espèces du couple O_2/O^{2-}.

CHAPTER 1

INTRODUCTION

In high temperature industries, most of the metallic parts normally consist of nickel-based alloys with high chromium and aluminium contents, which can lead to the formation of chromia, Cr_2O_3 and alumina, Al_2O_3 when in contact with air atmosphere at high temperature. These two oxides are very well known to provide good protection against oxidation as they usually form homogeneous and protective layers on the alloys.

The biggest challenge faced by the production of glass is related to the lifetime of the glass processing equipments which are in contact with molten glass. These equipments are expected to have the ability to withstand harsh environments and thus to resist against high temperature corrosion since they are normally consist of chromia (Cr_2O_3) forming alloys with chromium mass content ranging from 25 to 30 wt.%. However, the stability of these alloys in molten glasses, which is mainly governed by the dissolution of the protective chromia in the melts, is one of the crucial factors that determine the lifetime of these metallic parts.

During the last 20 years, the team "Surface et Interface : Réactivité Chimique des Matériaux" has been focusing on the corrosion of different materials in molten glass media. In a first approach, electrochemical methods has been used in order to characterise the corrosion behaviour of the metals/alloys in molten glass. The ability of the alloys to build a protective chromia layer has been emphasized as the best candidates for long term corrosion resistance in molten glass media. As a

consequence, the works have been continued by a more specific study devoted to the behaviour of chromia in molten silicates. In this work, a focus has been given on the characterisation of the basicity of the media; a crucial property of the glass which gives a profound influence on the behaviour of chromia in the melt. A previous PhD work led by Sandra Abdelouhab has contributed to the development of the *in situ* measurement of the activity of the strong base, sodium oxide (Na_2O). This work proved the profound effect of different parameters on the corrosivity of molten silicates, *i.e.* temperature, oxygen fugacity and basicity. As a continuity, a second PhD work performed by Hichem Khedim, dealt with the study of the solubility of chromia in simple binary glasses (Na_2O-$xSiO_2$ system). Through this work a specific device has been developed, allowing the control of the temperature, oxygen fugacity and glass composition parameters independently.

The work proposed here is an extension of the study of the solubility of chromium in glasses whose basic composition is similar to the most common industrial glass. In this present work, an introduction of the calcium oxide (CaO) to the simple binary glass has been taken into account. The aim is to have a closer investigation towards a well-known corrosive system *i.e.* CMAS (CaO-MgO-Al_2O_3-SiO_2), which is directly involved in the corrosion of TBC (Thermal Barriers Coatings). In addition, CaO which is a basic oxide also behaves as a network modifier as Na_2O. Therefore, it is necessary to evaluate the effect of CaO addition to binary glassy matrix Na_2O-$xSiO_2$ on the physicochemical properties of the ternary system.

The present work is a continuity of the previous studies in the binary soda silicate Na_2O-$xSiO_2$ melts. The objectives of this work are (i) to evaluate the performances of chromia forming and alumina forming alloys in simplified soda silicate and soda-lime silicates in order to compare the ability of these oxides to give protection against corrosion in molten glasses (ii) to extend the knowledge of the physicochemical properties of chromia in simplified molten silicates of the Na_2O-$xSiO_2$ system by an addition of a second network modifier which is the basic oxide CaO. The manuscript is organised as follows:

Firstly, a literature review is proposed in the second chapter. A description of the molten glass media is given, in terms of structure, acid base properties, and redox properties. Then, the state of art on the corrosion of metals and alloys in molten glass is presented. Chromia and alumina forming alloys are thus emphasised. Then, a part deals with the previous studies devoted to the behaviour of chromia in silicate melts is presented in the final part of this chapter.

The materials and experimental methods used in this work are presented in the third chapter. The characterisation of the raw materials, alloys and glasses used in this study is detailed in Appendices. The specific electrochemical characterisation of the corrosion in molten media is detailed herein. The electrodes used in molten glass at high temperature are an adaptation from the methods used in aqueous media. The reactor allowing the independent control of temperature, oxygen fugacity and glass composition which has been developed in a previous oxide solubility study is also described in this chapter.

The fourth chapter is devoted to the determination of the corrosion of (i) chromia forming and (ii) alumina forming Ni-based simplified alloys in different types of silicate melts. A 'Raw immersion' test followed by a thorough observation of the samples give informations about the general aspects of the corrosion by the molten glass (surface morphology, glass penetration, thickness loss, oxide thickness, etc.). Correlation is then made with the electrochemical measurements, which allows an access to further information on the redox reactions and the kinetics ruling the corrosion process. An accurate comparison is made between chromia and alumina about their ability to give an efficient protection against glass corrosion.

Since the chromia has the ability to provide protection to the alloys due to its low solubility in molten glass, its physicochemical properties are then detailed in the fifth chapter. Firstly, the dissolution kinetics of chromia in different conditions (*i.e.* temperature, oxygen fugacity, melt composition are thoroughly studied herein. The aim is to choose the best duration of heat treatment in order to be as close as possible to the equilibrium, thus allowing a pertinent thermodynamic study. The mechanisms which are strongly correlated to the diffusion of oxygen species in the melt are also discussed.

The last part deals with the solubility of chromia in the ternary system Na_2O-CaO-xSiO_2. The influences of temperature and oxygen fugacity are first observed, in the same way as in the previous study performed in binary melts. Then, a specific attention is paid on the role played by CaO in the melts, and its influence on the physicochemical properties of the Cr oxo-complex species.

CHAPTER 2

LITERATURE REVIEW

Introduction

This chapter is devoted to a brief description of the physicochemical properties behind the word 'glass' as well as the corrosion phenomena occurring in molten glass. The prerequisite for this attempt is to have an understanding of the structure and the components of the glass which will be discussed in the first part. Secondly, the theoretical and experimental of the concept of acid-base in molten glass as well as the redox reactions in the melts will be discussed thoroughly through a synthetic review of the state of art of many previous studies. The phenomena of corrosion of metals and alloys in molten glasses will be described in the next part. As the protection of the alloys in molten glasses is related to the nature and stability of the oxide layer formed at the interface alloy/glass, hence the physicochemical behaviour of some important oxides in molten glasses will be presented in the final part.

2.1. General aspects of glass

The silicate glass has become a high-tech material with numerous applications in various fields including industry (aeronautic, power generation, glass fibre elaboration, etc.), architecture, arts and as very recently, in waste management's with the use of glass matrices for the stabilisation and the storage of nuclear waste. The term 'glass' brings many contradictions among scientists whether it should be classified as a solid or as a liquid. However, by considering the definition behind the term 'glass', it actually refers to a state of matter, usually produced when a viscous

molten material is cooled rapidly to below its glass transition temperature, with insufficient time for a regular crystal lattice to form. Being neither a liquid nor a solid, but sharing the qualities of both, glass possesses its own state of matter which is called an amorphous solid. Unlike crystals, glass does not have a sharp melting point and does not cleave in preferred directions. Glass also shows elasticity like crystalline solids. Thus, instead of describing the glass by its definition, it is more appropriate to define it by considering the physicochemical properties of the glass itself which strongly depend on its structure.

2.1.1. Formation and structure of silicate network

Unlike crystal (Figure 2.1(a)), glass is a three-dimensional network of atoms forming a solid that lacks periodicity or ordered pattern (Figure 2.1(b)). Random atomic arrangement as would appear in a sodium silicate glass has been shown schematically in Figure 2.1(c). In this case, a Si^{4+} acts as the building block of the glass network which is known as a network-forming cation (NWF)[1]. The four positive charges of the silicon ion tend to form bonds with four oxygen atoms, forming SiO_4 tetrahedra *i.e.* four-sided pyramidal shapes, connected to each other at the corners. An oxygen atom that connects two tetrahedra is known as bridging oxygen while the oxygen atom which joins to only one silicon atom is called a non-bridging oxygen. In the example of sodium silicate glass (Figure 2.1(c)), a univalent sodium ion (Na^+) occupies an interstice adjacent to the SiO_4 tetrahedra in order to balance the remaining negative charge. The role played by Na^+ in the silicate network will be discussed thoroughly in the next part. This corner-sharing tetrahedral structure achieves a liquid-like randomness rather than a crystalline regularity

because of the random value of the Si-O-Si angle. Furthermore, there are twist angles arising between two connected tetrahedra.

Glass consists of network formers, network modifiers and intermediates[1,2]. In order to predict the oxides that tend to form glasses, Zachariasen[3] has proposed four rules for glass formation:

- No oxygen atom may be linked to more than two cations.
- The cation coordination number is small: 3 or 4.
- Oxygen polyhedra share corners, not edges or faces.
- For 3D networks, at least three corners must be shared.

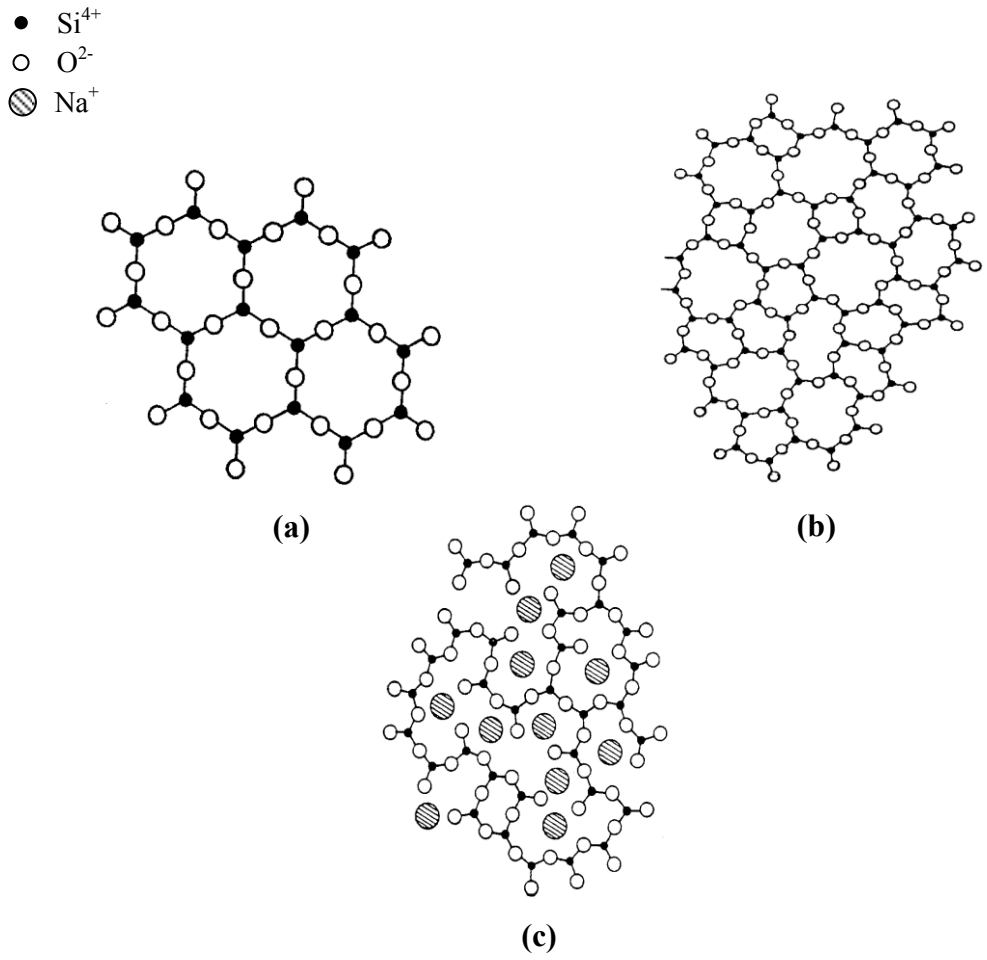

Figure 2.1: Schematic of two dimensions of (a) crystalline quartz (b) amorphous silica (c) soda silicate glass. The fourth Si-O bond is placed perpendicularly to the plane of the figure[1]

Apart from Zachariasen[3], Sun[4] has also introduced a correlation between the strength of the interatomic bonds and the ability of the material to form a glass. The classification of the substances with regard to their glass-forming ability has become the most important contribution of Sun's single bond criterion. Dietzel[5] has proposed to characterise the ability of the cations to form a network with oxygen ions by the Coulomb's force of attraction. It is known as the 'field strength' and can be described by the following equation:

$$A = \frac{Z_c}{\left(r_c + r_o\right)^2} \tag{2.1}$$

where Z_c is the cation valence, r_c and r_o are the cation and O^{2-} radii respectively and expressed in Å. The values of the field strength (A) for various cations are presented in Table 2.1. The value of $A > 1.0$ represents the cations of the network formers whereas $A < 0.35$ corresponds to the cations of the network modifiers.

Table 2.1: The field strength of various cations[5]

Elements	$\mathbf{Z_c}$	$\mathbf{r_c}$	$\boldsymbol{A = \frac{Z_c}{\left(r_c + r_o\right)^2}}$	
P	5	0.31	1.710	
V	5	0.49	1.400	
Si	4	0.40	1.235	Cation
B	3	0.25	1.102	formers
Sb	5	0.74	1.092	
Ge	4	0.53	1.074	
Ti	4	0.74	0.873	
Al	3	0.53	0.805	
Zr	4	0.86	0.783	Cation
Be	2	0.41	0.610	intermediates
Mg	2	0.86	0.392	
Zn	2	0.88	0.385	

Table 2.1: Continued[5]

Elements	Z_c	r_c	$A = \frac{Z_c}{(r_c + r_o)^2}$	
Ca	2	1.14	0.310	Cation modifiers
Pb	2	1.33	0.268	
Li	1	0.90	0.189	
Na	1	1.16	0.153	
K	1	1.52	0.117	

2.1.1.1. Network formers

According to Zachariasen[3], the cations which have the coordination number of 3 or 4 could readily form glasses and are commonly known as 'network formers' as they provide the backbone in other mixed-oxide glasses. However, this rule is not applicable for all cases. For example, Al_2O_3 is not able to form glass when the oxide is alone since the charges are not sufficient to form a stable polyhedron with four oxygen. The examples of network formers are B_2O_3, SiO_2, P_2O_5 and GeO_2.

2.1.1.2. Network modifiers

Alkali and alkaline-earth elements such as Li, Na, K, Ca and Mg play a role as a network modifiers in the glass network[2]. A network former such as SiO_2 is well-known for its high melting temperature which lies between 1600^{o}C - 1725^{o}C. At this temperature, the liquid is very viscous, making the processing of the glass difficult. Since the network modifiers have the ability to break up the covalent bonds between the network formers and the anions, a network modifier such as Na_2O which is known as a 'flux' is always added to the network formers such as SiO_2 in order to decrease the melting temperature of pure SiO_2 and also the viscosity of the melts.

There are two important effects by an addition of Na_2O to the network. Firstly, every Na_2O molecule will disrupt the network and will cause the formation of two groups of $Si-O^{-}Na^{+}$ (Figure 2.2). The oxides that have the ability to modify the network are called 'network modifiers' since they can transform the bridging oxygen (the oxygen that links to two cation formers) into non-bridging oxygen (oxygen which links to only one cation former). The breaking of the Si-O bonding lowers the viscosity of the melt, thus facilitating the fusion process. Secondly, an alkali oxide such as Na_2O has the ability to lower the liquidus temperature of the melt, thus limiting the risk of devitrification phenomenon.

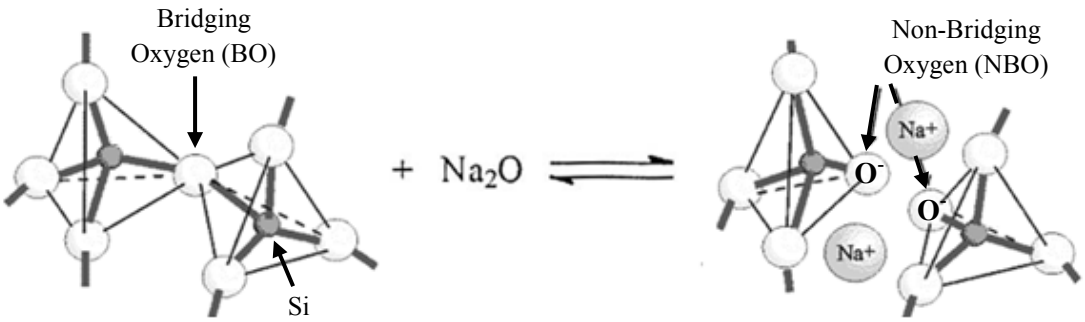

Figure 2.2: Schematic of the breaking of Si-O bonding by introducing a Na_2O molecule in the silicate network[2]

2.1.1.3. Intermediates

The intermediate oxides are less clearly defined compared to the network formers and network modifiers. The intermediates may act as network formers or network modifiers depending on the glass compositions. The oxides such as Al_2O_3, BeO, MgO and ZnO are examples of the intermediates[2]. The intermediate cations create a slightly covalent binding with the O^{2-} anions. The coordination tendency of these ions is insufficient to establish a three-dimensional network. Since the intermediates can establish a bond with two or three oxygen ions, the addition of intermediates to a silica glass does not lead to a complete breaking up of the

polyhedra network. The presence of the intermediates suppresses the tendency of the glass melt to form crystals during cooling.

2.1.1.4. The role of CaO

CaO is an alkaline-earth oxide playing a role as a glass modifier since it also breaks the Si-O bonding in the network[2]. The introduction of CaO into the network could be described by the following equation:

$$\equiv Si - O - Si \equiv + CaO \rightarrow \equiv Si - O^{-} Ca^{2+} O^{-} - Si \equiv \quad (2.2)$$

An addition of CaO to the network leads to the creation of two non-bridging oxygen. It can also decrease the viscosity of the molten glass but the effect is more moderate compared to the addition of alkali oxide. Furthermore, the effect of an addition of alkaline-earth oxide on the decreasing the liquidus temperature of the silicate network is less significant compared to the alkali oxide since the alkaline-earth oxides are more refractory compared to the alkali oxide.

In the case of soda-lime silicate glass, an addition of CaO will break the bridging of Si-O-Si bonds between silicate tetrahedron, thus decreasing the average silicate chain length. However, the electronic charge of calcium ion which is higher than sodium ion makes the $[SiO_4]^{4-}$ to be more easily associated with Ca^{2+} ions compared to the monovalent cation. Therefore, the Na^{+} ions are potentially freer in the Ca-bearing system relative to the sodium-silica binary. According to Abdelouhab *et al.*[6], the increased number of non-bridging oxygen in the Ca-bearing system (Na_2O-CaO-xSiO_2) may lead to an increase in the Na_2O activity relative to that

observed in the equivalent Na_2O-$xSiO_2$ melt. Addition of CaO to a binary alkali silicate glass is known to increase its durability[1]. They are chemically durable against water and acid and have fairly good weathering resistance. However, soda-lime silicate glass has high thermal expansion, thus prone to thermal shock failure.

2.1.1.5. The role of Al_2O_3

Al_2O_3 will never form glass itself but acts like a glass former or modifier if combined with other oxides[2]. Therefore Al_2O_3 is classified as an intermediate in the glass network. By introducing in the pure SiO_2, Al^{3+} has the coordination number of VI, thus playing a role as a network modifier. Al_2O_3 has the ability to be a network former in the alkali-containing glasses when Al^{3+} substitutes Si^{4+} in the network. Every Al_2O_3 introduced in the melt will remove a pair of non-bridging oxygen (associated with two Na^+ which must neutralise the two $[AlO_4]^{5-}$ tetrahedra) which leads to an increase of the glass viscosity due to the formation of aluminate tetrahedra[7]. However, the structural role of the Al^{3+} in alkali silicate glasses depends on the aluminium concentration and the temperature of the melts[8].

2.1.2. Acid-base properties in glass melts

As in the aqueous media, the acid-base properties play an important role in the molten glass for the theoretical understanding of the nature of some physicochemical processes in glass-forming melts and slags, as well as for applied tasks, *e.g.* the prediction of the process tendencies and design of the materials with necessary characteristics. Acid-base properties of the glass also show a significant influence on the corrosion of metal/alloys by molten glasses[9–11]. A large number of studies have been performed in order to reveal the theories of acid-base in the molten

glass[12–19] as well as to determine a scale to distinguish the acidity or basicity of the melts.

2.1.2.1. Acid-base concepts in glass melts

The Brönsted-Lowry[12,13] theory provides a broader definition of acids and bases in a protonic solvent. According to this theory:

- An acid is defined as a species which has the tendency to yield a proton.
- A base is a substance that can accept a proton.

The Brönsted-Lowry theory still does not present the full generalisation of acid-base phenomena. This theory does take into account the experimental fact that there are many substances besides the hydroxyl ion which exhibit typical basic properties, but fails to recognise complementary data with regard to acids. Therefore, the proton transfer acid-base theory has practically no application in glass.

As a contrary, Lewis[14] theory considers acid-base functions and related processes independently of the solvent. According to Lewis:

- An acid is any species that is capable of accepting a pair of electrons to form a covalent bond by sharing with the electron donor.
- A base is any species that can donate a pair of electrons to form a covalent bond with the acid.

Although it can overcome many difficulties in aqueous solution, the application of Lewis theory in glass melt raises doubt since there is a close relationship between acid-base function and oxidation-reaction in the molten glass. Even though both acids and oxidising agents tend to accept electrons, however the acid accepts electron

pairs and forms coordinate covalent bonds whereas the oxidising agent keeps the electrons to itself.

The concept of acid-base in molten oxides was first introduced by Lux[15] in 1939. His definition can be represented by the following equation:

$$\text{Base} = \text{Acid} + O^{2-} \quad (2.3)$$

The concept of Lux was developed by Flood and Förland in 1947[16] and remains actual up to the present time. Flood and Förland have summarised that the acid-base in an oxide system is characterised by the transfer of an O^{2-} ion from one state of polarisation to another. The degree of basicity of an oxide is determined by the ability of oxygen atoms to give up electrons. The basicity is greater when the O^{2-} ion is unaffected by surrounding cations. As a summary of Lux and Flood theory in the case of molten oxides and molten salts, the exchange of O^{2-} ions between the base and the acid can be assimilated to the exchange of electrons in the Lewis theory. A strong base is capable of combining with electron acceptor which is known as oxoacid. The species resulting from these combinations are called oxobase. For example:

- Metal oxides (Na_2O, BaO, Al_2O_3, ...) are bases and metal cations (Na^+, Ba^{2+}, AlO^+, ...) are conjugate acids.
- Oxoanions (SiO_3^{2-}, SO_4^{2-}, CO_3^{2-},...) are bases and the oxides (SiO_2, SO_3, CO_2,...) are conjugate acids.

These couples react according to the following equilibrium:

$$\text{oxobase} \leftrightharpoons \text{oxoacid} + O^{2-} \tag{2.4}$$

The equilibrium constant, K:

$$K = \frac{a_{acid} \times a_{O^{2-}}}{a_{base}} \tag{2.5}$$

will be a measure of the strength of the acid-base pair.

By analogy with the aqueous solution where the H^+ ion activity allows to establish an acidity scale ($pH = -\log a(H^+)$), the activity of O^{2-} ions has been used as a basicity indicator in the molten glass[15,17,18] or in a medium where the O^{2-} ions exist as free ions according to the following equation:

$$pO^{2-} = -\log a(O^{2-}) \tag{2.6}$$

where $a(O^{2-})$ is the activity of the oxide ions in the medium. It is noteworthy that the pO^{2-} scale works in the reverse direction as compared with the pH scale in protonic solvents. In contrary with the case of aqueous solution where the standard state of H^+ ion can be defined precisely (water is a universal solvent), no standard state can be defined for molten glass because the composition of the solvent varies from one glass to another. Furthermore, the basicity of the oxide melts depends on the force of the ionic bonding between O^{2-} and the cation modifier[1]. The basicity increases with the increase in ionic radii of the alkali ions and alkaline-earth ions. Therefore, the basicity increases by descending the column of alkali and alkaline-earth elements and decreases by going through the group of alkali and alkaline-earth in the periodic

table. Since the terms "acidity" and "basicity" are determined via O^{2-} activity, both characteristics become indiscernible. Therefore, the boundary dividing "acid" and "base" in melts is a problem of standardisation and quantitative of pO^{2-} measurement[19].

2.1.2.2. Evaluation of acid-base properties in molten glass

The acid-base properties in the molten glass have been defined through theoretical and calculation models by several authors. Moreover, some efforts have been made in order to measure the basicity of the molten glass through *ex situ* and *in situ* measurements.

(a) Theoretical models of calculation

Many studies have been devoted to develop theoretical models of calculation of acid-base properties in molten glass in order to quantify the activity of oxide ion (O^{2-}) and the activity of non-bridging oxygen as a function of glass composition.

- *Model of Sun*

In 1948, Sun[20] estimates the strength of cation-oxygen bonding by the formation enthalpy of the glass. The strength of cation-oxygen bonding depends on the dissociation energy of the oxides in the molten glass and the coordination of oxygen with the cation. According to this model, an acid is a network former which has a high electron affinity. Cameron[21] has proposed to calculate the glass basicity based on the value of oxides basicity from Sun[20]. The basicity of boric oxide has been randomly chosen as the origin of the scale. The glass basicity is proportional to the basic number « B »:

$$a(O^{2-}) = Cst \times B \tag{2.7}$$

where

$$B = 119 - \left(\frac{A_{Sun(oxideA)} \times \%mol}{100} + \frac{A_{Sun(oxideB)} \times \%mol}{100} + ... \right) \tag{2.8}$$

The basicity value of oxides (A_{Sun}) which has been proposed by Sun is compiled in Table 2.2:

Table 2.2: The values of A_{Sun} allowing to determine the acid-base properties of the glass[20]

Oxides	A_{Sun}
K_2O	13
Na_2O	20
BaO	33
Li_2O	36
MgO	37
PbO	36-39
Al_2O_3	53-67
Sb_2O_3	68-85
B_2O_3	119
As_2O_3	70-87
SiO_2	106

- *Model of Sanderson*

Sanderson[22–25] has proposed a model to calculate the acid-base properties in the glass by considering a magnitude (x) which is attributed to the size of an atomic electron density. The magnitude x can be related to the Pauling electronegativity (χ) by the following equation:

$$x = \frac{\sqrt{\chi} - 0.77}{0.21} \tag{2.9}$$

For an oxide M_mO_n, the value x can be calculated according to the following equation:

$$xM_mO_n = \left[(x_M)^m (x_O)^n \right]^{\frac{1}{m+n}} \quad (2.10)$$

Thus, the acidity/basicity of the glass A_{glass} can be determined by the following equation:

$$A_{glass} = (x_1^{N_1} \times x_2^{N_2} \times ..... \times x_n^{N_n} \times 5.02)^{\frac{1}{(N_1+N_2+....+N_m+1)}} \quad (2.11)$$

where x_i is the Sanderson electronegativity of element i, and N_i is the total number of oxygen in the system.

➢ *Model of Toop and Samis*

In 1962, Toop and Samis[26] have proposed the existence of three different forms of oxygen:

- The bridging oxygen which links to two silicon atoms (O^0).
- The non-bridging oxygen which links to one silicon atom (O^-).
- The free oxide ion (O^{2-}).

It is possible to develop an equilibrium between these three forms of oxygen and thus to derive the equilibrium constant as expressed by the following equations:

$$2O^- \Leftrightarrow O^0 + O^{2-} \quad (2.12)$$

$$K = \frac{a(O^{2-}) \times a(O^0)}{a(O^-)^2} \quad (2.13)$$

The value of K is constant for a given temperature and it represents the characteristic of cations present in the molten glass. In this equation, Toop and Samis have replaced the activities of the components by their concentrations, hence specified the equilibrium proportions for each form of presented oxygen. For a molten oxide with a composition nM_2O-(1-n)SiO_2, the number of moles of oxygen atoms bonding to silicon atoms 4(1-n) can be written as the following equation:

$$2N(O^0) + N(O^-) = 4(1-n) \tag{2.14}$$

where $N(O^0)$ and $N(O^-)$ are the number of bridging and non-bridging oxygens. Thus, the following equation can be derived:

$$N(O^0) = \frac{4(1-n) - N(O^-)}{2} \tag{2.15}$$

The number of free oxide ions can be represented by the following equation:

$$N(O^{2-}) = n - \frac{N(O^-)}{2} \tag{2.16}$$

Since the reaction of one mole of oxide modifier with silica gives rise to two moles of non-bridging oxygen, the equilibrium constant between the three forms of oxygen can be written in assimilating the activities with their concentrations:

$$K = \frac{N(O^{2-}) \times N(O^0)}{N(O^-)^2} \tag{2.17}$$

By replacing the $N(O^{2-})$ *and* $N(O^{0})$ by Eq. 2.16 and Eq. 2.15 respectively, the following equation can be derived:

$$K = \frac{[(4-4n) - N(O^{-})] \times [2n - N(O^{-})]}{4N(O^{-})^{2}} \tag{2.18}$$

Eq. 2.18 can be simplified by the following equation:

$$(4K-1) \times N(O^{-})^{2} + (4-2n)N(O^{-}) + 8(n^{2}-n) = 0 \tag{2.19}$$

The resolution of this equation for various values of equilibrium constants and for different stoichiometries allows the determination of the distribution of the three forms of oxygen present in the melt under the considered environment. However, Konakov[19] has pointed that the states of O^{0} in SiO_2 and the formed silicates, as well as O^{-} in these silicates, are indiscernible. Therefore, the Toop and Samis model was rather limited and could not be used for an adequate description of the acid-base interactions in real oxide melts. However, the approach by Toop and Samis was partly used in many known models[1,27,28].

(b) Experimental measurements

Due to the importance of the knowledge of acid-base properties in the molten glass and the difficulties in predicting it, many authors have developed some techniques in order to measure experimentally the acid-base properties in molten glass.

- *Gaseous solubility*

The relative basicity of molten glass can be evaluated experimentally by the solubility of certain gases (H_2O[29,30], CO_2[31–33], SO_2[34]) which dissolve in the glass network. The solubility of the gas will increase at any constant pressure of oxygen as the oxygen ion activity in the melt increases. Since the oxygen ion activity is related to the basicity of the melt, an increase in the solubility of the gas can be used as an indicator of an increase in the basicity of the melt.

- *Transition metal ions as acid-base indicators*

Paul and Douglas[35–37] have proposed a method by using transition metal ions as acid-base indicators in glass. The transition metals which have been introduced in molten glass behave like a Lewis acid and interact with the free oxide ions in order to form an oxocomplex. The possibility of using transition metal ions as indicators in silicate glasses is due to the fact that the coordination symmetry of these ions changes with the basicity of the melt. Due to their incompletely filled inner shell, the oxocomplex formed can be studied thoroughly by spectroscopic and magnetic measurements. The cations that are widely used in this method are Ni^{II} [35],Co^{II} [36] and Cr^{VI} [37]. In the case of Ni^{II} and Co^{II}, a change of coordination from octahedral symmetry to tetrahedral symmetry with increasing basicity can be determined by spectroscopic measurements since the optical absorption characteristics of octahedral and tetrahedral are distinctly different.

- *Transpiration method*

Since basicity of the melt links to the content of network modifiers in the glass, the transpiration method is dedicated to determining the activity of sodium

oxide ($a(Na_2O)$) which plays a role as a network modifier by measuring the vapour pressure of the distillation gas of the molten oxides. Rego *et al.*[38] have used the transpiration technique to measure the vapour pressures of Na above the stirred Na_2O-$xSiO_2$ melts which are in equilibrium with graphite crucible and CO. The experiments have been performed at 1300°C and 1400°C for silica-rich melts under a system pressure of one atmosphere. Under these reducing conditions, the expected reaction is:

$$Na_2O_{(l)} + C_{(s)} = 2Na_{(g)} + CO_{(g)} \tag{2.20}$$

The equilibrium constant for the above reaction allows the determination of the activity of Na_2O in the silicate melts according to the following equation:

$$\log(a_{Na_2O}) = \log[(p_{Na})^2 \times p_{CO}] - \log K \tag{2.21}$$

The quantity log $[(p_{Na})^2$ x $p_{CO}]$, which is related to the $a(Na_2O)$ is plotted as a function of compositions for each two temperatures. The second-order curve fits give an access to the log K values, thereby allowing the determination of aNa_2O by the following equations:

at 1300°C,

$$\log a_{Na_2O} = -9.86 + 6.22X_{Na_2O} + 6.75(X_{Na_2O})^2 \tag{2.22}$$

and at 1400°C,

$$\log a_{Na_2O} = -9.01 + 2.44X_{Na_2O} + 11.8(X_{Na_2O})^2 \tag{2.23}$$

where X_{Na2O} is the mole fraction of Na_2O in the glass. An extension of this work, using an encapsulation technique to study the Na_2O-CaO-SiO_2 and Na_2O-MgO-SiO_2 systems and some synthetic blast-furnace slags have been described by Rego *et al*.[39] in another work.

- *EMF measurement*

The oxygen ion activity of two melts can be compared by measuring the difference of the electrochemical potential of oxygen in the melts. The only direct method by which oxygen ion activities can be compared independently without interference from other reactions is through an electromotive force measurement (EMF)[1]. This method requires the use of a reversible oxygen electrode immersed in molten glass. Thus, a platinum electrode which has been flushed by air is the best candidate for this type of application. It is also necessary to provide a bridge between the glasses being compared which has negligible junction potential. The basicity of the molten glass has been determined by measuring the different potentials between the working melt (studied melt) and the reference melt (melt with well-known basicity). The junction between the two glasses is ensured either by a β alumina[6,40–42] refractory or by a direct contact between these two glasses through a small diameter of orifice[43,44].

The potential generated by the electrochemical cell of type:

Platinum $O_{2(g)I}$	$Glass_{(I)}$	Ionic junction	$Glass_{(II)}$	Platinum $O_{2(g)II}$

is given by the following equation if $O_2(Pt)_I = O_2(Pt)_{II}$:

$$\Delta E = \frac{-RT}{2F} \times \ln \frac{a\left(Na_2O\right)_{(II)}}{a\left(Na_2O\right)_{(I)}} \tag{2.24}$$

where $Glass_{(I)}$ is the reference glass and the $Glass_{(II)}$ is the working glass. The Eq. 2.24 can be expressed as:

$$\ln a\left(Na_2O\right)_{II} = \ln a\left(Na_2O\right)_{I} - \frac{2F\Delta E}{RT} \tag{2.25}$$

This method allows a direct access to the relative basicity of a molten glass. Unlike the other methods which have been discussed before, the EMF measurement allows the determination of the basicity of the molten glass without modifying the solvent by an addition of gas or an indicator. Furthermore, a wide range of glass compositions can be studied using this technique especially for a higher acidity melt where the conventional method such as gas dissolution may not give an accurate result.

The activity of Na_2O in Na_2O-SiO_2 and Na_2O-CaO-SiO_2 systems has been measured by Neudorf and Elliott[40] by using this method. It has been demonstrated that an addition of CaO to the binary Na_2O-SiO melt causes an increase in the activity of Na_2O. The experimental activity data seems to have a good agreement with the values calculated using Richardson ideal mixing model[40].

The EMF measurement has been also applied by Abdelouhab *et al.*[6] in order to quantify the activity of Na_2O in a series of sodium-bearing silicate melts at high temperature. Abdelouhab has tried to make a comparison between the log a(Na_2O) obtained via EMF measurement and the calculated basicity using theoretical model

of Sun[20], Sanderson[22–24] and Duffy and Ingram[45]. It has been found that there is a linear relationship between the calculated glass basicity and the measured log a(Na_2O) for each compositional series. However, none of the considered models provides a good correlation between measured a(Na_2O) and calculated glass basicity if all compositions are taken into account[6].

2.1.2.3. Optical basicity

The optical basicity (Λ) concept has been introduced by Duffy and Ingram[45–47] by taking into account both Lux-Flood[15,16] and Lewis[14] theories. This method is based on the donating electron power of O^{2-} in the glass which can be measured by UV spectroscopy. An addition of a small concentration of a solute metal ion to a glass will cause the oxygen of the glass to donate some of their negative charges to the metal ions. The metal ions which are surrounded by bridging oxygen and non-bridging oxygen will act like Lewis acids whereas the oxygen will behave as Lewis base. The ability of oxygen to donate the negative charge is at maximum when it exists as the "free" O^{2-}, surrounded by almost non-polarising cations, for example Na^+, K^+ or Ca^{2+}. The metal ions such as Pb^{2+}, Bi^{3+}, Ti^+ can undergo observable changes depending upon the degree of electron donation they receive from oxygen and therefore make it possible to be used as a 'probe' for measuring the basicity in the glass. Duffy and Ingram have constructed a scale (Table 2.3) for the optical basicity of the oxides based on the position of absorption spectrum of the s → p electronic transition of the probes. The frequency of the absorption band is dramatically lowered by an increase in the basicity of the glass. This is due to orbital expansion of the probe ions while receiving the electron donation by the oxygen with high electron donor power.

Table 2.3: Optical basicity of oxydes determined by Duffy and Ingram[45]

Oxides	B_2O_3	SiO_2	Al_2O_3	MgO	CaO	Li_2O	BaO	Na_2O	K_2O
Λ_{oxyde}	0.42	0.48	0.60	0.78	1.00	1.00	1.15	1.15	1.40

The probe ion spectroscopic studies of many glass systems, *e.g.* borates, silicates, phosphates and other oxidic media which allow the construction of optical basicity of individual oxides (Table 2.3) have induced the so-called "theoretical" or "ideal" optical basicity of multi-component glasses on the basis of the following equation proposed by Duffy and Ingram[45,48]:

$$\Lambda = X_A \times \Lambda_A + X_B \times \Lambda_B + ... \tag{2.26}$$

where X_A, X_B are equivalent fractions based on the amount of oxygen that each oxide contributes to the overall glass stoichiometry and Λ_A, Λ_B are the optical basicities assigned to the individual oxides. As stated by Duffy and Ingram, Eq. 2.26 can only predict the 'trends' in optical basicity rather than the 'true' basicity value. Eq. 2.26 expresses the average bulk basicity of all oxide species and it cannot estimate the coordination number changes of the cations. Therefore, in some cases it is expected to observe a difference between the theoretical and experimental trends of optical basicity. However, Eq. 2.26 seems to work well on the silicate and phosphate glasses[45]. On the other hand, a discrepancy exists between the calculation and measurement of the optical basicity by UV spectroscopy for borate glasses[49,50].

Since the optical basicity calculation seems to work well on the silicate glasses, the Eq. 2.26 will be used in this work for indicating the trend in (average) basicity as the proportion of basic oxide that is increased or decreased.

2.1.2.4. Influence of the acid-base properties of the melts on the solubility of oxides

As in the aqueous medium, the solubility of oxides in the melts depends on the acid-base properties of the system. In the case of amphoteric oxides (*e.g.* Al_2O_3 and Cr_2O_3), the dissolution in acid medium (high pO^{2-}) can be expressed by the following equation:

$$MO \Leftrightarrow M^{2+} + O^{2-} \quad \text{with } K_1 = [M^{2+}][O^{2-}] \tag{2.27}$$

This is known as acid fluxing. In basic medium (low pO^{2-}), dissolution or basic fluxing is represented by the following reaction:

$$MO + O^{2-} \Leftrightarrow MO_2^{2-} \quad \text{with } K_2 = \frac{[MO_2^{2-}]}{[O^{2-}]} \tag{2.28}$$

The variation of solubility of amphoteric oxide in a medium where O^{2-} is the active species, as a function of pO^{2-} can be represented by the following diagram (Figure 2.3):

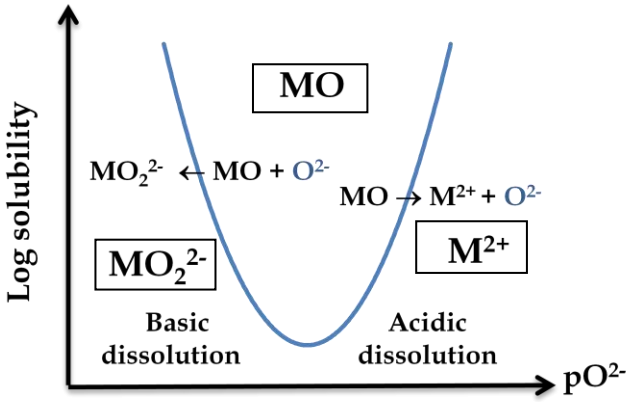

Figure 2.3: Log solubility of amphoteric oxides as a function of melt basicity (pO^{2-})[51]

As an example, the solubilities of the important oxides NiO, Co_3O_4, Fe_2O_3, CeO_2, Cr_2O_3, Al_2O_3 and also for SiO_2 have been determined as a function of melt basicity and oxygen activity for pure fused Na_2SO_4 at 1200 K. A compilation of these results has been shown (Figure 2.4) and discussed thoroughly by R. A. Rapp[51]. The "V" shape curves prove the dependence of the solubility of oxides with the basicity/acidity of the melts. As a conclusion, it is important to have a knowledge of melt basicity in order to predict the behaviour of the oxides in the melts.

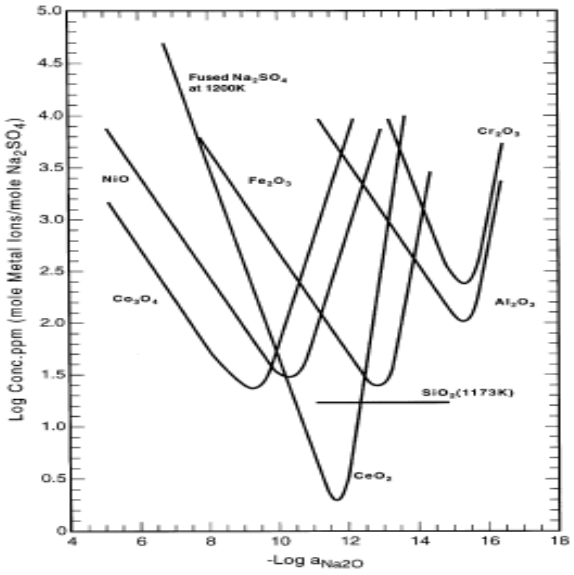

Figure 2.4: Compilation of solubility of several oxides in fused pure Na_2SO_4 at 1200K[51]

2.1.3. Redox properties in silicate melts

The molten glass is a solvent in which the reaction of oxidation-reduction (redox) can occur. When a metal is immersed in molten glass at high temperature, an electronic exchange can be established between the oxygen of the glass and dissolved species (oxidant with higher standard potential), which is actually the origin of the problem of corrosion of materials by molten glass. Furthermore, in molten glass, many species occur in more than one valence or oxidation states and

the valence state of these ions governs many physico-chemical properties of the molten glass (*e.g.* viscosity, quality of refining) and the final material (colour, viscoelasticity, crystallisation, aging resistance)[1,52,53].

In the molten glass environment at temperatures higher than 1000°C, the O_2/O^{2-} couple plays an important role in the redox equilibrium according to the following equation:

$$\frac{1}{2}O_2 + 2e^- \Leftrightarrow O^{2-} \tag{2.29}$$

2.1.3.1. Equilibrium constant

The reactions in the molten glass between polyvalents ions and O_2/O^{2-} couple have been described by several authors[54–57] according to the following equations:

$$M^{m+} \Leftrightarrow M^{(m+n)+} + ne^- \tag{2.30}$$

$$\frac{n}{4}O_2 + ne^- \Leftrightarrow \frac{n}{2}O^{2-} \tag{2.31}$$

$$M^{m+} + \frac{n}{4}O_2 \Leftrightarrow M^{(m+n)+} + \frac{n}{2}O^{2-} \tag{2.32}$$

The Le Châtelier principle allows the prediction of the influence of the modification of the variables of the Eq. 2.32 on the redox equilibrium:

- An increase in the oxygen fugacity (fO_2) will lead to an increase of the oxidised species for a given temperature and melt basicity.

- On the other hand, an increase in the oxide ion activity (O^{2-}) will favour an increase of the reduced species for a given temperature and oxygen fugacity (fO_2).

Many studies[11,58–60] have proved the first prediction but some authors[11,56,61–64] have shown an opposite behaviour from the second prediction where an increase in the melt basicity leads to an increase of the oxidised species. This disagreement can be explained by taking into account the nature of the metal cations which interact with the oxide ions. This leads to the formation of oxocomplexes where their stabilities, charges, symmetries and the coordination numbers vary depending on the oxidation state of the solute[65].

By taking into account the combination of redox and acid-base properties in the glass, Eq. 2.32 can be expressed according to the following reaction:

$$MO_x^{(2x-m)-} + \frac{n}{4}O_2 \Leftrightarrow MO_y^{(2y-m-n)-} + \left(x - y + \frac{n}{2}\right)O^{2-} \tag{2.33}$$

In this equilibrium, the oxidised and reduced states of multivalent species $M^{(m+n)+}$ and M^{m+} are complexed by oxygen where the x and y represent the coordination numbers for resulting oxocomplexes respectively. The value of stoichiometric coefficient of O^{2-} plays an important role to determine the redox species that will be stabilised by increasing the melt basicity. The equilibrium constant can be derived from Eq. 2.33 and is given by Eq. 2.34:

$$K(T) = \frac{a(MO_y^{(2y-m-n)-}) \times a(O^{2-})^{(x-y+n/2)}}{a(MO_x^{(2x-m)-}) \times (fO_2)^{n/4}} \quad (2.34)$$

where a_i is the chemical activity of element i and fO_2 is the oxygen fugacity imposed on the system. As discussed in the previous part, the activity of oxide ion (O^{2-}) is related to the composition of the glass. By replacing activities by the expression ($a_i = \gamma_i.C_i$), the equilibrium constant can be expressed as:

$$K^*(T) = \frac{\gamma_{M^{(m+n)+}} \times [MO_y^{(2y-m-n)-}] \times a(O^{2-})^{(x-y+n/2)}}{\gamma_{M^{(m)+}} \times [MO_x^{(2x-m)-}](fO_2)^{n/4}} \quad (2.35)$$

where γ_i is the activity coefficient of the i component in the melt and [i] is the concentration of the i component in the melt. The concentration of the polyvalent element is usually low compared to the concentration of the oxide ion. As a consequence, by applying Henry's law, the activity of the polyvalent element can be assimilated to its concentration[1,65]. Furthermore, it is assumed that oxygen behaves as a perfect gas so that the oxygen fugacity is equal to the internal partial oxygen pressure of the melt. The equilibrium constant $K^*(T)$ can thus be expressed by using only the concentration of the polyvalent element, the partial oxygen pressure and the activity of the oxygen ions:

$$K^{**}(T) = \frac{[MO_y^{(2y-m-n)-}] \times a(O^{2-})^{(x-y+n/2)}}{[MO_x^{(2x-m)-}] \times (PO_2)^{n/4}} \quad (2.36)$$

where

$$\frac{[MO_y^{(2y-m-n)-}]}{[MO_x^{(2x-m)-}]} = \frac{[ox]}{[red]} = \Re \tag{2.37}$$

with $\Re$ represents the redox ratio.

Thus,

$$\Re = K^{**}(T) \times a(O^{2-})^{(y-x-n/2)} \times PO_2^{n/4} \tag{2.38}$$

This equation shows that the redox ratio depends on the temperature, the basicity of the glass melt and the partial oxygen pressure imposed on the system.

2.1.3.2. Redox properties by electrochemical measurement

As in the aqueous media, an electrochemical technique can be used to characterise the redox properties in the melt. The oxidising power of the redox couple M^{m+} and $M^{(m+n)+}$ in Eq. 2.30 can be characterised by its redox potential E, given by the Nernst relation:

$$E = E^0_{(M^{(m+n)+}/M^{m+})} + \frac{RT}{nF} \ln \frac{a(M^{(m+n)+})}{a(M^{m+})} \tag{2.39}$$

where $E^0_{(M^{(m+n)+}/M^{m+})}$ is the standard potential of the couple. Since the concentration of the redox elements is relatively low in the melt, the activities notation can be assimilated to its concentration according to the following equation:

$$E = E^0_{(M^{(m+n)+}/M^{m+})} + \frac{RT}{nF} \ln \frac{[M^{(m+n)+}]}{[M^{m+}]} \tag{2.40}$$

Since there is no absolute value of the potential of the redox couple, the potential has to be defined with respect to a potential of a reference couple. In the standard condition (25°C, P = 1 atm) for aqueous solutions, the reference couple that is used is H^+/H_2. However, the protons are not stabilised in the molten glass, thus making it impossible to be used as a reference couple in the melts. As a consequence, the O_2/O^{2-} couple has been used as a reference couple in the molten glass due to its reversible behaviour towards the platinum[58] electrode or zirconia[66,67] electrode.

The potential of the half-cell on the platinum or zirconia electrodes is given by the following Nernst law:

$$E = E^0_{O_2/O^{2-}} + \frac{RT}{4F}\ln\frac{P(O_2)}{a(O^{2-})^2} \tag{2.41}$$

where $P(O_2)$ is the partial oxygen pressure in equilibrium with the melt and $a(O^{2-})$ is the oxide ion activity. For any potential E, the following equation is valid:

$$E = E_{\text{working electrode}} - E_{\text{reference}} \tag{2.42}$$

and thus,

$$E = E^0_{M^{(m+n)+}/M^{m+}} + \frac{RT}{nF}\ln\frac{[M^{(m+n)+}]}{[M^{m+}]} - E^0_{O_2/O^{2-}} - \frac{RT}{4F}\ln PO_2 \tag{2.43}$$

Many studies[66,68–71] have been devoted to determining the formal potentials of redox couples in various glasses at different temperatures. The results allow a potential scale (Figure 2.5) to be drawn for the prediction of corrosion reactions[72]. The potentials of the redox couples are expressed relative to the zirconia reference

electrode. It seems that this scale is valid in simple silicate glasses (soda-lime silicate, borosilicate, etc.) for a range of temperatures from 1000°C to 1300°C[72].

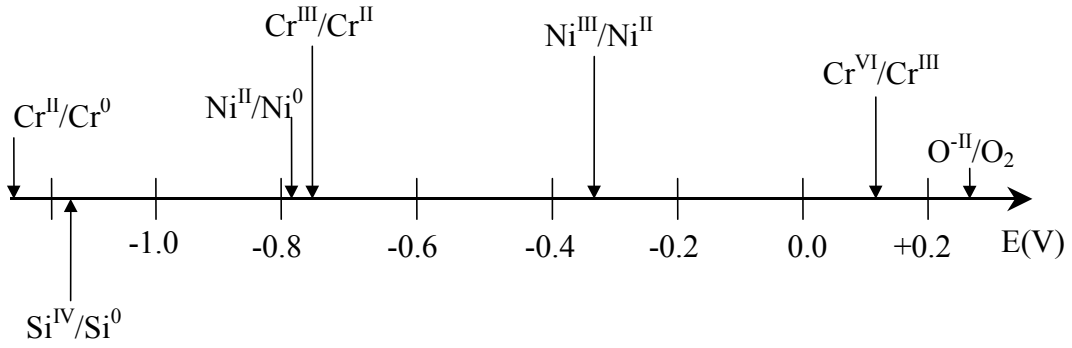

Figure 2.5: Scale potential used for prediction of corrosion in silicate glasses between 1000°C - 1300°C[72]

2.2. Corrosion of metals and alloys by molten glass

The glass melts behave as a solvent and they are extremely corrosive towards metallic materials. As shown in the previous part, corrosion of metals and alloys in molten glass is the result of the coupling of acid-base properties and redox reactions in the systems. As a consequence, the studies of the corrosion of metals and alloys in molten glasses can be carried out experimentally by an electrochemical technique.

2.2.1. Corrosion of pure metals in molten glasses

The study of the corrosion behaviour of pure metals in molten glasses was performed by several authors. It has been divided into two categories which are:

a) Case of noble metal

b) Case of metals used in glass and nuclear industries

2.2.1.1. Case of noble metal

To date, platinum and platinum alloys are still preferentially used in glass industry due to their very high corrosion and erosion resistance, as well as low solubility when in contact with molten glass. The platinum is used in the glass industry for melting pots, coating of melting vats, stirrers and for other auxiliary equipments. However the high temperature mechanical properties of this element at temperatures above 1200^{o}C is limited due to low creep resistance and recrystallisation phenomena[68]. Furthermore, the Pt alloys can react in reducing atmospheres with metallic or semi-metallic elements to form low melting point compounds[68,73].

The platinum is exposed to recrystallisation[68] phenomenon when it is subjected to high temperature. This phenomenon leads to the grain growth, thus allowing the penetration of molten glass along the grain boundaries. As a consequence, the decohesion of material will occur.

In a very reducing condition, species such as tellurium can be reduced as shown by Gaillard Allemand[68]. In this condition, the potential of the glass (-0.5 V) becomes lower than the formal potential of Te^{IV}/Te^{0} (-0.35 V). As a consequence, the Te metal exists in the molten glass. The contact of this metal with platinum leads to a formation of an eutectic component with low melting point, thereby causing a faster degradation of the material as shown in Figure 2.6(a) and (b).

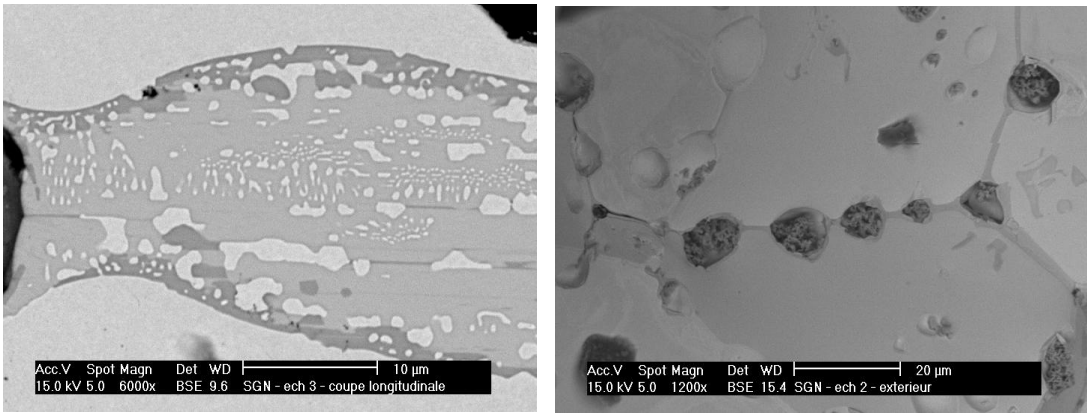

(a) **(b)**

Figure 2.6: (a) Pt sample immersed in a waste glass containing TeO_2 under argon atmosphere and (b) Higher magnification of the micrograph of Pt-Te eutectic grain boundary[68]

Furthermore, platinum also undergoes a catastrophic corrosion when it is immersed in molten glass equilibrated under reducing conditions. For example, in the case of the existence of $MoSi_2$[68], the formation of eutectic Pt-Si (Figure 2.7) with low melting point which is responsible for the degradation of the platinum has been observed according to the following equations:

$$Si^{IV} + 4e^{-} \Leftrightarrow Si^{0} \tag{2.44}$$

$$Si^{0} + 3Pt \Leftrightarrow Pt_3Si \tag{2.45}$$

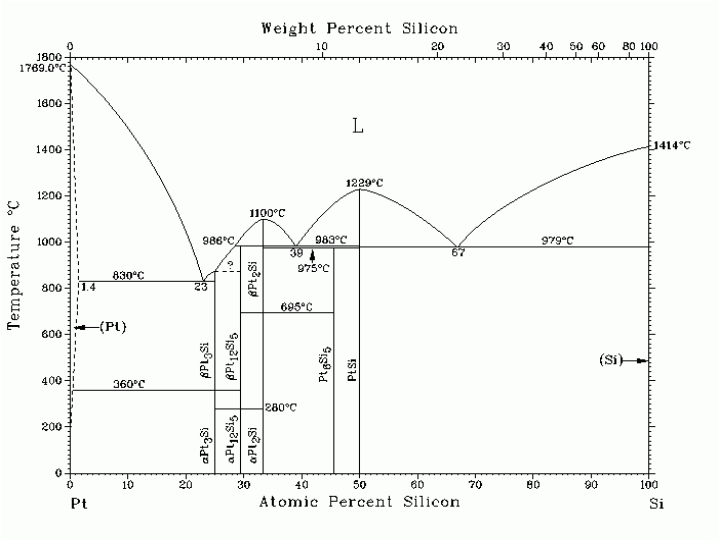

Figure 2.7: Binary phase diagram of Pt-Si[74]

2.2.1.2. Case of metals used in glass and nuclear industries

The studies on the corrosion of pure Nb[75], Ta[76], Zr[77] and Ti[78,79] metals have been performed by several authors in order to tackle the industrial problems especially for the nuclear industry. The development of the glass for vitrification of radioactive waste in nuclear industry which is performed by induction melting in a cold crucible requires a specific study on the possible materials for this kind of application. The materials should be chosen by taking into account the electrical resistivity of the metals which must be compatible with the high frequency induction. In addition, the metals should possess an acceptable resistance to the oxidation in air and corrosion in the molten glasses as well.

The studies on the corrosion of the four pure metals[75–79] have been performed on three different borosilicate glasses at T = 1050°C - 1040°C. The corrosion behaviour in molten glass has been characterised by immersion test followed by electrochemical measurements. The authors proved that each of the metal-glass

couples possesses a unique corrosion-degradation process for a studied temperature range.

The corrosion mechanisms of the four pure metals in the three different borosilicate glasses can be summarised as follows:

- The metal M is oxidised to metal oxide MO_x by one or more oxidising species of the glass.
- The corrosion products which are formed on the interface metal/glass are often complex but can be determined by combining the knowledge of the redox couples and the phase diagrams.
- The accummulation of the corrosion products tends to increase the oxidation reaction of the substrate.
- The complete corrosion of the metals is observed by the prolongation of the mechanisms described above or by the dislocation of the metallic parts due to the difference in the density between the corrosion products and the substrates.

It is noted that all the phenomena demonstrated by the authors have never been precisely described. The approach has helped to determine the complexity of the corrosion products by combining the knowledge of redox couples present in the system and the phase diagrams in order to predict the possible corrosion layers formed at the interface. An example of this approach is shown in Figure 2.8 where the corrosion products obtained after immersing a Zr plate in G-Fe glass have been determined by combining the redox scale and the phase diagram of Zr-Si-O system.

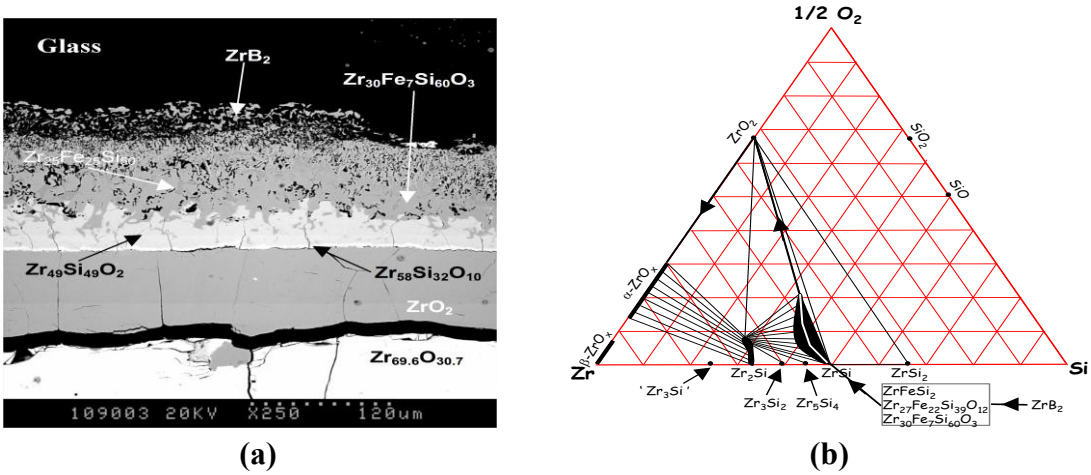

(a) (b)

Figure 2.8: (a) SEM micrograph of a zirconium plate immersed in G-Fe glass (borosilicate glass containing iron oxide) at 1418°C for 13 h and (b) the corrosion layers formed are determined by the phase diagram of Zr-Si-O-(Fe-B). The diffusion path is shown by the arrows[77]

The study of the pure Fe[71], Co[71], Ni[71] and Cr[10,71] has been performed by several authors in order to characterise the main components of superalloys (cobalt or nickel-based superalloys) used in the glass industry. The corrosion behaviour of these metals in an industrial soda lime silicate glass has been conducted using two complementary methods. The first method which is thickness loss measurement has been used to determine the corrosion rates of these metals. Among the tested metals, only Cr shows an ability to form a protective chromia (Cr_2O_3) layer at the interface metal/glass when it has been immersed in an industrial soda lime silicate glass at 1025°C.

The second method which is the conventional electrochemical method with the use of specific electrodes adapted to molten glasses has been performed on these four metals. The results show an existence of a wide passivation plateau with very low current densities (~0.4 mA/cm^2) in the case of Cr (Figure 2.9) which proves the ability of Cr to build a protective chromia (Cr_2O_3) layer by increasing the potential.

This characteristic shows the potential of Cr to be used as a main protective component of superalloys in molten glasses.

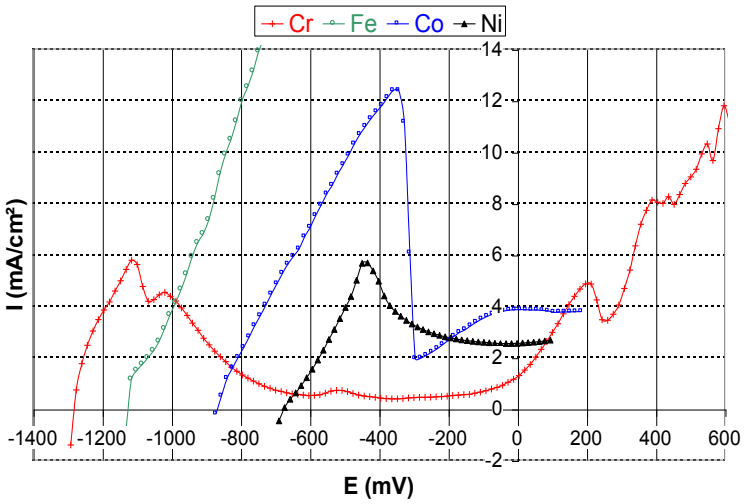

Figure 2.9: Anodic polarisation of Cr, Fe, Co and Ni at 1050°C in an industrial soda-lime silicate glass[71]

Even though Cr possesses an ability to develop a Cr_2O_3 layer, the stability of this layer in molten glass plays a crucial role for protecting the superalloy. Carton *et al.*[80] have demonstrated the influence of temperature on the stability of the passivity state in molten glass as shown in Figure 2.10. It can be seen from the curves that a transition from passive to active states occurs at a critical temperature when there is a decrease of corrosion potential (E_{corr}) and polarisation resistance (Rp). In the case of preoxidised pure Cr rod immersed in G-S glass, the transition occurs at 1160°C. As a consequence, 1160°C is known as a depassivation temperature at this condition where the protection is not efficient anymore.

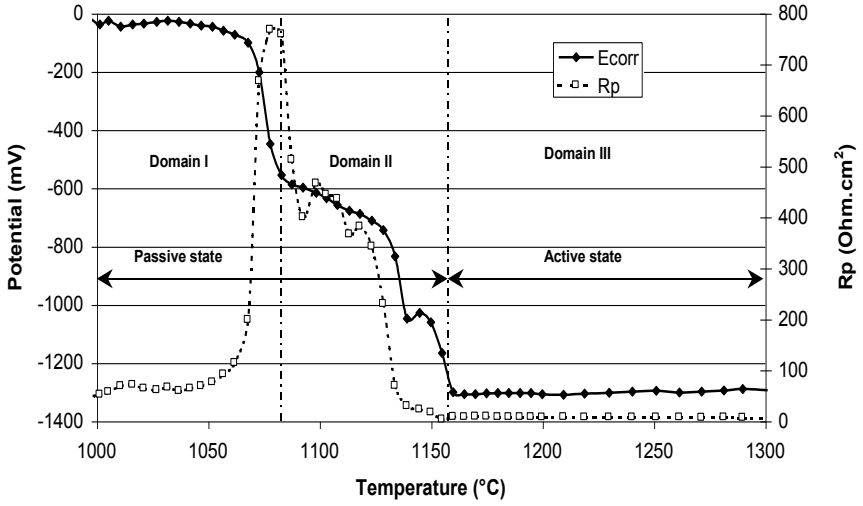

Figure 2.10: E_{corr} and Rp of preoxidised pure Cr immersed in G-S glass as a function of temperature[80]

As compared to the thickness loss measurement, the electrochemical technique possesses an advantage as a tool to characterise the corrosion behaviour in molten glass since it allows the identification of the mechanisms involved in the system. This is an important step to improve the behaviour of the materials. In addition, it has been proved that the corrosion rates calculated from the polarisation curve are close to the ones determined from the measurements of thickness loss[71]. Therefore, the electrochemical method can serve as a semi-quantitative indicator for the classification of the performance of metals and alloys in molten glasses.

2.2.2. Corrosion of alloys in molten glasses

Since the behaviour of several important pure metals in molten glasses has been documented, the studies have been extended on the corrosion behaviour of alloys in molten glasses. In the hot corrosion context, Ni-based superalloys with high Cr content and with Al as an alloying element are the best candidates for high temperature applications (*e.g.* heating elements, gas turbine engines, etc.) since Cr

and Al are well known to have the ability to develop thermodynamically stable oxides (Cr_2O_3 and Al_2O_3). However, the nature of the formed oxides depends on the composition of the alloy and the conditions of the heat treatment. At sufficient concentration of Cr and Al, they will be selectively oxidised to form a continuous layer of Cr_2O_3 and Al_2O_3. The selective oxidation of Cr takes place in Ni-Cr alloy with approximately more than 20 wt.% Cr[81]. Higher concentrations of Al are needed in binary alloys (*e.g.* Ni-Al) than in ternary alloys (*e.g.* Ni-Al-Cr) in order to achieve a formation of continuous Al_2O_3 scale. This is due to the fact that the oxygen flux into the alloy is reduced when there is an internal oxidation of Cr in the case of ternary alloys[81]. The reaction during the steady state changes depending on the critical concentration of the alloying components. This behaviour is simplified in Figure 2.11, which is an oxide map developed for Ni-Al-Cr system at 1000°C.

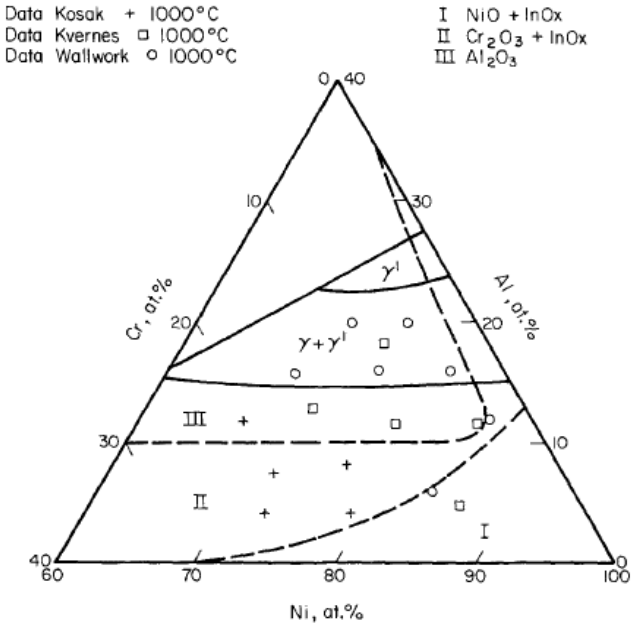

Figure 2.11: Oxide map for the ternary system Ni-Al-Cr at 1000°C[82]

Since Cr_2O_3 and Al_2O_3 are the most probable oxides to be formed in this kind of alloys at high temperature, attention will be paid on the behaviour of chromia and alumina forming alloys in molten silicates.

2.2.2.1. Chromia forming alloys in molten glasses

Chromia forming alloys are often used in glass industry. For example, they can be materials of construction for processing pot and susceptor in metallic melter pot furnace, as well as electrodes in Joule-heated ceramic melter pot employed for high level nuclear waste immobilisation process[83,84]. It has been previously shown that a sufficient chromium content has the ability to build a thick and adhesive chromia layer which can protect the alloy from the glass corrosion[41,71,85–87]. As a consequence, several studies have been devoted to the characterisation of the behaviour of chromia forming alloys in molten glasses.

Lizarazu *et al.*[87] have performed a study devoted to the corrosion of Ni-Cr alloys in float glass (soda lime silicate glass with small additions of MgO, Al_2O_3 and Fe_2O_3) at 1100°C by using an electrochemical technique. This work has shown that the Ni-Cr alloys with intermediate chromium content (Ni-30Cr and Ni-50Cr (wt.%)) exhibit spontaneously low corrosion current (< 0.2 mA/cm^2), whereas the alloys with both low (Ni, Ni-20Cr (wt.%)) and high (Cr, Ni-70Cr (wt.%)) chromium content display important corrosion current (> 3 mA/ cm^2). A low Cr content in the alloy is not sufficient to provide enough chromium to build a protective oxide layer. On the contrary, a too high Cr content will induce a spallation of the layer due to the development of compressive stress because of the great thickness of the formed chromia. Other works confirm the spontaneous development of a protective chromia

layer, as shown by Dutta *et al.*[83] who studied the corrosion of superalloy 690 (Ni-Cr-Fe alloy with 28 wt.% of Cr) in borosilicate glass at 1248 K.

Di Martino *et al.*[86] have extended the study on the corrosion of high chromium (~ 30 wt.%) Ni-based and Co-based commercial superalloys in borosilicate glass at 1050°C. The comparison between spontaneous behaviour of Co-based alloy and the behaviour of the alloy after preoxidation treatment has been illustrated in Figure 2.12. In this case, the spontaneous behaviour leads to corrosion of the alloy with very low corrosion potential (E_{corr}). The protection could be only obtained by performing a preoxidation treatment in air before immersing the alloys in the molten glass. This preoxidation treatment 'helps' the alloy to build a compact and adhesive chromia (Cr_2O_3) scale at the interface. As a consequence the alloy which consists of a protective chromia scale will be subjected directly to the passivation region right after immersion with high corrosion potential (E_{corr}) and polarisation resistance (Rp).

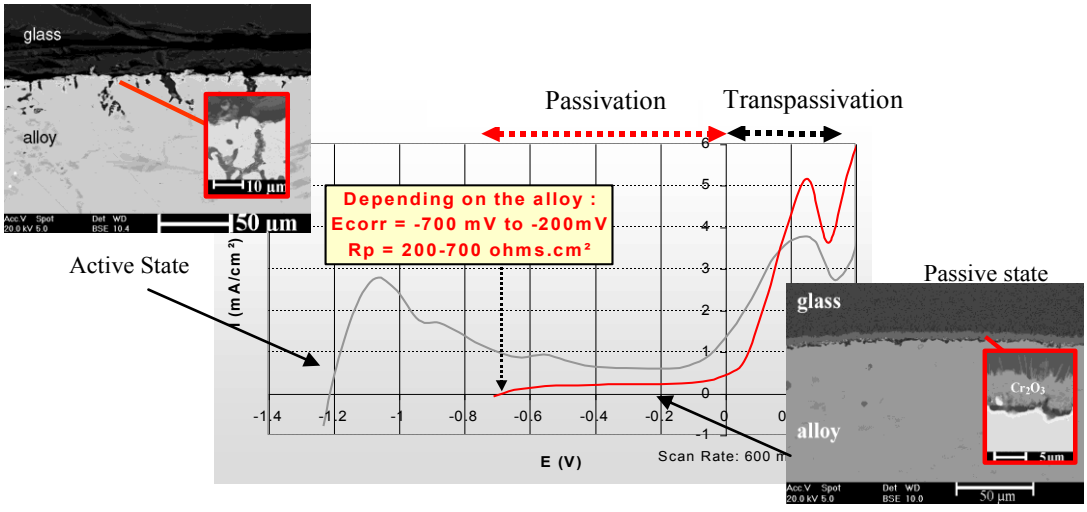

Figure 2.12: Anodic polarisation curves of Co-based alloy in borosilicate glass for active and passive states at 1050°C with scan rate, υ = 10 mV/min. The interpretation of the curves is supported by the SEM micrographs for both conditions[85]

As a conclusion, a sufficient Cr content is required to allow the development of a protective oxide layer. Nevertheless, depending on the conditions (temperature, melt composition, etc.), a preoxidation is necessary in order to "help" the alloy to build the protective chromia layer before having contact with the molten glass.

2.2.2.2. Alumina forming alloys in molten glasses

The behaviour of alumina forming alloys in molten glasses is poorly documented in the literature. Recently, Dutta *et al.*[83] have performed an aluminisation of superalloy 690 (Ni-Cr-Fe alloy with 28 wt.% of Cr) by pack-cementation. The cemented alloy has then been oxidised for 4 h at 1273 K, leading to a formation of ~ 2 μm thickness of Al_2O_3 layer on the topmost surface. The alloy was then exposed to borosilicate glass at 1248 K for 192 h. Their conclusion is that the sample has shown a good stability without any phase formation at the coating/glass interface which is attributed to modification of glass composition at the coating/glass interface. This composition has been modified due to the partial dissolution of Al_2O_3 from preexisting Al_2O_3 layer. However, no data has been recorded concerning the prediction of the corrosion rate/life time of this alloy in the melts.

As a conclusion, the ability of the alloys to develop a homogeneous and adherent oxide layers as well as their durability in the melts play an important role in order to ensure their resistance against corrosion by molten glasses. Thus, the next part will deal with the state of art of the physicochemical behaviour of the most important oxides in molten glasses.

2.3. Solubility of important oxides in molten glasses

Since the performance of the alloys in molten glasses depends on the stability of their protective layers in contact with the melts, many works have been devoted to the study of the solubility of the refractory oxides in the melts. Manfredo *et al.*[88] have measured the solubility limit of Cr_2O_3, SnO_2, ZrO_2 and Al_2O_3 in soda-lime glass at 1300°C - 1600°C. The results are compiled as shown in Table 2.4:

Table 2.4: Solubility limit for refractory oxides in soda-lime glass[88]

T (°C)	Solubility limit in at.%			
	Cr_2O_3	SnO_2	ZrO_2	Al_2O_3
1300	0.6	4.4	9.7	21.3
1340	0.5	4.2	9.6	/
1400	1.2	/	/	/
1410	1.0	5.2	10.9	23.4
1500	0.9	5.5	/	24.4
1550	1.5	/	12.1	27.8
1600	1.8	6.3	12.8	28.1

The results show that the order of solubility in soda-lime glass is $Al_2O_3 > ZrO_2 > SnO_2 > Cr_2O_3$ at 1300°C - 1600°C.

Tin oxide (SnO_2) is used in the glass industry for specific applications such as heating electrodes and high temperature devices[89–91]. Gateaux *et al.*[92] have performed a study on the solubility of tin oxide in soda-lime silicate melts at 1200°C - 1400°C. This study reveals a correlation between the basicity of the glass and the solubility of tin oxide. SnO_2 shows a significant solubility in silica-rich glass. Indeed, the presence of Sn^{II} is suspected as the acidity of the glasses increases and the total solubility of SnO_2 might be assimilated to the sum of dissolved Sn^{II} and Sn^{IV} [92].

Zirconium oxide (ZrO_2) can be used in high temperature applications as Thermal Barrier Coatings (TBCs)[93]. TBCs are used to protect the blades and vanes in the hot sections of gas turbines and they consist of several layers: (i) a Ni-based superalloy substrate (ii) an alumina forming metallic bond coat and (iii) a porous ceramic top coat of yttria partially stabilised zirconia (8YPSZ-ZrO_2-8wt% Y_2O_3)[93]. In service, the engine ingests dust, sand and ash particles, which then melt and adhere on the hot TBC surface (~1200^oC) made of ZrO_2. During this process, calcium-magnesium-alumino-silicate (CMAS) is incorporated in the molten phase. In this context, the solubility of zirconia in CMAS has been studied by Chellah[94], confirming the order of magnitude of the values obtained by Manfredo *et al.*[88] in other types of glasses (Table 2.4).

According to Manfredo *et al.*[88], Al_2O_3 exhibits the highest solubility in soda-lime silicates. This is coherent with the parts 2.1.1.3 and 2.1.1.5, where it is stated that alumina can behave as a network former or a network modifier in melts, depending on the conditions which have been discussed in the previous part. Monteiro[95] has performed a study on the chemical and physical interactions that take place during glass vitrification process; a process which is conducted in order to store high-level radioactive waste. The results show that a high chemical reactivity of cullet has been observed when $NaAlO_2$ is preferentially oxidised in the cullet. As a contrary, the crystalline phases rich in Al_2O_3 ($NaAl_{11}O_{17}$, $NaAl_6O_{9.5}$) severely limit the reactivity of the cullet and thus induce the difficulty in the dissolution process. In the case of power generation plants, Al_2O_3 ceramic has been used as the combustion chamber refractory due to its superior properties, *e.g.* easy to handle, less expensive and easy to produce. Furthermore Al_2O_3 shows a better corrosion resistance in low

basicity of slags as compared to the MgO based materials[96]. However the corrosion of this refractory by molten oxides is still considered as a serious problem in this industry. As a consequence, Hirata *et al.*[97] have tried to develop a more stable ceramic material in molten slag by adding Cr_2O_3 to Al_2O_3. From this work, they have drawn out a conclusion that the corrosion resistance of Al_2O_3 based ceramic in CaO-Al_2O_3-SiO_2 melt has been improved by an addition of Cr_2O_3[97] since the diffusion rate of Cr ion through the boundary layer is considered to be slower than that of other metal ions.

The work on Cr_2O_3 has been thoroughly investigated previously in this laboratory (LCSM), through the works of Abdelouhab[98] and Khedim[99]. The main discussions are detailed in the next paragraphs.

2.3.1 Physicochemical behaviour of chromium oxide in molten glass

An understanding of the physicochemical behaviour of chromium oxide in molten glass has been facilitated by a schematic in Figure 2.13.

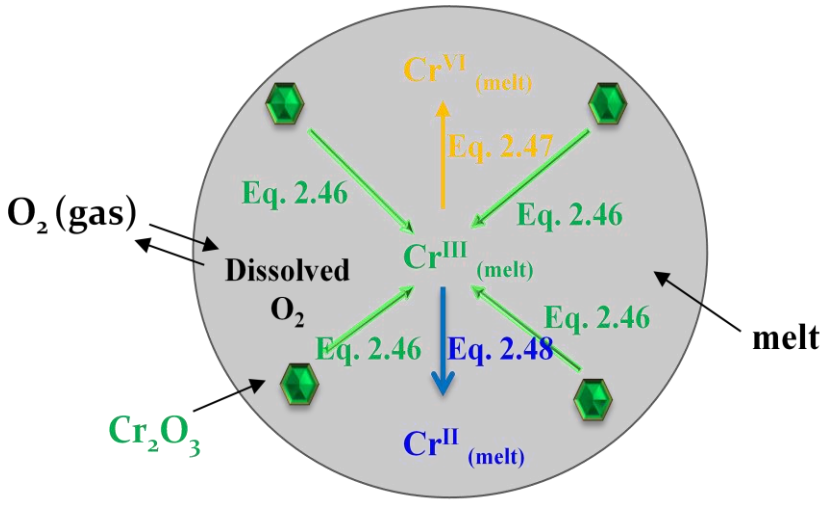

Figure 2.13: Schematic of the Cr_2O_3 dissolution and redox reactions in molten glass

Upon a contact with molten glasses, the dissolution of Cr_2O_3 into Cr^{III} oxocomplex will occur by following an acid-base reaction which is independent of the oxygen fugacity (fO_2) (Eq. 2.46).

$$\frac{1}{2}Cr_2O_{3(crystal)} + \left(x - \frac{3}{2}\right)O^{2-}{}_{(melt)} \Leftrightarrow Cr^{III}O_x^{(2x-3)-}{}_{(melt)} \quad \text{(dissolution)} \tag{2.46}$$

Depending on the oxygen fugacity, Cr^{III} oxocomplex can be oxidised to Cr^{VI} oxocomplex (Eq. 2.47) under oxidising conditions or reduced to Cr^{II} oxocomplex (Eq. 2.48) under reducing conditions. The notation of Cr^{II}, Cr^{III} and Cr^{VI} will be used hereafter to represent the oxocomplexes of these species.

$$Cr^{III}O_x^{(2x-3)-}{}_{(melt)} + \frac{3}{4}O_{2(gas)} \Leftrightarrow Cr^{VI}O_y^{(2y-6)-}{}_{(melt)} + \left(x - y + \frac{3}{2}\right)O^{2-}{}_{(melt)} \tag{2.47}$$

(oxidation)

$$Cr^{III}O_x^{(2x-3)-}{}_{(melt)} + \left(z - x + \frac{1}{2}\right)O^{2-}{}_{(melt)} \Leftrightarrow Cr^{II}O_z^{(2z-2)-}{}_{(melt)} + \frac{1}{4}O_{2(gas)} \tag{2.48}$$

(reduction)

The behaviour of chromium in the melts is complicated due to the volatility of Cr^{VI} species which normally occurs for a system exposed to oxidising atmosphere (air) where Cr^{VI} is known to be stable[55,100]. This observation may occur due to the volatilisation of Cr^{VI} from the melts in the form of $CrO_{3(g)}$[101]. At T > 1000 ^oC, the volatilisation of Cr^{VI} may occur by the direct oxidation of Cr_2O_3 grains (Eq. 2.49) or by the volatilisation of the Cr^{VI} oxocomplex in the melts (Eq. 2.50)[102].

$$Cr_2O_{3(crystal)} + \frac{3}{2}O_{2(gas)} \Leftrightarrow 2CrO_{3(gas)} \quad (2.49)$$

$$2Cr^{VI}O_y^{(2y-6)-}{}_{(melt)} \Leftrightarrow 2CrO_{3(gas)} + (2y-6)O^{2-}{}_{(melt)} \quad (2.50)$$

The solubility of Cr_2O_3 in soda silicate melts has been determined in binary, ternary and industrial glasses by Abdelouhab[98] for different temperatures ($1050^oC \leq T \leq 1250^oC$) under different partial pressures of oxygen which have been imposed by air, CO_2, CO_2 99.21% + CO 0.79% and CO_2 95% + CO 5%. The results on the binary glasses (Na_2O-$xSiO_2$) under oxidising conditions (air) show that the variation of Na_2O leads to either a basic fluxing (basic dissolution) or acid fluxing (acidic dissolution). In the case of basic fluxing, an increase in the total dissolved Cr in the melts is due to an increase of the Cr^{VI} species. For acid fluxing, Cr^{III} species is the predominant species and an increase in the total dissolved Cr is due to an increase of the dissolution of Cr^{III} species in the melts. However, under reducing conditions, the concentration of Cr^{VI} species decreases and Cr^{III} species is stabilised here. The solubility of Cr^{III} seems to possess low dependency on the melt basicity[98]. Furthermore, the study[98] also reveals that the Cr_2O_3 solubility depends on the melt compositions, melt structure and the valence state of the dissolved Cr in the molten glasses.

The works have been continued thoroughly by Khedim *et al.*[11,99,103,104] for different temperatures ($1125^oC \leq T \leq 1250^oC$), glass compositions ($Na_2O$-$xSiO_2$; $1.5 \leq x \leq 3$) and oxygen fugacities ($-15 < \log fO_2 < -0.61$). In this study, a closed-system[105] has been used in order to control the parameters (temperature, glass compositions and oxygen fugacity) imposed on the samples which will be described

thoroughly in Chapter 3. The Cr solubility as a function of oxygen fugacity (log fO_2) for four different compositions at T = 1125°C has been shown in Figure 2.14. The results reveal the dependence of Cr solubility on the fO_2 and melt compositions as well. The shape of the curves which reveal three significant domains of Cr solubility which is supported by the schematic in Figure 2.13 and Eq. 2.46 - 2.48 verifies the existence of three Cr species (Cr^{II}, Cr^{III} and Cr^{VI}) in the melts.

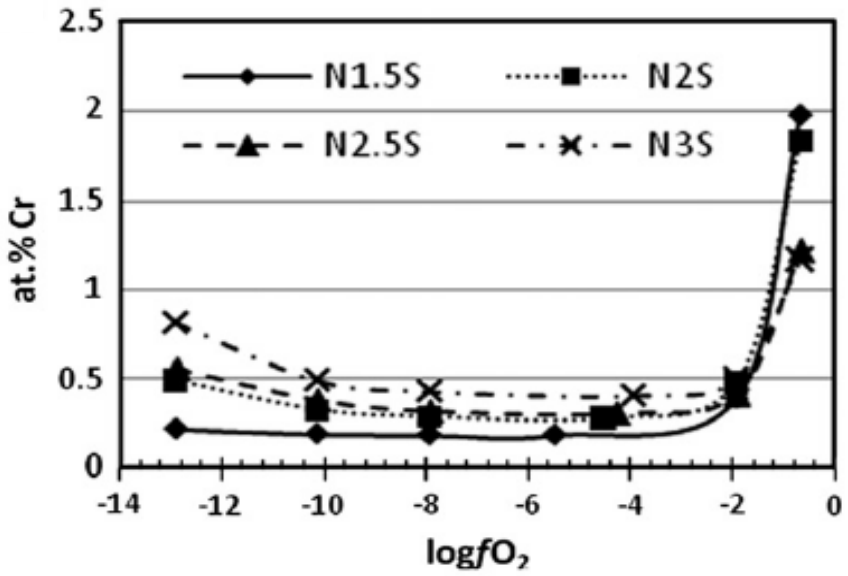

Figure 2.14: Total Cr contents reported as a function of log fO_2 for four different glass compositions at 1125°C[11]

As a consequence, Khedim *et al.*[11,99,103,104] have made an effort in order to quantify the contribution of each chromium species (Cr^{II}, Cr^{III} and Cr^{VI}) in the binary melts by using a model describing the chromium chemistry in the melts involving dissolution, redox and oxocomplex reactions. By considering Eq. 2.46 - 2.48, the equilibrium constants for dissolution (K_{diss}), oxidation (K_{ox}) and reduction (K_{red}) reactions can be written as:

$$K_{diss} = a[Cr^{III}]a[O^{2-}]^{\left(\frac{3}{2}-x\right)} \tag{2.51}$$

$$K_{ox} = \frac{a[Cr^{VI}]a[O^{2-}]^{\left(x-y+\frac{3}{2}\right)}}{a[Cr^{III}]fO_2{}^{3/4}} \tag{2.52}$$

$$K_{red} = \frac{a[Cr^{II}]fO_2{}^{1/4}}{a[Cr^{III}]a[O^{2-}]^{\left(z-x+\frac{1}{2}\right)}} \tag{2.53}$$

where $a_i = \gamma_i X_i$ and a_i is the activity, γ_i is the activity coefficient and X_i is the molar fraction of species *i*. In glass melts, the content of polyvalent ions is generally very low. Hence, in conformity with Henry's law, the activity can be equated to the concentration and thus the preceding equations can be developed to:

$$log[Cr^{III}] = logK_{diss} + \left(x - \frac{3}{2}\right)a(O^{2-}) \tag{2.54}$$

$$log\frac{[Cr^{VI}]}{[Cr^{III}]} = \frac{3}{4}logfO_2 - \left(x - y + \frac{3}{2}\right)loga[O^{2-}] + logK_{ox} \tag{2.55}$$

$$log\frac{[Cr^{II}]}{[Cr^{III}]} = -\frac{1}{4}logfO_2 + \left(z - x + \frac{1}{2}\right)loga[O^{2-}] + logK_{ox} \tag{2.56}$$

For a given oxygen fugacity and glass composition, Eq. 2.54 - 2.56 can be written as:

$$log[Cr^{III}] = A \tag{2.57}$$

$$log\frac{[Cr^{VI}]}{[Cr^{III}]} = \frac{3}{4}logfO_2 + B \tag{2.58}$$

$$log\frac{[Cr^{II}]}{[Cr^{III}]} = -\frac{1}{4}logfO_2 + C \tag{2.59}$$

where

$$A = logK_{diss} + \left(x - \frac{3}{2}\right)a(O^{2-}) \tag{2.60}$$

$$B = -\left(x - y + \frac{3}{2}\right)loga[O^{2-}] + logK_{ox} \tag{2.61}$$

$$C = \left(z - x + \frac{1}{2}\right)loga[O^{2-}] + logK_{ox} \tag{2.62}$$

The above equations allow an access to the log redox as a function of oxygen fugacity as has been illustrated by Khedim *et al.*[11] in Figure 2.15. The plots show a good agreement between the theoretical equations (Eq. 2.58 and 2.59) where the slopes obtained under oxidising and reducing conditions are 0.75 and -0.25 respectively. One may conclude that the above equations seem to work well in the case of soda silicate melts.

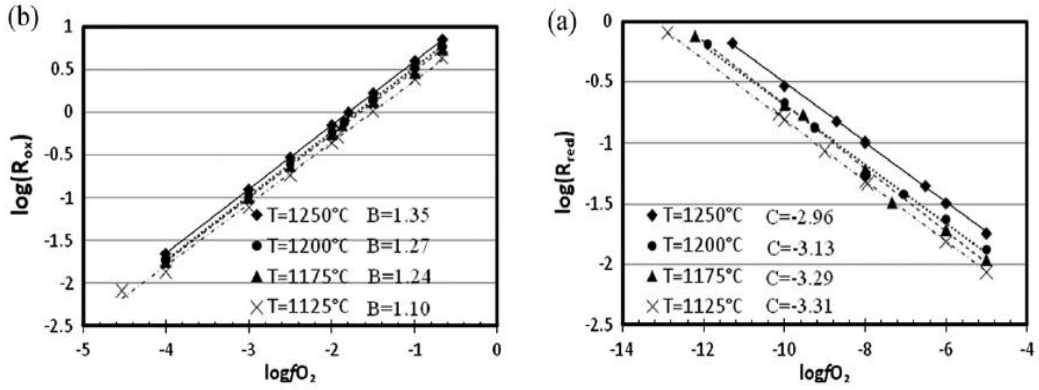

Figure 2.15: Plots of log (R_{red}) (a) and log (R_{ox}) (b) determined in the Na_2O-$2SiO_2$ system as a function of log fO_2 for different temperatures. The obtained equations of the lines are in agreement with the theoretical equations: log (R_{red}) = -0.25 log fO_2 + C and log (R_{ox}) = 0.75 log fO_2 + C for reducing and oxidising conditions respectively[11]

The treatment of the results also allows the determination of the physicochemical properties of chromium species in melts (chromium complex formulas) as well as thermodynamic properties (entropies and enthalpies) related to the dissolution, reduction and oxidation processes of chromium oxide in binary melts[11,99,103,104].

Summary

Glass possesses a unique and complex structure which is attributed to the specific roles played by the components in the glass. As in the aqueous media, the acid-base properties show a profound influence on the corrosion of metal/alloys by molten glass. As a consequence, a large number of studies have been devoted to theoretically as well as experimentally determine the basicity/acidity of the glass. The molten glass which behaves like a solvent also allows the redox reactions to take place in it. The coupling of acid-base properties and redox reactions results in the corrosion of metals/alloys in molten glass. The corrosion of the metal/alloys in the

melts can be characterised by an electrochemical technique and also a thickness loss measurement. Since the corrosion of the metals/alloys in the melts depends on the stability of the protective layer formed at the interface, many works have been performed on the determination of the solubility of some important oxides in molten glass. Furthermore, the physicochemical behaviour of the Cr_2O_3 in binary melts is also demonstrated thoroughly in this chapter.

The information that has been compiled in this chapter has led to the development of the present works in this thesis:

- The works will be focused on the corrosion behaviour of pure Cr as well as chromia and alumina forming alloys in molten glasses. An electrochemical technique and thickness loss measurement will be used herein in order to characterise the corrosion of the metal/alloys in the melts.
- The study will be extended on the kinetics and thermodynamic properties of the Cr_2O_3 in the ternary system which is soda-lime silicate melts.

CHAPTER 3

MATERIALS AND EXPERIMENTAL METHODS

Introduction

The first part of this chapter deals with the preparation of the raw materials used in this study which are pure chromium, Ni-based alloys and the glasses. The characterisation results of the raw materials are included in Appendices. The second part involves the experimental methods used to study the corrosion of pure chromium and Ni-based alloys in molten glasses. The procedure for the study on the solubility of Cr_2O_3 in silicate glasses has been also explained in this part. Finally, the metallographic preparation and the different techniques used to characterise the samples have been focused.

3.1. Raw materials

3.1.1. Metal and alloys

3.1.1.1. Pure chromium

The pure chromium rods were supplied by GoodFellow (Ø = 5.0 mm, purity = 99.7%). The rods were cut into 2 cm of length and were polished with SiC abrasive paper grit 1200 on the cutting plane of the rods before being used as an electrode.

3.1.1.2. Ni-based alloys

The alloys used in this study are Ni-30Cr (wt.%), Ni-8Al-28Cr (wt.%) and NiAl. The alloys were prepared using two different techniques which are high frequency induction melting and pack cementation.

(a) High frequency induction melting

High frequency induction melting was used to prepare Ni-30Cr, Ni-8Al-28Cr, Ni rods (for producing cemented NiAl) and NiAl (bulk). The raw materials used are listed in Table 3.1.

Table 3.1: The elements used as starting materials

Elements	Purity	Supplier
Ni	99.5%	Alfa Aesar
Al	99.9%	Alfa Aesar
Cr	99.5%	Alfa Aesar

The required amounts of the metallic elements were weighed and were placed in an induction furnace. The fusion took place in a copper crucible with an enclosed silica tube (Figure 3.1) under argon atmosphere. The generator can provide the power of 50 kW that allows the melting of more refractory elements (*e.g.* chromium). In order to have a rod shape, a silica tube with Ø = 6 mm and h ~ 30 cm was attached to the pumping system of the furnace. This silica tube was immersed in molten alloy and the pressure was carefully controlled while sucking the alloy into the tube.

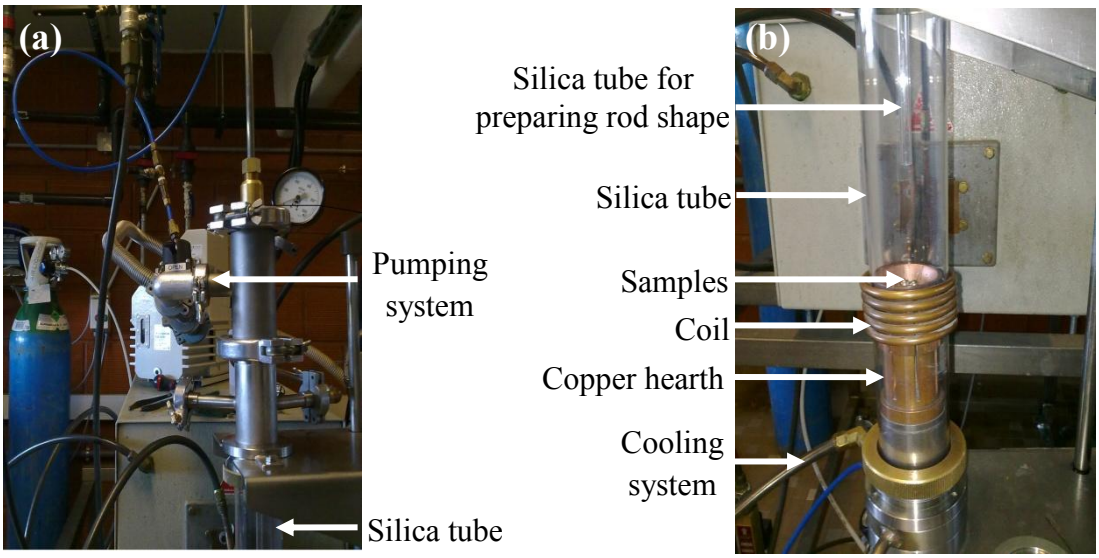

Figure 3.1: High frequency induction system. (a) upper part (b) lower part

After the synthesis, the alloy rods were cut into pieces before being subjected to the annealing process at T = 1200^{o}C for 24 h in order to have a homogeneous microstructure. The heat treatment was performed in a silica tube which was sealed under secondary vacuum.

In the case of NiAl which will be used for 'raw immersion' test, the metallic elements were just mixed and heated in the induction furnace in order to form a bulk NiAl. It is noteworthy that a rod shape is difficult to be formed due to the exothermic reaction between Ni and Al which is very high and difficult to control. This alloy will be noted hereafter as NiAl (bulk). The NiAl (bulk) was then cut into pieces with the thickness of ~ 1.5 mm. The characterisation of the prepared alloys by using this technique is detailed in Appendix A.

(b) Pack cementation technique

The NiAl (rod) alloy was not prepared by high frequency induction melting since the reaction between Ni and Al is very exothermic and the heat of the reaction is difficult to control, thereby making it difficult to have a rod shaped alloy. As a consequence, pack cementation process which is a type of chemical vapour deposition (CVD) was used to produce the NiAl coating on the Ni rod.

The fundamentals and parameters for this aluminising process were discussed precisely by several authors[106–108]. The Ni rod (which was produced by high frequency induction melting) with Ø = 5 mm and length ~ 2.5 cm was immersed in a mixture of powders which is called cement (Figure 3.2). The cement consists of 40% of master alloy (Ni_2Al_3) which provides the element (or elements) to deposit, 60% of inert filler (Al_2O_3) to avoid sintering of the cement and ~ 20 mg (this quantity is sufficient to limit the pressure to 1 bar inside the silica tube with 15 cm^3 of volume at high temperature during the deposition process) of halide activator ($CrCl_3$) which transports the master alloy in gas phase. All the elements were sealed in a silica tube and were subjected to the heat treatment at T = 1000°C for 16 h. The characterisation of the prepared NiAl alloy by using this technique is shown in Appendix B.

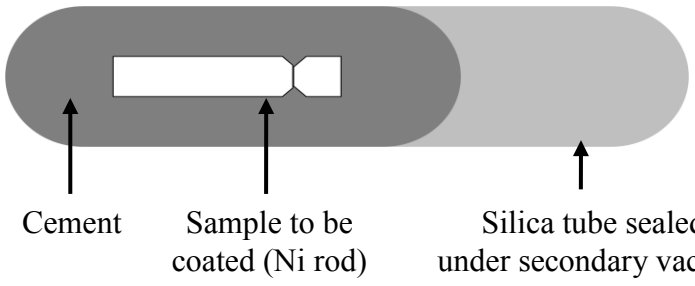

Figure 3.2: Schematic of pack cementation which was performed in a silica tube

3.1.2. Glass synthesis

Bulk amounts of homogeneous soda lime silicate glasses were prepared by mixing an appropriate amount of reagent-grade of powders as listed in Table 3.2:

Table 3.2: The powders used as starting materials

Elements	Purity	Supplier
Na_2CO_3	99.5%	Chempur
$CaCO_3$	99.0%	Chempur
SiO_2	99.9%	Chempur

100 g - 130 g of glass were produced per cycle in a muffle furnace (Nabertherm HFL 16/17). After being mechanically mixed, the batch was melted in a Pt-10% Rh crucible (Ø = 120 mm, h = 130 mm, thickness = 2 mm) which possesses a greater hardness and higher strength than other platinum alloys. Moreover, it is capable of maintaining its shape at very high temperature. Not more than one third of the crucible was filled up with the powders in order to avoid the overflow of the batch during the heat treatment.

The batch was heated up slowly to 1200^{o}C (4^{o}C/min) in order to avoid the overflow of the batch from the crucible during the decomposition of calcium carbonate. It was then maintained at 1200°C for 1 h. After that the temperature of the furnace was increased up to 1500^{o}C (10^{o}C/min) and the batch was subjected to this temperature for 2 h in order to ensure a complete melting of the mixture. The melt was then held at 1300°C (10^{o}C/min) for 10 h for the refining process. Finally, the melt was rapidly quenched in air at T = 1300^{o}C in order to avoid any crystallisation phenomenon. In order to facilitate the removal of the obtained glass from the crucible, the quenching process took place in several steps. After few seconds in air,

the crucible was quenched in water in order to induce thermal shock for breaking the glass. However, a precaution was taken while handling the water quenching for a hygroscopic glass (glass with high Na content) in order to avoid a contact between the hygroscopic glass with water.

The glass compositions were systematically checked by Electron Probe Micro Analysis (EPMA) and are reported in Table 3.3. The glasses that are supplied by Cerfav (Centre Européen de Recherches et de Formation aux Arts Verries) are also listed in Table 3.3. The resulting glasses which were analysed by EPMA show no significant deviation from the theoretical compositions except in the case of the glasses supplied by Cerfav. Since the glasses were prepared by Cerfav in such a big quantity, the compositions of the resulting glasses might not be as accurate as the glasses that were prepared in the laboratory.

Table 3.3: Chemical compositions (theoretical and experimental in wt.%) of soda-lime silicate glasses used in this study

Glass compositions	Theoretical (wt.%)			Experimental (wt.%)			Experimental (at.%)		
	Na_2O	CaO	SiO_2	Na_2O	CaO	SiO_2	Na/2Ca	Si/Ca	2Si/Na
Na_2O-CaO-3SiO_2 (NC3S)	20.78	18.80	60.42	20.68 (0.16)	18.36 (0.30)	60.80 (0.32)	1.02 (0.02)	3.09 (0.04)	3.03 (0.02)
Na_2O-CaO-4SiO_2 (NC4S)	17.29	15.65	67.06	17.11 (0.19)	14.83 (0.15)	65.69 (0.50)	1.04 (0.02)	4.14 (0.06)	3.96 (0.03)
Na_2O-CaO-5SiO_2 (NC5S)	14.81	13.40	71.79	14.84 (0.19)	13.35 (0.60)	71.33 (0.73)	1.01 (0.04)	5.00 (0.28)	4.96 (0.10)
Na_2O-CaO-6SiO_2 (NC6S)	12.95	11.72	75.33	12.95 (0.17)	11.62 (0.20)	75.31 (0.28)	0.98 (0.02)	5.98 (0.08)	6.07 (0.06)
1.5Na_2O-0.5CaO-6SiO_2 (0.5C)	19.31	5.82	74.87	19.41 (0.23)	6.52 (0.14)	72.96 (0.27)	2.69 (0.07)	10.45 (0.25)	3.88 (0.05)
Na_2O-CaO-3SiO_2 (NC3S) - Cerfav	20.78	18.80	60.42	20.10 (0.16)	16.94 (0.22)	60.00 (0.27)	1.07 (0.02)	3.31 (0.05)	3.08 (0.02)
Na_2O-CaO-6SiO_2 (NC6S) - Cerfav	12.95	11.72	75.33	12.86 (0.15)	12.05 (0.19)	72.44 (0.35)	0.96 (0.02)	5.61 (0.11)	5.81 (0.07)
Na_2O-2SiO_2 (N2S) - Cerfav	34.03	/	65.97	31.37 (0.29)	/	69.48 (0.48)	/	/	2.29 (0.03)

* The values in ( ) represent the standard deviations

For the glass synthesis, the chosen quenching temperature is a critical requirement in order to form a homogeneous glass. In this present work, the quenching process was performed at 1300^{o}C for all compositions of the glasses. Previous experiments have indeed shown that lower quenching temperatures lead to the formation of precipitates in the glasses, specifically in NC3S. The characterisation of these glass precipitates is detailed in Appendix C.

3.2. Experimental procedures

3.2.1. Corrosion by molten glasses

3.2.1.1. Preparation of electrodes

Three different types of electrodes were used in this technique which are the reference, counter and working electrodes. All electrodes were fabricated by using specific materials and particular methods in order to withstand high temperatures for a long run duration.

(a) Reference electrode

Reference electrode is an electrode which has a constant electrochemical potential. In this work, a self-constructed yttria stabilised zirconia (YSZ) was used as a reference electrode due to its stability at high temperatures. It has been used and established in this laboratory since many years ago. The zirconia (ZrO_2) with an addition of yttria (Y_2O_3) possesses a good resistance at a wide range of temperatures. It is chemically inert in the molten glass and also a good ionic conductor of O^{2-} ions. The ability to conduct O^{2-} ions makes yttria stabilised zirconia well suited to be used as a reference electrode based on the redox couple O_2/O^{2-}. The electrode (Figure 3.3) consists of a twin holes mullite tube (6) with a platinum wire which was introduced into one of the holes. The platinum wire (7) was connected with the molten glass by the YSZ stick (1) (Ø = 5 mm, length ~ 2.5 cm). Platinum ink (4) was used in order to enhance the ceramic-platinum contact. All the different elements were sealed by zirconia-based cement (2) (supplied by Final Advanced Materials) and were mechanically fixed to the outer mullite tube (5) by introducing a small alumina stick

(3) as shown in Figure 3.3(b). This alumina stick could avoid the YSZ stick from dropping into the molten glass if the cement failed. The electrode was flushed with air (P_{O_2} = 0.21 atm) as a reference gas which was introduced with a syringe needle into another hole of the inner mullite tube.

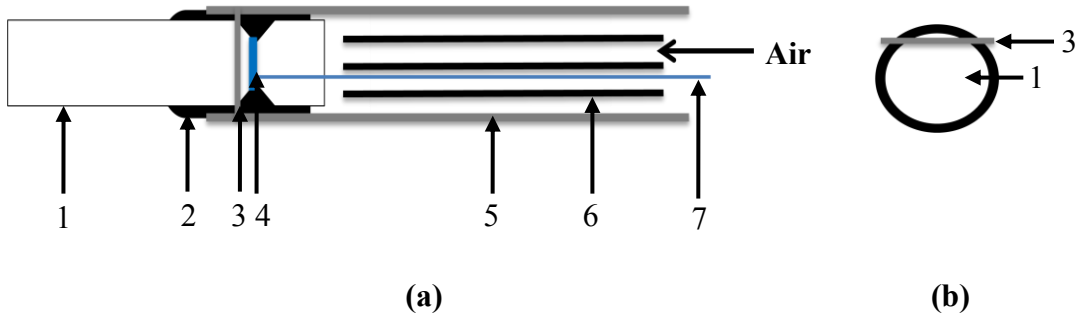

Figure 3.3: Reference electrode (yttria-stabilised zirconia electrode) used in the electrochemical study (a) side view (b) top view

1: YSZ stick
2: Zirconia cement
3: Alumina stick
4: Platinum ink
5: Outer mullite tube
6: Inner mullite tube
7: Platinum wire (Ø = 0.5 mm)

The yttria stabilised zirconia reference electrode is a reversible electrode which possesses the following reaction:

$$O^{2-} \Leftrightarrow \tfrac{1}{2} O_{2(g)} + 2e^{-} \qquad (3.1)$$

The potential of the electrode is equivalent to the total of the interface potentials of Pt/zirconia (α/β) and zirconia/glass (β/γ) (Figure 3.4):

Pt	Yttria stabilised zirconia	Glass
(α)	(β)	(γ)

Figure 3.4: Schematic of the interfaces of platinum, zirconia and molten glass

At the air/zirconia interface, the potential, E^R of the electrochemical reaction can be described as:

$$\tfrac{1}{2} O_2(g) + 2e^-_{(\alpha)} \Leftrightarrow O^{2-}_{(\beta)} \tag{3.2}$$

$$\Delta G_R = -nFE^R \tag{3.3}$$

$$E^R = \frac{\left(\mu_{O_2(g)} - \mu_{O^{2-}_{(\beta)}}\right)}{2F} \tag{3.4}$$

where $\mu_{O^{2-}_{(\beta)}} = RT \ln a(O^{2-})$ is the chemical potential of O^{2-} ion in the β phase, $\mu_{O_2(g)} = \frac{RT}{2} \ln P_{O_2(g)}$ is the chemical potential of oxygen in the gas phase, F is the Faraday constant (F = 96500 C/mol) and ΔG_R is the Gibbs free energy of the reaction. At the zirconia/glass interface, the junction potential, E^j of the reaction can be described as:

$$E^j = \frac{1}{F} \sum_{i=1}^{n} \int_{\gamma}^{\beta} \frac{t_i}{Z_i} d\mu_i \tag{3.5}$$

where t_i is transport number of species i (t_i = 1), Z_i is the charge of species i (Z_i = 2) and n is the number of species which diffuse (n = 1).

$$E^j = \frac{1}{2F}\left(\mu_{O^{2-}_{(\beta)}} - \mu_{O^{2-}_{(\gamma)}}\right) \tag{3.6}$$

where $\mu_{O^{2-}_{(\gamma)}} = RT \ln a(O^{2-})_{\gamma}$ is the chemical potential of O^{2-} ions in the γ phase.

The total:

$$E = E^R + E^j = \frac{1}{2F}\left(\mu_{O_2(g)} - \mu_{O^{2-}_{(\gamma)}}\right) = \frac{1}{2F}\left(\frac{1}{2}RT\ln P_{O_2(g)} - RT\ln a\left(O^{2-}\right)_\gamma\right)$$

$$= \frac{RT}{4F}\ln P_{O_2(g)} - \frac{RT}{2F}\ln a\left(O^{2-}\right)_\gamma \qquad (3.7)$$

Therefore, the potential of the electrode is constant for a given glass composition ($a(O^{2-})_\gamma$ = constant) and P_{O_2}. Since the P_{O_2} was systematically fixed to 0.21 atm (air atmosphere), this electrode has a constant potential for a given glass composition.

(b) Counter electrode

Counter electrode is a current-carrying electrode that completes the cell circuit. It consists of a platinum plate with length of ~ 2.5 cm and width ~ 1.4 cm (1) (Figure 3.5). The platinum plate and the platinum wire (5) were welded by Soudax Equipment SD100 in order to ensure the connectivity in the system. All the elements were sealed with silico-aluminous cement (supplied by final advanced materials) (2).

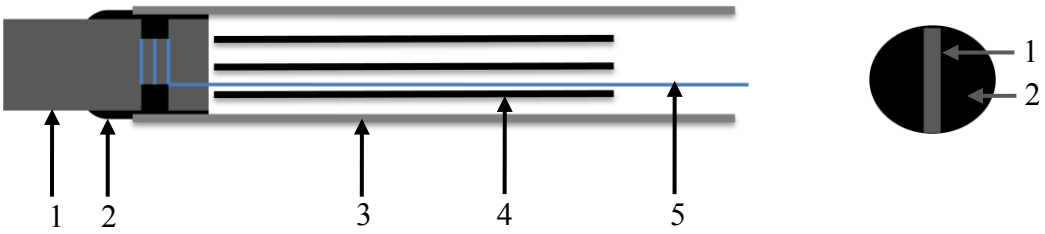

Figure 3.5: Schematic of a counter electrode (a) side view (b) top view

1: Platinum plate
2: Silico-aluminous cement
3: Outer mullite tube
4: Inner mullite tube
5: Platinum wire (Ø = 0.5 mm)

(c) Working electrodes

Working electrode is an electrode on which the reaction of interest is occurring. There are two types of working electrodes which were used in this study.

➢ *Electrochemical characterisation of the molten glasses*

The working electrode which was used for the characterisation of electroactivity domain of the studied molten glasses has to be chemically inert. Therefore it was composed of a platinum wire with diameter of 1 mm and length of ~2.5 cm (1) (Figure 3.6). This platinum wire was welded to a smaller platinum wire (5) (Ø = 0.5 mm) by Soudax Equipments SD100. Finally the elements were sealed with silico-aluminous cement (2) in order to avoid the contact of the platinum wire with the air/glass interface.

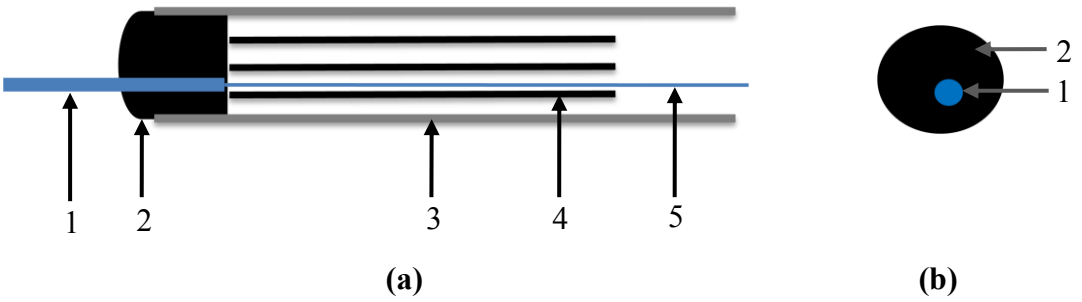

Figure 3.6: Schematic of a working electrode for an electrochemical characterisation of molten glasses (a) side view (b) top view

1: Platinum wire (Ø = 1 mm)
2: Silico-aluminous cement
3: Outer mullite tube
4: Inner mullite tube
5: Platinum wire (Ø = 0.5 mm)

➢ *Corrosion characterisation of pure chromium and Ni-based alloys by molten glasses*

The electrode was composed of pure chromium (99.7%, GoodFellow) and Ni-based alloy rods (prepared by high frequency induction melting and pack cementation techniques) with diameter = 5 mm and length of ~ 2.5 cm (Figure 3.7). The contact between the platinum wire and the metals was secured by performing a spot welding. All the elements were sealed with silico-aluminous cement.

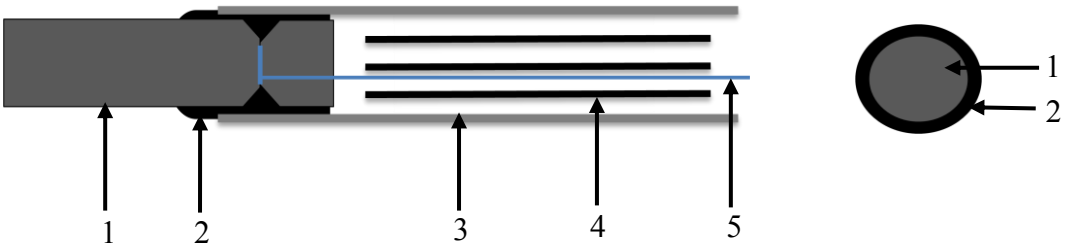

Figure 3.7: Schematic of a working electrode for the corrosion characterisation of metal and alloys (a) side view (b) top view

1: Pure chromium/alloys
2: Silico-aluminous cement
3: Outer mullite tube
4: Inner mullite tube
5: Platinum wire (Ø = 0.5 mm)

3.2.1.2. Elelctrochemical measurements

The experiments on the electrochemistry were performed by using an apparatus as shown in the Figure 3.8. The measurements were realised by a Potentiostat/Galvanostat model 263A which is equipped with the software of corrosion EG&G Perkin Elmer M352 and M270. A quantity of 1.3 kg of glass (6) was placed in a clay crucible (5). A clay crucible was used in this study instead of a

platinum crucible due to the fact that the reduction of SiO_4^{4-} to Si^0 will lead to a formation of eutectic Pt-Si with low melting point which is responsible for the platinum degradation. In order to avoid any leak from the molten glass that could damage the furnace, the crucible was put in another clay crucible which has a bigger dimension. These crucibles were supported in Carbolite HTF 17/10 furnace (4) by a refractory cement which is known as 'Zircoram' (80% Cr_2O_3, 20% ZrO_2) (7). Before starting the electrochemical measurements, the glass was annealed at 1200°C (10°C/min) for 2 h in order to ensure a complete melting of the glass and also to remove the bubbles that could interfere with the electrochemical signals.

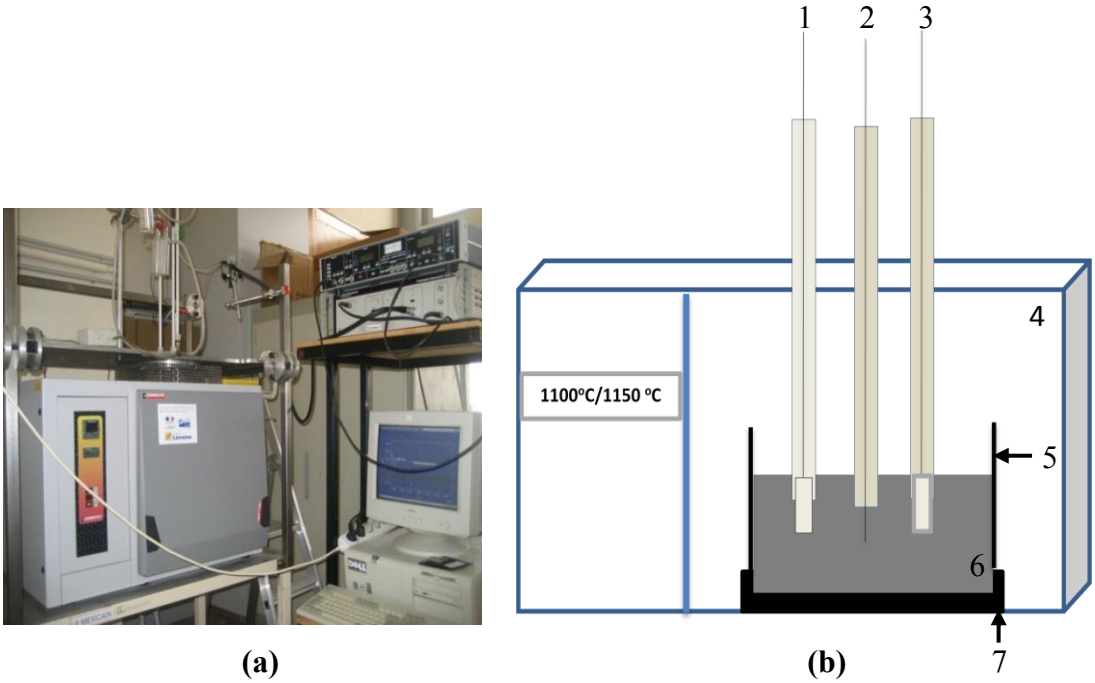

Figure 3.8: Apparatus used for an electrochemical measurements at high temperatures (a) full overview (b) schematic of the furnace and electrodes

All the electrodes (reference elecrode (1), working electrode (2) and counter electrode (3)) were placed in the furnace through the specific holes at the top of the furnace. Since there is a possibility that the performance of the electrodes might fail,

normally 2-3 set of counter and reference electrodes were installed in the furnace along with the working electrode. The first consideration while positioning the relative location of the electrodes is to minimize the solution resistance by keeping the tips of the three electrodes as close as possible especially for the working electrode and the reference electrode, while not interferring the current path between one another. The solution resistance between these electrodes causes an ohmic (iR) drop that leads to an error in the measured potential difference between them.

The working and counter electrodes were totally immersed in the molten glass in order to avoid the presence of triple point contact between the molten glass, the atmosphere and the electrodes. The existence of this triple point could cause a perturbation of cathodic curve according to the following equation:

$$O_{2(atm)} + 4e^{-} \Leftrightarrow 2O^{2-}_{(glass)} \tag{3.8}$$

After the experiment, the working electrode was lifted up from the glass melt for few seconds before being quenched in air. In order to preserve the glass surrounding the sample which might detach from the metal/alloy during the polishing process, a heat shrinkable tube was applied on the sample a few seconds after the quenching. Finally the sample was embedded in the resin for the metallographic preparation as shown in Figure 3.9.

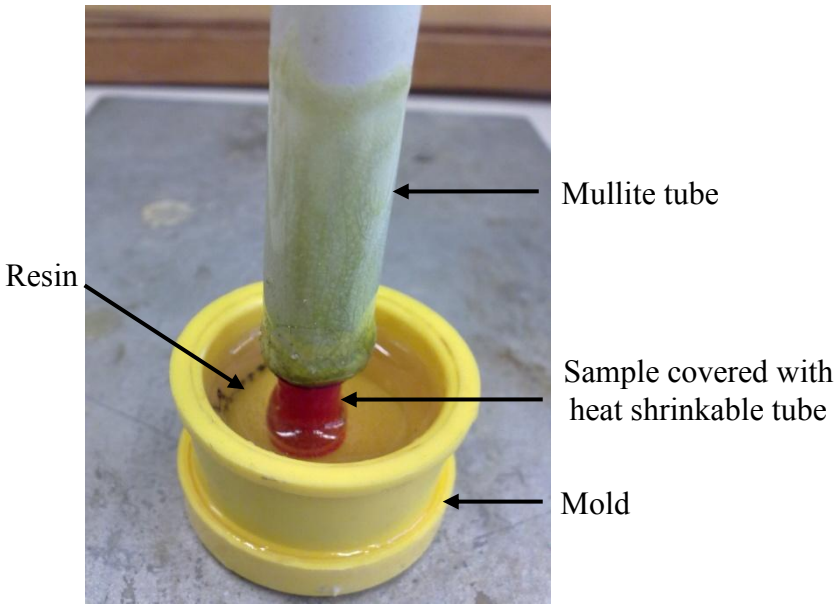

Figure 3.9: The sample embedded in resin for metallographic preparation

(a) Electrochemical characterisation of the glass

Before the corrosion behaviour of the pure chromium and Ni-based alloys could be characterised, it is necessary to study the electrochemical behaviour of the molten glass itself. The platinum working electrode which was used in this work is inert, so the electrochemical signals gave the direct indicative of the characteristic of the molten glass at the given experimental temperature. The polarisation curve of the Pt working electrode was plotted by first polarising the anodic field from free potential to +600 mV. After that the cathodic field was polarised from the free potential to -1300 mV. These two polarisations were carried out at a scan rate of 1 mV/s.

(b) Corrosion of pure chromium and Ni-based alloys by molten glass

The characterisation of different materials was performed by the conventional electrochemical methods which have been established for aqueous corrosion *i.e.*

measurement of polarisation resistance (Rp) by the Stern-Geary method and tracing of the potential-current curve.

➢ *Measurement of the polarisation resistance and calculation of the corrosion rate*

The measurement of the polarisation resistance was performed by polarising the working electrode from -10 mV to +10 mV around the corrosion potential (E_{corr}) with a scan rate of 600 mV/h. The corresponding current allows the potential-current curve of this domain to be plotted, hence leading to the determination of the slope (1/Rp) according to the following equation:

$$\frac{1}{Rp} = \frac{di}{dE} \text{ at } E = E_{corr} \tag{3.9}$$

By taking into account the number of electrons involve in the anodic and cathodic reactions, the kinetic constants, β_a and β_c could be obtained by the following equations:

$$\beta_a = \frac{2.3RT}{\alpha_a nF} \tag{3.10}$$

$$\beta_c = \frac{2.3RT}{\alpha_c nF} \tag{3.11}$$

with R is the gas constant (8.31 J/mol.K), T is the temperature in Kelvin, α_a is the transfer coefficient of the anodic reaction, α_c is the transfer coefficient of the cathodic reaction, n is the number of electron involved and F is the Faraday constant (96500 C/mol). The Stern-Geary relation leads to the derivation of the corrosion current according to the following equation:

$$I_{corr} = \frac{\beta a \beta c}{2.3(\beta a + \beta c)} \times \frac{1}{Rp} = \frac{B}{Rp} \quad (3.12)$$

Finally the corrosion rate could be determined by the Faraday law:

$$V_{corr} = \frac{I_{corr} tM}{n\rho F} \quad (3.13)$$

where I_{corr} is the corrosion current density (A/cm^2), t is the time in s, M is the average molecular weight of the alloy (g/mol), n is the number of electron involved, ρ is the average density of the alloy (g/cm^3) and F is the Faraday constant (96500 C/mol).

- *Potential-current curve*

The anodic potential-current curve was plotted from the equilibrium potential up to 0.5 V with a scan rate 1 mV/s. This method is destructive since it modifies the spontaneous behaviour of the surface of the materials.

3.2.1.3. 'Raw immersion' technique

A 'raw immersion' experiment was always coupled with the electrochemical measurement since the latter technique will modify the spontaneous behaviour of the surface of the studied material when the potential is polarised. This technique was performed in order to predict the real corrosion mechanism at the interface of the alloys without the interference from any destructive method. A raw immersion technique was performed on the Ni-30Cr rod, Ni-8Al-28Cr rod and NiAl plate (bulk) which were prepared by using high induction melting. The schematic of the device was illustrated in Figure 3.10. The alloys with rod/plate shape were sealed in a mullite tube (Ø = 10 mm) with silico-aluminuos cement. The alloy which was

embedded in the mullite tube was suspended in the molten glass thank to a smaller mullite tube (Ø = 4 mm) which was joined horizontally to the system with silico-aluminous cement.

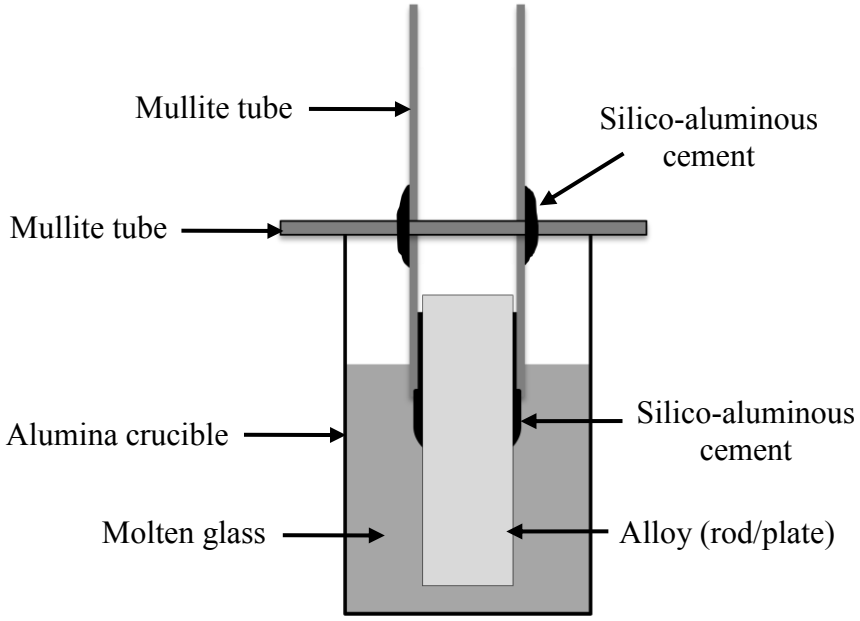

Figure 3.10: Schematic of the 'raw immersion' technique performed on the alloys

A sufficient amount of glass was filled up in an alumina crucible. Before immersing the alloy, the glass was annealed at 1200^{o}C for ~15 min in order to ensure a complete melting of the glass. The alloy was then immersed in the molten glass depending on the experimental conditions. Finally, the metal/alloy was then quenched in air. A heat shrinkable tube was also applied on the sample in order to preserve the glass surrounding of the metal/alloy.

3.2.1.4. Thickness loss measurement

The diameter or the thickness of every sample before and after the corrosion tests was determined by using micrometer (type Palmer) and also by stereo microscope ZEISS Stemi 2000-C (SIP 50147) which is equipped with a digital camera AxioCam ICc 1. This microscope is operated with AxioVision 4 software.

3.2.2. Solubility of chromia (Cr_2O_3) in molten glasses

3.2.2.1. Glass balls (samples) preparation

The method for the glass balls preparation was already optimised by Khedim[99] in binary melts. Chromium-containing glasses were obtained by mixing 5-10 wt.% Cr_2O_3 with the soda-lime silicate glasses. This sufficient amount of Cr_2O_3 has been chosen in order to be higher than the solubility limit of Cr_2O_3 in the melts. These values have been predicted based on the work which has been performed by Khedim *et al.*[11,99,103,104] on the binary melts. The mixtures were finely grounded, heat-treated at 1200°C in a Pt plate for about 2 minutes and rapidly quenched in air. This procedure was performed two times in order to ensure a good homogeneity of the Cr_2O_3-rich glass. Then, approximately 100 mg of the homogeneous Cr_2O_3-rich glass were melted again in a graphite crucible (Ø = 17 mm, length = 18 mm) at 1200 °C for about 1 minute and rapidly quenched in air. Due to the low wettability between the melt and crucible, the sample formed a spherical shape with an average diameter of 4 mm.

3.2.2.2. Control of the experimental parameters

In order to control the experimental parameters *i.e.* temperature (T), basicity (melt compositions) and oxygen fugacity (fO_2), the experiments were performed in a closed system (Figure 3.11) which was developed in a previous work[105]. The system consists of a sealed silica tube containing several components that impose the thermochemical parameters of this study.

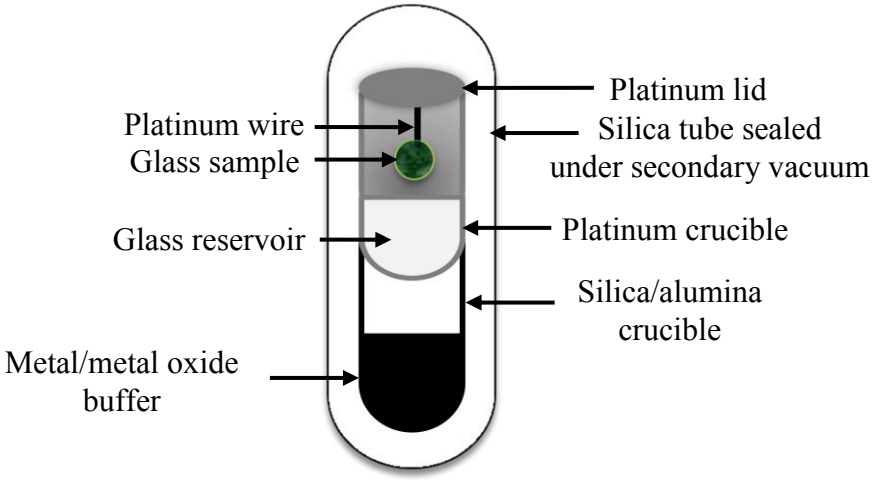

Figure 3.11: Schematic of a closed system which allows the control of the different experimental parameters (temperature, basicity (melt composition) and oxygen fugacity (fO_2) simultaneously

The Cr_2O_3-rich glass ball with the required composition was suspended on a loop of platinum wire. In order to minimize the Na volatilisation from the sample, Na vapour partial pressure was imposed around the sample by adding a platinum crucible (Ø = 16 mm, length = 35 mm) containing a glass which has the same composition as the sample. The amount of the glass should be sufficient to buffer the sample that corresponds to (the glass should occupy at least one third of the platinum crucible) approximately 4 g of glass. The volatilisation of the alkali oxide from the reservoir occurs according to the following equation:

$$Na_2O_{1/2(reservoir)} \rightarrow Na_{(g)} + \frac{1}{4}O_{2(g)} \quad (3.14)$$

The alkali vapour will dissolve in the sample (glass ball) by the condensation process according to Eq. 3.15:

$$Na_{(g)} + \frac{1}{4}O_{2(g)} \rightarrow Na_2O_{(sample)} \quad (3.15)$$

At the thermodynamic equilibrium, the activity of alkali oxide is fixed by the glass reservoir according to Eq. 3.16:

$$aNa_2O_{(reservoir)} = aNa_2O_{(sample)} \quad (3.16)$$

The oxygen fugacity (fO_2) of the system was controlled by solid MO_x/MO_y buffers (M = metallic element) which were determined by Ellingham diagram. The values of the equilibrium constants (K) were calculated by using a thermodynamic software (HSC 5.1)[109] by considering the following equations:

$$\frac{2}{y-x}MO_{x(solid)} + O_{2(g)} \Leftrightarrow \frac{2}{y-x}MO_{y(solid)} \quad (3.17)$$

$$K = \frac{1}{fO_2} \quad (3.18)$$

$$\Delta G^o = -RT \ln K = -RT \ln \frac{1}{fO_2} \quad (3.19)$$

The buffers that were used in this study are Fe_3O_4/Fe_2O_3, Cu/Cu_2O, Ni/NiO, Co/CoO, FeO/Fe_3O_4 and Fe/FeO which can impose a wide range of fO_2 ($-12 \leq \log$

$fO_2 \leq -0.6$). The calculated values of fO_2 imposed on the samples as a function of temperature are shown in Figure 3.12.

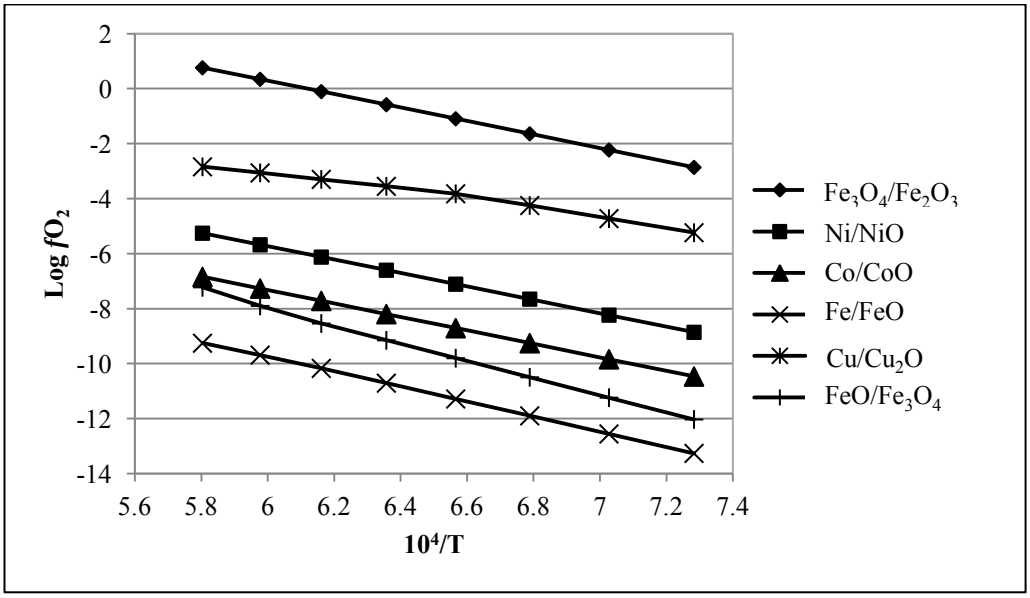

Figure 3.12: The values of fO_2 for the MO_x/MO_y buffers as a function of temperature

About 1 g of the mixture of MO_x/MO_y powder was placed in a silica crucible (Ø = 18 mm, h = 25 mm) or alumina crucible ((Ø = 18 mm, h = 15 mm) depending on the nature of the powders. While imposing the reducing atmosphere with powders containing wüstite (FeO), a precaution was taken by incorporating them into an alumina crucible in order to avoid any reaction of the powders with silica tube which might lead to the formation of undesirable fayalite (Fe_2SiO_4). The oxidising buffer (Fe_3O_4/Fe_2O_3) was imposed on the samples just at T = 1200°C since the fO_2 value for this buffer at T > 1200°C is superiour than the air atmosphere which might cause a dangerous explosion.

All the components were then placed in a silica tube (Ø = 22 mm, length ~120 mm) and were sealed under secondary vacuum (~10^{-6} mbar). The experiment

for oxidising condition (air atmosphere) was performed in the same manner as the other atmospheres except no solid MO_x/MO_y buffers were needed and the silica tube was not sealed under vacuum. A small hole was introduced on the top of the silica tube in order to expose the sample to the oxidising atmosphere (air).

The silica tube containing samples were subjected to the experimental temperatures in a muffle furnace (Nabertherm HT16/16). In order to preserve the redox species in the glass which might change with the atmosphere condition and the temperature, the tube was directly quenched in air right after the heat treatment. The presence of both metal and oxide phases of the buffers was systematically confirmed by X-ray diffraction (XRD) after each experiment in order to ensure that the desired value of fO_2 was effective at high temperatures.

3.3. Sample characterisation

3.3.1. Metallographic preparation

Some of the alloys (*i.e.* samples of isothermal oxidation test) were subjected to the Ni electroplating before being embedded in the cold resin type Epoxy (Escil) in order to preserve the oxide scale at the interface. The samples for corrosion test (*i.e.* alloys in molten glasses) were subjected to the mechanical polishing starting with SiC abrasive paper grit 120 followed by 240, 400, 400, 600, 800, 1200, 2400 and 4000. The finishing process was performed by using colloidal silica on a polishing disk type Magnet Politex. For the alloys which were immersed in soda silicate melt (hygroscopic glass), the dry polishing must be performed by using an oil based lubricant (Kerdane).

The samples containing just soda-lime silicate glasses were polished with the SiC abrasive paper grit 240 until 4000 before completing with diamond suspension (diameter of 1 μm) on a polishing disk type Magnet ST. The hygroscopic glasses (*i.e.* soda silicate) were subjected to the dry polishing (without water).

The non-hygroscopic samples were rinsed with water, cleaned with alcohol in the ultrasonic tank and finally dried in air. For the hygroscopic samples, the water was replaced with absolute ethanol.

3.3.2. Technique of analysis

3.3.2.1. Thermogravimetric analysis (TGA)

The isothermal oxidation behaviour of the alloys was characterised by Thermogravimetry (SETARAM SETSYS). The thermogravimetric analysis of the alloys led to the knowledge of the nature and thickness of the oxides formed during high temperature treatment in air. The cylinder shape samples (Ø = 5 mm, length ~ 5 mm - 7 mm) were suspended in a furnace with a platinum system which was connected to a beam balance. The oxidation tests were performed in aerated atmosphere. All the samples were subjected to the constant heating and cooling rates of 20^{o}C/min and 5^{o}C/min respectively. The characterisation of the oxidised samples as well as the method used for the treatment of the thermogravimetric data were explained in details in Appendix D.

3.3.2.2. X-ray diffraction (XRD) analysis

The X-ray diffraction analysis was performed with a goniometer type Philips X'PERT PRO which operates in the θ-2θ mode. This device is equipped with a copper anticathode ($\lambda K\alpha_1$ = 1.54056 Å), a furnace (HTK 450) which operates in air and a fast detector (X'Celerator). The studied angular domain is in the range of 25° and 140° (in 2θ) with a step of 0.01671°. The phase identification was performed by module EVA with the software of Diffract Plus equipped with JCPDS database.

3.3.2.3. Differential thermal analysis (DTA)

The glass transition, crystallisation and melting temperatures of the glasses were determined by using differential thermal analysis (DTA). The experiment was performed in a simultaneous TG/DTA SETARAM 92-16.08. The sample was heated in air flow up to 1300°C with a rate of 10°C/min. The sample was then cooled down to the ambient temperature at 10°C/min.

3.3.2.4. Optical microscope

The surface of the polished samples was controlled by an optical microscope Polyvar MET (Reichert-Jung) with maximum magnification of 1000x. It is equipped with a CCD DP12 camera which is controlled by AnalySIS (Soft Imaging System) software.

3.3.2.5. Scanning electron microscope (SEM)

The information about the sample's surface topography and composition were obtained by two types of scanning electron microscope (SEM) which are the JEOL JSM-7600F and JEOL JSM 6010LA. JEOL JSM-7600F is equipped with both

energy dispersive spectrometer (EDS) and wavelength dispersive spectrometer (WDS). As a consequence, the qualitative and quantitative analyses could be performed simultaneously. The analyses were performed with an accelerating voltage of 15 kV and beam current of 6 nA. JSM-6610A/6610LA is a high-performance scanning electron microscope for fast characterisation and imaging of fine structures on both small and large samples.

3.3.2.6. Electron probe micro-analysis (EPMA)

The chemical analysis was performed by electron probe micro-analyser (CAMECA SX 100). This equipment is equipped with wavelength dispersive spectrometer (WDS) which provides a better accuracy on quantitative analysis for trace elements.

The analyses on glasses were performed using the spot size of 20 µm in order to minimize the Na loss from the samples whereas focalised analyses could be performed on metal samples. The acceleration voltage and beam current used are 15 kV and 10 nA respectively. The determination of the elements required a calibration of the spectrometers with 'standards' each time before performing the analyses. For the glass analyses, albite ($NaAlSi_3O_8$) was used as a standard for Na and Si whereas andradite ($Ca_3Fe_2Si_3O_{12}$) was used as a standard for Ca. Cr_2O_3 was used to calibrate the element of Cr. The oxygen content was determined by stoichiometry. For the metal analyses, the Ni, Cr and Al were calibrated by using their pure elements while the Cr_2O_3 was used as a standard for oxygen.

CHAPTER 4

CORROSION OF CHROMIA FORMING AND ALUMINA FORMING ALLOYS BY MOLTEN GLASSES

Introduction

As described in the literature review in chapter 2, the glass melts are extremely corrosive towards metallic materials. In the hot corrosion context, Ni-based superalloys with high Cr content and with Al as an alloying element are the best candidates for high temperature application, since Cr and Al are well known to have the ability to develop thermodynamically stable oxides (chromia Cr_2O_3 and alumina Al_2O_3 respectively). This chapter is devoted to the study of the behaviour against corrosion by molten glass of two kinds of alloys: chromia forming alloys and alumina forming alloys. The aim here is to evaluate their ability to resist against corrosion by molten glass.

In the first part of this chapter, the use of chromium as an alloying element is thoroughly studied, through the characterisation of the corrosion resistance of two materials: pure chromium and a simplified chromia forming Ni-based alloy containing 30 wt.% of chromium (noted here as Ni-30Cr) which contains sufficient Cr to allow the formation of a protective oxide layer.

The second part of the chapter deals with two alumina forming alloys. The first alloy is supposed to contain enough aluminium to develop an Al_2O_3 layer at 1100°C (composition: Ni-based with 28 wt.% Cr and 8 wt.% Al, noted here as Ni-

8Al-28Cr). The second alloy is a nickel rod cemented with NiAl layer. The synthesis of these different alloys is detailed in Chapter 3.

Firstly, the oxidation behaviour of the alloys in hot air was first accurately studied and detailed in Appendix D. The formed oxides were characterised, then the kinetics of the oxide growth are determined through the analysis of thermogravimetry measurements. The aim is to have an evaluation of the morphology and thickness of the oxide layers formed through preoxidation treatments. In this chapter, the corrosion of the alloys by molten glass is studied. 'Raw immersion' and a thorough observation of the alloys will provide the knowledge of the general aspects of the corrosion by molten glass (glass penetration, thickness loss, surface morphology). Electrochemical measurements will bring further information about the redox couples involved in the corrosion process, and also the kinetics of corrosion through E_{corr} and Rp measurements.

4.1. Corrosion of pure Cr and Ni-30Cr by molten glass

The first part of this chapter deals with the behaviour of chromia-forming materials against corrosion by molten glass. Pure chromium and Ni-30Cr present different Cr activities and their performances against glass corrosion will be compared.

After a detailed study of the isothermal oxidation in hot air of Ni-30Cr at 1100°C and 1150°C which have been discussed in Appendix D, electrochemical method will give further information about the corrosion by molten glass. Three different melts will be used herein; a binary melt (Na_2O-$2SiO_2$ *i.e.* N2S) and two

compositions of ternary melts (Na_2O-CaO-$3SiO_2$ *i.e.* NC3S and Na_2O-CaO-$6SiO_2$ *i.e.* NC6S). The corrosion behaviour of pure Cr and Ni-30Cr will be studied by taking into account the influence of different parameters; glass composition, temperature and preoxidation treatment of the alloys.

4.1.1. Electrochemical characterisation of the solvents

Since the electrochemistry experiments require a big amount of glass to fill the clay crucibles (~1.3 kg), the glasses which have been elaborated by Cerfav have been used in these studies. The raw glasses prepared by Cerfav have been presented in Table 3.3 (Chapter 3).

The electroactivity domain of the glasses at T = 1100°C were measured for soda-lime silicate melts (Na_2O-CaO-$3SiO_2$ (NC3S) and Na_2O-CaO-$6SiO_2$ (NC6S)) and soda silicate melt (Na_2O-$2SiO_2$ (N2S)) by using a platinum working electrode. The free potentials measured for the glasses are:

- NC3S: -7 mV
- NC6S: +22 mV
- N2S: +32 mV

The free potentials of the three glasses are quite high and lie in the same range of values. These values represent the characteristic of the glasses which have been elaborated in oxidising atmosphere (air). Thus, one may conclude that these glasses exhibit a high oxidation power.

The polarisation curves were plotted for the three glasses as shown in Figure 4.1. The curves were obtained by first exploring the anodic field from the free potential to ~ +1000 mV. The polarisation curve was started by anodic field due to the fact that the cathodic polarisation leads to the reduction of the active species (*e.g.* Si^{IV}) which might contaminate and thus alter the surface of the platinum working electrode. After a purge time of about 1 h, the cathodic field was polarised from the free potential to ~ -1400 mV. All the experiments were performed with a scan rate (υ) of 1 mV/s.

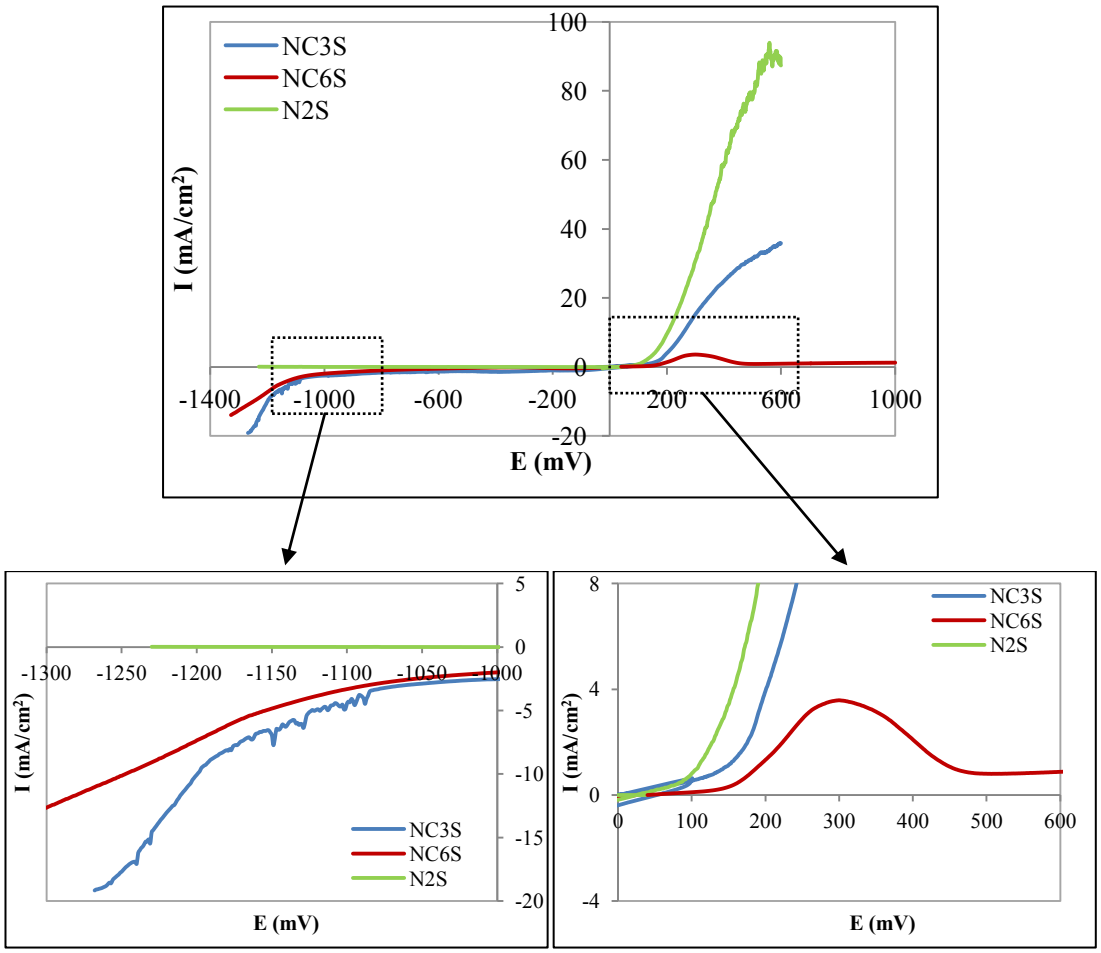

Figure 4.1: Electroactivity domains of NC3S, NC6S and N2S at 1100°C measured on the Pt working electrode with υ = 1 mV/s. The potentials are reported with respect to the potential of yttria-stabilised zirconia reference (YSZ) electrode

The electroactivity domain of the molten glasses extends approximately from -1100 mV to +150 mV. However, in the case of N2S, the experiment in the cathodic field was just carried out until -1230 mV due to the aggressiveness of N2S, thereby leading to a difficulty in determining the cathodic limit of this glass. The cathodic limit of the molten glasses as could be observed in NC3S and NC6S corresponds to the reduction of the silicate network[71,86,87] according to the following equation:

$$SiO_4^{4-} + 4e^- \Leftrightarrow Si^0 + 4O^{2-} \tag{4.1}$$

The anodic limit of the molten glasses corresponds to the oxidation of the O^{2-} ions and the oxidation of silicate network according to the following equations:

$$O^{2-} \Leftrightarrow \tfrac{1}{2} O_{2(g)} + 2e^- \tag{3.16}$$

$$SiO_4^{4-} \Leftrightarrow SiO_3^{2-} + \tfrac{1}{2} O_{2(g)} + 2e^- \tag{4.2}$$

For the glass of NC6S, it is obviously seen that the current density decreases when the imposed potential is higher than +300 mV. A similar behaviour has been observed in the electroactivity domain of binary glasses (Na_2O-$3SiO_2$ and Na_2O-$3.5SiO_2$) at 1050°C[10]. According to a thorough observation by Abdelouhab *et al.*[10], there is an existence of a thin SiO_2 layer around the platinum electrode which limits the exchange current and yields to the observed curve inflection. The SiO_2 layer is observed due to the impoverishment of Na_2O for the glass which is directly in contact with the platinum working electrode. The Na^+ ions migration is probably due to the imposed electric field on the system. A similar cation migration has been observed in the case of titanium electrode immersed in an industrial glass[79].

4.1.2. Electrochemical measurements of the corrosion of pure Cr and Ni-30Cr alloy in silicate melts

Since the past several years, a lot of efforts have been dedicated in the LCSM on the research concerning the corrosion behaviour of chromia forming superalloys while having contact with molten glasses. As has been discussed in the Chapter 2, an electrochemical technique is able to provide a good measurement of the interface reactions in the systems. Although pure Cr is not technologically important as an oxidation-resistant structural material, the behaviour of pure Cr in molten glass will be discussed herein to acquire a fundamental insight into the corrosion mechanism of Ni-based alloys with high Cr content in molten silicates.

The behaviour of pure Cr and Ni-30Cr alloy were studied in soda-lime silicate melts (Na_2O-CaO-$xSiO_2$) and soda silicate melt (Na_2O-$2SiO_2$) at different temperatures depending on the experimental conditions. The electrochemical technique is able to demonstrate the spontaneous behaviour of the pure Cr in the molten glass. However, it is possible to reach a passivation state right after the immersion by development of a chromia (Cr_2O_3) protective layer. The development of the protective Cr_2O_3 layer might be performed by:

- an oxidation of the metal in air at high temperature. This treatment is known as 'preoxidation'[85].
- an anodic polarisation[71,86].

The work presented here deals with the spontaneous behaviour of pure Cr and Ni-30Cr alloy while directly immersed in NC3S at 1100^{o}C. Then, the behaviour of

the preoxidised samples in molten glass has been discussed by taking into account the influences of temperature and the melt basicity.

4.1.2.1 Spontaneous behaviour of pure Cr and Ni-30Cr alloy in NC3S at 1100°C

(a) Pure Cr

A pure Cr sample (5 mm diameter rod) was immersed in NC3S at 1100°C for 24 hours and quenched in air. Micrographs of the cross section of the sample are presented in Figure 4.2.

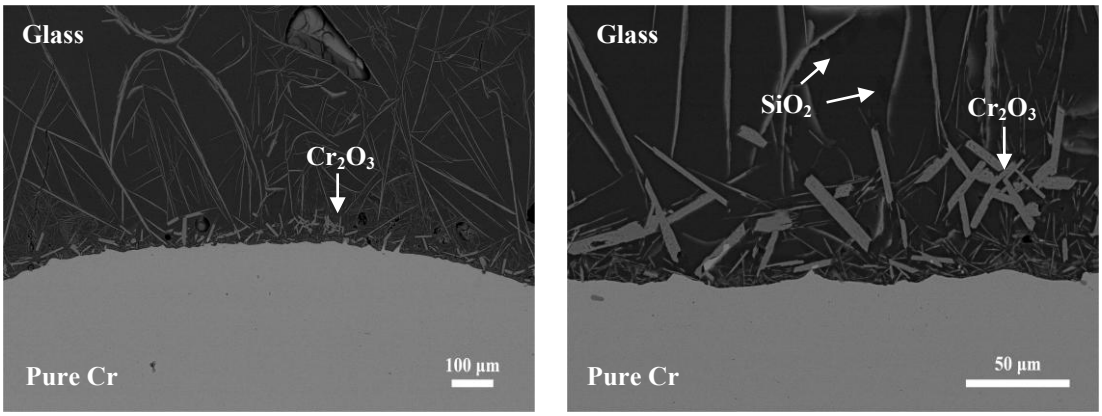

(a) **(b)**

Figure 4.2: Micrographs of pure Cr after 24 h of immersion in NC3S at 1100°C with magnification of (a) 100x and (b) 500x

The surface has been corroded by the molten glass since there are dissolutions of Cr from the sample. A lot of needle-like shaped Cr_2O_3 that have been precipitated in the glass. It is noteworthy that no compact and adherent oxide layer is detected on the surface of the sample and the metal is still directly in contact with the melt.

The electrochemical measurement of pure Cr electrode which was directly immersed in NC3S at 1100°C is presented in Figure 4.3. It shows a very low corrosion potential (E_{corr}) and polarisation resistance (Rp) which are < -1300 mV and 6 Ω.cm^2 respectively. This behaviour proves that the metal is in active state right after immersion. The anodic polarisation curve of pure Cr after ~ 40 min of immersion in NC3S at 1100°C was recorded from E_{corr} - 20 mV until +500 mV with a scan rate of 1 mV/s.

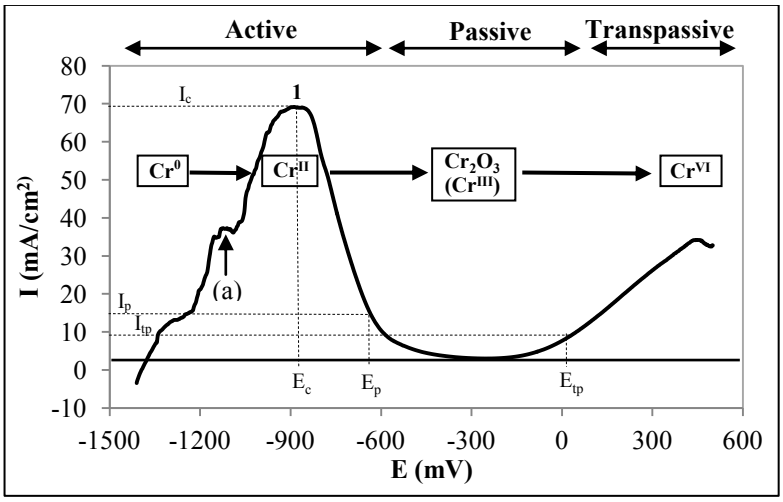

Figure 4.3: Anodic polarisation curve of pure Cr after ~ 40 min of immersion in NC3S at 1100°C (υ = 1 mV/s)

The individual reaction steps that occur when the Cr electrode is polarised from the low to the high potential in different melt compositions have been discussed in previous electrochemical studies[85,98,110]. The knowledge of the redox reactions in these previous studies has been used herein in order to describe thoroughly this intensity-potential curve. A scale giving the order of magnitude of the potentials in molten glass of the redox couples studied here has been presented in Figure 2.5.

- Right after immersion, the Cr electrode exhibits an active dissolution with a very low potential (Ecorr < -1300 mV). According to the scale in Figure 2.5, the chromium oxidation might be due to the Si^{IV}/Si^{0} couple (peak (a) on Figure 4.3).

  Reduction of the silica from the glass network:

  $$SiO_4^{4-} + 4e^- \Leftrightarrow Si^0 + 4O^{2-} \quad (4.1)$$

  Oxidation of the chromium rod:

  $$Cr^0 \Leftrightarrow Cr^{II} + 2e^- \quad (4.3)$$

- The Cr_2O_3 needles observed in the glass might be due to the oxidation of the dissolved Cr^{II} into Cr^{III}. The oxidation is due to the presence of dissolved O_2 in the melt (experiments performed in air).

  Reduction of the dissolved O_2:

  $$\frac{1}{2}O_2 + 2e^- \Leftrightarrow O^{2-} \quad (2.9)$$

  Oxidation of the chromium rod:

  $$Cr^{II} \Leftrightarrow Cr^{III} + e^- \quad (4.4)$$

- The peak 1 in Figure 4.3 which is known as critical passivation potential, E_c is the potential where the passivation reaction prevails over the dissolution reaction. At this stage, the Cr^{II} may transform to the protective Cr_2O_3 layer (Cr^{III}) which possesses a low solubility in molten glass[11,88,99]. The corresponding potential (~ -0.8V) is related to the potential of the Cr^{II}/Cr^{III} reported in Figure 2.5. The current density of peak 1 which is known as

critical current density, I_c is the current density which should be overcome by the metal/alloy to stabilise its passive state.

- Beyond the passivation potential E_p, the current density which is called the passivation current density I_p is very low, thereby exhibits the protection behaviour served by Cr^{III}. The potential between E_c and E_p is called as the pre-passivation range.

- Beyond the transpassivation potential E_{tp}, the protection due to the Cr_2O_3 layer is less effective due to the dissolution of Cr^{III} to Cr^{VI} via the oxidation reaction:

$$Cr^{III} \Leftrightarrow Cr^{VI} + 3e^- \quad (4.5)$$

The potential domain between E_p and E_{tp} is known as the passivity or passivation range. Here, it is comprised between ~ -0.6 V and ~ 0 V.

(b) Ni-30Cr alloy

The study has been continued by investigating the behaviour of Cr_2O_3 forming alloy (Ni-30Cr) in silicate melt. The Ni-30Cr rod was immersed in NC3S at 1100^{o}C for 24 h. The backscattered electron (BSE) images of this sample (Figure 4.4) show that there is no protective oxide layer on the surface of the alloy. Some Cr_2O_3 agglomerates are observed, but they are isolated and cannot provide any protection to the alloy. An EPMA measurement performed in the glass close to the surface of the alloy reveal a Cr content of around 0.3 at.%, proving the dissolution of this element in the glass. A strong corrosion has occurred, with a glass penetration of

about 12 μm from the surface. This corrosion particularly affects the grain boundaries of the alloy.

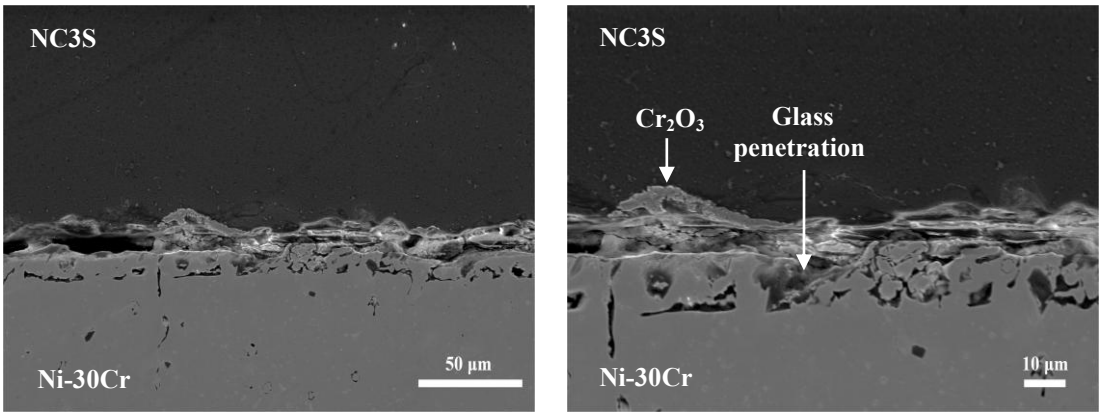

(a) **(b)**

Figure 4.4: Micrographs of Ni-30Cr alloy after 24 h of immersion in NC3S at 1100°C with magnification of (a) 500x and (b) 1000x

In order to reveal the corrosion behaviour of this alloy, an anodic polarisation curve was performed as a comparison with pure Cr electrode. The anodic polarisation curve was recorded for Ni-30Cr from E_{corr} - 20 mV up to +500 mV with a scan rate of 1 mV/s after ~ 40 min of immersion in NC3S at 1100°C. The comparison of the anodic polarisation curves between pure Cr and Ni-30Cr alloy which were subjected to the same experimental parameters is shown in Figure 4.5:

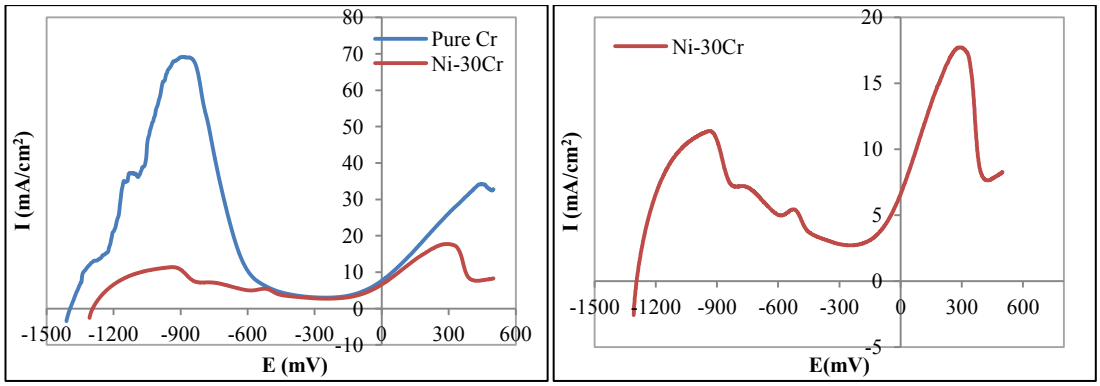

(a) **(b)**

Figure 4.5: Anodic polarisation curves of pure Cr and Ni-30Cr in NC3S at 1100°C after ~ 40 min of immersion (a) comparison of pure Cr and Ni-30Cr alloy (b) anodic polarisation curve of Ni-30Cr alloy

The results reveal the same trend of plots for pure Cr and Ni-30Cr alloy. Both curves exhibit a passivation plateau with very low current density (~ 3 mA/cm^2) at the same potential range (between -0.6 and 0 V) in both cases. As the passivation plateau possesses the same characteristic for both cases, one may conclude that both samples tend to form the same passivation layers, *i.e.* Cr_2O_3.

The critical current density measured for a potential around -0.9 V, is much lower in the case of the Ni-30Cr alloy (~ 12 mA), compared to the case of pure Cr (~ 70 mA). This observation clearly shows that Ni-30Cr alloy will develop a passivation layer much more easily than pure Cr.

The corrosion potentials just after immersion in the molten glass are quite different between the two metals; the corrosion potential of the Ni-30Cr alloy (~ -1.3 V) is a bit higher than the corrosion potential of pure Cr (~ -1.4 V). This phenomenon can be explained by the difference of Cr activity between the two

metallic samples. The thermodynamic potential of the Cr^{II}/Cr^0 couple can be expressed through the Nernst law as follows:

$$E_{Cr^{II}/Cr^0} = E^0_{Cr^{II}/Cr^0} + \frac{2.3RT}{2\Im}\log\frac{a_{Cr^{II}}}{a_{Cr^0}} \tag{4.6}$$

As the Cr activity is much lower in the Ni-30Cr alloy than in the pure Cr rod, the thermodynamic potential of the Cr^{II}/Cr^0 couple is higher in the case of Ni-30Cr alloy. By assuming that the cathodic reduction of silica into silicon is always the same, independently of the oxidation reaction, the measured corrosion potential is increasing when the chromium activity is decreasing in the corroded alloy, as shown in Figure 4.6.

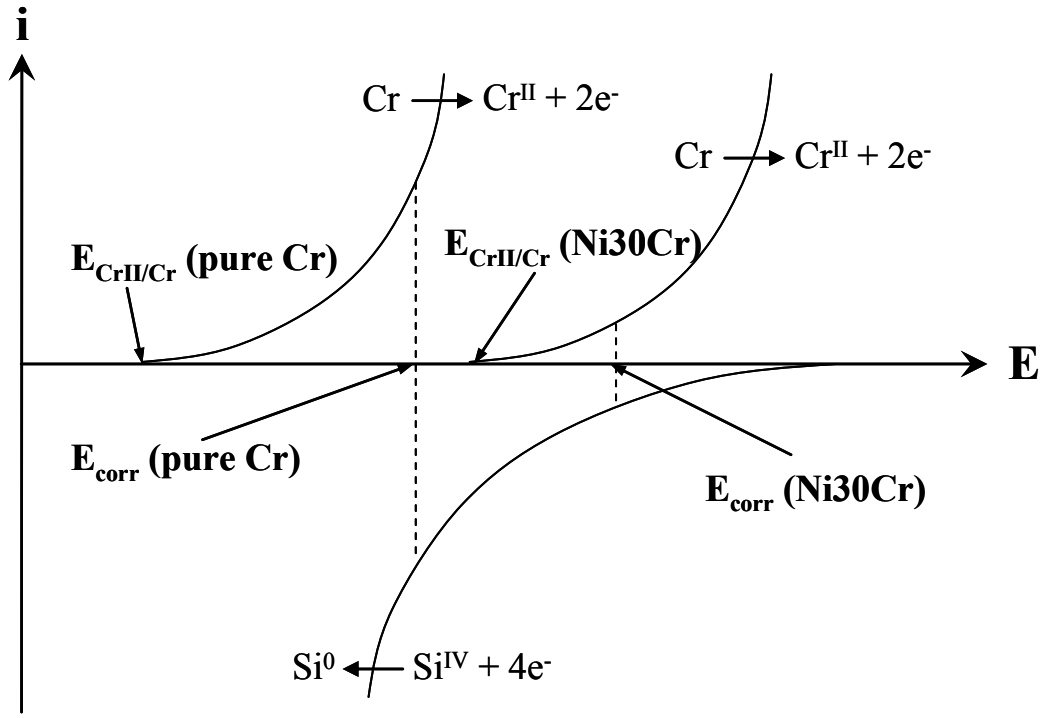

Figure 4.6: Trends of current density as a function of potential plots of Cr^{II}/Cr^0 and Si^{IV}/Si^0 redox couples in the case of pure Cr and Ni-30Cr samples

(c) Determination of corrosion rates

The corrosion rates for the pure Cr and Ni-30Cr alloy which were immersed in NC3S for 24 h have been determined at 1100°C by using two methods. The first method which is noted herein as V_{corr} is based on the Stern-Geary law which has been described in Chapter 3. The other method which is known as thickness loss measurement is calculated based on the thickness loss of the sample after the corrosion test. This second method is noted herein as $V_{thickness\ loss}$. The formal potentials of some redox couples that have been displayed in Figure 2.5 lead to the prediction of the anodic and cathodic reactions as summarised in Table 4.1.

Table 4.1: The main corrosion data concerning the spontaneous behaviour of pure Cr and Ni-30Cr alloy in NC3S at 1100°C

Samples	**Pure Cr**	**Ni-30Cr**
E_{corr} (mV)	-1390 (± 20)	-1290 (± 20)
State	Active	Active
Anodic reaction	$Cr \rightarrow Cr^{II} + 2e^-$	$Cr \rightarrow Cr^{II} + 2e^-$
Cathodic reaction	$Si^{IV} + 4e^- \rightarrow Si^0$	$Si^{IV} + 4e^- \rightarrow Si^0$
B (V)	0.04	0.04
Rp ($\Omega.cm^2$)	6 (± 1)	9 (± 1)
V_{corr} (cm/year)	15.4 (± 0.5)	5.2 (± 0.3)
$V_{thickness\ loss}$ (cm/year)	15 (± 2)	2 (± 0.9)

The corrosion rate is much lower in the case of Ni-30Cr alloy as compared to the pure chromium. This result is in a good agreement with the observation on the SEM micrographs. It is noteworthy that no oxide layer is observed on the surface of pure chromium whereas some agglomerates are observed on the surface of Ni-30Cr. This SEM observation can be related to the electrochemical behaviour which has shown that the critical current density is much lower for the Ni-30Cr alloy in order to obtain passivation. Even though the Ni-30Cr alloy is spontaneously in active state, the existence of a few agglomerates of oxide on its surface will provide a slight

protection (compared to the pure Cr sample which totally remains in contact with the molten glass), thus leading to a lower corrosion rate.

A very good correlation is observed for the corrosion rates determined by both methods on the pure Cr samples. The Rp measurements can thus be considered as a good indicator of the corrosion phenomena. However, this is less obvious in the case of Ni-30Cr alloy. The V_{corr} determined by Rp measurements shows a lower value as compared to the pure Cr sample; 5.2 cm/year is equivalent to 140 µm/day, which is quite difficult to measure on a 5 mm rod. As a consequence, another geometry should be considered for the samples, or the thickness loss should be measured after much longer time of contact between the alloy and the molten glass.

4.1.2.2. Behaviour of preoxidised pure Cr and Ni-30Cr alloy in NC3S at 1100°C

In order to improve the spontaneous behaviour of pure Cr and Ni-30Cr alloy against corrosion, both electrodes were preoxidised in air before immersion in the molten glass. This treatment allows development of a chromia layer at the interface of the metal/alloy, hence providing a better protection to the metal/alloy against corrosion by the molten glass[71,86]. The 2 h of preoxidation time has been used herein for the both samples.

The parabolic and linear constants determined for Ni-30Cr alloy allow the evaluation of the thickness of the Cr_2O_3 layer obtained right after the preoxidation treatment (before immersion in the molten glass). After conversion of k_p' and k_l' into k_{pe} and k_{le} by using Eq. 9 and 10 from Appendix D, it is possible to evaluate the oxide thickness through Eq. 6 as has been discussed in Appendix D.

In the case of pure Cr, the data reported by Taneichi *et al.*[111] on the oxidation behaviour of pure Cr in atmosphere has been used in order to estimate the thickness of Cr_2O_3 layer formed at the interface. The calculated values of the oxide (Cr_2O_3) thickness formed at the interface pure Cr and Ni-30Cr alloy after 2 h of preoxidation in air at different temperatures are listed in Table 4.2.

Table 4.2: Evolution of oxide (Cr_2O_3) thickness layer formed at the interface pure Cr and Ni-30Cr alloy after 2 h of preoxidation in air at different temperatures

	1050°C	1100°C	1150°C
pure Cr	6.3 µm	7.7 µm	-
Ni-30Cr alloy	-	5.5 µm	8.9 µm

In the present electrochemical experiments, the preoxidation treatment of the sample was performed a few centimetres above the molten glass. In order to avoid the spallation of the oxide layer which is induced by the thermal shock, the electrodes were directly immersed in NC3S right after the preoxidation process.

After 24 hours of immersion in NC3S at 1100°C, the preoxidised Ni-30Cr sample still exhibits a compact, thick (6 µm < e < 10 µm) and adherent Cr_2O_3 layer, as illustrated in Figure 4.7. EPMA measurements performed in the glass close to the oxide layer reveal a chromium content of around 0.3 at.% Cr, which is in the same range as the value measured in the case of the non-preoxidised sample. Some Cr_2O_3 has been dissolved in the glass, but the oxide growth seems to prevail over the dissolution of the oxide in the melt. This is due to the fact that the thickness of the oxide layer formed during the preoxidation treatment is sufficient to provide the protection. Since there is no contact between the alloy and the molten glass, the preoxidised sample is assumed to still be in passive state with a good resistance

against corrosion even after 24 h of immersion in NC3S at 1100°C. The $Na_2Ca_2Si_3O_9$ precipitates observed in the glass are the phase which has been identified in Chapter 3 *i.e.* the solid solution $(Na_2,Ca)Na_2CaSi_3O_9$. According to the DTA analysis in Appendix C, this phase is expected to be formed since the experimental temperature (*i.e.*1100°C) is just below the melting point.

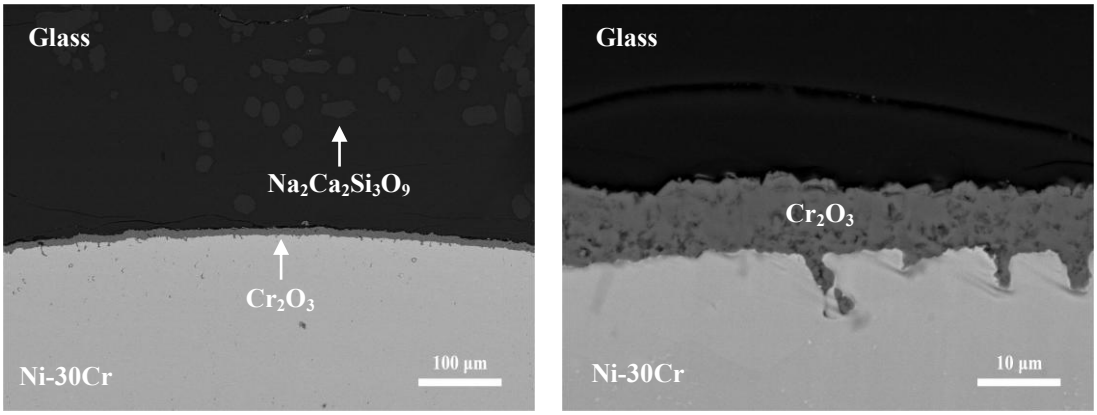

(a) **(b)**

Figure 4.7: Cross section of preoxidised Ni-30Cr alloy after 24 h of immersion in NC3S at 1100°C (a) 200x magnification (b) 2000x magnification

A 'raw immersion' experiment in NC3S at 1100°C for 24 h has also been performed on a pure chromium sample after 2 h of preoxidation. After quenching, the sample has been prepared in a resin for SEM characterisation. However a detachment of the metal from the glass has occurred which makes the observation by SEM not possible. As a consequence, it seems like only the glass remains in the resin. An observation on the remaining pure Cr electrode shows that no oxide layer is attached on the surface of the metal. The spallation of the Cr_2O_3 layer might happen due to the thermal shock during quenching or due to its poor adherence on the metallic substrate. Furthermore, Buscail *et al.*[112] have observed a development of nitride layer beneath the Cr_2O_3 layer after an oxidation in air at high temperature. This nitride layer seems to have a bad effect on the adherence of the Cr_2O_3 layer on

the pure metal substrate[112]. As a consequence, it is assumed that the pure Cr metal is not protected in this condition. However, a thorough investigation by an electrochemical measurement will give a complementary explanation on this phenomenon.

(a) Measurement of E_{corr} and Rp for 24 h of immersion

As an attempt to characterise the efficiency of the preoxidation step on the stability of the pure Cr and Ni-30Cr alloy in molten glass, the E_{corr} and Rp were recorded on these samples depending on the experimental conditions. In order to preserve the original state of the sample which will be modified when the potential is polarised, the E_{corr} and Rp were first recorded for several hours up to 24 hours of immersion. The anodic polarisation curves of the sample were then recorded right after the experiment. The recorded E_{corr} and Rp for pure Cr and Ni-30Cr alloy are displayed in Figure 4.8.

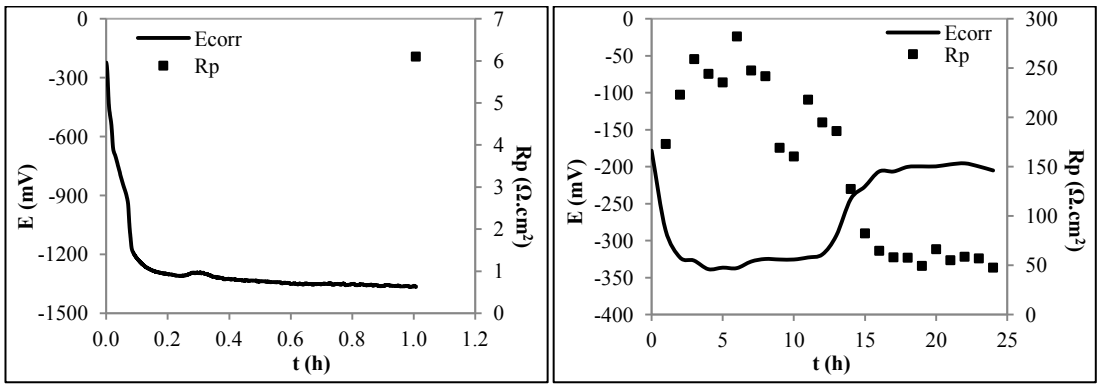

(a) **(b)**

Figure 4.8: Evolution of corrosion potential (E_{corr}) and polarisation resistance (Rp) of (a) preoxidised pure Cr (b) preoxidised Ni-30Cr alloy during the immersion in NC3S at 1100°C

The recorded E_{corr} of preoxidised pure Cr electrode (Figure 4.8(a)) right after the immersion shows that the metal is in passive state with high potential (~ -200

mV). However, the metal demonstrates a rapid decrease of potential just after a few minutes of immersion in NC3S at 1100°C. After about 10 min of immersion, the potential is stabilised at ~ -1300 mV - ~ -1400 mV with very low Rp (6 $\Omega.cm^2$). These values are very close to the ones measured on the non preoxidised pure Cr sample. Thus, it can be assumed that after 10 minutes of immersion, the preoxidised sample returns to its active state by possessing a direct contact between the metal and the molten glass. This behaviour is in accordance with the anodic polarisation plots in Figure 4.5(a) where the pure Cr sample exhibits a much higher critical current density than the Ni-30Cr alloy, thus demonstrating a lower ability for pure Cr to develop a protective oxide layer.

A fast deterioration of pure Cr electrode might happen due to the insufficient protection provided by the Cr_2O_3 layer. Since the potential stabilises at a very low value, the involved anodic reaction is: $Cr^0 \rightarrow Cr^{II} + 2e^-$. An oxidation of pure Cr in air at 1100°C might induce a development of a thick polycrystalline Cr_2O_3 scale which thickens rapidly, hence generating compressive stress and causing wrinkling of the formed scale[113,114]. Furthermore, as has been discussed previously, a poor adherence of Cr_2O_3 scale on the substrate might be due to the formation of nitride beneath the oxide layer. The nitride formation is more significant at higher temperature[112]. Since the metal returns to its active state after few minutes, the experiment was just performed up to 1 h of immersion in the case of preoxidised pure Cr.

In contrast with pure Cr, the preoxidised Ni-30Cr alloy shows a much better stability in NC3S at 1100°C. The electrochemical behaviour of the sample can be explained in two steps:

- from 0 to ~15 h: E_{corr} ~ -320 mV and Rp ~ 150 Ω.cm²
- from ~15 to 24 h: E_{corr} ~ -200 mV and Rp ~ 60 Ω.cm²

A change of E_{corr} domain might be an indication of a change in the electrochemical phenomena occurring at the surface of the electrode. However, these two values are in the range corresponding to the passivation plateau of chromia forming alloys (-600 mV < E < 0 mV, Figure 4.5). The Rp values are decreasing with the immersion time. However the preoxidised Ni-30Cr alloy still exhibits a Rp value which is an order of magnitude higher than the non-preoxidised sample even after 24 h of immersion. Therefore one may conclude that the sample is still in passive state after 24 h of immersion. This result is indeed in perfect correlation with the micrographs in Figure 4.7.

Since the Rp values shows a quite significant difference for these two steps, a preoxidised sample was immersed in molten NC3S at 1100°C for 5 h before being quenched in air in order to make a comparison with the samples immersed for 24 h. The SEM micrographs observed after 5 h of immersion reveal a protective Cr_2O_3 layer with 5 - 7 µm of thickness at the interface (Figure 4.9). The characteristics of the oxide formed after 5 h of immersion does not show any difference with the Cr_2O_3 formed after 24 h of immersion. As a consequence, it is difficult to have a concrete explanation on the change of electrochemical behaviour of the sample after 15 h of immersion.

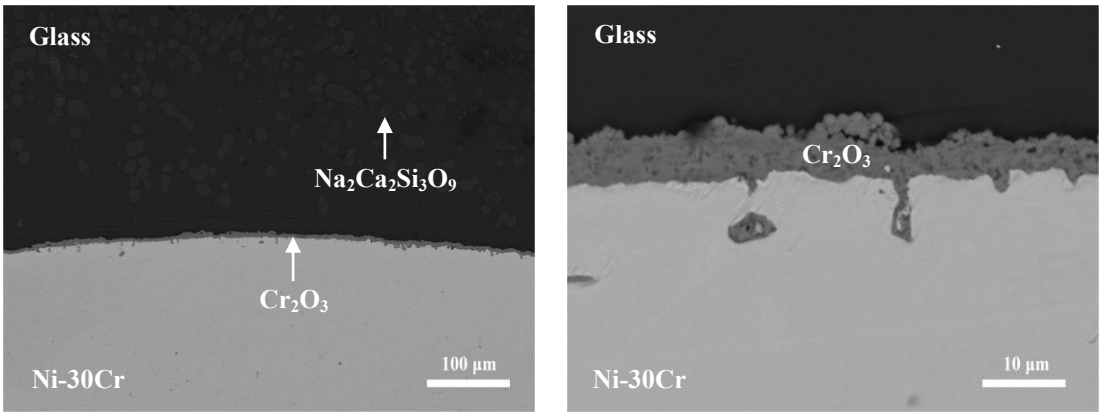

(a) **(b)**

Figure 4.9: Cross section of preoxidised Ni-30Cr alloy after 5 h of immersion in NC3S at 1100°C with (a) 200x magnification (b) 2000x magnification

(b) Intensity-potential curve of preoxidised Ni-30Cr alloy

An anodic polarisation curve (Figure 4.10) of preoxidised Ni-30Cr was recorded after 24 h of immersion in NC3S at 1100°C. The curve has been compared with the behaviour shown by the non-preoxidised Ni-30Cr alloy at the same experimental conditions.

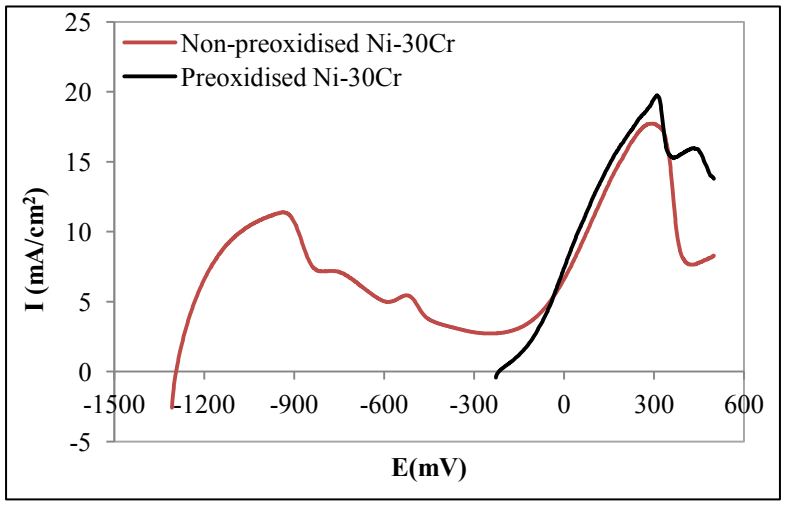

Figure 4.10: Anodic polarisation curves for both non-preoxidised and preoxidised Ni-30Cr alloy after 24 h of immersion in NC3S at 1100°C

The preoxidised Ni-30Cr curve does not present an anodic peak. The curve exhibits a high corrosion potential ($E_{corr} \approx$ -200 mV) right after immersion. The value

of E_{corr} indicates that the alloy is in Cr^{III} domain which is in the passivation region of the curve. By increasing the potential, the alloy exhibits an increasing of the current density as observed in the non-preoxidised Ni-30Cr alloy. At high potential (E > 0 mV), the alloy is subjected to the transpassivation state as previously discussed.

4.1.2.3. Influence of temperature on the stability of the passivity state

The influence of temperature on the stability of the Cr_2O_3 layer has been proved by several authors[66,98]. Since the investigated temperatures herein were just focusing on 1100°C and 1150°C, this study is able to compare the stability of Ni-30Cr alloy at these two different temperatures.

(a) 'Raw immersion' of preoxidised Ni-30Cr alloy in NC3S at 1150°C

A Ni-30Cr rod was preoxidised at 1150°C for 2 h (the oxide layer thickness is ~ 8.9 µm determined by the isothermal oxidation of Ni-30Cr in Appendix C) before being subjected to the immersion in NC3S at the same temperature. Figure 4.11 presents the cross section of the sample after 24 h of 'raw immersion' in NC3S at 1150°C.

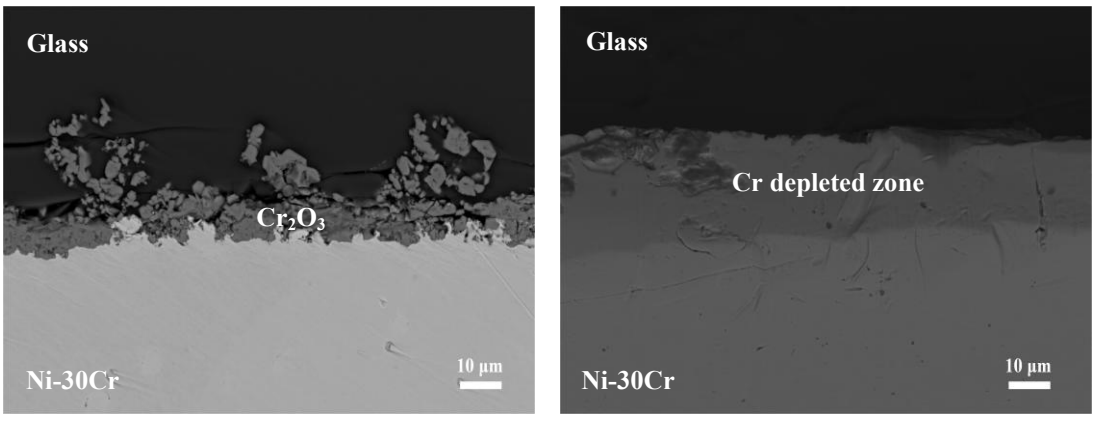

Figure 4.11: Cross section of preoxidised Ni-30Cr after 24 h of immersion in NC3S at 1150°C (a) region with chromium oxide (b) region with no oxide

It is noteworthy that two kinds of region have been observed at the interface of the sample. A Cr_2O_3 layer is detected on the major zone but it is not compact and adherent enough to the substrate. Furthermore, a thorough investigation on the micrographs reveal an existence of a direct contact between the substrate and the melt. The chromia layer obtained from the preoxidation process has been partially dissolved. EPMA measurements performed in the glass close to the oxide layer reveal a Cr content of around 0.3 at.% Cr. It seems that all the oxide which can develop at the interface during the immersion is instantaneously dissolved in the melt. Thus the protection of the alloy is minimum on these zones. On minor regions, no oxide layer can be detected. Furthermore, a Cr depleted zones is detected on the surface of the alloy, with a thickness of about 20 - 25 µm. In these zones, the Cr layer has been totally dissolved, and the impoverishment of the surface of the alloy in chromium shows that the dissolution has been much more preponderant than the oxide growth.

(b) Measurement of E_{corr} and Rp for 24 h of immersion

The E_{corr} and Rp values were recorded for 24 h at 1100°C and 1150°C. The results have been compiled in Figure 4.12. The alloy is in the passivation region for both temperatures right after the immersion. This behaviour is characterised by a high E_{corr} (~ -200 mV) and Rp (~ 180 Ω.cm^2) values recorded during the first hour of immersion. After 24 h of immersion at 1100°C, the alloy seems to show a good protection with a stabilised Rp value around 60 Ω.cm^2. In the case of immersion at 1150°C, the protective Cr_2O_3 layer seems to be totally inefficient after 9 h of immersion when the values of E_{corr} and Rp stabilise at ~ -1200 mV and 9 Ω.cm^2 respectively which are the characteristic of the active region.

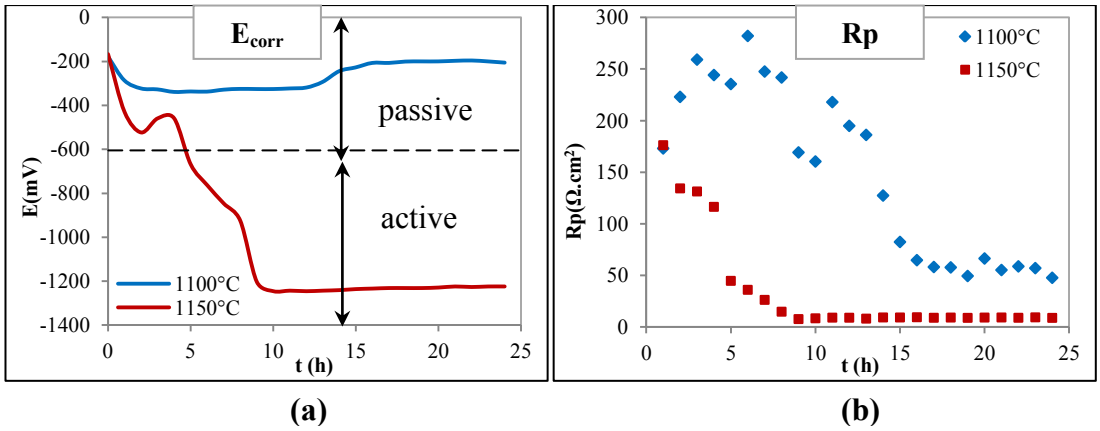

(a) (b)

Figure 4.12: The corrosion potentials (E_{corr}) (a) and polarisation resistance (Rp) (b) of preoxidised Ni-30Cr alloy in NC3S at 1100°C and 1150°C

After 24 h of immersion in NC3S at 1100°C and 1150°C, anodic polarisation curves were plotted for both samples as displayed in Figure 4.13.

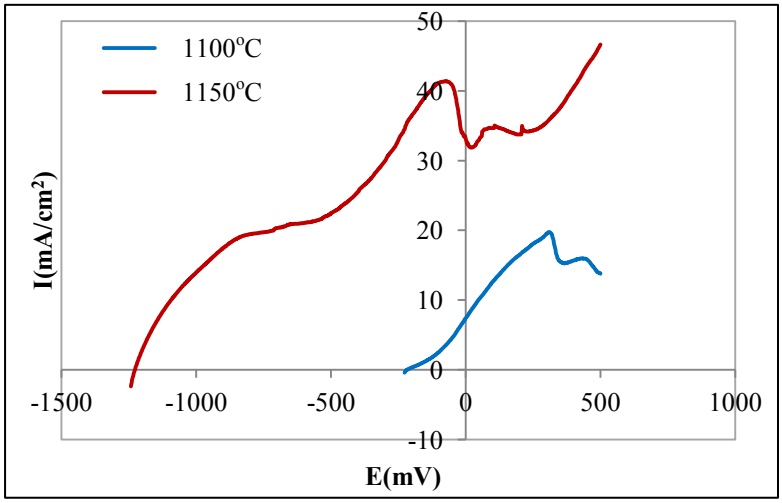

Figure 4.13: Anodic polarisation curves of preoxidised Ni-30Cr alloy after 24 h of immersion in NC3S at 1100°C and 1150°C

The plots in Figure 4.13 reveal that the preoxidised alloy is still in passive state after 24 h of immersion in NC3S at 1100°C. On the contrary, the plot shows that it is impossible to obtain the passivation state at 1150°C. At higher temperature, the solubility of Cr_2O_3 supposed to be higher and the dissolution might occur much faster than the formation of the oxide layer. So one may conclude that the critical

temperature, where the dissolution of the chromia layer becomes faster than its formation is between 1100°C and 1150°C in the case of the Ni-30Cr alloy.

(c) Determination of corrosion rates

The corrosion rates for the preoxidised Ni-30Cr alloy which was immersed in NC3S for 24 h have been determined at 1100°C and 1150°C. The corrosion rates were calculated based on the Stern-Geary relation which has been described in Chapter 3. The anodic and cathodic reactions which are displayed in Table 4.3 have been predicted based on the scale presented in Figure 2.5.

The average values of E_{corr} and Rp as well as the standard deviations have been calculated for the last 9 h of immersion at 1100°C and for the last 16 h at 1150°C as these two parameters are not stable in the first hours of immersion. The results of V_{corr} calculated from Rp values in Table 4.3 show that the corrosion rate is one order of magnitude higher when the temperature increases from 1100°C to 1150°C. At 1100°C, the alloy is still in passive state even after 24 h of immersion whereas it is in active state at 1150°C, thus explaining the significant increase of the corrosion rate between these two temperatures. As shown previously by Khedim *et al.*[99,104], the temperature dependence of the Cr solubility follows an Arrhenius law. The critical temperature where the dissolution of the Cr_2O_3 layer becomes more important than its formation on the surface of the alloy has been previously emphasised as "depassivation temperature" in a previous study[110].

In this case, the corrosion rates have not been determined by measurement of thickness loss. Since the corrosion rates of this alloy are very low, the 'raw

immersion' experiment required a much longer time in order to measure significant thickness losses. This phenomenon has already been explained in the Table 4.1.

Table 4.3: The main corrosion data concerning the corrosion of the preoxidised Ni-30Cr alloy after the immersion in NC3S for two different temperatures

Temperature (^{o}C)	**1100**	**1150**
E_{corr} (mV)	-201 (± 4)	-1234 (± 8)
State	Passive	Active
Anodic reaction	$Cr \rightarrow Cr^{III} + 3e^{-}$	$Cr \rightarrow Cr^{II} + 2e^{-}$
Cathodic reaction	$O_2 + 4e^{-} \rightarrow 2O^{2-}$	$Si^{IV} + 4e^{-} \rightarrow Si^{0}$
B (V)	0.034	0.041
Rp ($\Omega.cm^2$)	60 (± 6)	9 (± 1)
V_{corr} (cm/year)	0.5 (± 0.1)	5.5 (± 0.2)

4.1.2.4. Influence of melt basicity on the corrosion behaviour of pure Cr and Ni-30Cr alloy

The objective of this part is to comprehend the influence of the melt basicity on the corrosion behaviour of pure Cr and Ni-30Cr. The influence of the melt basicity will be discussed for soda-lime silicate glass by modifying the stoichiometry of SiO_2 in the system. This work will be extended to comparing the corrosion behaviour for different types of glass (soda silicate and soda-lime silicate melts). The latter study allows to have a view on the influence of the CaO addition in the glass system on the corrosion behaviour of the studied materials.

As discussed in the previous chapter (Chapter 2), the theoretical optical basicity equation seems to work well on the silicate glasses. As a consequence, this concept will be used herein in order to predict the 'trend' of the basicity for the binary (soda silicate) and tenary (soda-lime silicate) melts. The optical basicity values as

well as the activity of Na_2O (aNa_2O) for the binary and ternary silicate glasses are displayed in Table 4.4.

Table 4.4: The values of theoretical optical basicity (Λ_{th}) and activity of Na_2O (aNa_2O) for binary and ternary silicate melts

Glasses		Theoretical optical basicity (Λ_{th})	aNa_2O	
			(1050 °C)	(1100 °C)
Soda silicate melts (Na_2O-$xSiO_2$)	N1.5S	0.6475	4.89×10^{-9} *	7.21×10^{-9} *
	N2S	0.6140	1.09×10^{-9} *	1.68×10^{-9} *
	N2.5S	0.5917	2.23×10^{-10} *	3.80×10^{-10} *
	N3S	0.5757	7.04×10^{-11} *	1.14×10^{-10} *
	N3.5S	0.5638	2.82×10^{-11} *	/
Soda-lime silicate melts (Na_2O-CaO-$xSiO_2$)	NC3S	0.6288	4.35×10^{-10} **	6.29×10^{-10} **
	NC4S	0.5990	8.66×10^{-11} **	1.10×10^{-10} **
	NC5S	0.5792	/	/
	NC6S	0.5650	2.24×10^{-11} **	2.57×10^{-11} **

* Values given by Neudorf and Elliot[40]
** Values reported by Abdelouhab[98]

(a) Pure Cr

Abdelouhab *et al.*[10,98] have revealed the influence of the melt basicity on the corrosion behaviour of preoxidised pure Cr in soda silicate melts. According to these previous studies, the protective Cr_2O_3 layer is more stable in more acidic glass in the Na_2O-$xSiO_2$ (NxS) system. However, the comparison of the corrosion behaviour of pure Cr in the same melt basicity for the different types of glasses is not well-documented. As a consequence, the electrochemical behaviour of preoxidised pure Cr at 1050°C after 24 h of immersion in NC3S will be compared with the behaviour of the metal in NxS (x = 1.5, 2, 3 and 3.5) at the same conditions. The values of E_{corr} and Rp for these melt compositions have been compiled in Figure 4.14. According to the Table 4.4, the basicity of NC3S is approaching the basicity of N1.5S and N2S in the case of binary silicate melts. The question arising here is whether the preoxidised pure Cr after 24 h of immersion in NC3S exhibits the same corrosion behaviour as in

the binary melts which possesses almost the same optical basicity *i.e.* N1.5S and N2S.

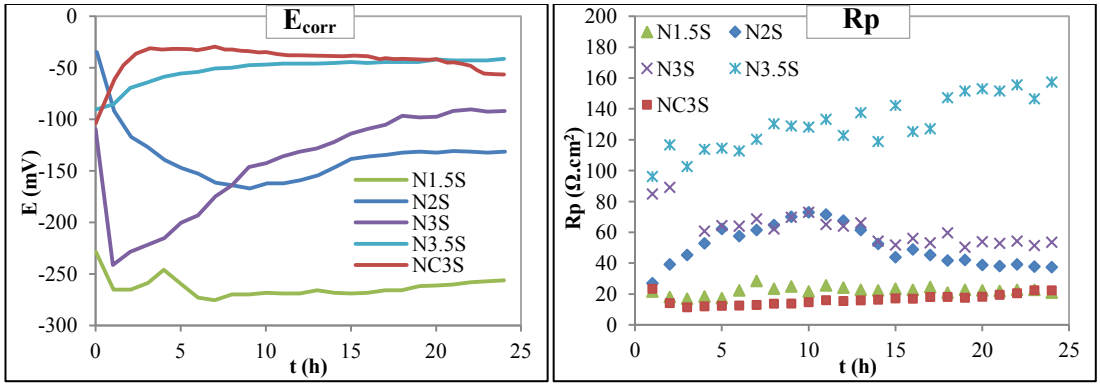

Figure 4.14: Measurement of (a) E_{corr} and (b) Rp of preoxidised pure Cr during the 24 h of immersion in N1.5S[10,98], N2S[10,98], N3S[10,98], N3.5S[10,98] and NC3S[this study] at 1050°C

As discussed by Abdelouhab *et al.*[10,98] in binary melts, the protection of the metal by Cr_2O_3 layer is more efficient in more acidic melts. This behaviour can be explained by decreasing E_{corr} and Rp values with the increasing of the optical basicity (Figure 4.15(a)) and decreasing of the pa(Na_2O) (Figure 4.15(b)).

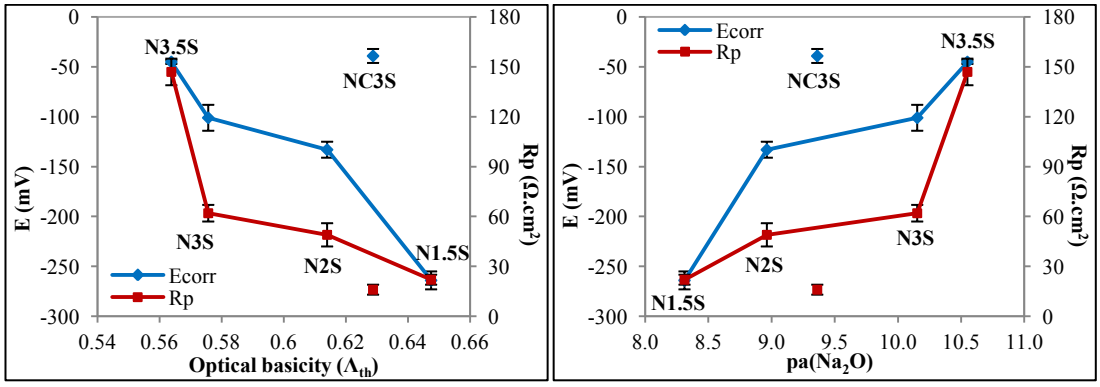

Figure 4.15: The values of E_{corr} and Rp of the preoxidised pure Cr after 24 h of immersion in binary melts (Na_2O-xSiO_2; x = 1.5, 2, 3 and 3.5) and ternary melt (NC3S) at 1050°C, reported as a function of (a) optical basicity (Λ_{th}) and (b) activity of Na_2O (pa(Na_2O))

If NC3S and the binary soda silicate melts were compared based on their Λ_{th} and pa(Na_2O) without taking into account the type of melts, it is obviously seen that NC3S does not fit with the trend of E_{corr} and Rp shown in binary melts. Even though NC3S possesses almost the same optical basicity with N1.5S and N2S, it seems that the preoxidised pure Cr in NC3S exhibits a significant difference of E_{corr} as compared to N1.5S and N2S. However, the Rp values in the case of NC3S seem to be very close to N1.5S. In spite of the deviation from the trend, the E_{corr} and Rp values show that the alloy is in passive state after the immersion in all the melts presented above. In order to have a thorough discussion of these behaviours, the interface of metal/glass for the case of NC3S has been systematically compared with N1.5S and N2S as shown in Figure 4.16.

The micrographs in Figure 4.16 show an existence of Cr_2O_3 layer at the metal/glass interface which proves that the metal is in passive state for all the experimental conditions. It was observed also the existence of the chromium nitride (CrN) at the border of the sample in the case of N2S and NC3S. The nitride might presence during the oxidation treatment of the metal in air at 1050^{o}C due to inward diffusion of nitrogen, thereby leading to the formation of solid solution of nitrogen in chromium[112]. In the case of NC3S, the existence of $Na_2Ca_2Si_3O_9$ precipitate is evident which is expected to be formed at this experimental temperature as described in Appendix C.

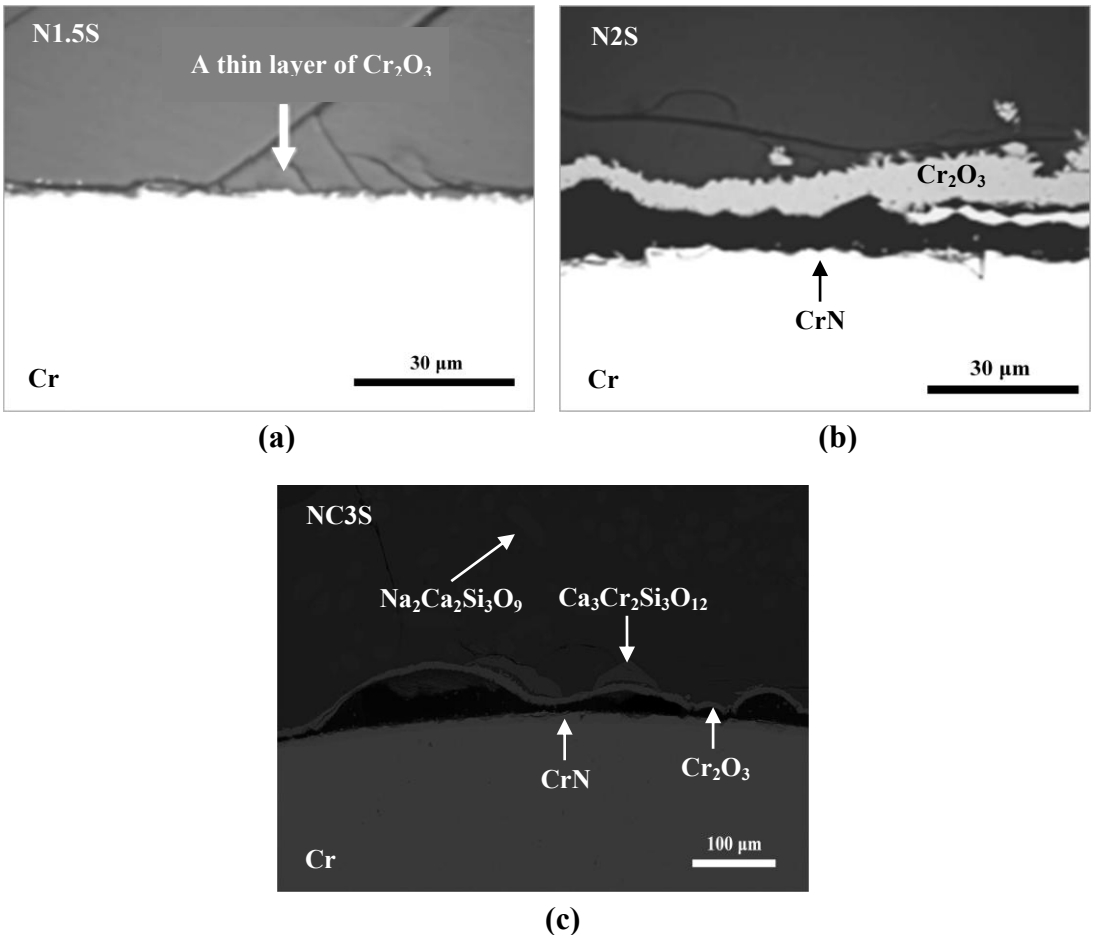

Figure 4.16: Metal/glass interface of pure Cr which has been preoxidised in air at 1050°C for 2 h, after 24 h immersion in (a) N1.5S[10,98] (b) N2S[10,98] and (c) NC3S at 1050°C

The micrographs also reveal the evolution of the thickness of Cr_2O_3 layer with the different melt compositions after 24 h of immersion as shown in Table 4.5.

Table 4.5: The thickness of Cr_2O_3 layer and the Cr content at the glass/oxide layer interface after 24 h of immersion of preoxidised pure Cr in three different melt compositions at 1050°C

Glasses	Thickness (e) of Cr_2O_3 layer (µm)	Cr content in the glass at the interface (at.% Cr)
N1.5S[10,98]	≈ 1	2.15
N2S[10,98]	4 < e < 8	1.60
NC3S	8 < e < 10	0.51

As in the case of N2S[10,98], the Cr_2O_3 thickness measured in NC3S is quite thick which is between 8 - 10 μm. Even though the formed layer is quite thick and continuous, the numerous blistering of the scale has been observed after the cooling down process. However, the thickness and the continuity of the Cr_2O_3 layer do not allow the penetration of the molten glass into the metal. Therefore, the zones that are still in contact with the metal are passive while those which are peeled off are active. This phenomenon might be the reason to the identical Rp values for N1.5S and NC3S even though the Cr_2O_3 layer in N1.5S is very thin as compared to NC3S.

Even though the Rp values are quite identical for N1.5S and NC3S, the Cr concentration measured at the metal/NC3S interface is lower than in the other glasses. This observation can be explained by the existence of $Ca_3Cr_2Si_3O_{12}$ (uvarovite) precipitate at the Cr_2O_3 layer/glass interface. The Cr_2O_3 might dissolve into Cr^{III} and react with the molten glass to form the uvarovite.

The evolution of the thickness of the Cr_2O_3 layer as a function of Cr content measured in the glass is presented in Figure 4.17. The evolution observed in Figure 4.17 has been expected since there is a competition between the formation of the Cr_2O_3 layer and its dissolution in the molten glass. After 24 h of immersion, the more the oxide layer that has been corroded by the molten glass, the higher the Cr content in the glass is.

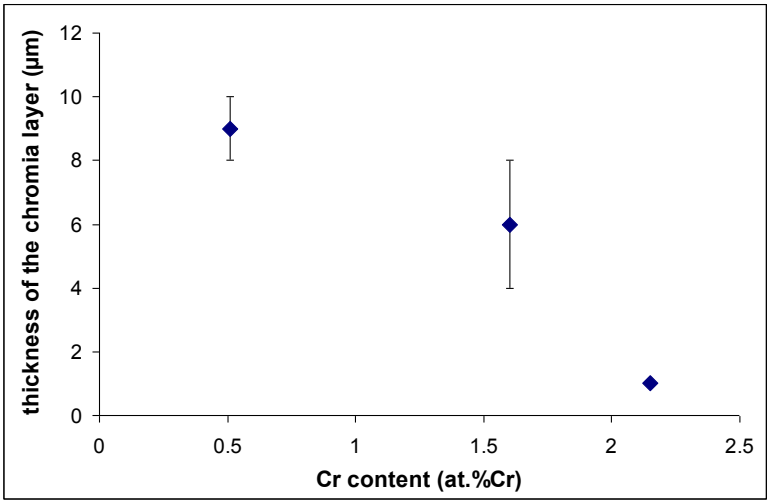

Figure 4.17: Thickness of the Cr_2O_3 layer on the preoxidised Cr samples after 24 h of immersion in N1.5S, N2S and NC3S at 1050°C as a function of Cr content measured near the glass/oxide layer interface

The corrosion rates of the preoxidised pure Cr have been determined after 24 h of immersion in NC3S at 1050°C. The results have been compared with the previous studies performed by Abdelouhab *et al.*[10,98]. The data concerning of the corrosion of this metal in the three different melt compositions are presented in Table 4.6.

Table 4.6: The main corrosion data concerning the corrosion of the preoxidised pure Cr after the immersion in three different melt compositions at 1050°C

Glass	**N1.5S**[10,98]	**N2S**[10,98]	**NC3S**
E_{corr} (mV)	-264 (± 9)	-133 (± 8)	-39 (± 7)
State	Passive	Passive	Passive
Anodic reaction	$Cr \rightarrow Cr^{III} + 3e^-$	$Cr \rightarrow Cr^{III} + 3e^-$	$Cr \rightarrow Cr^{III} + 3e^-$
Cathodic reaction	$O_2 + 4e^- \rightarrow 2O^{2-}$	$O_2 + 4e^- \rightarrow 2O^{2-}$	$O_2 + 4e^- \rightarrow 2O^{2-}$
B (V)	0.033	0.033	0.033
Rp ($\Omega.cm^2$)	22 (± 5)	50 (± 7)	16 (± 5)
V_{corr} (cm/year)	1.2 (± 0.2)	0.5 (± 0.1)	1.6 (± 0.4)

The data in Table 4.6 show that the preoxidised pure Cr exhibits the highest corrosion rate in NC3S as compared to N1.5S and N2S. The V_{corr} calculated from Rp measurement seems to deviate from the observation on the oxide thickness and Cr

content measured at the interface where the sample in NS3S exhibits the highest oxide thickness and the lowest Cr concentration as compared to others. However, the value of calculated V_{corr} is quite close to the value of preoxidised pure Cr in N1.5S. Since the system in the electrochemical experiment is not in equilibrium, an appropriate discussion on the relation between the corrosion rate and the Cr concentration in the melt should be done by performing a thorough analysis on the physicochemical behaviour of Cr_2O_3 in different type of glasses from kinetics and thermodynamic point of view. This study will be discussed in the following chapter.

(b) Ni-30Cr

In this study, the corrosion behaviour of the glass with the highest Na content (NC3S) has been compared with the melt which has the lowest amount of Na (NC6S). Since the theoretical optical basicity (Λ_{th}) for NC3S is closer to N2S in binary system, an experiment was also performed in N2S melt in order to have a view on the corrosion behaviour of the alloy in the different types of glass with the same optical basicity. Raw samples of Ni-30Cr alloy have been immersed at 1100°C for 24 h in N2S, NC3S and NC6S. Micrographs of the samples after immersion in NC3S and NC6S are presented in Figure 4.18.

As described previously, a strong corrosion with glass penetration in the alloy (~ 12 μm) is observed after immersion in NC3S. The oxide agglomerates on the surface are not sufficient to give any protection to the alloy. The same trend has been observed after the immersion in NC6S but it seems like the corrosion is not as severe as in the case of NC3S. The oxide layer is not homogeneous and has a lot of vacant spaces for contact between the alloy and the molten glass. Furthermore, the glass

penetration is still observed (~ 1 - 2 µm), even if it is less severe than in the case of NC3S.

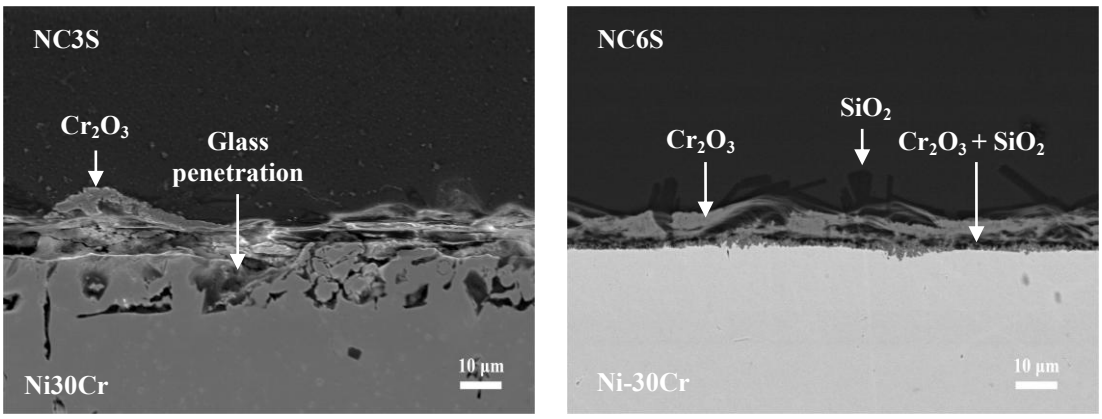

(a) **(b)**

Figure 4.18: Micrographs of Ni-30Cr alloy after 24 h of immersion in (a) NC3S and (b) NC6S at 1100°C

As discussed in the part devoted to the physicochemical behaviour of Cr in the melt (part 2.3.1 in Chapter 2), the equilibrium of Cr dissolution mainly depends on the oxide ions O^{2-} activity. As a consequence, it is coherent to observe a lower corrosion in the case of a less basic glass, *i.e.* NC6S.

Cross section of the sample immersed in N2S could not be presented here. As in the case of preoxidised pure Cr immersed in NC3S at 1100°C, there is a detachment of the alloy from the glass, thereby leading to a separation of the alloy from the resin. As a consequence, the SEM observations are difficult to be performed. Further investigations by electrochemical method are thus required in order to have a thorough understanding on the behaviour of Ni-30Cr alloy in N2S.

➢ *Anodic polarisation curves*

The anodic polarisation curve of Ni-30Cr has been observed for three different melt compositions at 1100°C. The anodic polarisation curves of the alloy in the molten glasses have been compiled in Figure 4.19.

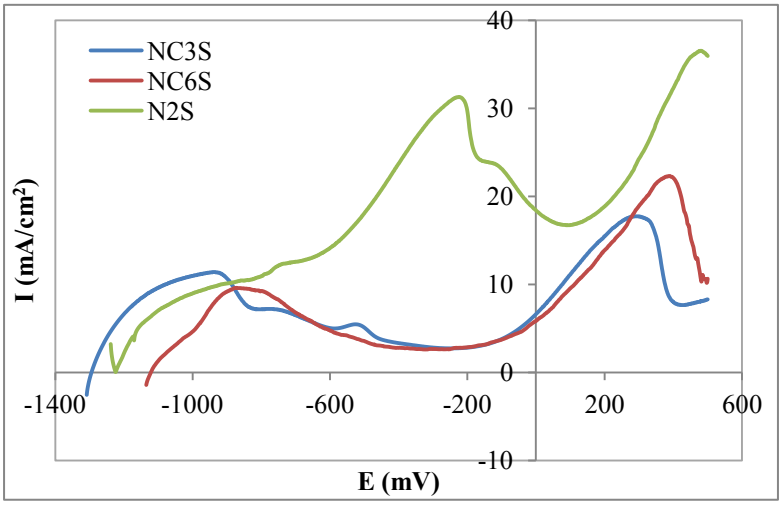

Figure 4.19: Anodic polarisation curves of non-preoxidised Ni-30Cr in the three different glasses at 1100°C

- Na_2O-CaO-3SiO_2 (NC3S) and Na_2O-CaO-6SiO_2 (NC6S)

Both plots exhibit a very similar trend. The alloy is in active state right after immersion in these melts with very low E_{corr} (E_{corr} < -1100 mV). The anodic polarisation in the case of these glasses possesses the same trend of the curve with an existence of a passivation plateau with low current density. The values of the electrochemical characteristics of the Ni-30Cr in NC3S and NC6S determined by the curves have been compiled in Table 4.7.

Table 4.7: Electrochemical characteristics of Ni-30Cr alloy extracted from the I = f(E) curves

Glass	E_c (mV)	I_c (mA/cm^2)	E_p (mV)	I_p (mA/cm^2)	E_{tp} (mV)
NC3S	-937	11.4	-437	3.5	-147
NC6S	-850	9.4	-508	3.5	-80

Table 4.7 reveals that the critical passivation potential, E_c is higher as the basicity decreases. However, the critical current density, I_c decreases with the basicity of the melts since the number of the soluble species that takes part in the reaction becomes more important when the Na content in the melt increases. This peak corresponds to the oxidation of Cr^0 to the Cr^{II} species. In this case, the quantity of Cr^{II} dissolved in the melts increases with the basicity. This phenomenon has been observed by Abdelouhab *et al.*[98] for the pure Cr in binary melt.

The current density on the passivation plateau I_p is exactly the same in both glasses. As a consequence, the alloy is subjected to the same passivation mechanism for both samples, *i.e.* formation of protective Cr_2O_3.

- N2S

Even though N2S possesses almost the same theoretical optical basicity as NC3S, the non-preoxidised Ni-30Cr exhibits a different behaviour when the potential was polarised up to +500 mV. There is no existence of a passivation plateau by increasing the potential. The solubility of Cr in different kinds of glasses must be taken into account. The thermodynamic data on the Cr solubility in the ternary melts will be discussed thoroughly in the next chapter. However, some of data are displayed in this part as reported in Table 4.8.

Table 4.8: Cr solubility (at.% Cr) in soda silicate melts and soda-lime silicate melts at 1200°C in oxidising atmosphere (air)

Cr solubility (at.% Cr)		Glasses		
		N2S[99]	NC3S[This study]	NC6S[This study]
Temperatures	1200°C	2.13(± 0.11)	0.74(± 0.06)	0.42 (± 0.06)
	1300°C (1250°C for N2S)	2.76(± 0.15)	0.84(± 0.03)	0.50(± 0.03)

Even if the temperature range is higher than in the present study, it is obviously seen that the Cr solubility is three times higher in N2S compared to NC3S, and five times higher compared to NC6S. As a consequence, the formation of a protective scale is difficult to be achieved due to the high solubility of Cr in N2S.

The electrochemical behaviour can be directly correlated to the Cr solubility in an equilibrium system. Indeed, the binary melt seems to be much more corrosive than the ternary melt at a given optical basicities (*e.g.* $\Lambda_{N2S} \approx \Lambda_{NC3S}$). Hence, the role played by CaO on the chemical properties (*i.e.* real contribution to basicity, oxide ions activity of the melt) of the ternary glasses seems to be of great importance to explain these phenomena.

- *E_{corr} and Rp measurements for 24 h of immersion*

Since the alloy which has been subjected to the preoxidation treatment in air before the immersion in the melts exhibits a better corrosion protection behaviour, the E_{corr} and Rp values of the preoxidised (2 h at 1100°C in air) alloy have been recorded for 24 h in NC3S and NC6S at 1100°C. The obtained values are compiled in Figure 4.20.

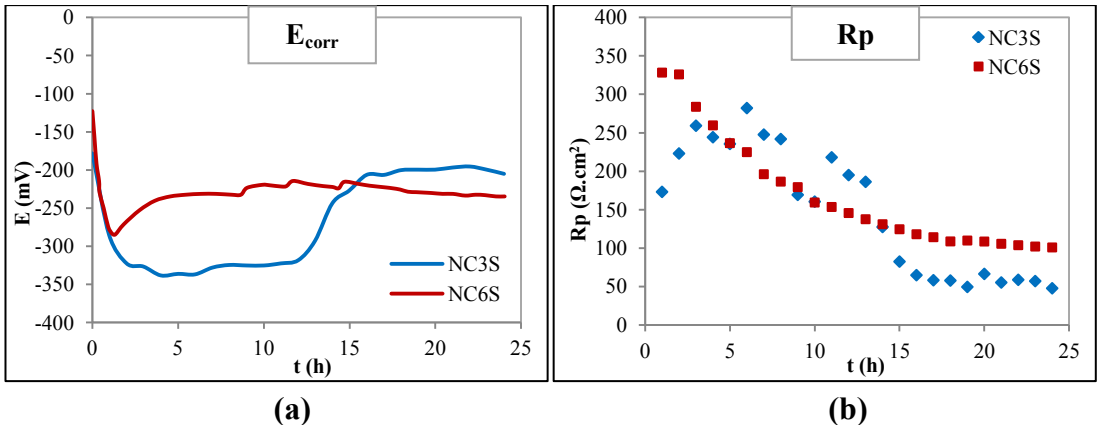

Figure 4.20: Evolution of corrosion potential (E_{corr}) (a) and polarisation resistance (Rp) (b) of preoxidised Ni-30Cr alloy during 24 h of immersion in NC3S and NC6S at 1100°C

The values of the corrosion potentials right after immersion for both NC3S and NC6S are -180 mV and -120 mV respectively. The Rp values which have been recorded after 1 h of immersion in NC3S and NC6S are 170 Ω.cm^2 and 330 Ω.cm^2 respectively. These characteristics show that the alloy is in passive state (domain of Cr^{III}, *i.e.* Cr_2O_3 layer) while having contact with both molten glasses (NC3S and NC6S). In the case of both melts, the potential decreases for the first hours of immersion before starting to increase again. This is called as transition domain. The transition domain corresponds to the region where there is a competition between the dissolution and the development of a protective Cr_2O_3 layer. The transition domain in NC3S is much longer (~ 16 h) as compared to the NC6S (~ 4 h). This behaviour might be explained by a higher Cr content at the interface of alloy/melt in the case of NC3S as shown in Table 4.9.

After 24 h of immersion, the alloy in both melts still exhibits high E_{corr} and Rp values. The alloy in NC3S exhibits a higher E_{corr} after 24 h of immersion, nevertheless the Rp value is higher in NC6S (106 Ω.cm^2) as compared to NC3S (57

$\Omega.cm^2$). The micrographs of this alloy in both melts after 24 h of immersion at 1100°C are represented in Figure 4.21.

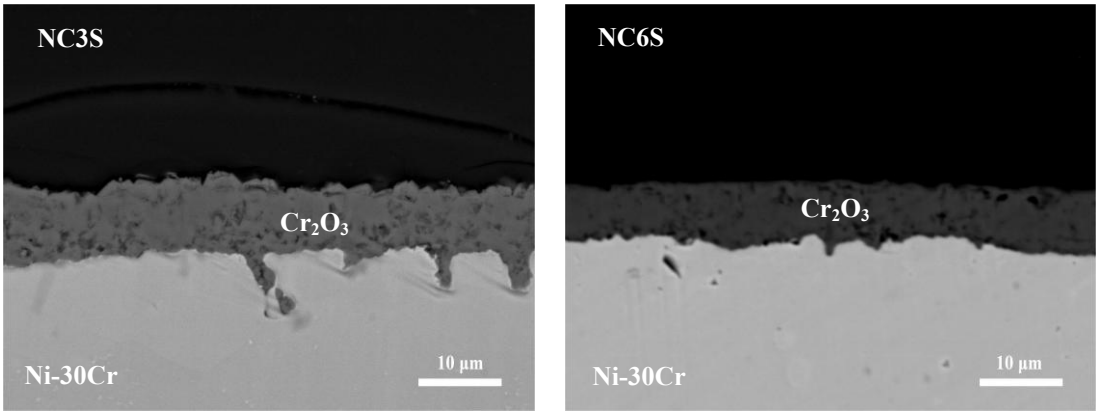

(a) **(b)**

Figure 4.21: Micrographs of preoxidised Ni-30Cr after 24 h immersion at 1100°C in (a) NC3S and (b) NC6S

The micrographs reveal that the protective Cr_2O_3 layer is still effective even after 24 h of immersion at 1100°C in both melts. The X-ray mapping proves that no glass penetration exists in the alloy. The thickness of Cr_2O_3 layer as well as the Cr concentration at the interface has been compiled in Table 4.9.

Table 4.9: The thickness of Cr_2O_3 layer and the Cr concentration measured at the glass/oxide layer interface after 24 h of immersion of preoxidised Ni-30Cr in two different melt compositions at 1050°C

Glasses	Thickness (e) of Cr_2O_3 layer (µm)	Cr content measured at the glass/oxide layer interface (at.% Cr)
NC3S	$6 < e < 10$	0.29
NC6S	$7 < e < 9$	0.15

Figure 4.22 presents a superimposition of these data on the graph presented in Figure 4.17. These new data are in good agreement with the results presented in Figure 4.17 even though the substrate and the experimental temperature are different.

One may conclude that the durability of the Cr_2O_3 layer seems to be dependant on the Cr solubility in the melt. It seems that there is a critical limit of Cr solubility. Beyond this critical value, the dissolution process prevails over the oxide growth, thus leading to the loss of the protective scale.

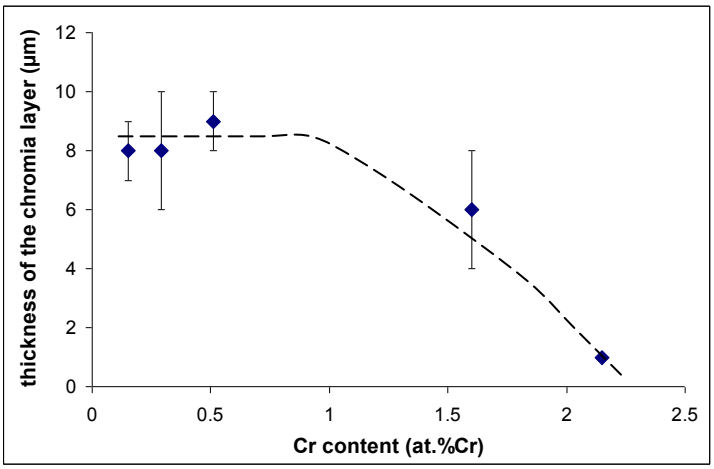

Figure 4.22: Thickness of the Cr_2O_3 layer on the preoxidised Cr or Ni-30Cr samples after 24 h of immersion in N1.5S, N2S and NC3S at 1050°C (or 1100°C for the Ni-30Cr alloy) as a function of Cr content measured near the glass/oxide layer interface. The dotted line is a guide to the eyes.

➢ *Determination of corrosion rates*

The data concerning of the corrosion of preoxidised Ni-30Cr in the two ternary melts are presented in Table 4.10.

Table 4.10: The main corrosion data concerning the corrosion of the preoxidised Ni-30Cr alloy after the immersion in two different melt compositions at 1100°C

Glass	NC3S	NC6S
E_{corr} (mV)	-201 (± 4)	-227 (± 7)
State	Passive	Passive
Anodic reaction	$Cr \rightarrow Cr^{III} + 3e^-$	$Cr \rightarrow Cr^{III} + 3e^-$
Cathodic reaction	$O_2 + 4e^- \rightarrow 2O^{2-}$	$O_2 + 4e^- \rightarrow 2O^{2-}$
B (V)	0.034	0.034
Rp ($\Omega.cm^2$)	60 (± 6)	106 (± 12)
V_{corr} (cm/year)	0.5 (± 0.1)	0.16 (± 0.01)

Even though there is no significant difference of the Cr_2O_3 layer observed after 24 h of immersion of the preoxidised Ni-30Cr in NC3S and NC6S, the corrosion rates calculated from the electrochemical data show that the most basic glass leads to a much higher corrosion rate. This result is coherent with the solubility limit given in Table 4.8, which clearly shows that for a given type of glass (*i.e.* NCxS), the dissolution of the Cr_2O_3 layer will be more severe in a basic glass.

4.1.3. Summary of the behaviour of chromia forming alloys in molten glass media

The isothermal oxidation of Ni-30Cr alloy at 1100°C and 1150°C has proved that the composition contains a sufficient amount of Cr to allow the formation of a protective Cr_2O_3 layer. The exploitation of thermogravimetric analysis allows an access to the parabolic and linear constants, thus allowing the calculation of the oxide thickness as a function of the duration of the heat treatment for both temperatures.

When immersed in molten glass media, both pure Cr and Ni-30Cr alloy are in active states for all studied range of temperatures. Since the corrosion potential is low, the metallic Cr is first oxidised to Cr^{II}. In the case of pure Cr, some needle-like Cr_2O_3 are observed in the glass. This phenomenon is due to the oxidation of Cr^{II} to Cr^{III}, thus inducing the precipitation of the oxide in the glass. A direct immersion of Ni-30Cr in the melt leads to a strong corrosion with ~ 12 μm of glass penetration into the alloy after 24 h of immersion. The corrosion rates are very high, specifically for the pure Cr sample; ~ 15 cm/year for pure Cr, and ~ 5 cm/year for Ni-30Cr.

A preoxidation treatment in air has been performed in order to develop a Cr_2O_3 layer on the surface of the samples before the immersion in the melt. Its resistance against corrosion by molten glass was then tested. After 24 h of immersion in NC3S at 1100°C, Ni-30Cr is in a passive state with an oxide layer a bit thicker (6 - 10 µm) than the one initiated during the preoxidation process (5.5 µm). This observation proves that the oxide formation is still effective during the immersion in the glass and prevails over the dissolution of the oxide. At 1150°C, the immersion of a preoxidised sample leads to an active state. It seems like the dissolution is preponderant as the solubility limit of Cr in the glass increases with the temperature. A depassivation temperature can thus be emphasised in the 1100°C - 1150°C temperature range. However, the pure Cr is in an active state when subjected to the preoxidation at 1100°C before being immersed in the melt at the same temperature. The preoxidation process at 1100°C does not seem to be efficient for the metal. Since the Cr activity is too high, the higher temperature of heat treatment might induce cracks due to compressive stress, thus leading to a direct contact between the metal and the melt. The development of a nitride layer might also contribute to the poor adherence of the Cr_2O_3 layer on the pure metal substrate.

The influence of the melt basicity on the corrosion behaviour has been also studied. In the case of pure Cr, a comparison has been made with previous of the corrosion by binary glasses Na_2O-$xSiO_2$. The overlay of the data (E_{corr} and Rp) of ternary glasses Na_2O-CaO-$xSiO_2$ (Figure 4.15) did not show the expected trend as measured in binary melts when optical basicity or Na_2O activity have been taken into account. A specific role of calcium oxide in the physicochemical properties of molten glass is thus emphasised.

A correlation between the thickness of the Cr_2O_3 layer and the solubility limit has been examined. When only considering these parameters, it is possible to observe an existence of a critical solubility limit. Beyond this limit, it is impossible to maintain the stability of the protective oxide layer.

4.2. Corrosion of NiAl and Ni-8Al-28Cr by molten glass

The study of the corrosion of the alumina forming alloys by molten glass proposed here follows the same approach as in the previous part devoted to the chromia forming alloys. The study of the isothermal oxidation in hot air of these materials which will give information about the growth kinetics of the Al_2O_3 layer has been detailed in Appendix D.

4.2.1. Electrochemical measurements of the corrosion of NiAl and Ni-8Al-28Cr alloys in silicate melt

The corrosion behaviour of NiAl and Ni-8Al-28Cr in soda-lime silicate melts (Na_2O-CaO-$3SiO_2$) was studied at 1100^{o}C. The studies were carried out with the same procedures as in the case of pure Cr and Ni-30Cr alloy.

4.2.1.1. Spontaneous behaviour of NiAl and Ni-8Al-28Cr alloys in NC3S at 1100°C

The spontaneous behaviour of the alloys was first characterised after 24 h of immersion in the melts. Then electrochemical measurements were performed on the samples.

(a) 'Raw immersion' of the alumina forming alloys in the melt

The NiAl plate (NiAl bulk) and Ni-8Al-28Cr rod were directly immersed in NC3S at 1100°C for 24 h. Micrographs of these alloys have been displayed in Figure 4.23 and Figure 4.24 respectively.

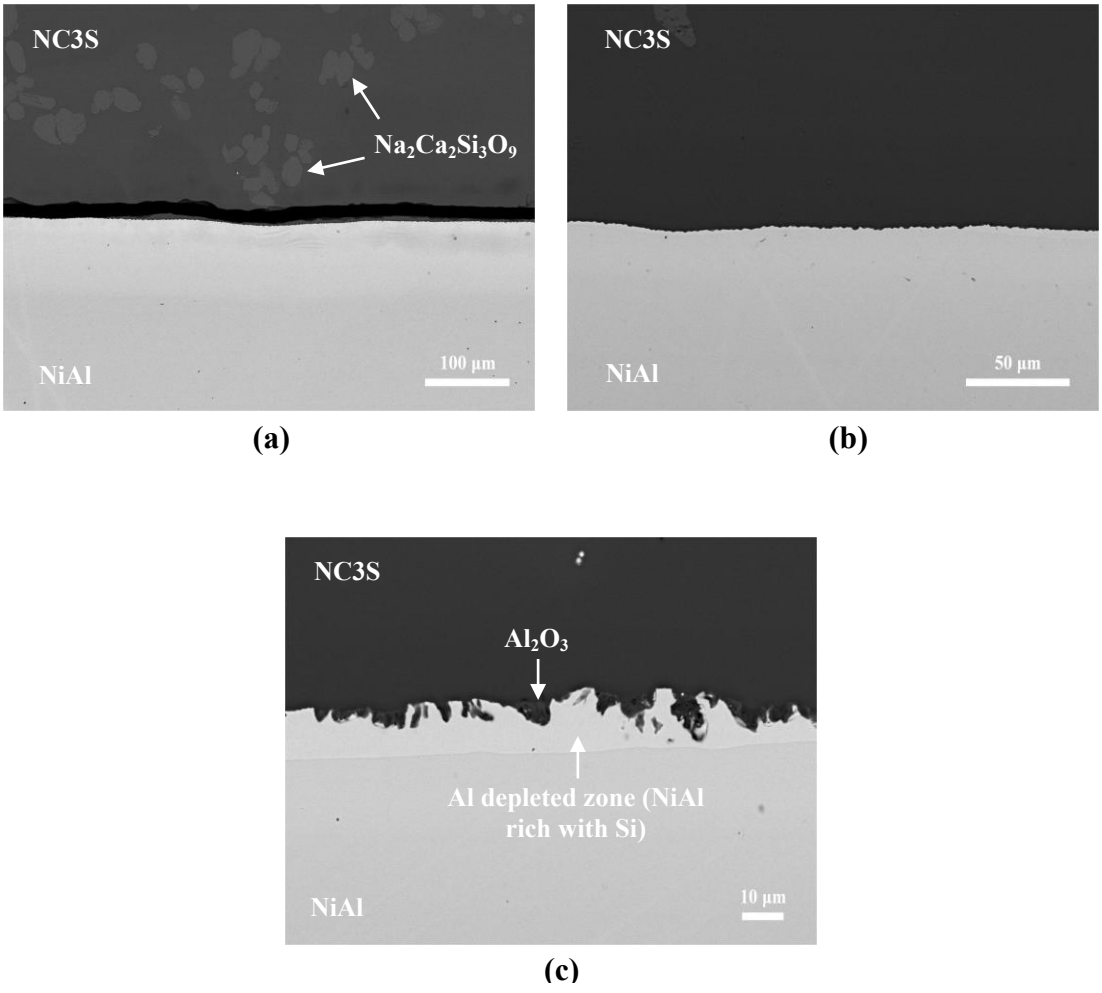

Figure 4.23: Micrographs of NiAl after 24 h of immersion in NC3S at 1100°C with magnification of (a) 200x, (b) 500x and (c) 1000x

In the case of NiAl (Figure 4.23), no oxide layer can be observed. However, some Al_2O_3 agglomerates can be detected. A strong corrosion of the surface is observed, thus leading the alloy to be in an active state. A 10 - 20 µm thickness of aluminium depleted zone is observed, with the presence of silicon. The Al alloy

might have been oxidised by the silica from the glass according the following equations:

Reduction of the silica from the glass network:

$$SiO_4^{4-} + 4e^- \Leftrightarrow Si^0 + 4O^{2-} \quad (4.1)$$

Oxidation of the aluminium:

$$Al^0 \Leftrightarrow Al^{III} + 3e^- \quad (4.7)$$

Some aluminium have been detected in the glass, close to the surface of the alloy. A concentration about 4.4 at.% Al have been measured by EPMA, showing that the main proportion of the alumina formed through Eq. 4.7 has been dissolved in the melt.

The micrographs of Ni-8Al-28Cr (Figure 4.24) reveal the existence of Cr_2O_3 and Al_2O_3 at the interface. The internal oxidation of Al occurs underneath the Cr_2O_3 layer. However, the Cr_2O_3 layer existing at the interface is not compact and adherent enough to provide any protection to the alloy.

As described in Appendix A, the raw Ni-8Al-28Cr alloy consist of γ-(Ni, Al, Cr) matrix in equilibrium with β-NiAl precipitates. The secondary electron images in Figure 4.24(a) clearly shows that all the β-NiAl precipitates have disappeared in a zone close to the surface (with depth around 110 μm). As the β-NiAl phase is much richer in aluminium than the γ-(Ni, Al, Cr) matrix, this Al diffuses to the surface in order to be oxidised into Al^{III} (Eq. 4.7) before being dissolved in the melt. The higher magnification of the SEM micrographs (Figure 4.24(c) and (d)) reveal the existence

of Ni agglomerates at the surface of the alloy/melt. The oxidation of Ni to Ni^{II} will not be occur in this condition since the potential observed in this case (~ 1.4 V) is very low for the reaction of Ni → Ni^{II} to take place.

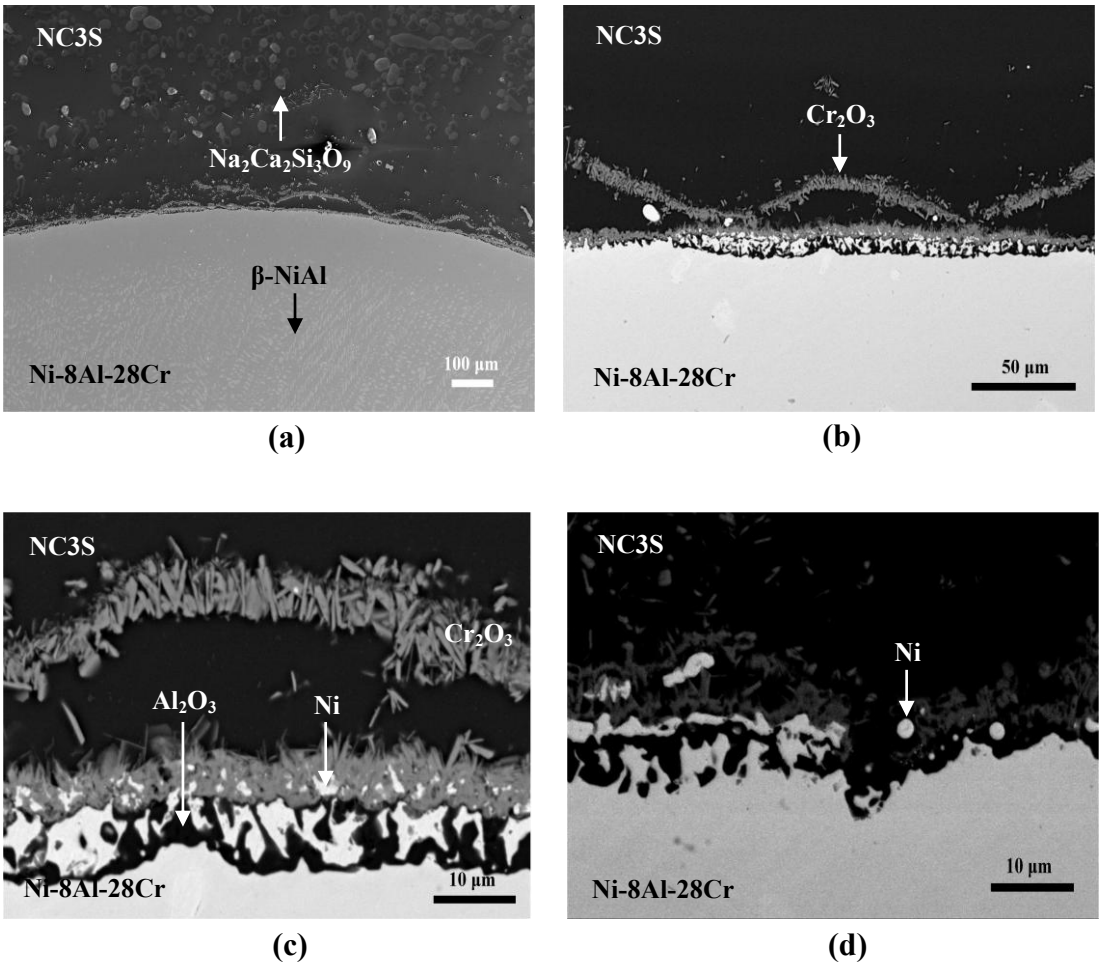

Figure 4.24: Micrographs of Ni-8Al-28Cr after 24 h of immersion in NC3S at 1100°C with magnification of (a) 100x – Secondary Electrons, (b) 500x – Back Scattered Electrons, (c) 2000x – Back Scattered Electrons and (d) 2000x - Back Scattered Electrons

Concentration profiles of the important elements have been performed by EPMA in both cases. Figure 4.25 represents the evolution of the concentration of the metallic elements in the glass, starting from the interface between the alloy and the glass. The plots show that Ni is never detected in the glass whereas a significant

amount of Al is observed in the glass. The amount of Al has been detected starting from more than 5 at.% at the interface and decreasing regularly to 0 after 300 µm from the interface for NiAl sample and 170 µm in the case of Ni-8Al-28Cr sample. One may conclude that a significant amount of Al has been dissolved in the glass and diffuses from the surface alloy/glass.

In the case of Ni-8Al-28Cr, a very few Cr has been detected at the interface of alloy/glass. However, no Cr has been observed after ~ 10 µm of distance from the interface.

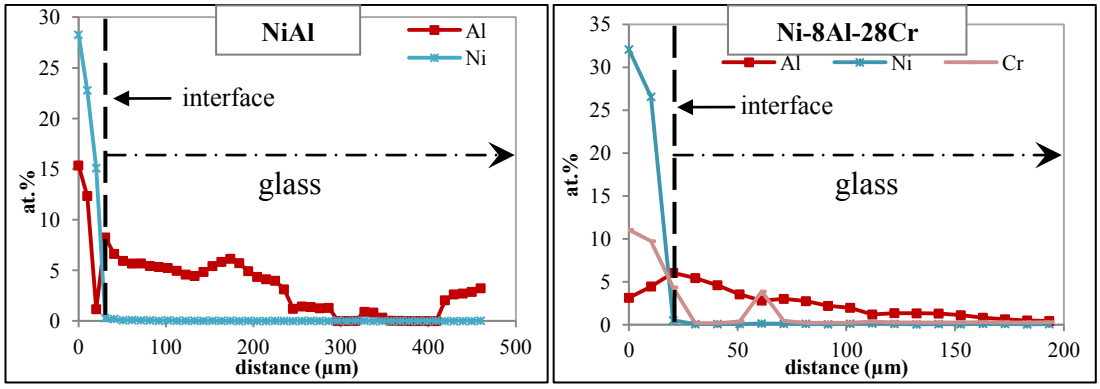

(a) **(b)**

Figure 4.25: The concentration profile of the metal elements in the glass for (a) NiAl (bulk) and (b) Ni-8Al-28Cr after 24 h of immersion in NC3S at 1100°C

The long distance of diffusion which has been observed in Al for both alloys in a given glass composition and temperature represents the high solubility characteristic of this element in the melt. This phenomenon has been previously demonstrated by Manfredo *et al.*[88] (*cf.* Table 2.4 in Chapter 2), who have shown that for a given glass, the Al_2O_3 solubility is > 20 times higher than the Cr_2O_3 solubility.

Figure 4.26 and Figure 4.27 reveal the concentration profile of glass and metal elements measured by EPMA in the NiAl bulk sample and in the Ni-8Al-28Cr sample respectively, after 24 h of immersion in NC3S at 1100°C.

In NiAl sample, Al depletion in the substrate can be clearly observed about 100 µm from the alloy/melt interface. Metallic silicon can also be detected in the alloy, with a concentration decreasing from 5 at.% down to 0 after 60 µm of depth. The presence of silicon confirms the oxidation / reduction reactions proposed in Eq. 4.1 and 4.7.

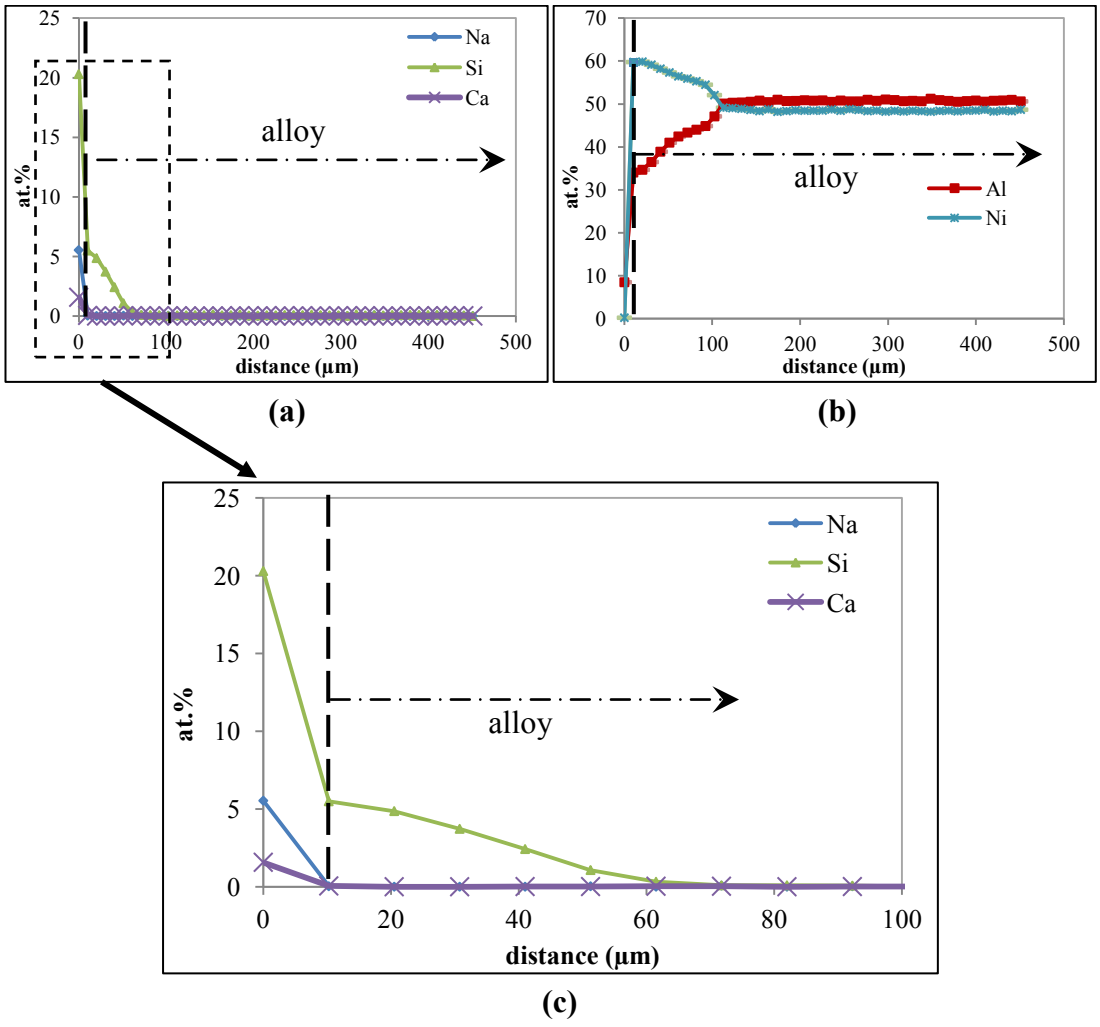

Figure 4.26: The concentration profiles of the (a) Glass elements and (b) Metal elements in the alloy for NiAl (bulk) after 24 h of immersion in NC3S at 1100°C. The plots in (c) represent the enlargement of the concentration profile in (b) for the distance of 100 µm from the surface of alloy/glass

Figure 4.27(a) shows that no metallic silicon can be detected in the Ni-8Al-28Cr alloy. The Al depletion can also be detected in the γ-(Ni, Al, Cr) matrix around 100 - 110 µm. This depletion zone in the matrix corresponds generally to the zone free of β-NiAl precipitates observed in Figure 4.24(a).

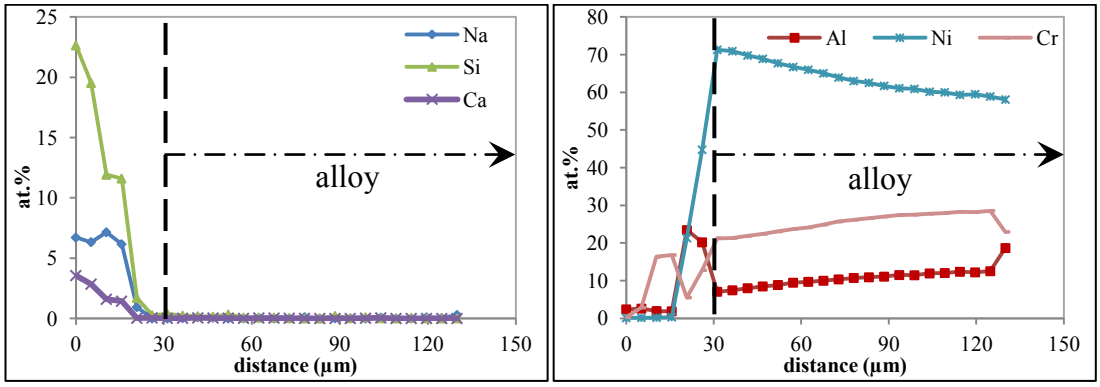

Figure 4.27: The concentration profiles of the (a) Glass elements and (b) Metal elements in the alloy for Ni-8Al-28Cr after 24 h of immersion in NC3S at 1100°C

(b) Measurement of Ecorr and Rp

The measurement of the corrosion indicators (E_{corr} and Rp) have been performed on cemented NiAl and Ni-8Al-28Cr. The electrodes have been directly immersed in NC3S at 1100°C. The E_{corr} and Rp as a function of experimental duration have been plotted in Figure 4.28 for both alloys.

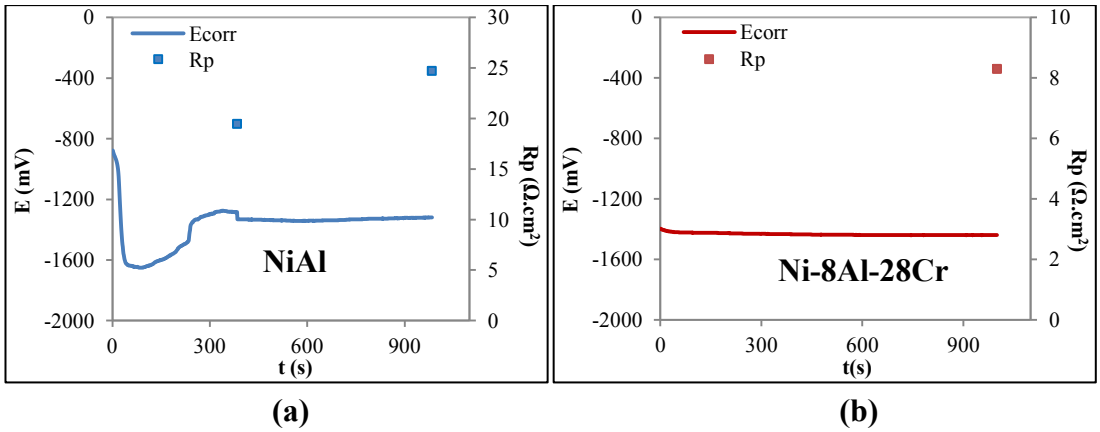

Figure 4.28: Corrosion potentials (E_{corr}) and polarisation resistance (Rp) of (a) NiAl (cemented) and (b) Ni-8Al-28Cr in NC3S at 1100°C

In the case of NiAl alloy, the alloy has been stabilised at the potential of ~ 1.3 V. However the Rp values measured are quite high and not coherent with the observed E_{corr}. Some phenomena might occur in cemented NiAl at this condition. If the NiAl is totally dissolved during the immersion, the high Rp values could be attributed to the oxidation of Ni to Ni^{II} from the substrate. However the measured E_{corr} shows a very low value for this reaction which is supposed to occur at E = -0.8 V (Figure 2.5). The second hypothesis is related to the change in the viscosity of the glass when there is a partial dissolution of aluminium in the melt. Aluminium which can behave as a network modifier or network former exhibits a high dissolution in the melt. The melt might be saturated with Al, thus restricting any further reaction at the surface of the alloy/melt. As a consequence, the further corrosion might decrease, thus high Rp values have been observed.

For Ni-8Al-Cr, the E_{corr} (< 1.2 V) and Rp (< 10 Ω.cm²) values are very low, thereby confirming the non-protective behaviour (active state) of the alloy. According to the potentials scale presented in Figure 2.5, the potentials are low enough to explain the oxidation of Cr^0 to Cr^{II}. As a consequence, the oxidation of Ni^0

to Ni^{II} which exhibits a higher former potential is not possible to occur. Thus, this explanation can be a reason to the presence of pure metallic nickel agglomerates in Figure 4.24.

(c) Anodic polarisation of NiAl and Ni-8Al-28Cr alloys in NC3S at 1100°C

The anodic polarisation curves were recorded for NiAl and Ni-8Al-28Cr from E_{corr} - 20 mV up to +500 mV with a scan rate (υ) of 1 mV/s after ~ 20 min of immersion in NC3S at 1100°C. The curves are reported in Figure 4.29.

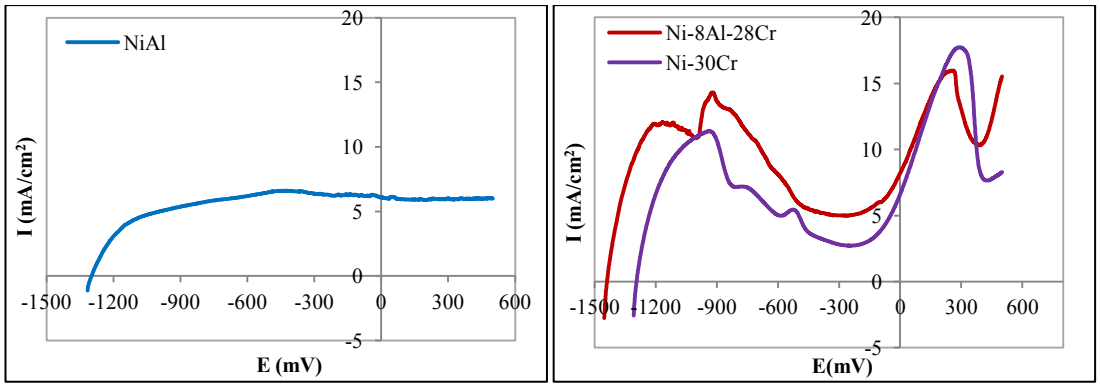

(a) **(b)**

Figure 4.29: Anodic polarisation curves of (a) NiAl (cemented) and (b) Ni-8Al-28Cr after ~ 20 min of immersion in NC3S at 1100°C

The anodic polarisation curve of NiAl does not exhibit the general trend of the curve. The current density seems to be constant when the potential is polarised. This phenomena might be attributed to the faster dissolution of Al to Al^{III} when the potential is polarised. As a consequence, only the bare Ni rod might be in contact with the melt after a very short of experimental duration due to the faster dissolution of NiAl coating in the melt. Hence, a quite high current density (~ 5 mA/cm^2) might represent the reaction of pure Ni rod.

The anodic polarisation plot of Ni-8Al-28Cr presents the same trend as pure Cr and Ni-30Cr alloy. The critical current density measured here (~ 15 mA/cm²) is a bit higher than Ni-30Cr (~ 12 mA/cm²) but much lower than pure Cr (~ 70 mA). As a consequence, it seems that the Ni-8Al-28Cr alloy has the same ability as Ni-30Cr alloy to develop a passivation layer. The passivation plateau observed in Ni-8Al-28Cr is as wide as for pure Cr and Ni-30Cr alloy and it is comprised between ~ -0.6 V and ~ 0 V. The passivation plateau of Ni-8Al-28Cr exhibits slightly higher current density (~ 5 mA/cm²) as compared to Ni-30Cr (~ 3 mA/cm²). This result reveals the possibility of forming the different oxides for Ni-30Cr and Ni-8Al-28Cr *i.e.* Cr_2O_3 and Al_2O_3 respectively.

4.2.1.2. Behaviour of preoxidised NiAl and Ni-8Al-28Cr alloys in NC3S at 1100°C

As in the case of chromia forming alloys, a preoxidation treatment has been performed here in order to form an oxide layer on the surface, before immersion of the sample in molten glass. The results of the isothermal oxidation study (Appendix D) reveal that the kinetics of formation of an alumina layer is much slower than for chromia. As an example, Table 4.11 gives the theoretical thickness of an alumina layer formed after 2 h of preoxidation of Ni-8Al-28Cr at 1100°C. It is 10 times thinner than the chromia layer formed in the same conditions as Ni-30Cr.

Table 4.11: Thickness of the alumina layer formed after 2 h and 24 h of preoxidation in air for Ni-8Al-28Cr alloy at 1100°C

Time of preoxidation (h)	2	24
Ni-8Al-28Cr alloy (µm)	0.5	1.6

As a consequence, in order to have a sufficient Al_2O_3 layer on the Ni-8Al-28Cr alloy, a preoxidation of 24 h at 1100°C has been performed on the alloy, leading to a 1.6 μm thick alumina layer. It has not been possible to determine any oxide growth kinetic data (k_p) on the NiAl sample, but as it is considered as an alumina forming alloy, the same treatment has been performed for preoxidation. In order to avoid any spallation of the oxide layer by thermal shock, the electrodes were preoxidised just above the crucible containing the melt before being immersed in the melt.

(a) Morphology of the preoxidised alloys after immersion in NC3S at 1100°C

Micrographs of the electrodes quenched after 2 h of immersion in NC3S are presented in Figure 4.30 and Figure 4.32. As they have not been polarised during the acquisition of the electrochemical data, these samples were not destroyed, thus representing the actual mechanisms occurring at the interface.

On the cemented NiAl sample (Figure 4.30), no NiAl coating has been observed on the surface of the sample due to the great dissolution of Al in the melt. Two different contrasts have been verified in the micrographs. The top layer with the thickness of ~ 150 μm from the surface is attributed to the Ni metal with few dissolved Al and Si in it whereas the second contrast represents the Ni substrate. A concentration of about 2 at.% Al has been measured in the glass close to the surface. It can be seen that a lot of Al_2O_3 particles are embedded in the surface of the alloy.

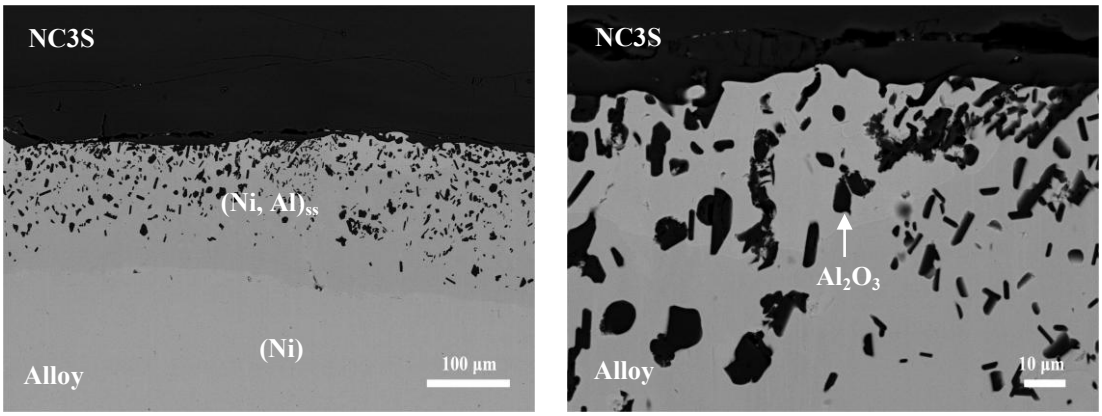

(a) (b)

Figure 4.30: Micrographs of preoxidised NiAl (cemented) (24 h in air at 1100°C) after 2 h of immersion in NC3S at 1100°C with magnification of (a) 200x and (b) 1000x

Figure 4.31 presents the concentration profiles of Si, Ni and Al in the alloy. Some metallic silicon is detected about hundred micrometers from the surface. This observation proves that some silica from the melt have been reduced to metal state and have diffused into the alloy.

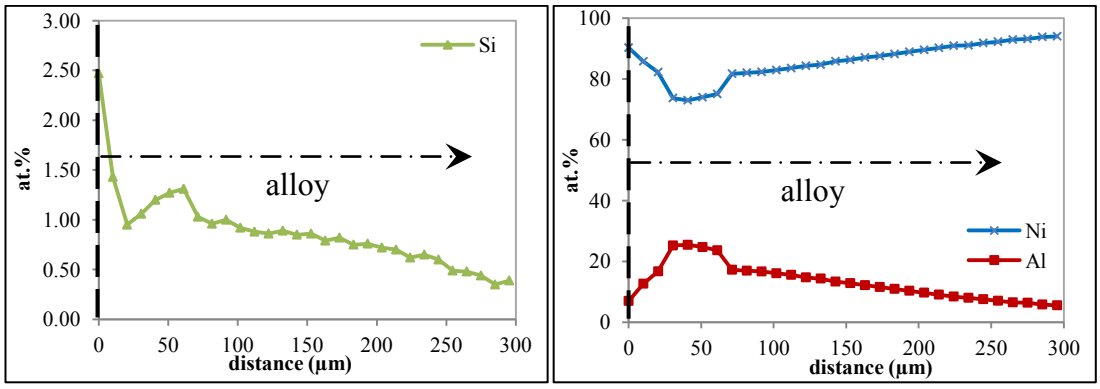

(a) (b)

Figure 4.31: The concentration profile of (a) Glass element and (b) Metal elements in the alloy for preoxidised NiAl (cemented) (24 h in air at 1100°C) after 2 h of immersion in NC3S at 1100°C

The concentration profiles of Al and Ni elements in Figure 4.31(b) shows a significant difference as compared to the profiles of NiAl (cemented) before the

immersion in the melt. After preoxidation and immersion in the melt, a very strong Al depletion is observed about 30 µm from the surface. The Al content never exceeds 30 at.%, thus making it out of the range of NiAl domain according to the phase diagram (Appendix B). Almost all the Al from the initial cemented coating has been dissolved in the glass. However, the traces of this element are still detected at 300 µm from the surface. A little amount of Al might also diffuse into the Ni substrate.

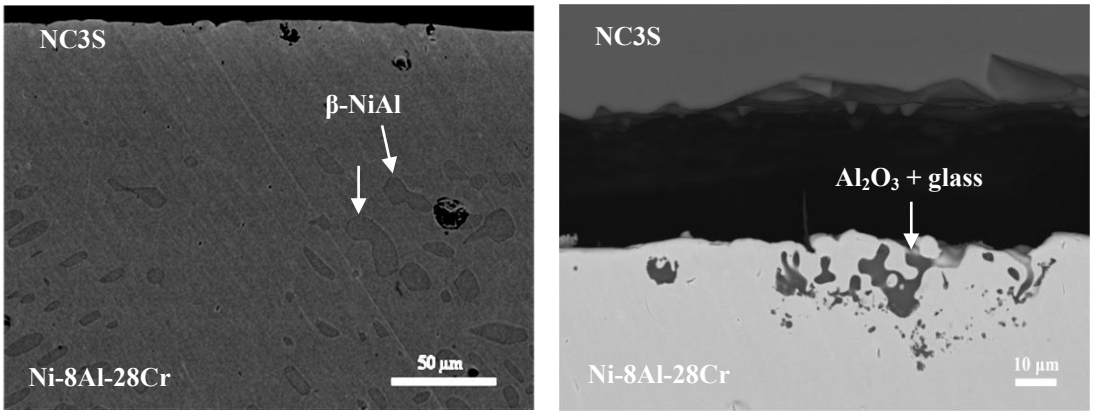

(a) **(b)**

Figure 4.32: Micrographs of preoxidised Ni-8Al-28Cr (24 h in air at 1100°C) after 2 h of immersion in NC3S at 1100°C with magnification of (a) 500x and (b) 1000x

The micrographs of the preoxidised Ni-8Al-28Cr after the immersion in NC3S are shown in Figure 4.32. An existence of grain-free zone is evident as has been observed in the case of the spontaneous behaviour of this alloy at 1100°C (Figure 4.24(a)). After 2 h of immersion, the depth of the zone is ~ 50 - 60 µm (compared to 110 µm after 24 h of immersion as shown in Figure 4.24(a)). Hence, as mentioned previously, this is due to the diffusion of Al through the alloy to the glass, where it is oxidised and dissolved in the melt. Few alumina particles are remaining at the surface but most of the oxide has been dissolved in the glass.

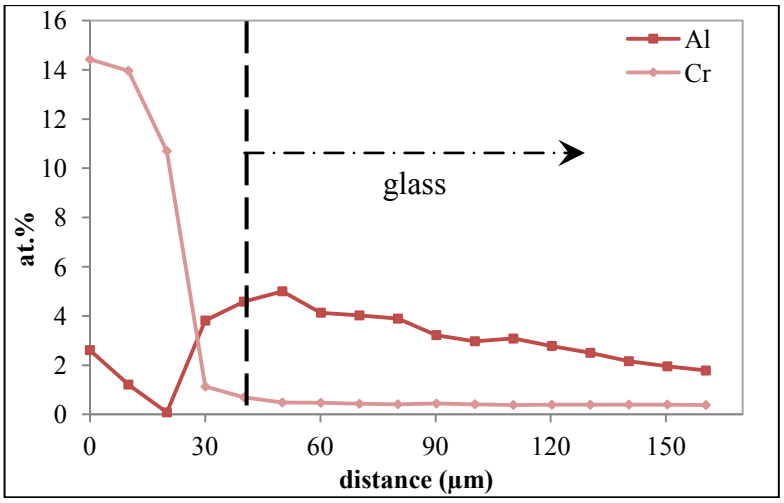

Figure 4.33: The concentration profile of metal elements in the glass for preoxidised Ni-8Al-28Cr (24 h in air at 1100°C) after 2 h of immersion in NC3S at 1100°C

The concentration profiles of Al and Cr have been measured by EPMA in the glass (Figure 4.33) close to the surface of the alloy. 4.79 at.% Al content has been detected at the interface. About 2 at.% of Al is still detected at 150 µm from the interface. However, the Cr content is very low (0.39 at.%) at the interface as compared to Al. These results emphasise the high solubility of Al compared to Cr.

As in Figure 4.31, the concentration profiles of Si and alloying elements in the alloy are reported in Figure 4.34. The metallic Si profile proves the reduction of silica from the melt and the diffusion of this element into the alloy. The Al depletion is also observed about 50 µm from the surface. A sudden increase in Al and a decrease in Cr represent the region with the remaining NiAl precipitates. It is noteworthy that the Al content in the β-NiAl phase after the immersion in the melt is lower than its initial composition; ~ 36 at.% for the raw alloy as presented in Appendix A and ~ 30 at.% after the immersion. Thus, one may conclude that the Al depletion can thus be observed in all phases of the alloy; β-NiAl and $(Ni, Al, Cr)_{ss}$.

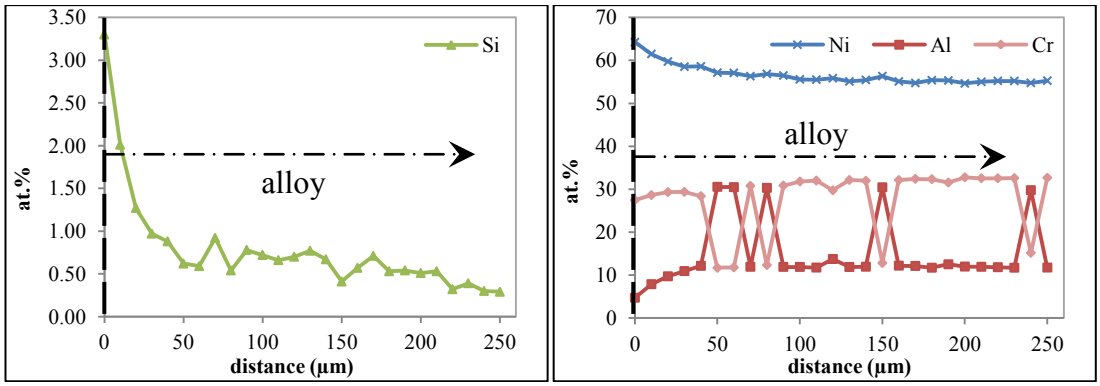

(a) **(b)**

Figure 4.34: The concentration profile of (a) Glass element and (b) Metal elements in the alloy for preoxidised Ni-8Al-28Cr (24 h in air at 1100°C) after 2 h of immersion in NC3S at 1100°C

(b) Measurement of Ecorr and Rp

The evolutions of E_{corr} and Rp as a function of time for the preoxidised samples are presented in Figure 4.35. For the Ni-8Al-28Cr sample which has been preoxidised during two hours (Figure 4.35(a)), the behaviour is exactly the same with the spontaneous behaviour of this alloy. The alloy exhibits very low E_{corr} (< -1.2 V) and Rp (< 10 Ω.cm²). The oxide layer formed during 2 h of preoxidation is not sufficient to give any protection to the alloy. This observation is coherent with the results of the calculation of oxide layer thickness in Table 4.11.

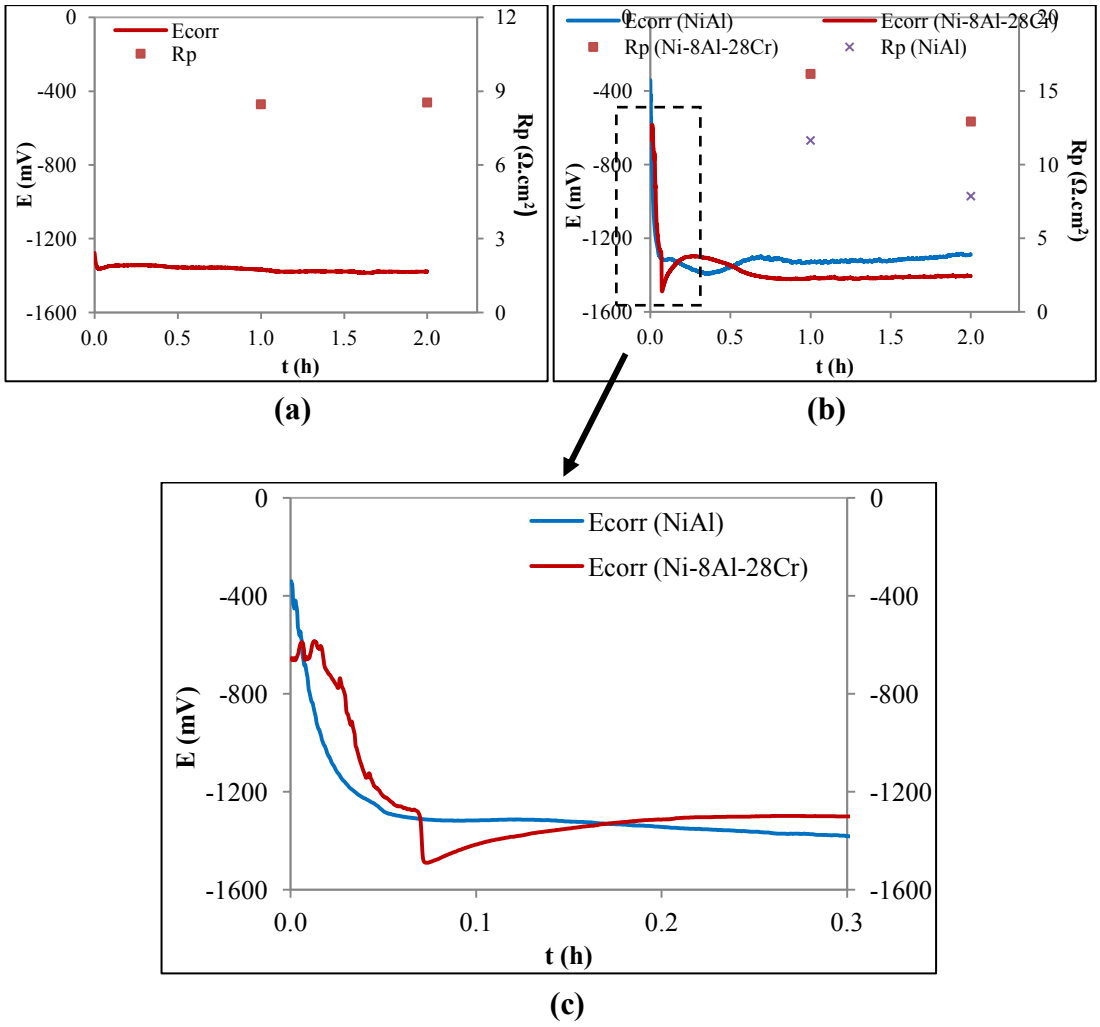

Figure 4.35: Corrosion potentials (E_{corr}) and polarisation resistance (Rp) of (a) preoxidised (2 h in air at 1100°C) Ni-8Al-28Cr, (b) preoxidised Ni-8Al-28Cr and NiAl (24 h in air at 1100°C) after 2 h of immersion in NC3S at 1100°C. Plots in (c) represent the enlargement of the first hour of immersion in graph (b)

After 24 h of preoxidation, for both NiAl and Ni-8Al-28Cr, the potential is much higher (> -0.6 V). Thus, It can be assumed that the alloys have been covered by the oxide before the immersion. However, the potential is decreasing very fast, and it goes down to the active domain in a few minutes (less than 5 minutes for both alloys). During this short time, the alumina layer is completely dissolved in the melt. After this, there is a direct contact between the glass and the alloy, thus explaining the low values of potential and Rp. It must be noted that the Rp values could not be

measured when the samples in the passive domain as they did not remain passive long enough to allow the measurement.

(c) Evaluation of the solubility of Al_2O_3 in ternary glasses

The poor behaviour of alumina forming alloys against corrosion can be explained by the high solubility of alumina in molten glass. As presented in the literature review (Chapter 2), Manfredo *et al.*[88] have evaluated the solubility of alumina which is around 21.3% (mol% of oxide), which corresponds to 23.8 at.% in a soda-lime glass at 1300°C.

In order to have an idea of the order of magnitude of alumina in the glasses of this study, the same kind of measurements have been performed in NC3S, NC4S, NC5S and NC6S. In a platinum crucible, 5 g of glass was mixed with 23 to 29 wt.% of amorphous Al_2O_3. The mixture was then placed in a furnace at 1200°C for 3 days before being quenched. The samples were then embedded in epoxy resin for the EPMA measurements. The Al content was measured close to the remaining Al_2O_3 grains. The results are reported in Table 4.12.

Table 4.12: Al_2O_3 solubility in ternary glasses at 1200°C

Glass	NC3S	NC4S	NC5S	NC6S
Al_2O_3 solubility (at.% Al)	9.8 (±0.1)	10.6 (±0.1)	10.0 (±0.3)	8.3 (±0.3)

The Al contents are in the same range for the four glasses. These values are 10 times higher than the Cr solubility measured by Khedim *et al.*[99] in NC3S at the same temperature (0.96 at.% Cr). This is thus coherent with all the results dealing with the alumina forming alloy. As alumina has a very high solubility in molten

glasses, this oxide cannot be used to protect any alloy against corrosion in this kind of media.

The solubility values are twice lower than the ones measured by Manfredo *et al*.[88] The immersion was performed in such a long time (3 days) in both cases. Other experiments performed in this study have shown that the dissolution kinetics of Al_2O_3 can be relatively long to reach the high limit of solubility. The goal of the experiments performed here is to show that alumina exhibits a much higher solubility than chromia, explaining the poor corrosion resistance of alumina forming alloys. A more accurate study would be required to determine the exact limit of solubility of alumina in ternary glasses, taking into account the time to reach equilibrium as well as the nature of the starting alumina powder.

4.2.2. Summary of the behaviour of alumina forming alloys in molten glass media

The isothermal oxidation of Ni-8Al-28Cr and NiAl showed that both alloys are alumina forming. The parabolic constant k_p could be determined for Ni-8Al-28Cr.

The raw immersion of both alloys in molten glass did not lead to the formation of an oxide layer. The alloys are in active state, and a huge Al loss is observed. This is in accordance with the high solubility values given in the literature and has been experimentally confirmed herein.

The polarisation curves show that passivation might be possible. After an adapted preoxidation treatment, no effect has been observed against corrosion: no oxide layer remaining after immersion in the glass and a huge amount of Al is dissolved in the glass. The alumina layer has dissolved in the melt in a few minutes for both materials, according to the potential measurements.

As a conclusion, the comparison between chromia forming alloys and alumina forming alloys give a huge advantage to chromia forming alloys. Alumina possesses such a high solubility in molten glass media, thus making it impossible to be used as a protective layer against corrosion. Chromia forming alloys possess a great potential since the solubility limit of chromia is one of the lowest amongst several oxides. It has been emphasised here that the solubility limit is the main parameter governing the ability of chromia to give protection to the alloy. The oxide growth is always in competition against the dissolution in the glass. Even if the solubility limit of chromia is low, there is an existence of a critical value. Beyond this value, the dissolution prevails over oxide growth, thus cancelling the protection of the alloy against glass corrosion.

As a consequence, the study of the different parameters governing the physicochemical properties of chromium oxide in the melts will be detailed in the next chapter.

CHAPTER 5

KINETICS AND THERMODYNAMIC APPROACH OF CHROMIA SOLUBILITY IN SILICATE MELTS

Introduction

This chapter is devoted to a thorough analysis on the physicochemical properties of chromia (Cr_2O_3) in soda-lime silicate melts. The studies in the previous chapter have proved the influence of the temperature and melt compositions on the corrosion behaviour of metal and alloys by molten glasses which is related to the stability of the chromia protective layer at the interface. The influence of the different atmospheres on the corrosion mechanisms of different alloys in industrial glasses have been also shown by several authors[68,115]. As a consequence, it is important to have a thorough investigation on the behaviour of Cr_2O_3 while having contact with molten glasses. This is due to the fact that chromium which is a multivalent element has an ability to exhibit several oxidation states depending on the conditions of the system.

The influence of temperature, basicity (*i.e.* glass composition) and melt compositions on the Cr_2O_3 solubility in binary soda silicate melts (simple binary system) has been proven by Khedim *et al.*[11,99,103,104]. Thus, the behaviour of Cr_2O_3 in melts will be thoroughly studied here by working on ternary soda-lime silicate melts at some specific conditions. The glasses that have been studied are soda lime silicate melts with Na_2O-CaO-$xSiO_2$ (x = 3, 4, 5 and 6; noted here as NCxS) compositions. In order to control the experimental parameters which are the temperature ($1200^oC \leq$

T ≤ 1350°C), the oxygen fugacity (-12 ≤ log fO_2 ≤ -0.6) and the melt basicity (*i.e.* glass compositions), the experiments were performed in a closed system which was developed in a previous work[105].

In order to quantify the solubility of Cr_2O_3 in melts, it is important to ensure an attainment of dissolution equilibrium which involves multistep reactions of chromium-bearing species. As a consequence, the first part of this chapter is devoted to the study of the dissolution kinetics of Cr_2O_3 in the melts. Then, the thermodynamic of Cr_2O_3 in the melts will be discussed in the second part of this chapter.

5.1. Dissolution kinetics of Cr_2O_3 in the Na_2O-CaO-xSiO_2 (NCxS) system

The physicochemical behaviour of Cr_2O_3 in molten glass has been reviewed and detailed in Chapter 2 (part 2.3.1.). All the important equations dealing with the acid-base and redox reactions have been defined in Chapter 2 (part 2.3.1).

A kinetic study on the dissolution of Cr_2O_3 in binary silicate melts (Na_2O-SiO_2) has been performed by Khedim *et al.*[103] at different temperatures, melt basicities and oxygen fugacities. Nevertheless, there is no experimental data dedicated to the dissolution equilibrium of Cr_2O_3 in soda lime silicate melts (Na_2O-CaO-SiO_2). Therefore, the work presented here is focused on the dissolution kinetics of Cr_2O_3 in soda lime silicate melt in order to evaluate the time required to reach the equilibrium of the process. The information from this work is not only important for the continuity of the research on the Cr solubility in the melt but it could also provide

an insight into the chemical mechanisms of redox reactions in the molten glass media.

The studies were carried out for different temperatures, melt compositions and oxygen fugacities. A thorough analysis has been performed on the samples in order to estimate the time to reach the equilibrium in the system. This information is important in order to have an accurate value of Cr solubility in the melts and to allow a comparison of the limit of Cr solubility measured in various conditions which may have a profound influence on the time to reach the equilibrium.

Focus is also drawn to the mechanisms and difficulties to achieve the dissolution equilibrium of Cr_2O_3 in the melt. Since the redox equilibrium is interrelated with the oxygen diffusion, a first attempt has been made in order to estimate the diffusion coefficient of oxygen in soda lime silicate melt for a given temperature, melt composition and oxygen fugacity.

The experiments were performed for different oxygen fugacity (fO_2), two different temperatures (1200^{o}C and 1300^{o}C) and melt compositions. However, only the significant results will be shown and discussed in detail herein. Since the aim of this work is to determine the time to reach the dissolution equilibrium in this system, the method of analysis is focused. The measurements were performed throughout the samples (rim and core) in order to measure the distribution of dissolved Cr in these two regions. The areas of analyses on the samples are shown in Figure 5.1. The equilibrium of Cr dissolution was expected to be achieved when there is a homogeneous Cr concentration throughout the samples. However, a deviation from

the conventional analysis existed when dealing with long duration of heat treatment which will be discussed precisely in this chapter.

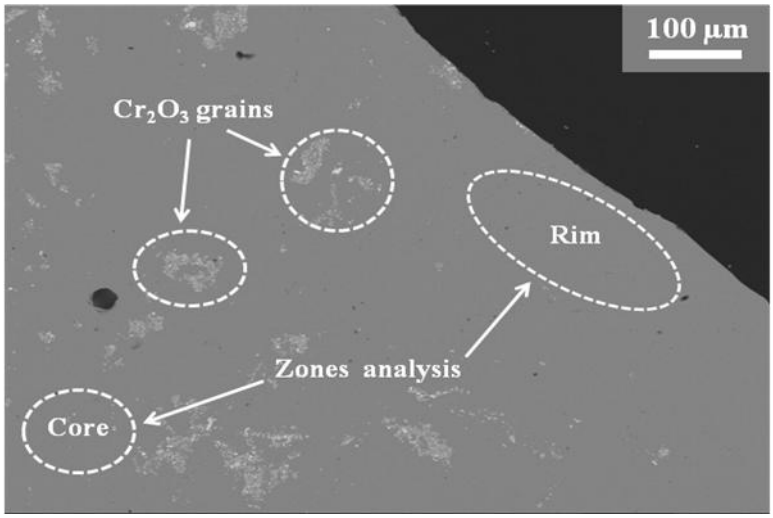

Figure 5.1: Cross section of a sample showing the analysed areas

5.1.1. Influence of oxygen fugacity (fO_2)

The oxygen fugacity (fO_2) of the system was controlled by solid MO_x/MO_y buffers (M = metallic element) which were determined by Ellingham diagram. The details of the experimental device have been discussed thoroughly in Chapter 3. The influence of oxygen fugacity on the dissolution equilibrium of Cr_2O_3 in silicate melts has been investigated for several melt compositions and different temperatures. However, the details of the mechanisms will be discussed based on the works performed on Na_2O-CaO-$5SiO_2$ (NC5S) at 1300°C for two different fO_2; oxidising (air) and reducing (Fe/FeO) conditions.

5.1.1.1. Oxidising condition (air)

The experiments were performed for a wide range of experimental durations (t = 1h, 4h, 9h, 24h and 48h). In order to be higher than the solubility limit of Cr (saturation) in the melt, 5 to 10 wt.% of Cr_2O_3 have been added in NC5S. Figure 5.2

illustrates the experimental results for the evolution of Cr solubility measured in soda-lime silicate glass (NC5S) when melted at 1300 ^{o}C under oxidising condition (air). The results are displayed as a plot of concentration of dissolved Cr (at. %) as a function of time (h) for both rim and core of the samples. The optical observation on all samples shows the existence of yellowish colouration which is an indication of the presence of Cr^{VI} species.

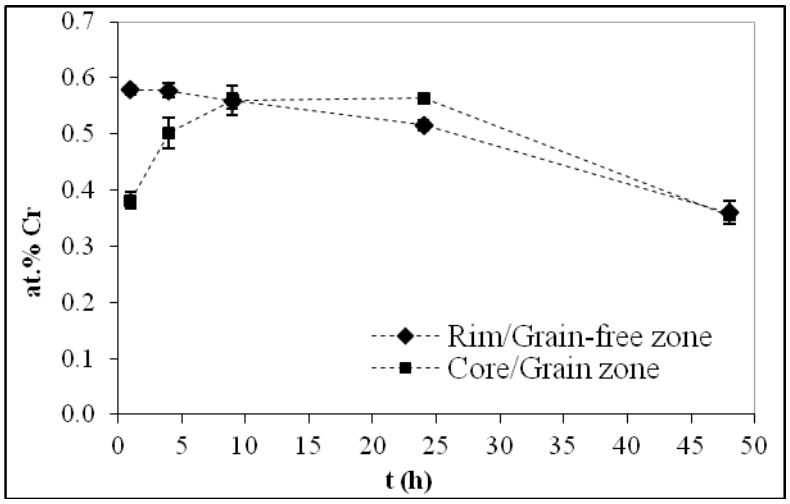

Figure 5.2: Plots of distribution of dissolved Cr (at.%) as a function of time in NC5S at 1300^{o}C under oxidising atmosphere (air). The dotted lines are guides to the eyes

(a) Short experimental duration (1 h ≤ t ≤ 4 h)

At t = 1 h, there is a noticeable difference of concentration of dissolved Cr between the rim and core of the sample where the Cr solubility seems to be higher at the rim of the glass ball (Figure 5.2). Nevertheless, the further investigation by SEM at t = 1 h (Figure 5.3) shows no significant difference of Cr_2O_3 grains distribution between these two regions (rim and core) of the sample. By prolonging the

experimental duration to 4 h, the difference of Cr solubility between the rim and the core seems to be minimised (Figure 5.2).

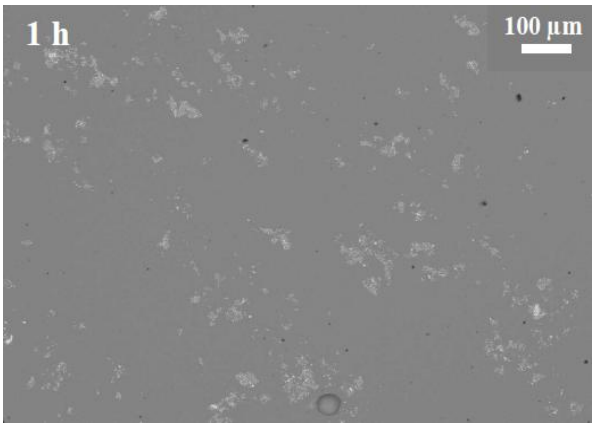

Figure 5.3: Distribution of Cr_2O_3 grains in NC5S at 1300^{o}C under oxidising atmosphere (air) after 1 h of experimental duration

In order to describe these phenomena, a mechanism of Cr_2O_3 dissolution in molten glass under oxidising atmosphere (air) has been proposed. This mechanism has been simplified by schematics in Figure 5.4. Since Cr is a multivalent element, it could exhibit different oxidation states depending on the environmental conditions. Upon heat treatment, the Cr_2O_3 grains will dissolve in the melts by following an acid-base reaction to form a Cr^{III} oxo-complex (*cf.* Eq. 2.46 in Chapter 2). By introducing the oxygen into the reaction, the Cr^{III} will be oxidised to Cr^{VI} depending on the dissolved oxygen content in the melt (*cf.* Eq. 2.47 in Chapter 2). Furthermore, Schreiber *et. al*.[116] have also proved that the rate determining step in the attainment of redox equilibrium in the melts is controlled by the diffusion of oxygen within the melt.

At a very short experimental duration (t = 1 h), the oxidation of Cr^{III} to Cr^{VI} may take place initially at the rim of the sample since the oxygen is higher at the surface of the sample that is in contact with the oxidising atmosphere (air) (Figure 5.4). Furthermore, an optical observation shows the existence of yellowish colouration at the rim and the greenish zone at the core of the sample which confirms the major contribution of Cr^{VI} and Cr^{III} respectively. The Cr solubility in the melt is higher at the rim of the sample due to the existence of Cr^{III} + Cr^{VI}. However, only Cr^{III} is expected to dominate in the core of the sample for a very short experimental duration. By prolonging the time to 4 h, the oxidation will move forward to the core of the sample, thus increasing the concentration of dissolved Cr in this region.

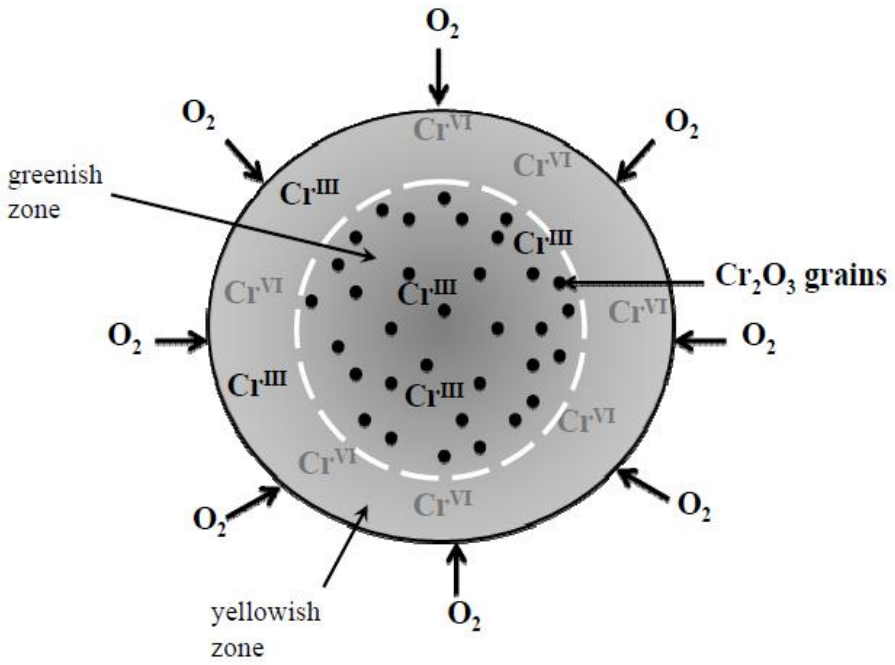

Figure 5.4: Schematic of dissolution mechanism of Cr_2O_3 in molten glass under oxidising condition (air) for a short run duration

(b) Long experimental duration (9 h ≤ t ≤ 48 h)

However, the gravity effect which influences the distribution of Cr_2O_3 grains in the melts should be taken into account while considering the time to reach the

equilibrium. At t ≥ 9 h, the grains assemble at the bottom of the glass ball. Consequently the rim and the core of the sample are no longer distinguishable. Thus, at t = 9 h and 24 h, the measurements have been performed for two different zones *i.e.* grain-free zone and grain zone (Figure 5.5). At t = 9 h, the Cr solubility in both regions has the same value. Nevertheless, the concentration of dissolved Cr increases in the grain zone while it decreases in the grain-free zone when the time is prolonged to 24 h (Figure 5.2).

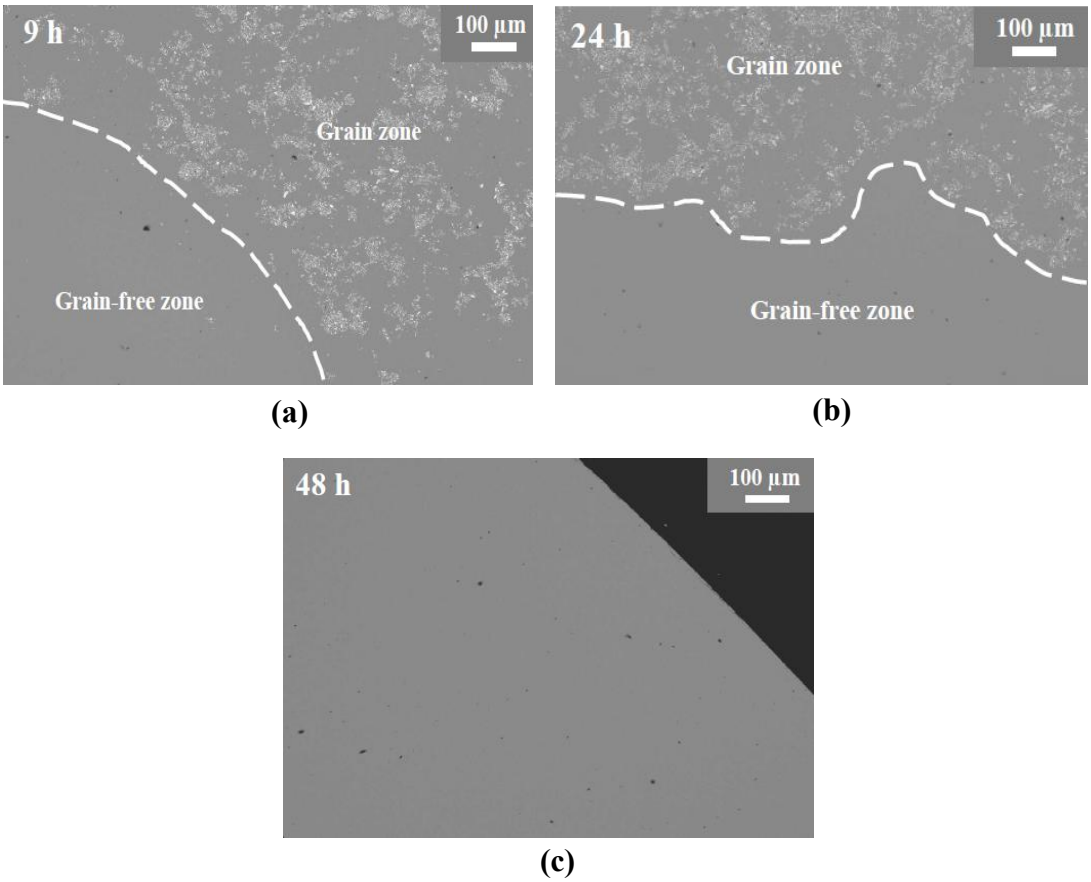

Figure 5.5: Distribution of Cr_2O_3 grains as a function of time in NC5S at 1300°C under oxidising atmosphere (air) after (a) 9 h, (b) 24 h and (c) 48 h of experimental duration

At a very long experimental duration (t = 48 h), all of the Cr_2O_3 grains dissolve (Figure 5.5(c)) in the melt but the total dissolved Cr seems to decrease. This observation may occur due to the volatilisation of Cr^{VI} from the melts in the form of

$CrO_{3(g)}$ (Figure 5.6) as has been described in Chapter 2 or due to the Na loss which changes the basicity of the melts.

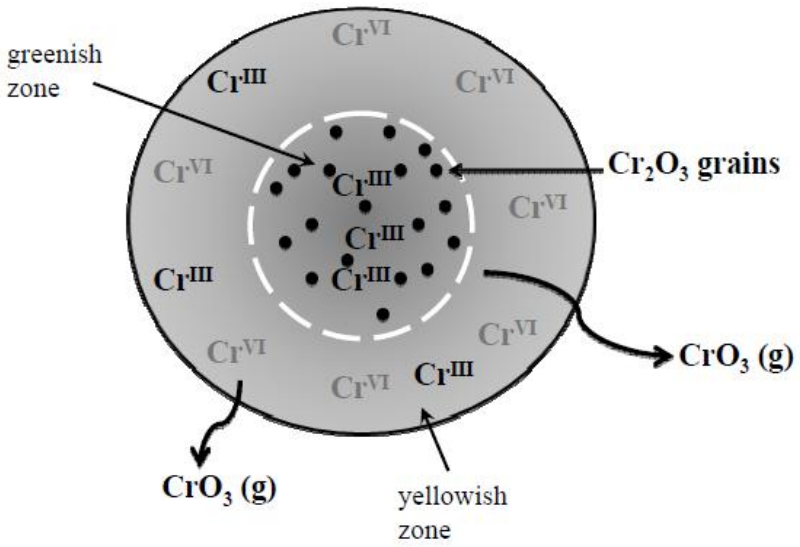

Figure 5.6: Schematic of dissolution mechanism of Cr_2O_3 in molten glass under oxidising condition (air) for a long experimental duration

The volatility of Na is a well-known phenomenon in molten silicates[92,117,118]. The Na_2O tends to volatilise by the following equation:

$$Na_2O_{(melt)} \leftrightarrow 2Na_{(gas)} + \frac{1}{2}O_{2(gas)} \quad (5.1)$$

Since the Si and Ca contents are quite stable with temperature and experimental duration, the evolution of 2Si/Na has been plotted as a function of experimental duration (Figure 5.7). Although the network structure of NC5S is more polymerised compared to a more basic glass (*e.g.* NC3S), a significant loss of Na can still be observed by increasing the experimental duration since the experiment has not been performed in a closed system. As a consequence, the basicity of the glass, which is

measured by aO^{2-} or pO^{2-} index ($-\log O^{2-}$)[1], decreases due to the loss of Na_2O acting as a network modifier. Therefore, the Na loss might change the dissolution behaviour of Cr in the melt since the reactions are influenced by the aO^{2-} (*i.e.* melt basicity) (*cf.* Eq. 2.46 - 2.48 in Chapter 2).

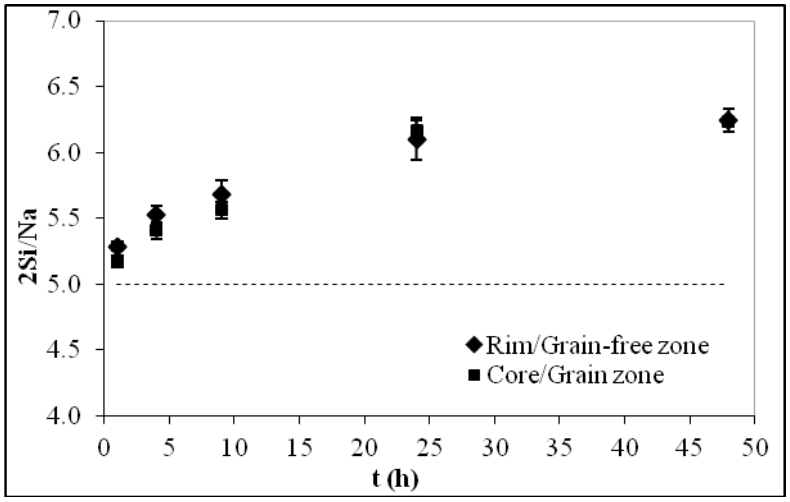

Figure 5.7: Plot of 2Si/Na ratio as a function of experimental duration at 1300°C under oxidising atmosphere (air). Theoretical ratio is in dotted line

(c) Time to equilibrium

In oxidising condition, the dissolution equilibrium will never be reached due to the fact that the solute and solution in this system are not stable with time since the volatilisation of Cr^{VI} and Na loss play a crucial role here. As noted above, the aim of this work is to determine the time to reach the dissolution equilibrium, to be applied for future study on the solubility measurement of Cr_2O_3 in soda lime silicate melts. As an effort to meet this goal, a compromise method of analysis has been proposed by taking into account all the problems encountered in this system. Since the Cr solubility in the rim of the samples remains constant for the first hours of experimental duration, it is suggested to consider just 1 h of heat treatment while

performing the analysis only on the rim of the samples. Furthermore, the Na loss could be minimised, thus stabilising the composition of the glass.

5.1.1.2. Reducing condition (Fe/FeO)

The mixture of NC5S with 5 wt.% of Cr_2O_3 has been subjected to 1 h of heat treatments while 10 wt.% of Cr_2O_3 has been added to the melt for 4 h, 9 h, 24 h and 48 h of heat treatments. A same procedure of analysis (already used for oxidising condition) has been performed on the samples in reducing atmosphere. The results have been demonstrated as a plot of dissolved Cr (at. % Cr) as a function of time (h) at 1300°C for both rim and core of the samples (Figure 5.8). The bluish colouration observed on the quenched samples proved the existence of Cr^{II} species.

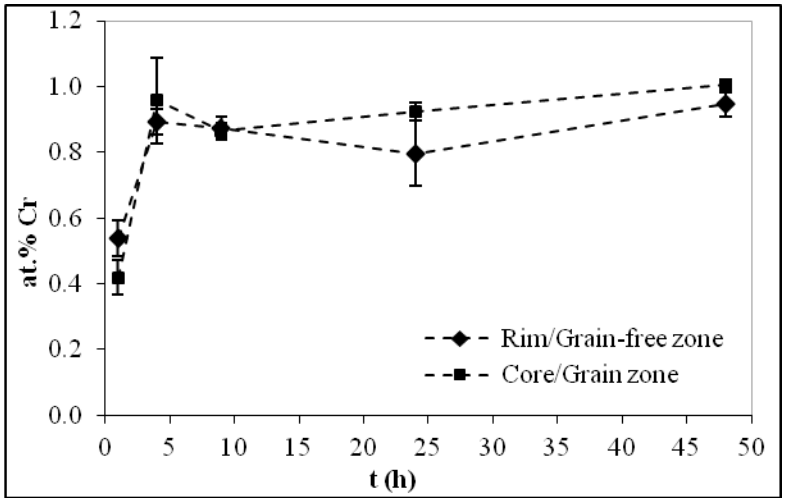

Figure 5.8: Plots of the distribution of dissolved Cr (at.%) as a function of time in NC5S at 1300°C under reducing atmosphere (Fe/FeO). The dotted lines are guides to the eyes

(a) Short experimental duration (1 h ≤ t ≤ 4 h)

At t = 1 h, the difference of Cr solubility in the rim and the core of the sample is quite significant (Figure 5.8). The SEM observation (Figure 5.9) shows the

existence of grain-free zone (thickness of ~100 μm) in the rim of the sample which is not the case for oxidising condition.

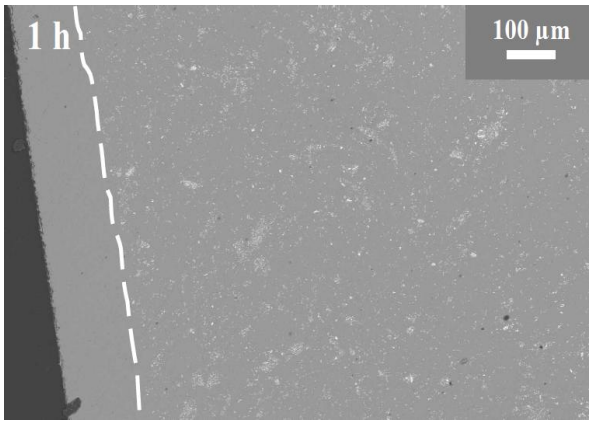

Figure 5.9: Distribution of Cr_2O_3 grains in NC5S as a function of time at 1300°C under reducing atmosphere (Fe/FeO) after 1 h of experimental duration

A schematic of the mechanism of Cr_2O_3 dissolution in the melts under reducing condition has been proposed in Figure 5.10. Since the raw glass balls were produced in the oxidising environment (air), the fO_2 imposed in the silica tube is lower than the fO_2 in the melt. As a consequence, the oxygen must diffuse out of the melt in order to achieve the equilibrium (Figure 5.10(a)). Upon heat treatment, the Cr_2O_3 will dissolve into the melt to form Cr^{III} oxo-complex (*cf.* Eq. 2.46 in Chapter 2). Since the fO_2 on the surface of the sample is lower than the fO_2 in the core of the sample, the reduction reaction will take place initially in the rim of the sample by following (*cf.* Eq. 2. 48 in Chapter 2). As a consequence, the dissolution of Cr in the rim is higher compared to the core due to the contribution of Cr^{II} and Cr^{III} in the rim of the sample. Therefore, the grain-free zone could be clearly observed on the surface of the sample with bluish colouration which is an indication of the existence of Cr^{II} species (Figure 5.10(b)). By prolonging the experimental duration to 4 h, the reduction reaction is expected to move forward to the core of the sample. The EPMA

results at t = 4 h shows a significant increase of Cr solubility in the melt compared to the very short experimental duration (t = 1 h).

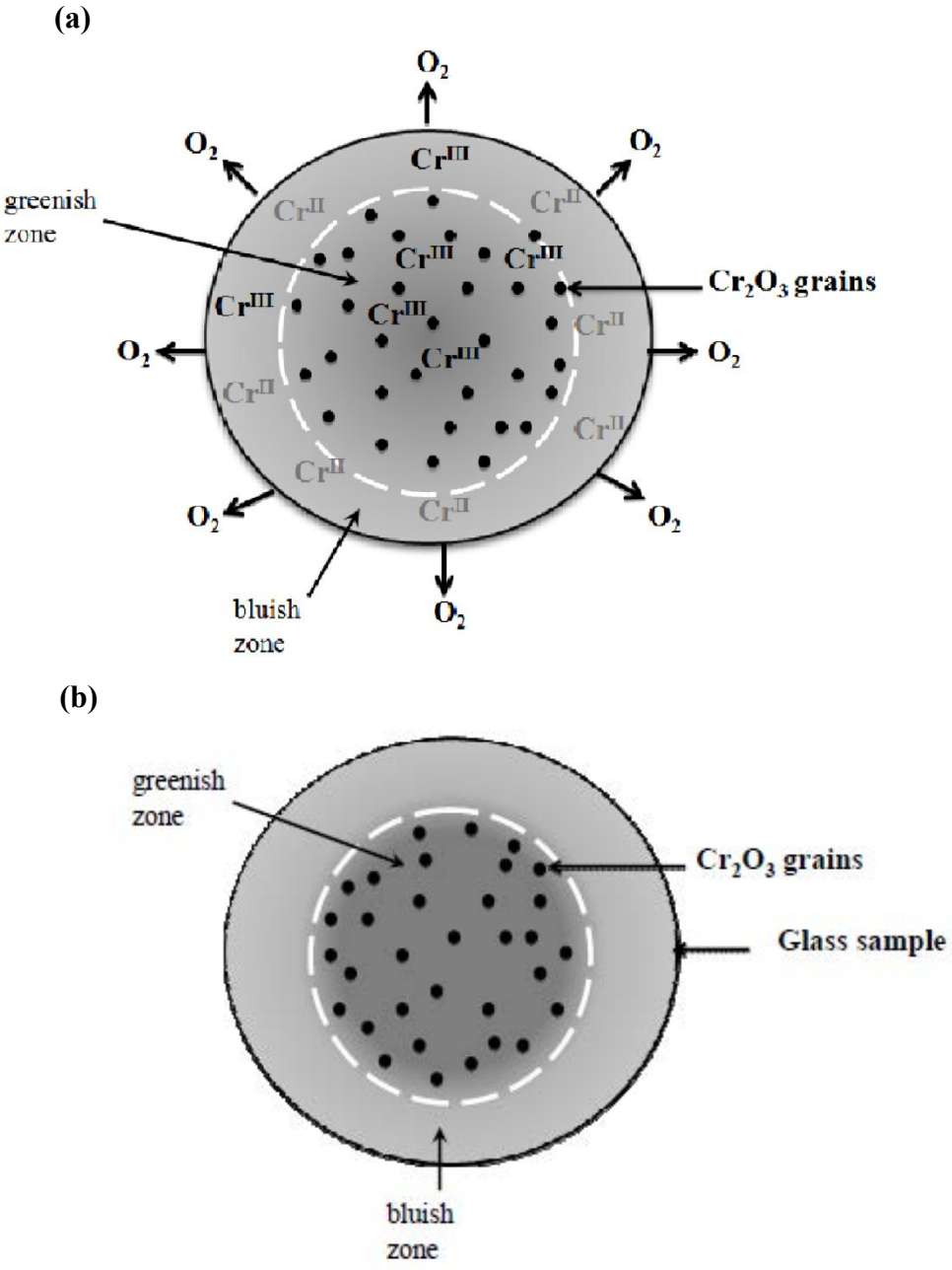

Figure 5.10: Schematic of dissolution mechanism of Cr_2O_3 in molten glass under reducing condition (Fe/FeO). (a) Short experimental duration (b) Optical observation

(b) Long experimental duration (9 h ≤ t ≤ 48 h)

Increasing the duration of the heat treatments seems to increase the area of the grain-free zone on the rim of the sample. For example the thickness of grain-free zone is ~300 µm for 9 h of heat treatment (Figure 5.11(a)) and it increases to ~ 450 µm when the heat treatment is prolonged to 24 h (Figure 5.11(b)). When $fO_{2core} = fO_{2rim}$, the reducing process will take place all over the sample, leading to a homogeneous dissolution of Cr_2O_3 grains in the glass ball. By extending the heat treatment to 48 h, the same behaviour as in the oxidising condition has been observed in the sample; the Cr_2O_3 grains assemble at the bottom of the glass ball due to the gravity effect. As a consequence, the results for 48 h of heat treatment has been classified into two different zones *i.e.* grains-free zone and grain zone (Figure 5.11 (c)). If the standard deviations have been taken into account, the Cr solubility in this domain of heat treatment is quite constant throughout the sample.

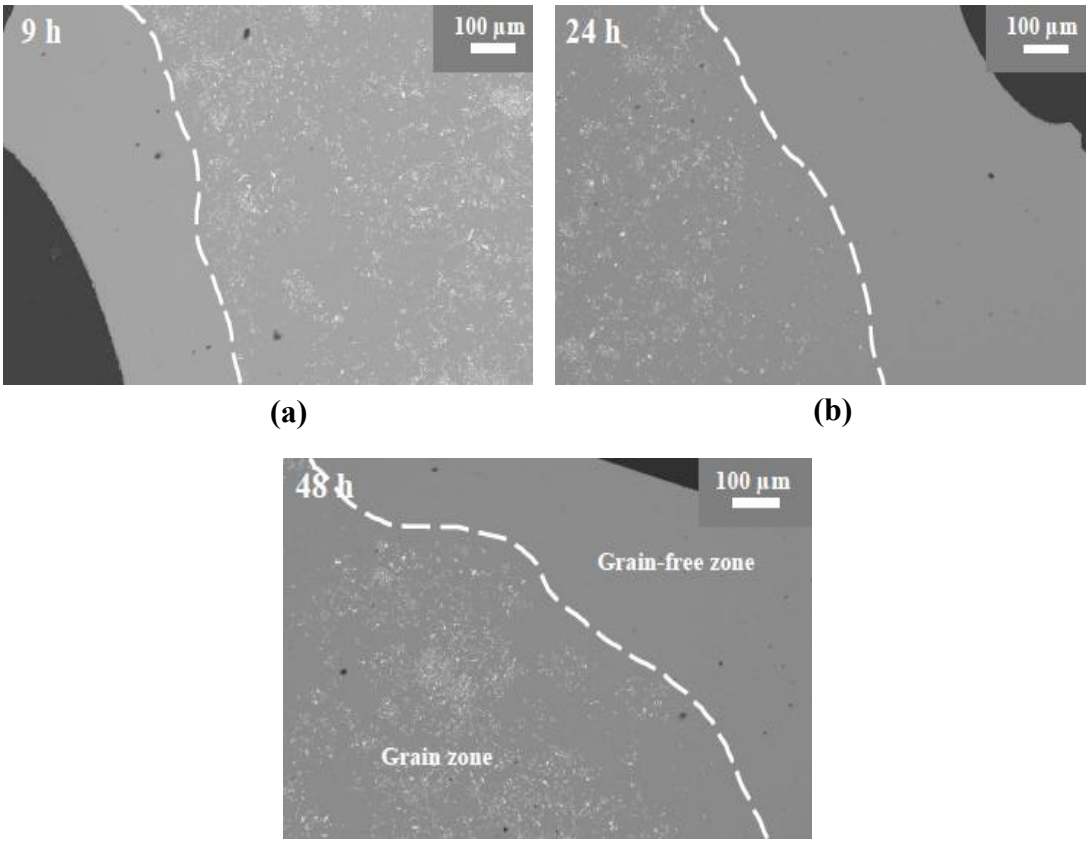

Figure 5.11: Distribution of Cr_2O_3 grains as a function of time in NC5S at 1300°C under reducing atmosphere (Fe/FeO) after (a) 9 h, (b) 24 h and (c) 48 h of experimental duration

(c) Time to equilibrium

In order to determine the time to reach the equilibrium, the change in the glass composition should be taken into account. The reduction experiment was performed in a closed system where the Na volatilisation is expected to be minimised. Figure 5.12 illustrates the evolution of 2Si/Na as a function of experimental duration. The results show that the Na loss is not very significant until 9 h of heat treatment and tends to reach a constant value around 5.3 for the 2Si/Na ratio. A slightly increase of this ratio up to 5.6 is measured after long experimental duration (48 h), showing here the efficiency of sodium buffer that was introduced in the device[105]. However, the deviation from the trend has been observed at 24 h of run

duration. 21 % Na loss was observed in this sample. Since there is no new phase in this sample, this significant Na loss might happen due to the longer heat treatment during the glass ball preparation.

By taking into account the standard deviations and the Na loss, the equilibrium is considered to be achieved at 4 h of heat treatment since the Cr solubility remains constant for both the rim and the core of the sample.

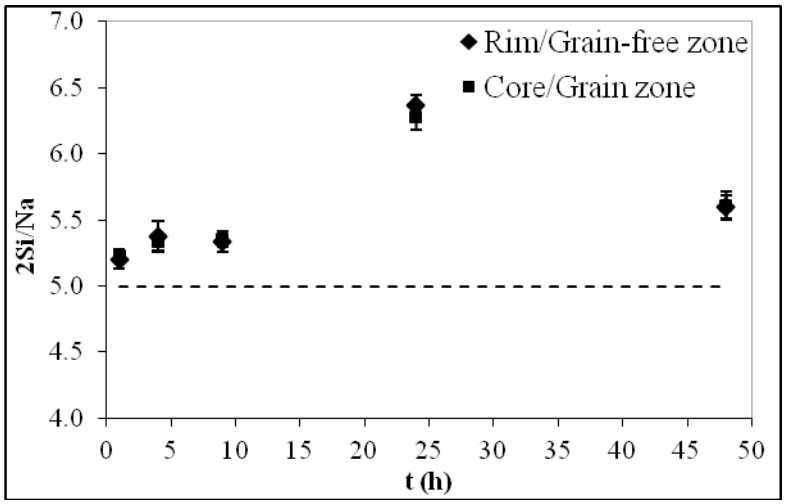

Figure 5.12: Plot of 2Si/Na ratio as a function of experimental duration for NC5S at 1300°C under reducing atmosphere (Fe/FeO). Theoretical ratio is in dotted line

5.1.2. Influence of temperature

The influence of temperature on the dissolution equilibrium of Cr_2O_3 in silicate melts was investigated on the highest viscosity of the studied range of the melts which is NC6S at 1200°C and 1300°C for two extreme conditions (air and Fe/FeO). Since the mechanisms of the Cr_2O_3 dissolution in the melts have been discussed thoroughly in the previous part, the results on the evolution of the Cr solubility and Na loss as a function of heat treatment for different temperatures will be discussed lightly.

5.1.2.1. Oxidising condition (air)

The distribution of dissolved Cr (at.%) and the melt compositions (ratio of 2Si/Na) as a function of experiemental duration in NC6S at 1200°C under oxidising atmosphere have been displayed in Figure 5.13.

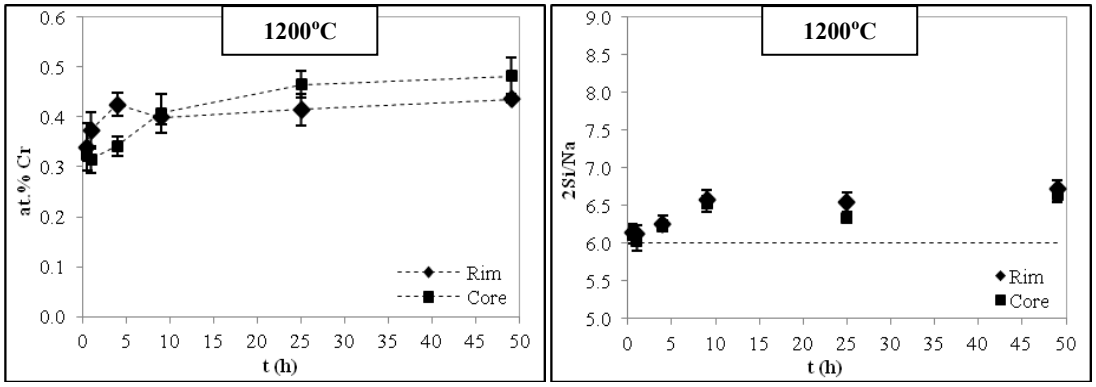

(a) **(b)**

Figure 5.13: Plots of (a) distribution of dissolved Cr (at.%) and (b) evolution of 2Si/Na ratio as a function of time in NC6S at 1200°C under oxidising atmosphere (air). The dotted lines in (a) are guides to the eyes whereas the dotted line in (b) is the theoretical ratio

The results show that the Cr solubility in the rim of the sample is higher than in the core of the sample until 9 h of experimental duration since the oxidation takes place initially at the rim of the sample. At t = 9 h, the Cr solubility in the rim of the sample has the same value as in the core of the sample. By prolonging experimental duration, the oxidation will move forward to the core of the sample, thus increasing the concentration of dissolved Cr in this region. The ratio of 2Si/Na shows a significant Na loss at $t \geq 9$ h of heat treatment which is expected for an experiment performed under oxidising condition. However, the Na loss seems to remain constant even until 49 h. At 1200°C, the grains are well-dispersed without the disturbance from the gravity since the viscosity of NC6S at 1200°C is quite high which is 96 Pa.s. The results have been compared with the same melt composition which has

been subjected to the heat treatment under oxidising condition (air) at 1300°C (Figure 5.14).

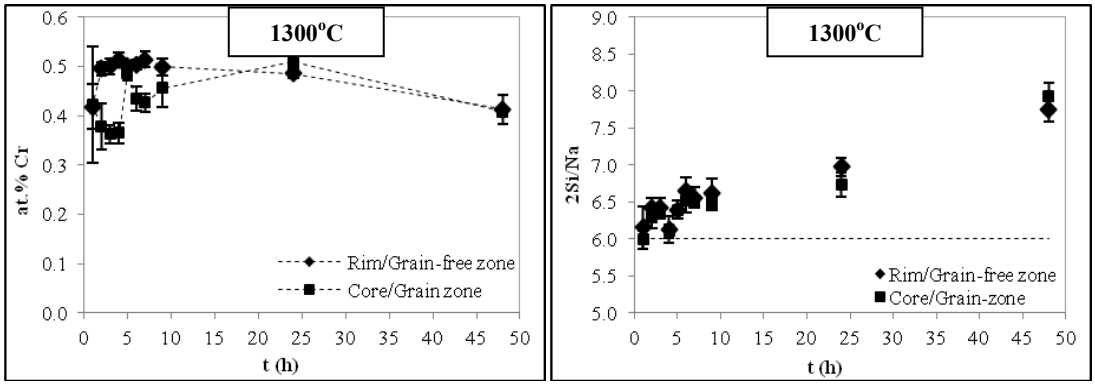

(a) **(b)**

Figure 5.14: Plots of (a) distribution of dissolved Cr (at.%) and (b) evolution of 2Si/Na ratio as a function of time in NC6S at 1300°C under oxidising atmosphere (air). The dotted lines in (a) are guides to the eyes whereas the dotted line in (b) is the theoretical ratio

The difference of Cr concentration between the rim and the core of the samples for the first hours of heat treatment is more significant at 1300°C as compared to 1200°C. However, the concentration of Cr is constant at the rim of the samples just after 2 h of heat treatment. For the first 9 h of heat treatment, there is no significant difference of Na loss between 1200°C and 1300°C. However, by prolonging the experimental duration, there is an obvious change in the glass composition at 1300°C.

The SEM micrographs (Figure 5.15) reveal the existence of SiO_2 crystals which are formed at higher temperature and at a long run duration. The crystallisation of SiO_2 occurs in SiO_2-rich melt (NC6S) at longer run duration when there is a significant Na loss in the melt.

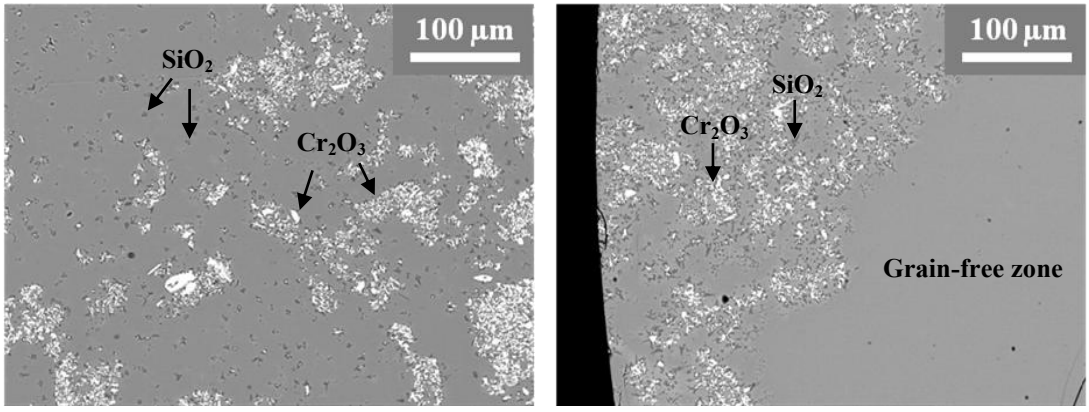

(a) **(b)**

Figure 5.15: Micrographs of the samples of NC6S + Cr_2O_3 which were subjected to (a) 24 h and (b) 48 h of heat treatments under oxidising condition (air) at 1300°C

As mentioned in the previous part, the rate determining step in the attainment of redox equilibrium in the melts is controlled by the diffusion of oxygen within the melt. By increasing the temperature, the viscosity of the melt will decrease; 96 Pa.s at 1200°C and 35 Pa.s at 1300°C. As a consequence, the diffusion of oxygen should be faster at 1300°C. However, in this work a direct comparison is quite difficult since the gravity influences the distribution of Cr_2O_3 grain at $t \geq 4$ h in the case of 1300°C. Thus, the measurements were performed by considering grain-free zone and grain zone.

At 1200°C, the equilibrium might be achieved at $t > 4$ h. However in the case of 1300°C, it is quite difficult to determine the time to reach the equilibrium. Nevertheless, the equilibrium seems to be achieved very fast at the rim of the sample at 1300°C. Therefore, it is suggested to consider just 2 h of heat treatment while performing the analysis only on the rim of the samples in the case of 1300°C.

5.1.2.2. Reducing condition (Fe/FeO)

The influence of temperature on the dissolution equilibrium of Cr_2O_3 in the melt was also studied for the reducing condition (Fe/FeO). The distribution of dissolved Cr in NC6S at 1200°C under oxidising condition is shown in Figure 5.16.

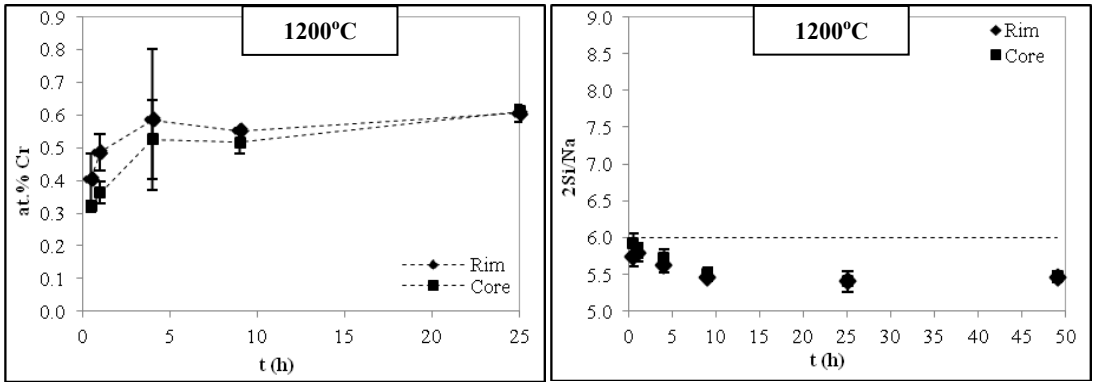

(a) **(b)**

Figure 5.16: Plots of (a) distribution of dissolved Cr (at.%) and (b) evolution of 2Si/Na ratio as a function of time in NC6S at 1200°C under reducing atmosphere (Fe/FeO). The dotted lines in (a) are guides to the eyes whereas the dotted line in (b) is the theoretical ratio

The results show the Cr solubility is higher at the rim of the sample for the first 9 h of heat treatment. At t = 9 h, the concentration of Cr in the rim is almost equivalent with the concentration in the core of the sample. However, the ratio of 2Si/Na (Figure 5.16(b)) shows that the Na concentration increases while increasing the time of heat treatment. This phenomenon might happen due to the overestimation measurement by Electron Probe Micro Analysis (EPMA).

The results on the distribution of Cr solubility in the NC6S at 1300°C under reducing condition (Fe/FeO) are displayed in Figure 5.17. At higher temperature, the gravity influences the distribution of the Cr_2O_3, hence leading to the measurement by considering the grain-free zone and grain zone as mentioned previously. However, at

t = 24 h, the average values of Cr solubility throughout the sample has been measured since the distribution of Cr_2O_3 grains in the sample is quite compact, making it difficult to find the spot for analysis.

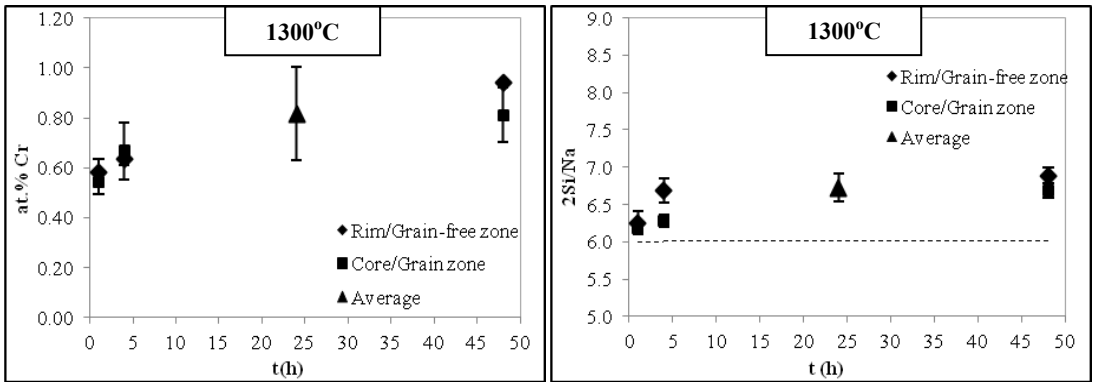

(a) **(b)**

Figure 5.17: Plots of (a) distribution of dissolved Cr (at.%) and (b) evolution of 2Si/Na ratio as a function of time in NC6S at 1300°C under reducing atmosphere (Fe/FeO). The dotted lines in (a) are guides to the eyes whereas the dotted line in (b) is the theoretical ratio

Figure 5.17(a) shows that there is no significant difference in Cr solubility between the rim and the core of the sample for the first hours of heat treatment. The ratio of 2Si/Na shows a significant change at the rim of the sample at 4 h of heat treatment. However, the melt composition seems to remain constant until 49 h of experimental duration. The SEM observation (Figure 5.18) on the samples reveal the existence of SiO_2 crystals as similarly found in the case of oxidising condition. However, the formation of SiO_2 crystals are much more obvious under oxidising condition. This phenomenon might happen due to the greater Na loss under oxidising condition which favours the formation of SiO_2.

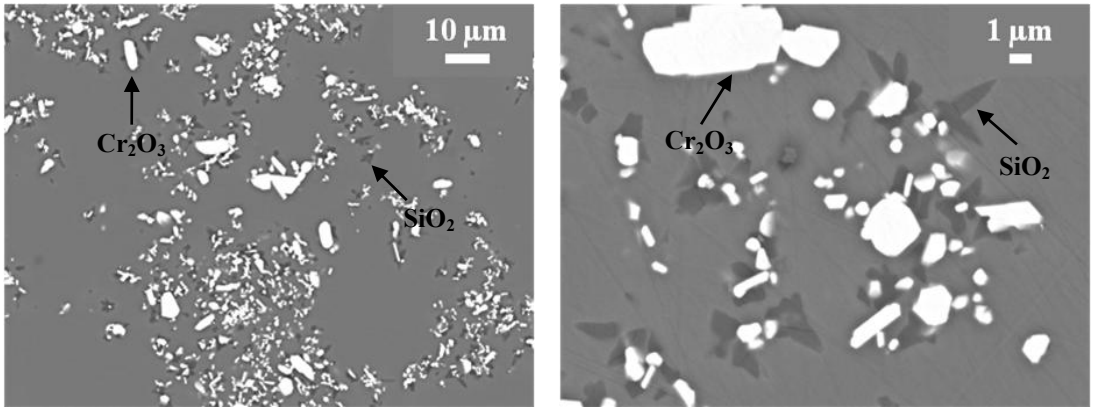

(a) **(b)**

Figure 5.18: Micrographs of the samples of NC6S + Cr_2O_3 which were subjected to (a) 24 h and (c) 48 h of heat treatments under reducing condition (Fe/FeO) at 1300^{o}C

At 1200^{o}C, the equilibrium seems to be achieved at 9 h of heat treatment. In the case of 1300^{o}C, the equilibrium can be achieved maybe at t > 4 h of run duration if the standard deviation and the Na loss are taken into account.

5.1.3. Influence of melt compositions

The influence of melt compositions has been studied by considering the influence of basicity and viscosity in the same type of glass which is soda-lime silicate melts and also the influence of network modifier in silicate melts. The latter study involves a variation in the Na_2O and CaO contents while fixing the stoichiometry of SiO_2 according to the following equation: $(1+x)Na_2O$-$(1-x)$CaO-$6SiO_2$ with x = 0, 0.5 and 1. Four different compositions were studied in this part which are Na_2O-CaO-$3SiO_2$ (NC3S), Na_2O-CaO-$6SiO_2$ (NC6S), $1.5Na_2O$-0.5CaO-$6SiO_2$ (0.5C) and Na_2O-$3SiO_2$ (N3S).

5.1.3.1. Influence of melt basicity in soda-lime silicate melts

The influence of melt basicity on the dissolution equilibrium of Cr_2O_3 has been investigated by performing the experiments on the two extreme melt compositions in the studied range of melts which are NC3S and NC6S. The experiments were performed at 1300°C under oxidising condition (air). The physical properties of these two glasses at 1300°C are listed in Table 5.1. The data from Table 5.1 reveals that the NC3S has a higher basicity as compared to NC6S. At 1300°C, the viscosity of NC6S is ~ 23 times higher than the viscosity of NC3S.

Table 5.1: The physical properties of the studied glasses at 1300°C

Glass	NC3S	NC6S
Optical basicity (Λ_{th})	0.6288	0.5650
aNa_2O	2.17×10^{-9}	4.09×10^{-11}
Viscosity, μ (Pa.s)	1.53	35.02

The experiments were performed up to 9 h for NC3S and 49 h in the case of NC6S. The average of Cr solubility measured throughout the samples and the ratio of 2Si/Na for both compositions were plotted as a function of time as shown in Figure 5.19. The results reveal that the Cr solubility in NC6S is constant with time if the standard deviations are taken into account. The ratio of 2Si/Na also shows that no significant loss occurs in NC6S up to 9 h of heat treatment. However, a prominent decrease of Cr solubility occurs in NC3S even at a very short experimental duration.

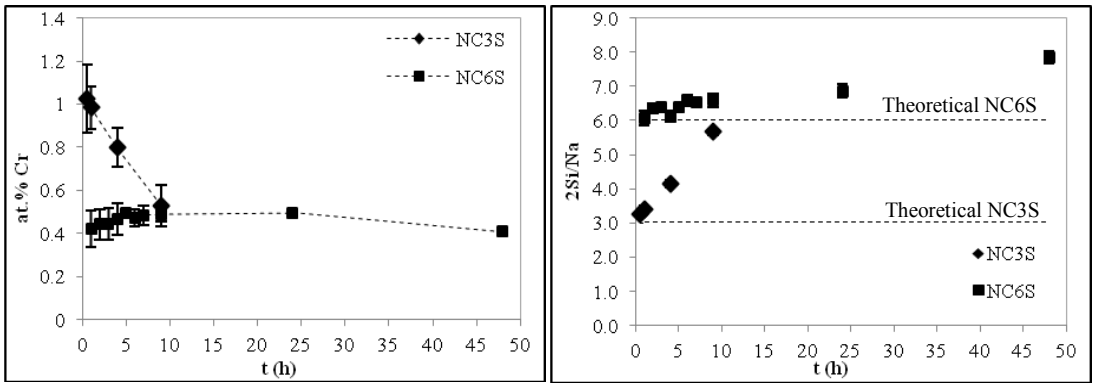

(a) **(b)**

Figure 5.19: Plots of (a) distribution of dissolved Cr (at.%) and (b) evolution of 2Si/Na ratio as a function of time in NC3S and NC6S at 1300°C under oxidising atmosphere (air). The dotted lines in (a) are guides to the eyes whereas the dotted lines in (b) are the theoretical ratio

In order to have a thorough understanding, the samples were studied by plotting the Cr solubility for the rim and the core of the samples. The plots of NC3S are displayed in Figure 5.20 while the distribution of Cr solubility in NC6S at 1300°C under oxidising condition has been shown in the previous part (Figure 5.14). Since the viscosity of NC3S at 1300°C is very low as compared to NC6S, the gravity has a great influence on the Cr_2O_3 distribution in the glass. Even after 1 h of experimental duration, the grains tend to assemble at the bottom of the glass ball, thereby leading to the classification of the measurement into two zones *i.e.* grain-free zone and grain zone (Figure 5.20).

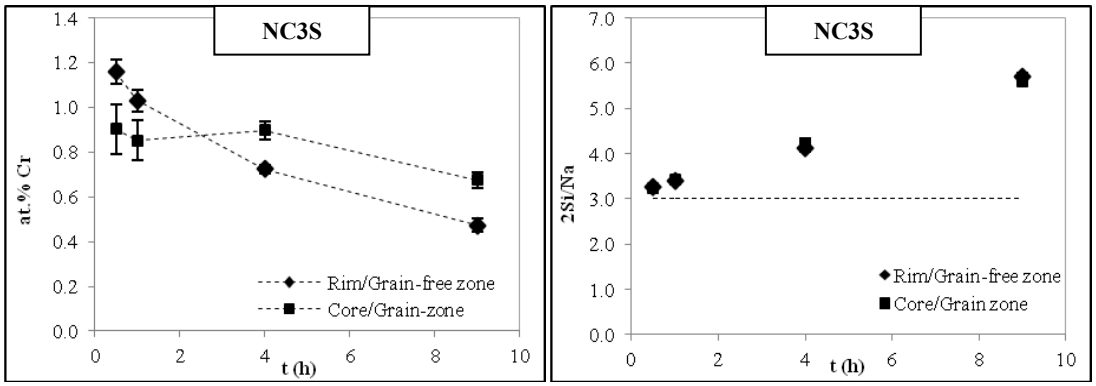

(a) **(b)**

Figure 5.20: Plots of (a) distribution of dissolved Cr (at.%) and (b) evolution of 2Si/Na ratio as a function of time in NC3S at 1300°C under oxidising atmosphere (air). The dotted lines in (a) are guides to the eyes whereas the dotted line in (b) is the theoretical ratio

Figure 5.20 reveals a higher Cr solubility at the rim/grain-free zone of the sample for the first hour of heat treatment. As a contrary to the NC6S (Figure 5.14(a)), the Cr solubility in NC3S at the rim/grain-free zone possesses a faster decrease by prolonging the experimental duration. However, the Cr solubility at the core/grain zone of the sample remains constant until 4 h of heat treatment. As can be seen from Figure 5.20(a), the Cr solubility for both rim and core of the sample for the first hours of experimental duration is higher than the Cr solubility of NC6S (Figure 5.14(a)). This is due to the fact that increasing the basicity will stabilise the higher oxidation state by taking into account the chemical bonding approach[64]. By considering Eq. 2.46 and 2.47 in Chapter 2, the Cr^{III} - Cr^{VI} equilibrium is assumed to dominate at higher fO_2 (oxidising condition). As a consequence, an increase of the total amount of Cr with the glass basicity for a given temperature might be explained by an increase of the Cr^{VI} species that are dissolved in the melt since Cr^{VI} is stabilised in more basic melt. Therefore, a faster decrease in the total dissolved Cr at the rim/grain-free zone in NC3S might occur due to the volatilisation of Cr^{VI} from the melt or/and due to the great Na loss which changes the basicity of the melt

(Figure 5.20(b)). Furthermore, NC3S melt has a very low viscosity, thus has less polymerised structure as compared to NC6S, thereby leading to a faster volatilisation of Cr^{VI} as well as Na from the melt.

The Cr solubility in NC3S at the core/grain zone is constant for the first 4 hours of heat treatment. It seems that the dissolution equilibrium of Cr_2O_3 in NC3S has been achieved in the core of the sample even at very short experimental duration. This phenomenon might happen due to the faster oxygen diffusion into the melt due to very low viscosity of NC3S at 1300°C as compared to NC6S.

5.1.3.2. Influence of oxide modifiers

Na_2O and CaO are the alkali and alkaline-earth oxides which behave as network modifiers in the glass network. However the roles played by these two oxides are still not well understood. Consequently, the study has been continued by verifying the Na_2O and SiO_2 contents while fixing the stoichiometry of SiO_2 according to the following equation: $(1+x)Na_2O$-$(1-x)$CaO-$6SiO_2$ with x = 0, 0.5 and 1. As a consequence, three different compositions were studied which are NC6S (x = 0), 0.5C (x = 0.5) and N3S (x = 1). The physical properties of the studied glasses at 1200°C are listed in Table 5.2. The data in this table reveals that N3S has the highest optical basicity and lowest viscosity while NC6S is the most acidic glass in this range. The experiments were conducted in the oxidising atmosphere (air) at 1200°C.

Table 5.2: The physical properties of the studied glasses at 1200°C

$(1+x)Na_2O$-$(1-x)$CaO-$6SiO_2$	NC6S (x = 0)	0.5C (x = 0.5)	N3S (x = 1)
Optical basicity (Λ_{th})	0.5650	0.5704	0.5757
aNa_2O	3.30×10^{-11} [98]	/	2.73×10^{-10} [40]
Viscosity, μ (Pa.s)	96.38	52.2	28.95

The Cr solubility was measured throughout the samples as displayed in Figure 5.21. The results show that the total dissolved Cr is always higher in N3S followed by 0.5C and NC6S. Therefore, this behaviour is in good agreement with the basicity of the melts (higher Cr solubility in more basic melts). The plots displayed in Figure 5.21 shows that the total dissolved Cr in NC6S seems to be constant as a function of experimental duration as compared to the other compositions.

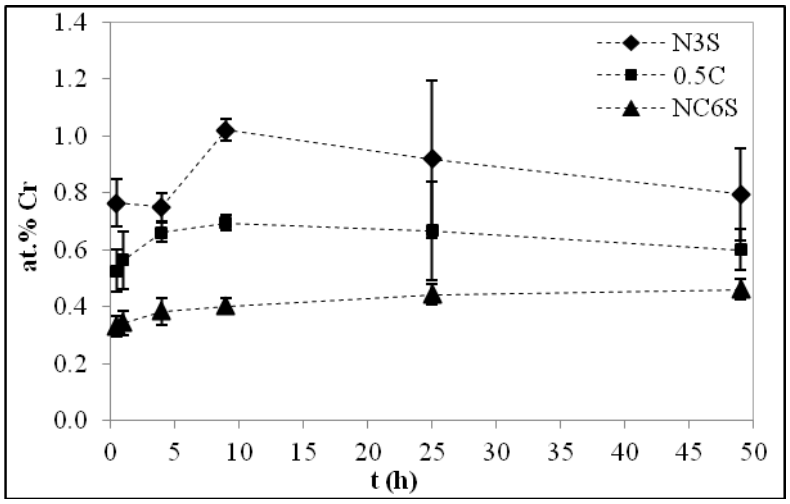

Figure 5.21: Plots of distribution of dissolved Cr (at.%) as a function of time in three different melts at 1200^{o}C under oxidising atmosphere (air). The dotted lines are guides to the eyes

However, the distribution of total dissolved Cr in the melts should be studied simultaneously with the distribution of Na loss as a function of heat treatment. The graphs of 2Si/Na ratio for three different compositions are displayed in Figure 5.22.

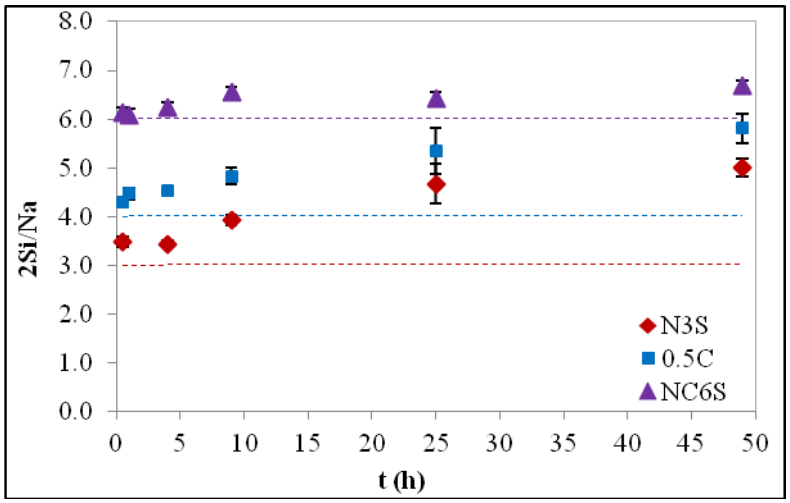

Figure 5.22: Plot of 2Si/Na ratio as a function of experimental duration at 1200°C under oxidising atmosphere (air) for three different melts. Theoretical ratios are in dotted line

The plots reveal that the N3S and 0.5C remains constant just until 4 h of experimental duration whereas the NC6S is stable up to 49 h of heat treatment. In order to have a thorough investigation, the plots of distribution of total dissolved Cr in the rim and the core of the samples were plotted as a function of experimental duration for these three glass compositions. The results are displayed in Figure 5.23. The plots reveal that the dissolution kinetics of Cr_2O_3 strongly depends on the nature of the glass itself. An equivalent molar of Na_2O and CaO (NC6S) resulted in a quite constant Cr solubility as well as the melt composition as a function of heat treatment. By replacing 0.5 mol of CaO with Na_2O, the total dissolved Cr increases since we have increased the more basic oxide in the melt. Furthermore, the viscosity decreases hence making the faster diffusion of oxygen to establish the equilibrium. Consequently, the equilibrium might reach first at 1 h of experimental duration at the rim of the sample. The total dissolved Cr is constant in the rim of the sample until 4 h of heat treatment. By replacing 1 mol CaO with Na_2O, the melt has a very low viscosity, leading to a faster equilibrium for both rim and the core of the sample as

compared to the other compositions. It is noteworthy that the total dissolved Cr after 9 h of heat treatment will not be taken into account in 0.5C and N3S since a significant Na loss has been observed in this condition.

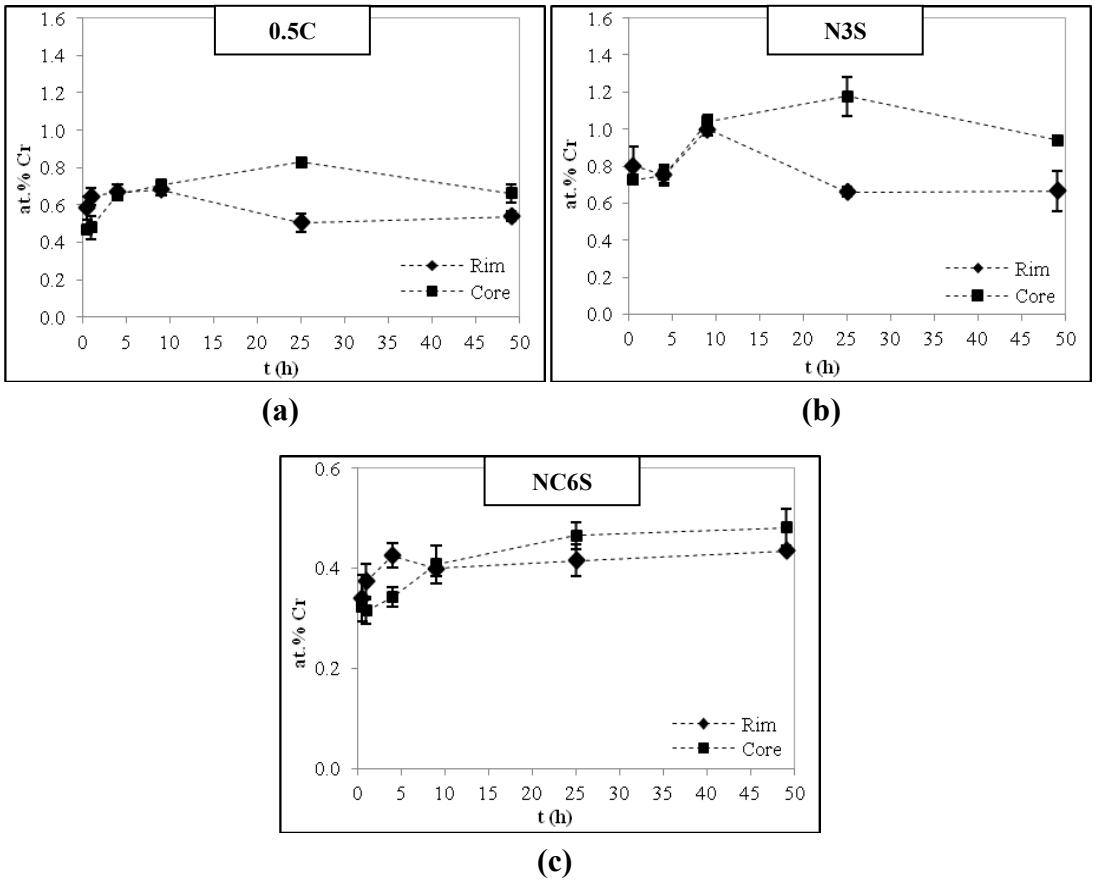

Figure 5.23: Plots of distribution of dissolved Cr (at.%) as a function of time in (a) 0.5C, (b) N3S and (c) NC6S at 1200^{o}C under oxidising atmosphere (air). The dotted lines are guides to the eyes

5.1.4. Diffusion of oxygen in the melt

Eq. 2.47 and 2.48 in Chapter 2 show the important role of oxygen to establish the redox equilibrium. However, only molecular oxygen dissolved in the melt can react with a multivalent element which is chromium in this study. Gaseous oxygen can be physically dissolved[119] in the melt as diatomic molecules according to the reaction:

$$O_2(gas) \rightarrow O_2(melt) \quad (5.11)$$

However, oxygen can also be chemically dissolved in the melt. The chemically dissolved O_2 behaves as an additional 'oxide' ion in the network as it exists only in latent form whereas the physically dissolved oxygen remains in the diatomic forms[116]. Basically, there are three routes available for oxygen migration in silicate glasses[120]:

- permeation of molecular oxygen through the channels of open space in the low density structures.
- exchange between network oxygen and network vacancy.
- interstitialcy diffusion which involves an exchange between network oxygen and molecular oxygen present either within the internal channels or at an external surface.

By considering Eq. 2.47 and 2.48 in Chapter 2, the chemically dissolved oxygen seems to give a predominant effect in the melt when there is a multivalent oxide introduced in the molten glass.

The oxidation and reduction equations also (*cf.* Eq. 2.47 and 2.48 in Chapter 2) reveal that the modification of the atmosphere (*i.e.* oxygen fugacity) of the system will lead to the reestablishment of a new redox equilibrium according to LeChâtelier's Principle. These speciation reactions involve the diffusion of oxygen into the melt (oxidation) or out of the melt (reduction). Thus, it can be concluded that the rate determining step in the attainment of redox equilibrium is controlled by the diffusion of oxygen within the melt as long as there are enough Cr_2O_3 grains in the melt to support the redox reactions by providing $Cr^{III}O_x^{(2x-3)-}$ oxo-complex through

acid-base dissolution (*cf.* Eq. 2.46 in Chapter 2). Many studies have been devoted to the determination of the oxygen diffusion coefficient (D)[68,116,121–124] and tracer or network oxygen diffusion coefficient (D*)[125–127] in the melts by using various methods. The difference between these two diffusion coefficients have been discussed in detail in the literature[116]. It has been proved that the value of oxygen diffusion coefficient is always greater than the value of tracer or network oxygen diffusion[128].

As mentioned above, the rate determining step in the attainment of redox equilibrium in the melt is controlled by the diffusion of oxygen within the melt. The kinetics behaviour of oxygen in the melt is not only important to understand the dissolution behaviour of Cr_2O_3 in the melt, it also provides a significant knowledge to understanding the melt structure, refining process, melt viscosity, phase separation and electrochemical transport[116].

A first attempt of determination of oxygen diffusion coefficient has been performed by taking into account the thickness of grain-free zone of the samples. As discussed previously, the grain-free zone exists due to the simultaneous process of acid-base reaction (*i.e.* dissolution) and oxidation or reduction reactions. Since gravity is likely to influence the distribution of Cr_2O_3 grains in the glass ball under oxidising condition, the oxygen diffusion coefficient has been determined only for the samples which have been subjected to the reducing atmosphere.

The results in this work show that the thickness of the grain-free zone increases with the time of heat treatment. The longer the time, the thicker the zone

will be. However, this observation is valid up to a certain duration of heat treatment depending on the composition of the melt and also the subjected atmosphere of the experiments. After a certain duration of heat treatment, the gravity affects the grains distribution in the melt. As a consequence, the first attempt of determination of oxygen diffusion coefficient has been performed on the NC5S at 1300°C under reducing condition (Fe/FeO).

Since the thickness of the grain-free zone is related to the redox equilibrium of the chromium in the melt, the evolution of the grain-free zone with time can be employed directly to calculate the oxygen diffusion coefficient in NC5S. The calculation was made by the following equation[129] by considering that a diffusion process is occurring in a semi-infinite diffusion couple:

$$D = \frac{x^2}{4t} \tag{5.12}$$

where D is the oxygen diffusion coefficient, x is the thickness of diffused oxygen in the melt (*i.e.* thickness of grain-free zone) and t is the time taken by oxygen to diffuse at x thickness (*i.e.* time of the heat treatment). This equation can be applied to this work as long as there is still a boundary between the grain-free zone and the grain zone. It means that there must be Cr_2O_3 grains remaining in the melts in order to avoid any limitation due to matter 'supply'. By plotting the thickness of grain-free zone, x as a function of $\sqrt{t}$, the value of oxygen diffusion coefficient has been obtained from the slope of the graph which is 2.5 x 10^{-9} cm^2/s. This obtained value is two orders of magnitude lower than the diffusion coefficient of molecular oxygen which has been determined by Gaillard Allemand[68] in an industrial glass (R7T7) by

an electrochemical measurement. By comparing with the oxygen diffusion coefficients in various melts which have been compiled by Schreiber *et al.*[116], the value of D obtained in this work seems to be in the range of the value of network or tracer oxygen diffusion coefficient. Even though the value of D cannot be directly comparable since it depends on the composition and temperature of the melts, the D value which has been determined in this work seems to be much lower than the average values of the molecular oxygen diffusion coefficient obtained in previous works.

When the initially 'oxidised' sample is subjected to the reducing atmosphere, the reduction process will take place initially at the surface of the sample (*cf.* Eq. 2.48 Chapter 2) by producing physically dissolved oxygen in the melt. In this condition, the movement of the oxygen out of the melt to the surface and into gas phase should be taken into account. Since the melt is saturated with the chromium oxo-complexes, it can be expected here that the diffusion of molecular oxygen will not be as simple as the diffusion of oxygen spheres in the liquid. The oxygen has to be transported to the surface of the sample through open channels within the melt structure. Since there is a limited number of channels due to the glass saturation by the various chromium oxo-complexes, the oxygen diffusion coefficient measured in this work may involve another mechanism through network oxygen diffusion. These mechanisms involve transportation of molecular oxygen by an exchange with the network oxygen that facilitate the movement of the oxygen to the surface of the melt[130]. Since the melt is saturated, the oxygen transport mechanism needs more energy, thus the lower oxygen coefficient is expected.

5.1.5. Summary of the dissolution kinetics of Cr_2O_3 in melts

This work has been devoted to determining the time and mechanism to reach the equilibrium for the dissolution of Cr_2O_3 in soda-lime silicate glasses at 1200°C and 1300°C. Due to the difficulties that have arisen, a compromising method has been proposed in order to meet the objective of this work. The important outcomes of the work have been listed down:

- Development of a method of analysis has led to the determination of the time required to reach the dissolution equilibrium of Cr_2O_3 in the melt. The equilibrium is expected to be achieved when there is no significant difference of Cr solubility between the rim and core of the sample.

- The complex mechanisms of Cr dissolution in soda-lime silicate glass have been underlined by taking into account several simultaneous reactions; *i.e.* basic dissolution, speciation (depending on the surrounding atmosphere) and Cr volatilisation. Furthermore, the evolution of the molten glass medium, oxygen diffusion and Na volatilisation have also been considered.

- The results presented in this part reveal that the time to reach the equilibrium varies with the oxygen fugacity (fO_2), temperatures and melt compositions. Furthermore, under oxidising condition, equilibrium will never be achieved since the volatilisation of Cr^{VI} and Na from the melt plays a crucial role here. As a consequence, a compromising equilibrium time and a specific method of analysis have been chosen in order to satisfy all the problems encountered.

- After considering all the problems that arise, a compromising equilibrium time of 2 h has been chosen while performing the analysis on the rim of the sample. However, a longer heat treatment (4 h) has been performed on an acid melts (NC5S, NC6S) under reducing condition (Fe/FeO) for a lower temperature of heat treatment ($1200^{o}C$).

- The oxygen diffusion coefficient has been calculated for the samples which have been subjected to the reducing atmosphere. The value has been determined to be D = 2.5 x 10^{-9} cm^2/s which is very low. The molecular oxygen probably diffuses within the melt by an interaction with the network oxygen.

5.2. Chromia solublity in silicate melts: Thermodynamic approach

The behaviour of chromia in melts will be thoroughly studied here by working on ternary glass system under some specific conditions. The glasses that have been studied are soda-lime silicate melts with composition Na_2O-CaO-xSiO_2 (x = 3, 4, 5 and 6; noted here as NCxS). In order to control the experimental parameters which are the temperature ($1200^{o}C \leq T \leq 1350^{o}C$), the oxygen fugacity ($-12 \leq \log fO_2 \leq -0.6$) and the melt basicity (*i.e.* glass compositions), the experiments were performed in the closed system which was described in Chapter 3. The influence of glass compositions on the chromia solubility will be studied by taking into account the theoretical optical basicity (Λ_{th}), the nature of the network modifiers in the binary soda silicate (NxS) and ternary soda-lime silicate melts (NCxS) and also the activity of Na_2O which has been determined experimentally in a previous study. All the numerical experimental data are displayed in Table 5.3.

Table 5.3: The experimental data of Cr solubility of NCxS (x = 3, 4, 5 and 6) for different temperatures (T = 1200°C, 1300°C and 1350°C) and different oxygen fugacity ($-12 \leq \log fO_2 \leq -0.6$)

1200°C					
Oxygen buffer	**log fO_2**	**NC3S**	**NC4S**	**NC5S**	**NC6S**
		at.% Cr	**at.% Cr**	**at.% Cr**	**at.% Cr**
Fe/FeO	-11.89	0.36 (±0.02)	0.45 (±0.03)	0.45 (±0.02)	0.53 (±0.03)
FeO/Fe_3O_4	-10.49	0.31 (±0.01)	0.34 (±0.02)	0.30 (±0.02)	0.28 (±0.01)
Co/CoO	-9.25	0.27 (±0.04)	0.33 (±0.02)	0.29 (±0.03)	0.25 (±0.01)
Ni/NiO	-7.65	0.25 (±0.02)	0.29 (±0.01)	0.27 (±0.02)	0.26 (±0.02)
Cu/Cu_2O	-4.25	0.26 (±0.01)	0.30 (±0.01)	0.29 (±0.03)	0.26 (±0.02)
Fe_3O_4/Fe_2O_3	-1.64	0.56 (±0.03)	0.33 (±0.02)	0.31 (±0.02)	0.26 (±0.03)
Air	-0.67	0.74 ± (0.06)	0.55 (±0.03)	0.44 (±0.02)	0.42 (±0.06)
1300°C					
Oxygen buffer	**log fO_2**	**NC3S**	**NC4S**	**NC5S**	**NC6S**
		at.% Cr	**at.% Cr**	**at.% Cr**	**at.% Cr**
Fe/FeO	-10.71	0.70 (±0.03)	0.50 (±0.06)	0.66 (±0.07)	0.66 (±0.11)
FeO/Fe_3O_4	-9.15	0.52 (±0.03)	0.47 (±0.01)	0.45 (±0.02)	0.38 (±0.03)
Co/CoO	-8.20	0.38 (±0.02)	0.41 (±0.01)	0.43 (±0.01)	0.42 (±0.02)
Ni/NiO	-6.60	0.30 (±0.02)	0.38 (±0.04)	0.39 (±0.03)	0.34 (±0.02)
Air	-0.67	0.84 (±0.03)	0.67 (±0.05)	0.45 (±0.05)	0.50 (±0.03)
1350°C					
Oxygen buffer	**log fO_2**	**NC3S**	**NC4S**	**NC5S**	**NC6S**
		at.% Cr	**at.% Cr**	**at.% Cr**	**at.% Cr**
Fe/FeO	-10.17	0.97 (±0.02)	1.05 (±0.02)	0.96 (±0.04)	0.92 (±0.13)
FeO/Fe_3O_4	-8.54	0.62 (±0.06)	0.58 (±0.03)	0.53 (±0.02)	0.38 (±0.03)
Co/CoO	-7.72	0.49 (±0.01)	0.50 (±0.02)	0.48 (±0.02)	0.43 (±0.02)
Ni/NiO	-6.13	0.38 (±0.02)	0.40 (±0.02)	0.41 (±0.02)	0.42 (±0.02)
Air	-0.67	1.05 (±0.04)	0.65 (±0.05)	0.57 (±0.02)	0.54 (±0.02)

5.2.1. Influence of different experimental parameters on the solubility of chromia in silicate melts

5.2.1.1. Influence of temperature

The temperature dependence of Cr solubility is presented as an Arrhenius plot (Figure 5.24) where the natural logarithm of the total dissolved Cr in NC3S (ln at.% Cr) is plotted as a function of reciprocal of absolute temperature (1/T) for different oxygen fugacities (arising from Fe/FeO, Ni/NiO, Co/CoO and Air). Both parameters are correlated, according to an Arrhenius law:

$$\ln C(at.\%Cr) = \ln C - \frac{E_a}{R}\left(\frac{1}{T}\right) \tag{5.13}$$

where E_a is an activation energy of Cr_2O_3 dissolution, C is a constant, R is the universal gas constant and T is the experimental temperature in Kelvin.

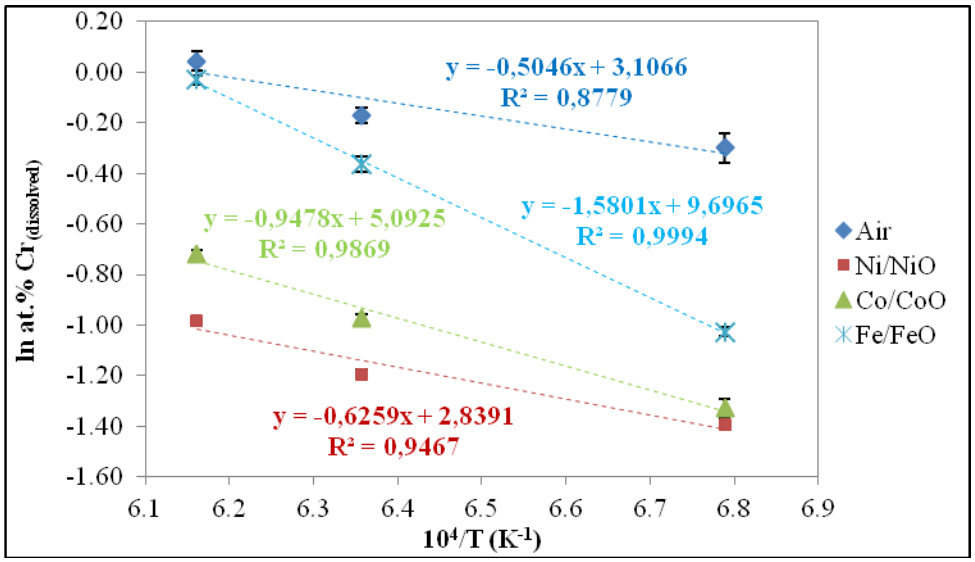

Figure 5.24: Correlation of the Cr solubility in NC3S with temperature (T = 1200°C, 1300°C and 1350°C) for different fO_2

The thermal dependence of the Cr solubility in NC3S shows a linear relationship with correlation coefficients higher than 0.90 except for the samples which have been heat treated under very oxidising condition (Air). As stated earlier in Eq. 2.47 in Chapter 2, the Cr^{III} complex will tend to oxidise to Cr^{VI} complex under oxidising atmosphere. However the volatilisation of Cr^{VI} as $CrO_3(g)$ at high temperature might induce an uncertainty to the concentration of the total Cr which could dissolve in the melts. As a consequence, the observed data might deviate from the expected values, thereby decreasing the quality of the linear fit. The poor quality of linear fit might be also caused by the equilibrium which could possibly not totally

be achieved in this condition. However, it is noteworthy that the experiments were devoted to be as close as possible to the equilibrium.

Figure 5.24 shows that the fO_2 variation modifies the slope of the lines (*i.e.* the activation energy). Application of Eq. 5.13 to the temperature dependence of the Cr solubility in the melt allows the calculation of E_a for the dissolution reaction of Cr_2O_3 as presented in Table 5.4.

Table 5.4: The activation energies (E_a) determined from an Arrhenius plot (Figure 5.23) for different fO_2

Buffers (log fO_2)	**E_a (kJ/mol)**
Air (-0.67)	42.0
Ni/NiO (-7.65)	52.0
Co/CoO (-9.25)	78.8
Fe/FeO (-11.89)	131.4

As demonstrated in Table 5.4, the activation energy increases with decreasing fO_2 showing a higher temperature dependence of the Cr solubility in a very reducing condition. In other words, the minimum energy required to initiate the reaction under oxidising condition is much lower than the one in reducing condition.

5.2.1.2. Influence of oxygen fugacity (fO_2)

The influence of fO_2 on the Cr solubility is demonstrated in Figure 5.25 where the total dissolved Cr in NC3S has been plotted as a function of log fO_2 for two different temperatures (1200°C and 1300°C) and also in the NC5S at 1200°C. The curves obviously indicate that an increase in the experimental temperature leads to an increase of the Cr solubility for all studied range of fO_2. It is noteworthy that,

under oxidising conditions (log fO_2 > -4), the Cr solubility is higher in more basic melt (NC3S) whereas the inverse phenomenon occurs in lower fO_2 (log fO_2 < -8).

The variation of Cr solubility with the fO_2 reflects the change in Cr oxidation states since the redox equilibrium expressed in Eq. 2.47 and 2.48 in Chapter 2 includes the O_2(g) as part of the dissolution/speciation reactions. Therefore, the significant region of solubility in the Figure 5.24 is observed due to the existence of different speciations of Cr in the melt.

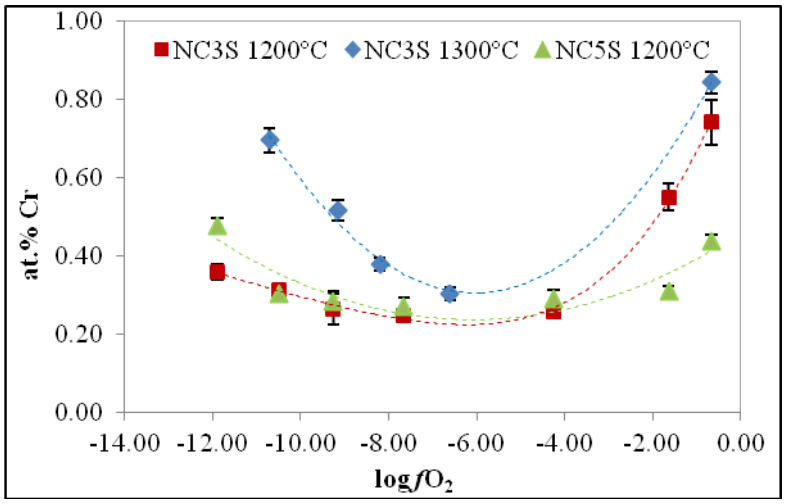

Figure 5.25: The plots of Cr solubility as a function of oxygen fugacity for two different temperatures and two different compositions. The dotted lines are guides to the eyes

The ultraviolet-visible spectroscopy (UV-Vis) was performed by Khedim[99] on a binary melt, undersaturated with Cr_2O_3 for three different atmospheres which are air (oxidising fO_2), Ni/NiO (intermediate fO_2) and Fe/FeO (reducing fO_2). The results of the works reach to the following conclusions[99]:

- Cr^{II} is the predominant species under reducing atmosphere
- Chromium is present in the valency of III under intermediate fO_2
- Cr^{VI} is the predominant species under oxidising condition

Furthermore, the observation from the glass balls colouration (blue, green and yellow) proves the presence of Cr^{II}, Cr^{III} and Cr^{VI} respectively.

Many authors[64,104,131,132] have proved that the higher oxidation states will be stabilised in more basic melts by taking into account the chemical bonding approach. By considering the Eq. 2.46 and 2.47 in Chapter 2, we assume that the Cr^{III} - Cr^{VI} equilibrium dominates at higher fO_2. As a consequence, an increase of the total amount of Cr with the glass basicity for a given temperature (Figure 5.25) might be explained by an increase of dissolved Cr^{VI} species in the melts since Cr^{VI} is stabilised in more basic melts. The same fact might be used to explain the phenomena occuring under the reducing conditions. When dealing with lower fO_2, it has been assumed that the Cr^{II} – Cr^{III} equilibrium dominates in the melts. Hence, increasing the basicity under reducing condition will lead to a decrease in Cr solubility since the Cr^{II} will be less stabilised in more basic melts compared to Cr^{III}. These significant data are in good agreement with the phenomena which have been observed in binary silicate melts[99].

5.2.1.3. Influence of glass compositions

The influence of the glass compositions on the redox equilibrium in molten glasses has received many attentions in the previous works[55,60,64,131]. As a consequence, the influence of glass compositions on the chromium behaviour will be discussed herein by taking into account the ratio of Si/Na, the theoretical optical basicity (Λ_{th}) and also the basicity which was determined by an in situ measurement of the activity of Na_2O (aNa_2O) in the melts.

(a) Influence of glass compositions on the Cr_2O_3 solubility in ternary soda-lime silicate melt

The influence of the glass compositions on the total dissolved Cr in the melt was first studied by taking into account the influence of the ratio of 2Si/Na and the theoretical optical basicity (Λ_{th}) in the Na_2O-CaO-xSiO_2. The stoichimetry of CaO has been fixed while verifying the ratio of 2Si/Na. The value of x is inversely proportional to the Na_2O content; the higher the x value, the lower the basicity of the glass since SiO_2 is an acidic oxide. The calculated Λ_{th} has been listed in Table 5.5.

Table 5.5: The values of theoretical optical basicity (Λ_{th}) for soda-lime silicate melts

Glasses		Theoretical optical basicity (Λ_{th})
Soda-lime silicate melts (Na_2O-CaO-xSiO_2)	NC3S	0.6288
	NC4S	0.5990
	NC5S	0.5792
	NC6S	0.5650

The results will be discussed based on the plots of total dissolved Cr (at.%) as a function of ratio 2Si/Na and Λ_{th} for the significant fO_2 which are oxidising (log fO_2 = -0.67), intermediate (log fO_2 = -7.65) and reducing atmospheres (log fO_2 = -11.89) (Figure 5.26). The results reveal that increasing basicity seems to increase the significance of fO_2 on the total dissolved Cr in the melts for two extreme fO_2, *i.e.* oxidising and reducing conditions. An increase in the basicity will lead to an increase of the total dissolved Cr in the melt under oxidising conditions whereas the opposite behaviour has been observed under reducing conditions. These phenomena has been thoroughly discussed previously (influence of oxygen fugacity).

The Cr solubility under intermediate atmosphere (Ni/NiO) seems to be constant with the glass basicity. As shown in the previous part, Cr^{III} is the

predominant species present under intermediate atmosphere. Therefore, the dissolution process which involves an acid-base reaction (*cf.* Eq. 2.46 in Chapter 2) presumably is dominant in this condition. However, the basicity does not show a profound influence here since the total dissolved Cr in the melt is very low.

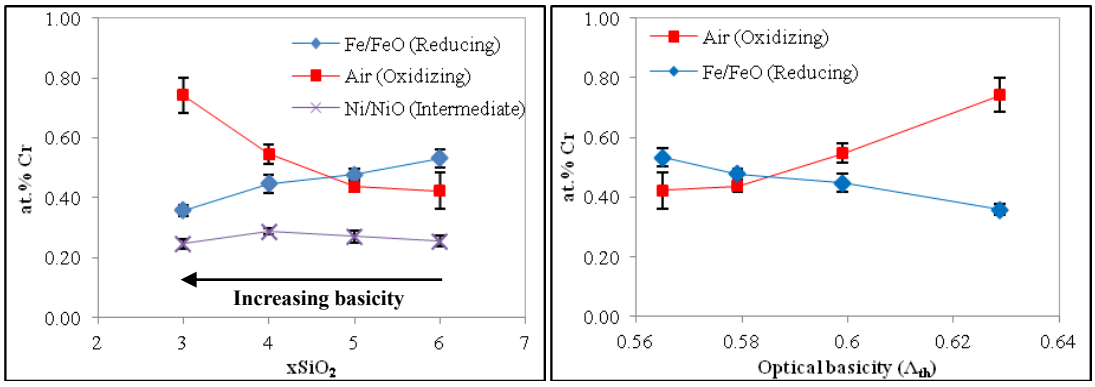

Figure 5.26: The variation of total dissolved Cr as a function of (a) 2Si/Na ratio and (b) theoretical optical basicity (Λ_{th}) for different fO_2 at 1200°C. The lines are guides to the eyes

(b) Influence of glass compositions on the Cr_2O_3 solubility: NxS vs NCxS

In the case of binary melt (Na_2O-xSiO_2), the basicity is directly related to the activity of Na_2O since an addition of Na_2O will induce the formation of O^{2-} ions. However, an uncertainty about the melt basicity exists in the case of ternary melt (Na_2O-CaO-xSiO_2) as an alkaline-earth oxide (CaO) has been introduced in the glass. A question has arisen concerning the influence of CaO on the melt basicity, hence the behaviour of multivalent elements in the melt. As a consequence, an attempt has been made to compare the Cr behaviour in these two melts with the same experimental parameters.

As discussed in Chapter 2, the theoretical optical basicity equation seems to work well on the silicate glasses. Hence, this concept will be used herein in order to predict the 'trend' of the basicity for the binary and tenary silicate melts. The optical basicity concept will be used in this part in order to have an overview of the trend of Cr solubility for the different types of melts. Since the basicity of the oxide melts depends on the force of the ionic bonding with the cation modifier, an in situ measurement on the activity of Na_2O (aNa_2O) which was performed in previous studies[6,40] will be also used in this work as an indicator of the glass basicity for these melts. The theoretical optical basicity values (Λ_{th}) as well as the activity of Na_2O (-log $a(Na_2O)$) for the binary and ternary silicate glasses have been calculated as displayed in Table 5.6:

Table 5.6: The values of theoretical optical basicity (Λ_{th}) and activity of Na_2O ($pa(Na_2O)$ at 1200°C for soda silicate and soda-lime silicate melts

Glasses		**Theoretical optical basicity (Λ_{th})**	**$pa(Na_2O)$ (1200°C)**
Soda silicate melts* (Na_2O-xSiO_2)	N1.5S	0.6475	7.84
	N2S	0.6140	8.44
	N2.5S	0.5917	9.01
	N3S	0.5757	9.56
	N3.5S	0.5638	10.15
Soda-lime silicate melts** (Na_2O-CaO-xSiO_2)	NC3S	0.6288	8.91
	NC4S	0.5990	9.77
	NC5S	0.5792	10.05
	NC6S	0.5650	10.48

* Values of $pa(Na_2O)$ given by Neudorf and Elliot[40]
** Values of $pa(Na_2O)$ reported by Abdelouhab[98]

Comparison of the behaviour of Cr in two different types of melts has been studied by plotting the evolution of the total dissolved Cr as a function of theoretical optical basicity (Λ_{th}) for NCxS (x = 3, 4, 5 and 6) and NxS (x = 2, 2.5, 3 and 3.5)[99] at 1200°C (Figure 5.27). The study was conducted on four different fO_2 which are air

(log fO_2 = -0.67), Ni/NiO (log fO_2 = -7.65), Co/CoO (log fO_2 = -9.25) and Fe/FeO (log fO_2 = -11.89) which represent the oxidising, intermediate, moderate reducing and very reducing atmospheres, respectively.

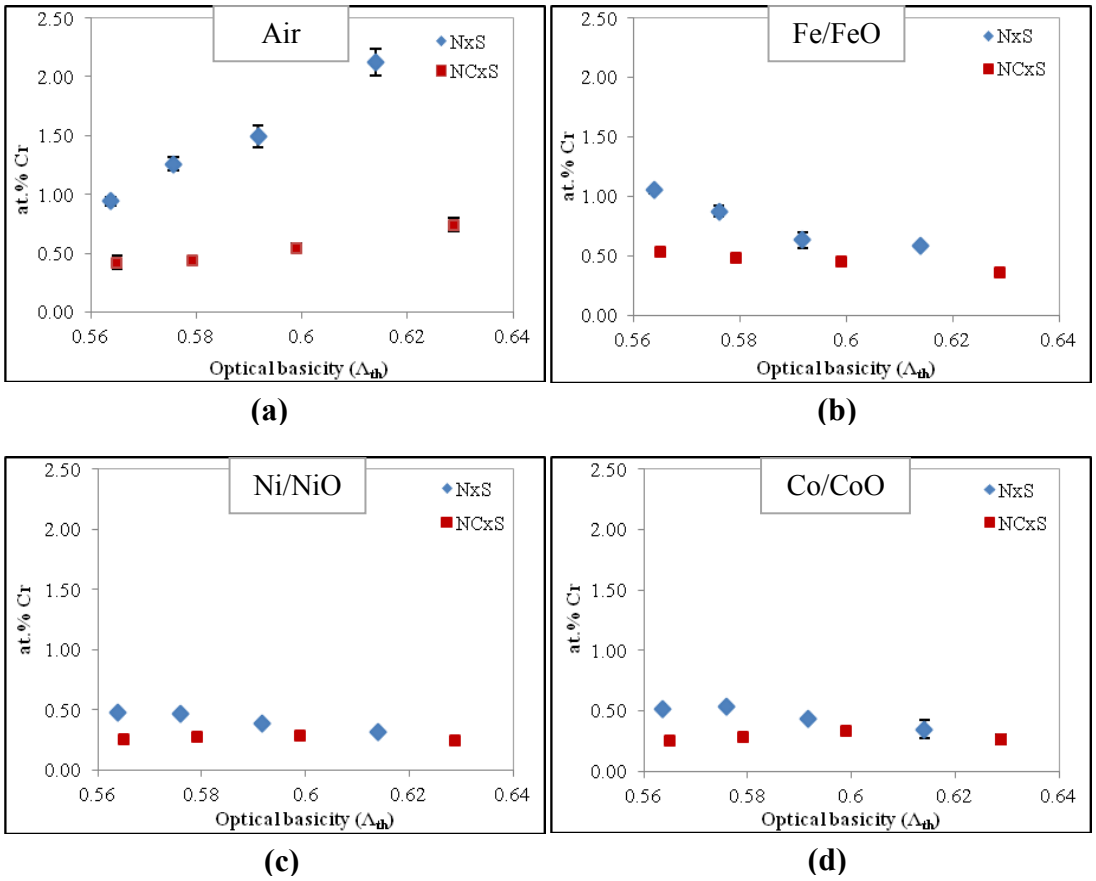

Figure 5.27: The evolution of total dissolved Cr as a function of optical basicity for soda-lime silicate melts (NCxS) and soda silicate melts (NxS) for four different fO_2 at 1200°C

The plots above reveal that there is a significant difference of the total dissolved Cr between the ternary and binary melts under oxidising (air) and reducing (Fe/FeO) conditions. The Cr solubility in binary melts is higher than in the ternary melts for these two extreme conditions (oxidising and reducing) at a given Λ_{th}. In oxidising condition (air), the difference of Cr solubility between NxS and NCxS becomes more significant as the Λ_{th} increases. However, an opposite behaviour has

been observed in the case of the reducing condition (Fe/FeO) where there is a significant difference of Cr solubility between NxS and NCxS as the Λ_{th} decreases.

However, the Cr solubility has almost the same solubility in both types of melts under intermediate (Ni/NiO) and moderate reducing (Co/CoO) conditions for all studied range of Λ_{th}. These results have induced an uncertainty on the optical basicity as an indicator of the trend of basicity for different melts. Thus, the experimental values of activity of Na_2O on soda silicate and soda-lime silicate melts have been used as complimentary results of this work. The results have been illustrated in Figure 5.28.

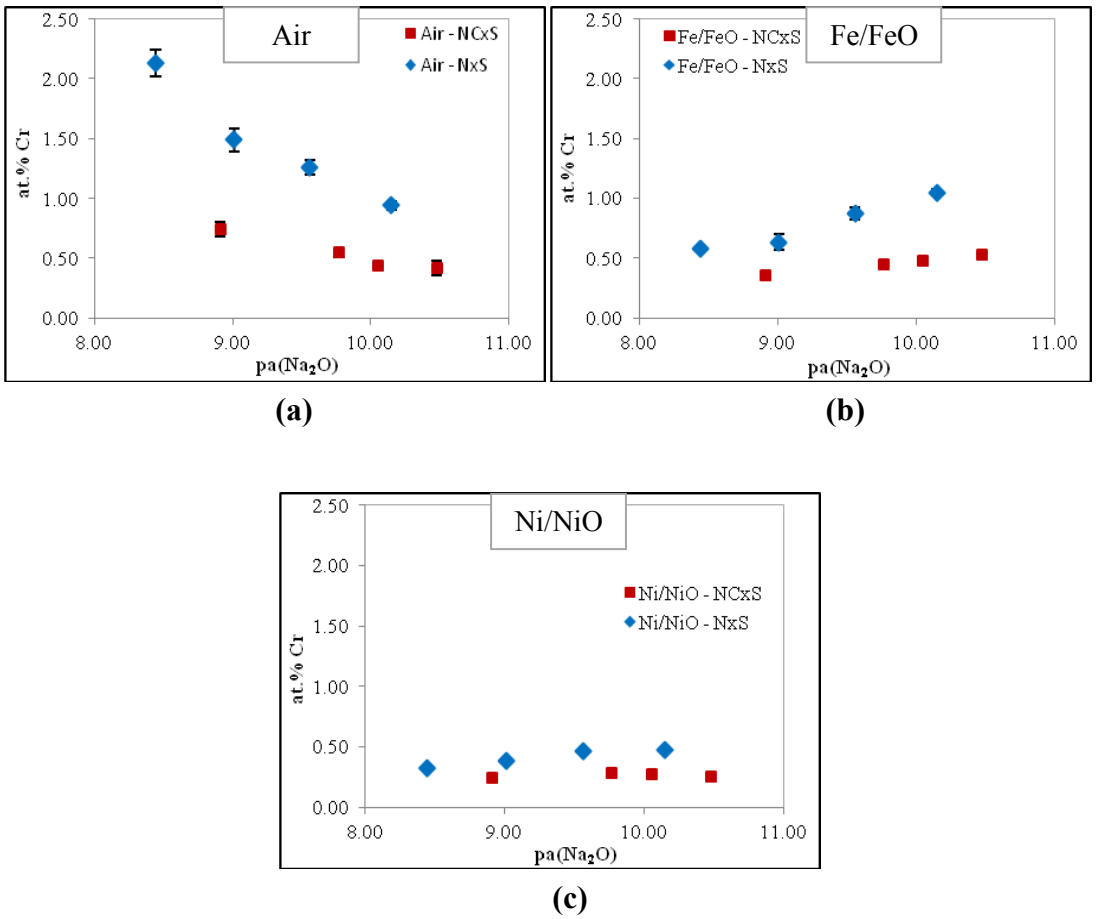

Figure 5.28: The evolution of total dissolved Cr as a function of activity of Na_2O ($pa(Na_2O)$) for soda-lime silicate melts (NCxS) and soda silicate melts (NxS) for different fO_2 at 1200°C

The results presented by the activity of Na_2O are in a good agreement with the Cr solubility observed as a function of theoretical basicity (Λ_{th}).

➢ *Intermediate (Ni/NiO) and moderate reducing (Co/CoO) conditions*

Under the intermediate atmosphere (Ni/NiO), the Cr_2O_3 has a very low solubility in the melt. If the minimum of the solubility is considered to be ruled by an acid-base reaction (*cf.* Eq. 2.46 in Chapter 2), therefore the dissolution of Cr_2O_3 in this condition only depends on the melt basicity. Hence, the total dissolved Cr in the melt is just dominated by Cr^{III} species. In the case of moderate reducing condition (Co/CoO), some of the Cr^{III} oxo-complex might be reduced to Cr^{II} oxo-complex (*cf.* Eq. 2.48 in Chapter 2). Thus, the total dissolved Cr in this case is dominated by Cr^{III} species with a little contribution of Cr^{II}. Khedim[99] has shown that there are slightly speciations in the case of binary NxS glasses which can explain the higher values of Cr solubility in NxS.

➢ *Oxidising (air) and reducing (Fe/FeO) conditions*

At present, understanding of this phenomenon remains incomplete and more research is needed to better define the actual mechanisms involve in this condition. However, some light assumptions have been proposed as an attempt to understand this phenomenon.

Under these conditions, the Cr solubility is more significant in binary NxS melts for a given melt basicity. Thus, one may conclude that the difference of Cr solubility between NxS and NCxS is significant only when there are speciation reactions in the melt (oxidation and reduction). As a consequence, the first

assumption might be done based on the influence of CaO on the reactions which are governed by O_2/O^{2-} couple.

The second assumption is the theoretical optical basicity (Λ_{th}) as well as the aNa_2O do not represent the full generality of basicity for different type of melts. When dealing with a series of different melts, it is necessary to consider the change in ionicity of the oxide species resulting from the different compositions. The tendency of the medium to release O^{2-} ions to participate in the redox reactions might not be very simple to be compared for different types of melts with different oxide modifiers. Consequently, the redox as well as the dissolution behaviour of Cr_2O_3 in different types of melts are difficult to have a linear comparison.

The second assumption deals with the nature of the melts themselves *i.e.* the viscosity of the glasses. The viscosity of the melts (log η) has been plotted as a function of temperature (Figure 5.29).

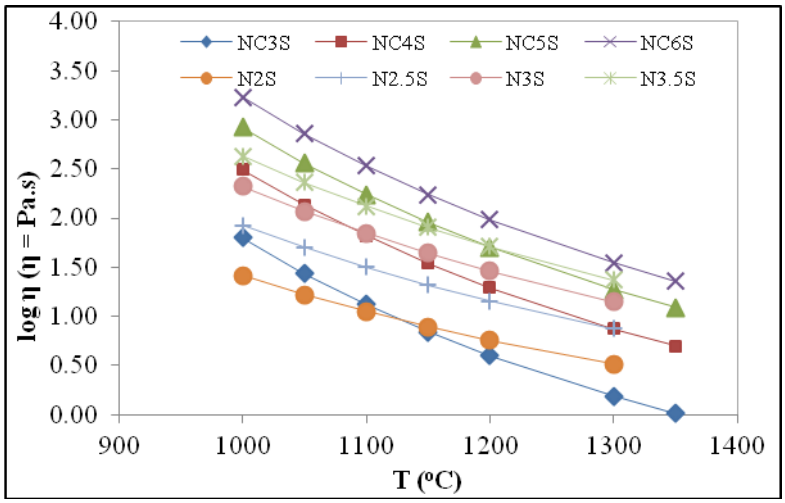

Figure 5.29: Calculated viscosity for soda silicate (NxS) and soda-lime silicate (NCxS) melts as a function of temperature (°C)[133]

Under oxidising conditions (air), the Cr^{III} oxo-complex will be oxidised to Cr^{VI} oxo-complex by following an oxidation reaction (*cf.* Eq. 2.47 in Chapter 2). If the viscosity of the melts at 1200°C is taken into account, it can be seen that the viscosity of NCxS is higher than NxS for the melts which possess almost the same Λ_{th}. As a consequence, the chemical reactivity of the elements in the system is very low, hence the oxidation of Cr^{III} which undergoes an octahedral-tetrahedral change in stoichiometry might be difficult to take place in more viscous melt. The low reactivity in more viscous melt could also be due to the low diffusion of oxygen which is responsible on the redox reactions. It has been shown in the kinetics part that the oxygen diffusion coefficient which has been determined in the ternary melt is quite low which is 10^{-9} cm^2/s. The same assumptions have been considered in the case of the reducing condition (Fe/FeO).

5.2.2. Redox behaviour in silicate melts

5.2.2.1. Determination of redox ratio

The determination of the Cr^n/Cr^{III} ratio values from the experimental data might be possible by treating the global curves of total dissolved Cr in the melts as a function of fO_2. In order to achieve this goal, the content of different Cr valences present in this melt should be determined. However, the experimental data reported in the previous part only concern the variation of total dissolved Cr in molten glass; *i.e*. the sum of all Cr valences (Eq. 5.14).

$$Cr(total) = Cr^{II} + Cr^{III} + Cr^{VI} \quad (5.14)$$

The following hypotheses have been introduced in order to determine the contribution of each Cr valences:

- Since the dissolution of Cr_2O_3 to Cr^{III} oxo-complex is an acid-base reaction, at equilibrium, the Cr^{III} is assumed to remain constant as long as Cr_2O_3 grains are remaining in the melts.
- The contribution of Cr^{II} is negligible under oxidizing atmosphere.
- The contribution of Cr^{VI} is negligible under reducing atmosphere.

As a consequence, Eq. 5.14 can be reduced to the following assumptions:

$$Cr(total) = Cr^{III} + Cr^{VI} \text{ (Oxidising condition)} \quad (5.15)$$

$$Cr(total) = Cr^{III} + Cr^{II} \text{ (Reducing condition)} \quad (5.16)$$

An example of the redox data refinement has been illustrated in Figure 5.30. The minimum of solubility in the intermediate fO_2 region corresponds to the constant Cr^{III} content. It has been estimated graphically after plotting the general trend given by the experimental points.

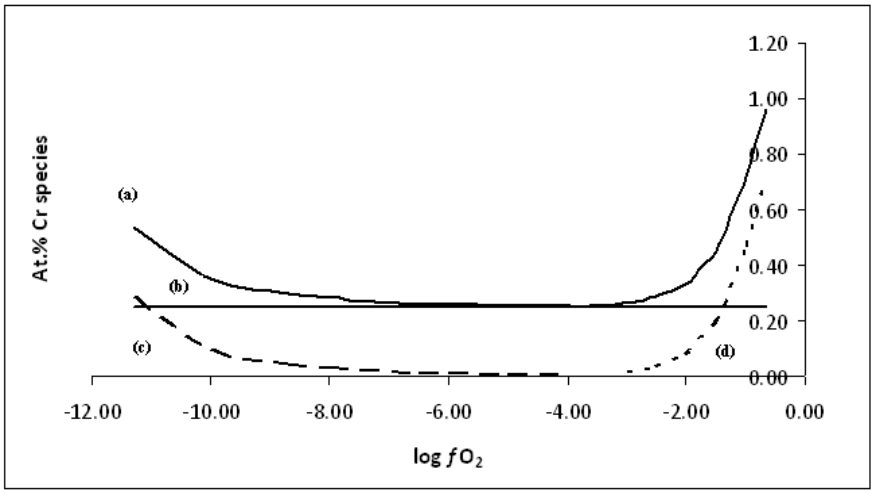

Figure 5.30: Cr species solubility representation as a function of log fO_2 (a) The total dissolved Cr in glass melt; (b) The Cr^{III} species contribution; (c) The Cr^{II} species contribution; (d) The Cr^{VI} species contribution

The plot above reveals that under oxidising atmosphere, an increase in the total dissolved Cr in the melt is due to an increase of the Cr^{VI} species. The same assumption has been performed under reducing conditions where an increase in the total dissolved Cr is due to an increase of Cr^{II} contribution in the melt.

5.2.2.2. Influence of oxygen fugacity (fO_2) on Cr redox behaviour in silicate melts

The influence of fO_2 on the Cr redox behaviour in silicate melts have been investigated in the case of NC3S at 1200°C. This is due to the difficulties to quantify the Cr speciations on the other compositions of the melts (NC4S, NC5S and NC6S) since the total dissolved Cr measured by EPMA is very low in soda-lime silicate melts, hence making the hypotheses of the redox difficult to be applied on the experimental data. A higher total dissolved Cr in the melt can be achieved by increasing the temperature of the heat treatment. However, less metal/metal oxide buffer is possible to induce a higher fO_2 (oxidising) at higher temperature.

The plot of log (Cr^n/Cr^{III}) as a function of log fO_2 is displayed in Figure 5.31. The slopes values arise from the chromium speciation (Eq. 2.47 and 2.48 in Chapter 2) and are linked to (i) the fact that O_2/O^{2-} is the couple reacting with the Cr^n/Cr^{III} couple (ii) Cr^{II} and Cr^{VI} are the species to consider in the reduction and oxidation reactions respectively. In the study of Khedim *et al.* previously performed on binary melts, the values of -0.25 and 0.75 have been verified in reducing and oxidising condition respectively.

However, in the case of NC3S at 1200°C the observation under oxidising condition seems to deviate from the theoretical slope.

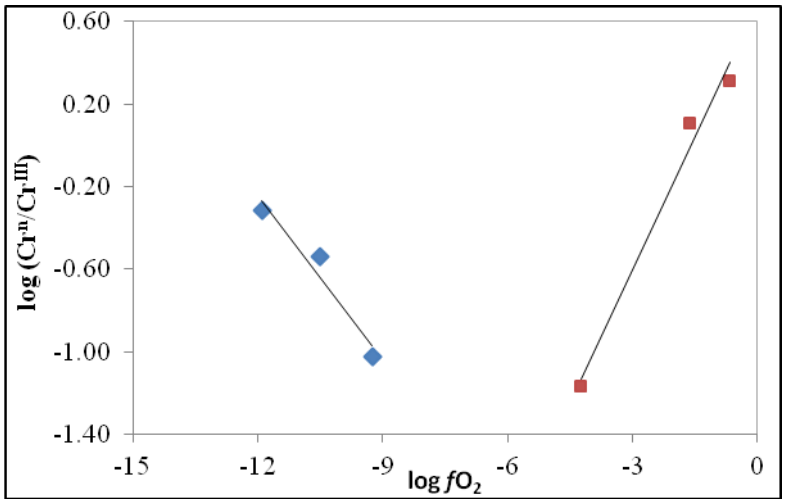

Figure 5.31: Variation of log (Cr^{n}/Cr^{III}) as a function of log fO_2 in the glass NC3S at T = 1200°C

- log (Cr^{II}/Cr^{III}) = -0.27x - 3.4263 (R^2 = 0.9405)
- log (Cr^{VI}/Cr^{III}) = 0.43x + 0.6904 (R^2 = 0.9822)

Some assumptions have been made in order to have an understanding of the deviation phenomenon under oxidising conditions. The first hypothesis has been made based on the formation of peroxide ion in the melt due to a reaction of the oxide ion and molecular oxygen according to the following equation:

$$O^{2-}(glass) + \frac{1}{2}O_2(gas) \Leftrightarrow O_2^{2-} \qquad (5.17)$$

Murata *et al.*[134] have observed the formation of Cr^{IV} in alkaline-earth aluminate, gallate and alumina-silicate glasses with modifier contents of ≥ 60 mol%. However, the optical observation on the colouration of the glass ball seems to contravene with this hypothesis. The yellowish colouration of the glass ball which has been confirmed with the UV-Vis[99] investigation prove the existence of Cr^{VI}. Furthermore, the peroxide ion is normally formed in very basic melts. However, the

peroxide ion was never formed in more basic melts of soda silicate glass[99]. So we can conclude that this assumption might be wrong.

The second hypothesis deals with the equilibrium of the system. The deviation from the theoretical slope might be due to the equilibrium which has not been reached in the system. Even though it is difficult to achieve the equilibrium in the case of oxidising condition since the solute and solvent are not stable with the heat treatment, however the kinetic study has allowed us to arrive as close as possible to the equilibrium state.

At present, understanding of this phenomenon remains incomplete and more research is needed to find a better explanation on this behaviour.

5.2.3. Summary of the thermodynamic approach of Cr_2O_3 in silicate melts

This part has been devoted to the investigation of the Cr_2O_3 behaviour in silicate melts by considering the thermodynamic approach. The influence of temperature (T), oxygen fugacity (fO_2) and melt basicity on the total dissolved Cr in the Cr_2O_3 saturated melts has been shown. The important outcomes have been listed down:

- The temperature dependence of Cr solubility seems to obey an Arrhenius law, *i.e.*, Cr solubility increases with an increase of temperature. The comparison of activation energies reveals that the minimum energy required to initiate the reaction under oxidising conditions is much lower than the one in reducing condition.

- The results indicate that fO_2 induces the oxidation states of Cr for a given glass composition and at fixed temperature. Cr^{II} and Cr^{VI} is the predominant species under reducing and oxidising conditions respectively. However, chromium is present in the valency of III under intermediate condition.

- Influence of basicity has been studied for two cases; ternary melt (soda-lime silicate melts) and different types of melts (comparison between ternary soda-lime silicate and binary soda silicate melts). The results show that increasing basicity seems to increase the significance of fO_2 on the total dissolved Cr for two extreme fO_2, *i.e.* oxidising (air) and reducing atmospheres (Fe/FeO). The comparison between different type of melts reveal a significant difference of the total dissolved Cr between ternary and binary melts for a given optical basicity and Na_2O activity under oxidising (air) and reducing (Fe/FeO) conditions. However, there is no profound effect of the different basicity for different types of melts under intermediate condition (Ni/NiO).

- The quantification of the redox ratio has been performed on the most reliable and complete set of data which is NC3S at 1200^{o}C. It seems like the slope under the reducing condition seems to obey the theoretical equation (-0.25). However, the obtained results under the oxidising condition seems to deviate from the theoretical slope. Some hypotheses have been detailed in the discussion. At present, understanding of this phenomenon remains incomplete and more research is needed to find a better explanation on this behaviour.

5.3. Chromia solubility in soda-lime silicate glass: Correlation with the corrosion of chromia forming alloy in the melt

The works performed in this chapter will lead to the determination of solubility limit of Cr_2O_3 at the thermodynamic equilibrium for different parameters *i.e.* temperature, oxygen fugacity and melt basicity. Hence, an effort has been made in order to have an insight on the correlation between these thermodynamic data with the Cr content measured in the corrosion study (Chapter 4) at a specific condition. A comparison between these two data has been determined for Ni-30Cr alloy in two different viscosities of the melts (NC3S and NC6S) at two different temperatures (1100°C and 1150°C) (Figure 5.29). Since the limit of solubility of Cr_2O_3 in the melts has been determined experimentally at higher temperature (≥ 1200°C) as compared to the corrosion study which has been performed at 1100°C, an extrapolation from an Arrhenius plot has been done in order to have an access to the Cr solubility at the lower temperature. It has been shown in this chapter that the dependence of Cr solubility on the temperature is in accordance with an Arrhenius law. The compilation of the comparison is displayed in Table 5.7.

Table 5.7: A comparison between the Cr concentration (at.%) determined in the corrosion study and the limit of Cr solubility which is determined from the thermodynamic study

Glass	Cr content at the interface (at.%)		Cr solubility (thermodynamic data) (at.%)	
	1100°C	**1150°C**	**1100°C**	**1150°C**
NC3S	0.33 (NPO) 0.25 (PO)	0.38 (NPO) 0.27 (PO)	0.27	0.36
NC6S	0.13 (NPO) 0.15 (PO)	/	0.09	0.11

*PO represents the preoxidised alloys
*NPO represents the non-preoxidised alloy

The values in Table 5.7 prove that there is no significant difference of Cr content and Cr solubility determined in corrosion and thermodynamic studies respectively for a given temperature and melt composition. Hence, one may conclude that the solubility measurement seems to be a good indicator on the corrosion behaviour of the alloy. The Cr content seems to achieve the steady state since they possess almost the same values with the Cr solubility which are already or very close to the thermodynamic equilibrium. Thus, it can be concluded that the driving force of the corrosion is the saturation of the glass by Cr. In the corrosion test, the experiments have been performed in a semi-infinite system and not in a close system. Since the temperature and viscosity of the melts may influence the behaviour of Cr diffusion, an effort has been made on the evolution of the Cr diffusion in the melt as a function of distance from the surface of alloy/melt for different temperatures and melt composition. The concentration profile of Cr is displayed in Figure 5.32.

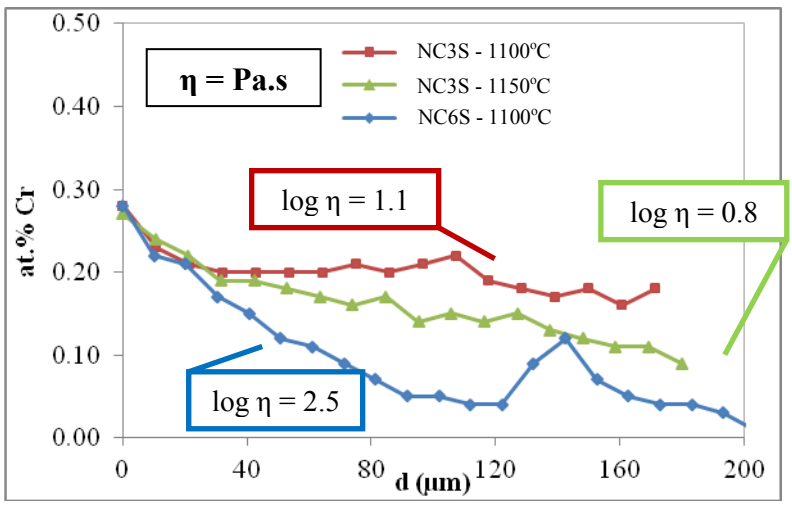

Figure 5.32: The concentration profile of Cr in the melts measured on Ni-30Cr alloy after immersion at 1100°C for 24 hours in NC3S and NC6S and at 1150 °C for 24 hours for NC3S

The concentration profiles observed in Figure 5.32 show that the Cr content exhibit quite the same value at the surface for the all three samples, *i.e.* the

equilibrium value of solubility. In the case of NC3S at 1100°C, the homogeneity of the Cr content can be obtained in a relatively a long distance from the surface. It seems like there is no significant difference of Cr diffusion in the case of NC3S at 1100°C and 1150°C.

By comparing the plot for NC3S and NC6S, it is obviously seen that the slope of the Cr concentration is more significant in the case of more acidic and higher viscosity melt, *i.e.* NC6S. The Cr content tends to decrease in such a shorter distance from the surface as compared to NC3S. As a consequence, due to the much higher viscosity of NC6S (more than one order of magnitude), Cr saturation can be achieved after 24 h of immersion at the interface: the chromium dilution in the glass is limited, thus restricting any further corrosion reaction at this region.

However, an opposite behaviour has been observed in the case of more basic and less viscous melts *i.e.* NC3S. The Cr diffuses in a relatively long distance as compared to NC6S, and is diluted in the glass. As a consequence, the Cr saturation will not be achieved in a short distance from the surface thereby allowing severe corrosion as compared to NC6S.

The results show that the determination of the limit solubility of Cr_2O_3 in the melt remains the best method as a complementary experiment to the electrochemical measurement of the alloy since the works have been performed in a close system and in such a shorter time. Furthermore, the system is certainly in equilibrium or as close as possible to the equilibrium. Therefore, it can be a good indicator to the real corrosion behaviour of the alloy by molten glass.

CHAPTER 6

CONCLUSIONS AND FUTURE RESEARCH RECOMMENDATIONS

The protection of Ni-based alloys against corrosion at high temperature by molten glasses is a great challenge faced by the industry. The efficiency of chromium and aluminium as added elements has been proved in the case of hot air corrosion, as they can lead to the formation of a protective and homogeneous oxide layer on the substrate. Molten glass is a specific media which exhibits redox and acid-base properties. As a consequence, the long term protection of the alloys is directly linked to the stability of the oxides in such harsh environments.

The 'raw immersion' and electrochemical techniques lead to a thorough observation on the corrosion behaviour of the alloys in molten glass. The results reveal that alumina can never provide the protection to the alloy in the molten glass, which is in contrary to the behaviour with hot corrosion phenomena where an alumina is a very stable oxide in hot air. This is due to the fact that alumina possesses a very high solubility in molten glasses. Thus, the thickness of alumina formed at the interface will not have any importance in the case of corrosion by molten glass since it will have a high dissolution in the melt.

On the contrary with alumina forming alloy, chromia forming alloy has a promising ability to resist against corrosion by molten glass since the solubility limit of chromia is one of the lowest amongst several oxides. It has been proved that the protection can be achieved by a preoxidation treatment in air before immersion in the molten glass. This treatment allows the development of homogeneous and adherent

chromia layer, thus providing an advance protection to the alloy before having contact with the melt. However, the spontaneous behaviour of chromia forming alloy leads to the corrosion phenomenon since the chromia dissolution prevails over the growth of the oxide. As a consequence, one may conclude that the competition between the dissolution and the growth of chromia plays a crucial role in determining the protection of the alloy in molten glass. It has been shown that there is an existence of a critical limit of solubility of chromia in the melt. Beyond this critical value, the dissolution process prevails over the oxide growth, thus leading to the loss of the protective scale. Even though chromia possesses a very low solubility in the melt, and since there is a critical limit of solubility, it is important to determine the limit of solubility of chromia in the molten glass. Hence, a thermodynamic study has been conducted on the physicochemical properties of chromia in the melts.

A preliminary study has been devoted to the dissolution kinetics of chromia in the ternary soda-lime silicate melts in order to determine the time and mechanism to reach the equilibrium. The results reveal that the time to reach the equilibrium varies with the oxygen fugacity (which is linked to the Cr speciation), temperatures and melt compositions (which is related to the melt viscosity and basicity). The rate determining step in the attainment of the equilibrium is controlled by the diffusion of oxygen within the melt provided that the glass has been prepared in oxidising atmosphere (air). Despite the difficulties arising due to the Na and Cr^{VI} volatilisation from the melt for a long experimental duration, a compromising equilibrium time and a specific method of analysis have been chosen in order to satisfy all the problems encountered. A heat treatment time of 2 hours has been chosen for almost all of the samples while performing the analysis on the rim of the sample. Indeed the

equilibrium will first take place in the rim as it is directly in contact with the imposed atmosphere. However, a longer heat treatment has been performed on most acidic melts under reducing condition (Fe/FeO) for the lowest temperature of heat treatment. In these conditions (high viscosity, lower temperature), the viscosity of the glass is a factor limiting the oxygen diffusion. Consequently a heat treatment time of 4 hours has been chosen as a sufficient time to reach the equilibrium.

The thermodynamic study of the chromia in ternary soda-lime silicate glass has been performed as a continuation of the study on binary soda silicate melts. Generally, it is obviously seen that the total dissolved chromium in ternary soda-lime silicate melts is lower than in the binary soda silicate melts. As most of the values are very low (< 1 at.% Cr), a specific attention has been paid on the significance of the results in subsequent discussions. The influence of temperature and oxygen fugacity on the Cr solubility in ternary melts seems to be in coherence with the observations in binary melts. The temperature dependence of Cr solubility seems to obey an Arrhenius law *i.e*. the Cr solubility increases with an increase of temperature. The oxygen fugacity induces Cr speciations at a given temperature and at a fixed glass composition. Cr^{II} and Cr^{VI} are the predominant species under reducing and oxidising conditions respectively. However, chromium is present in the valency of III under the intermediate condition.

The influence of melt basicity on the Cr solubility in ternary soda-lime silicate melts shows a dependency of this parameter on the oxygen fugacity, thus the Cr speciation. Under oxidising conditions, the Cr solubility seems to increase with an increase of the melt basicity since the Cr^{VI} is stabilised in this condition. However,

an opposite trend occurs under reducing conditions where the Cr solubility decreases with an increase of melt basicity. This phenomenon has been observed due to the fact that Cr^{II} is stabilised under reducing condition.

There is a concern on the trend of Cr solubility in the different types of melts possessing different oxide modifiers. For example, sodium oxide Na_2O in binary Na_2O-$xSiO_2$ system has been substituted by calcium oxide CaO to give the ternary Na_2O-CaO-$xSiO_2$ system. Thus, the aim is to make a comparison between the two families of glasses with constant silica content. An effort has been done in order to have a view on the comparison of Cr solubility for binary soda silicate and ternary soda-lime silicate melts by taking into account the theoretical optical basicity (Λ_{th}) and the activity of Na_2O as an indicator of the trend of basicity for different types of melts. The results reveal a significant difference of the total dissolved Cr between ternary and binary melts for a given optical basicity (Λ_{th}) and activity of Na_2O (log pa(Na_2O)) under oxidising (air) and reducing (Fe/FeO) conditions. It is obviously seen that the CaO shows a great influence when the redox reactions are predominant. As a consequence, one may assume that an introduction of CaO to the binary soda silicate melt might influence the reaction involving species from the O^{2-}/O_2 couple.

The real role played by this network modifier on the physicochemical properties of the system has not been clarified yet, and many outlooks could be proposed. CaO is considered as a basic oxide, but its real influence should be quantified. A development of electrochemical methods with specific electrodes to quantify the oxide ions O^{2-} activity should be implemented. These electrodes allow

the consideration of the contribution of all the oxides present in the melt on the oxide ions activity.

The redox ratios (Cr^{II}/Cr^{III} in reducing condition and Cr^{VI}/Cr^{III} under oxidising conditions) can be estimated through a mathematical refinement. The speciation reactions of Cr^{III} can be written by considering reduction to Cr^{II} and oxidation to Cr^{VI} through reactions with the O_2/O^{2-} couple. If these assumptions are correct, the plot of the log of these ratios as a function of log fO_2 are expected to lead to linear dependence with slopes equal to -0.25 and 0.75 under reducing and oxidising reactions respectively. This has previously been verified in the case of binary melts of the Na_2O-$xSiO_2$ system. In the case of the ternary Na_2O-CaO-$xSiO_2$ system, it is difficult to consider the data due to some significant reasons: (i) the solubility of chromium in these melts is very low, thus leading to a difficulty to discuss its evolution when changing the parameters (temperature, melt composition, oxygen fugacity), and (ii) less oxygen buffers are available at higher temperatures under oxidising atmospheres thus limiting the available experimental data. As a consequence, the data treatment of the redox ratio has been performed on the most reliable and complete set of data which is NC3S at 1200°C. The slope under the reducing condition seems to obey the theoretical value deduced from equation (-0.25), but a significant deviation is observed from the theoretical 0.75 expected in the oxidising condition. Some hypotheses have been detailed in the discussion. However, at present, understanding of this phenomenon remains incomplete and more research is needed to find a better explanation on this behaviour.

In order to tackle this problem, in-situ quantification of chromium speciation by different spectroscopic methods (XANES, UV-Visible, *etc*…) could be performed to give access to accurate values of the redox ratios. Furthermore, EXAFS spectroscopy could be used to give access to the coordination sphere of chromium. A better knowledge of the oxo-complexes corresponding to the different oxidation states of chromium in the different types of melts could be helpful to get further information about the physicochemical properties of these melts.

The main problem encountered during the treatment of the solubility data is the fact that the measured values are very low. The exploitation of the data in order to emphasise the influence of any parameters is thus quite difficult. Hence, the study of the physicochemical properties of other multivalent elements with higher limit of solubility could be of interest depending on the needs. For example, tin oxide SnO_2 could be studied, as it exhibits a limit of solubility about 5 times higher than Cr_2O_3. Furthermore tin also possesses the oxidation states of 2 and 4.

The limit of solubility of chromium determined at equilibrium by extrapolation compared with the chromium contents measured after the corrosion tests of the chromia forming alloy Ni-30Cr, revealed that close to the interface between the chromia layer and the considered glass, the chromium dissolution can be considered to be at equilibrium state. The glass saturated by dissolved chromium species can thus be considered as the driving force of corrosion.

As the corrosion tests occur in semi infinite media, the diffusion of chromium through the melt is also an important parameter that might be considered. The

chromium concentration profiles show that in the most viscous glass studied here (*i.e.* NC6S), the chromium diffusion is limited to a ~ 90 µm after 24 h, contrary to the less viscous glass (*i.e.* NC3S) where significant amounts of chromium can be detected at 200 µm from the interface in the same conditions. The viscosity is thus an important parameter that must be taken into account. In spite of the intrinsic ability of a glass to dissolve chromia, the corrosion will be restricted when there is a saturation of the glass with chromium. This phenomenon occurs if the viscosity of the melt is high enough to induce a slow diffusion of chromium. On the other hand, if the low viscosity of the glass allows a high diffusion rate of the chromium species, the chromia can be dissolved indefinitely as the glass will never be saturated. The influence of this parameter could be studied through electrochemical measurement performed with a rotating working electrode.

The physicochemical properties of silicate melts at high temperatures are complex, even in a simple ternary system, the composition which has been specifically studied in this present work. These properties play a crucial role to understanding the corrosion of alloys in contact with molten glass. The studies conducted on simple systems give an access to a lot of information. Furthermore, the introduction of CaO in this work is actually a first step to simulating real cases of glass corrosion. Thus, it can be of great interest to extend the works on a more complex systems such as CMAS (CaO-MgO-Al_2O_3-SiO_2). CMAS is a well known corrosive media, specifically in the aeronautic domain, where the TBC (Thermal Barrier Coatings) is subjected to catastrophic corrosion by this kind of glass. As a consequence, the understanding of the behaviour of alkaline-earth oxides appears to be very important in the high temperature corrosion phenomena.

REFERENCES

1. Paul, A. *Chemistry of Glasses*. (Chapmann & Hall, 1990).

2. Barton, J. & Guillemet, C. *Le verre Science et technologie*. (EDP Sciences, 2005).

3. Zachariasen, W. H. The atomic arrangement in glass. *J. Am. Chem. Soc.* **54,** 3841–3851 (1932).

4. Sun, K.-H. Fundamental condition of glass formation. *J. Am. Ceram. Soc.* **30,** 277–281 (1947).

5. Dietzel, A. Die kationenfeldstarken und ihre beziehungen zu Entglasungsvorgagen, zur Verbindungsbildung und zu den Schmelzpunkten von Silikaten. *Z Electrokem* **48,** 9–23 (1942).

6. Abdelouhab, S., Podor, R., Rapin, C., Toplis, M., Berthod, P. & Vilasi, M. Determination of Na_2O activities in silicate melts by EMF measurements. *J. Non-Cryst. Solids* **354,** 3001–3011 (2008).

7. Haussonne, J.-M. *Céramiques et verres: principes et techniques d'élaboration*. (PPUR presses polytechniques, 2005).

8. Neuville, D. R. & Mysen, B. O. Role of aluminium in the silicate network: In situ, high-temperature study of glasses and melts on the join SiO_2-$NaAlO_2$. *Geochim. Cosmochim. Acta* **60,** 1727–1737 (1996).

9. Duffy, J. A. & Baucke, F. G. K. Redox equilibria and corrosion in molten silicates: relationship with electrode potentials in aqueous solution. *J. Phys. Chem.* **99,** 9189–9193 (1995).

10. Abdelouhab, S., Rapin, C., Podor, R., Berthod, P. & Vilasi, M. Electrochemical study of chromium corrosion in Na_2O–$xSiO_2$ melts. *J. Electrochem. Soc.* **154,** C500–C507 (2007).

11. Khedim, H., Podor, R., Panteix, P. J., Rapin, C. & Vilasi, M. Solubility of chromium oxide in binary soda-silicate melts. *J. Non-Cryst. Solids* **356,** 2734–2741 (2010).

12. Bronsted, J. N. The conception of acids and bases. *Recl. Trav. Chim. Pays Bas Er Belg.* **42,** 718–728 (1923).

13. Lowry, T. M. Stability of coordination compounds. *Chem. Ind.* **42,** 711–715 (1923).

14. Lewis, G. N. *Valence and structure of atoms and molecules*. (Chemical Catalog Co, 1923).

15. Lux, H. Säuren und Basen im SchmelzfluB: Die Bestimmung der Sauerstoffionenkonzentration. *Z Elektrochem* **45,** 303–309 (1939).

16. Flood, H. & Forland, T. The acidic and basic properties of oxides. *Acta Chem Scand* **1,** 592–604 (1947).

17. Perander, M. & Karlsonn, K. H. Acidity and ionic structure of molten alkali silicates. *J. Non-Cryst. Solids* **80,** 387–392 (1986).

18. Stegmaier, W. & Dietzel, A. Die Bedeutung der Basizität von Glasschmelzen und Versuche zu deren Messung. *Glas. Ber* **18,** 297–308 (1940).

19. Konakov, V. G. From the pH scale to the pO scale. The problem of the determination of the oxygen ion O^{2-} activity in oxide melts. *J. Solid State Electrochem.* **15,** 77–86 (2010).

20. Sun, K. A scale of acidity and basicity in glass. *Glass Ind.* **98,** 73–74 (1948).

21. Cameron, R. A. Kinetics of arsenic-antimony fining. *Present. Symp. Gases Glass* **44,** 405 (1965).

22. Sanderson, R. T. Electronegativities in inorganic chemistry. *J. Chem. Educ.* **29,** 539–544 (1952).

23. Sanderson, R. T. Electronegativities in organic chemistry II. *J. Chem. Educ.* **31,** 2–7 (1954).

24. Sanderson, R. T. Electronegativities in organic chemistry III. *J. Chem. Educ.* **31,** 238–245 (1954).

25. Sanderson, R. T. Electronegativities in organic chemistry: A revision of atomic charge data. *J. Chem. Educ.* **32,** 140–141 (1955).

26. Toop, G. W. & Samis, C. S. Some new ionic concepts of silicate slags. *Can Met Quart* **1,** 129–152 (1962).

27. Dron, R. Acid-base reactions in molten silicates. *J. Non-Cryst. Solids* **53,** 267–278 (1982).

28. Shultz, M. M. Acid–base concept as applied to oxide melts and glasses and the D. I. Mendeleev theory of the vitreous State,. *Fiz Khim Stekla* **10,** 129–138 (1984).

29. Franz, H. Solubility of water vapor in alkali borate melts. *J. Am. Ceram. Soc.* **49,** 473–477 (1966).

30. Shakhmatkin, B. A. & Golubeva, O. Y. Thermodynamic modeling of dissolution of water in sodium borate melts. *Glass Phys. Chem.* **30,** 244–246 (2004).

31. Pearce, M. L. Solubility of carbon dioxide and the variation of oxygen ion activity in sodium borate melts. *J. Am. Ceram. Soc.* **48,** 175–178 (1965).

32. Pearce, M. L. Solubility of carbon dioxide and variation of oxygen ion activity in soda-silicate melts. *J. Am. Ceram. Soc.* **47,** 342–347 (1964).

33. Maeda, M., Mclean, A., Kuwatori, H. & Sano, N. Solubilities of carbon dioxide in sodium silicate melts. *Met. Mater. Trans. B* **16,** 561–566 (1985).

34. Holmquist, S. Oxygen ion activity and the solubility of sulfur trioxide in sodium silicate melts. *J. Am. Ceram. Soc.* **49,** 467–473 (1966).

35. Paul, A. & Douglas, R. W. Coordination equilibria of nickel(II) in alkali borate glasses. *Phys. Chem. Glas.* **8,** 233–237 (1967).

36. Paul, A. & Douglas, R. W. Optical absorption of divalent cobalt in binary alkali borate glasses and its relation to the basicity of glass. *Phys. Chem. Glas.* **9,** 21–26 (1968).

37. Paul, A. & Douglas, R. W. Ultraviolet absorption of chromium (VI) in some binary and ternary alkali and alkaline earth oxide glasses. *Phys. Chem. Glas.* **9,** 27–31 (1968).

38. Rego, D. N., Sigworth, G. K. & Philbrook, W. O. Thermodynamic study of Na_2O-SiO_2 melts at 1300° C and 1400° C. *Met. Mater. Trans. B* **16,** 313–323 (1985).

39. Rego, D. N., Sigworth, G. K. & Philbrook, W. O. Thermodynamic activity of Na_2O in Na_2O-CaO-SiO_2, Na_2O-MgO-SiO_2, and Na_2O-CaO-SiO_2-Al_2O_3 melts at 1400° C. *Met. Mater. Trans. B* **19,** 655–661 (1988).

40. Neudorf, D. A. & Elliott, J. F. Thermodynamic properties of Na_2O-SiO_2-CaO melts at 1000 to 1100 ^oC. *Met. Trans. B-Process Met.* **11,** 607–614 (1980).

41. Lin, R. Y. & Elliott, J. F. High-temperature electrochemical study of Na_2O-MoO_3 melts. *J. Alloys Compd.* **321,** 261–266 (2001).

42. Lin, R. Y. & Elliott, J. F. Thermochemistry of Na_2O-WO_3 system at 1065 to 1239 K. *Met. Mater. Trans.* **14,** 1713–1720 (1983).

43. Yokokawa, T., Tamura, S., Sato, S. & Niwa, K. Ferric-Ferrous Ratio in Na_2O-P_2O_5 Melts. *Phys. Chem. Glas.* **15,** 113–115 (1974).

44. Sato, S., Yokokawa, T., Kita, H. & Niwa, K. Thermodynamic Activity of Na_2O-B_2O_3 Melts. *J. Electrochem. Soc.* **119,** 1524–1526 (1972).

45. Duffy, J. A. & Ingram, M. D. An interpretation of glass chemistry in terms of the optical basicity concept. *J. Non-Cryst. Solids* **21,** 373–410 (1976).

46. Duffy, J. A. & Ingram, M. D. Behaviour of basicity indicator ions in relation to the ideal optical basicity of glasses. *Phys. Chem. Glas.* **16,** 119–123 (1975).

47. Duffy, J. A. & Ingram, M. D. Establishment of an optical scale for Lewis basicity in inorganic oxyacids, molten salts, and glasses. *J. Am. Ceram. Soc.* **93,** 6448–6454 (1971).

48. Duffy, J. A. & Ingram, M. D. Comments on the application of optical basicity to glass. *J. Non-Cryst. Solids* **144,** 76–80 (1992).

49. Duffy, J. A. & Harris, B. Reaction sites in network oxyanion systems. *Ironmak. Steelmak.* **22,** 132–136 (1995).

50. Nakamura, T., Yokokawa, T. & Toguri, J. M. Limitations in the metallurgical application of optical basicity. *Isij Int.* **33,** 204–209 (1993).

51. Rapp, R. A. Hot corrosion of materials: a fluxing mechanism? *Corros. Sci.* **44,** 209–221 (2002).

52. Rawson, H. *Glass Science and Technology 3, Properties and Applications of Glass*. (Elsevier Scientifc Publishing Company, 1980).

53. Bamford, C. R. *Colour generation and control in glass*. (Elsevier Scientific Pub. Co. : distributors for the U.S. and Canada, Elsevier North-Holland, 1977).

54. Tilquin, J.-Y., Duveiller, P., Glibert, J. & Claes, P. Comparison between high temperature UV-visible spectroscopy and electrochemistry for the in situ study of redox equilibria in glass-forming melts. *J. Non-Cryst. Solids* **224,** 216–224 (1998).

55. Tilquin, J. Y., Duveiller, P., Glibert, J. & Claes, P. Effect of basicity on redox equilibria in sodium silicate melts: An in situ electrochemical investigation. *J. Non-Cryst. Solids* **211,** 95–104 (1997).

56. Paul, A. & Douglas, R. W. Ferrous-ferric equilibrium in binary alkali silicate glasses. *Phys. Chem. Glas.* **6,** 207–211 (1965).

57. Laimbuck, P. R. Foaming of Glass Melts. PhD Thesis Technische Universiteit Eindhoven (1998).

58. Claes, P., Bacanamwo, Z. & Glibert, J. Influence of the partial pressure of oxygen on the redox chemistry of multivalent elements in molten sodium tetraborate. *J. Appl. Electrochem.* **22,** 293–300 (1992).

59. Schreiber, H. D., Peters, L. J., Beckman, J. W. & Schreiber, C. W. Redox chemistry of iron-manganese and iron-chromium interactions in soda lime silicate glass melts. *Glass Sci. Technol. Glas. Berichte* **69,** 269–277 (1996).

60. Thiemsorn, W., Keowkamnerd, K., Phanichphant, S., Suwannathada, P. & Hessenkemper, H. Influence of glass basicity on redox interactions of iron-manganese-copper ion pairs in soda-lime-silica glass. *Glass Phys. Chem.* **34,** 19–29 (2011).

61. Takahashi, K. & Miura, Y. Electrochemical studies on diffusion and redox behavior of various metal ions in some molten glasses. *J. Non-Cryst. Solids* **38–39, Part 2,** 527–532 (1980).

62. Douglas, R. W., Nath, P. & Paul, A. Oxygen ion activity and its influence on the redox equilibrium in glasses. *Phys. Chem. Glas.* **6,** 216–223 (1965).

63. Schreiber, H. D. Redox processes in glass-forming melts. *J. Non-Cryst. Solids* **84,** 129–141 (1986).

64. Baucke, F. G. K. & Duffy, J. A. The effect of basicity on redox equilibria in molten glasses. *Phys. Chem. Glas.* **32,** 211–218 (1991).

65. Decelle, E. Comportement redox de fontes d'oxydes non equilibrees avec leur atmosphere gazeuze. PhD Thesis Université Catholique de Louvain (2004).

66. Lizarazu, D. Comportement en oxydation a l'air et comportement electrochimique dans le verre fondu d'alliages nickel-chrome. PhD Thesis Université Henri Poincaré (1996).

67. Lizarazu, D., Steinmetz, P. & Bernard, J. L. Corrosion of Nickel-Chromium Alloys by Molten Glass at 1100 ^{o}C: An electrochemical study. *Mater. Sci. Forum* **251-254,** 709–720 (1997).

68. Gaillard-Allemand, B. Etude de la Corrosion de Materiaux Metalliques et Ceramique par le Verre de Confinement des Dechets Nucleaires Fondu. PhD Thesis Université Henri Poincaré (2001).

69. Schreiber, H. D., Wilk Jr, N. R. & Schreiber, C. W. A comprehensive electromotive force series of redox couples in soda-lime-silicate glass. *J. Non-Cryst. Solids* **253,** 68–75 (1999).

70. Rüssel, C. & Von Der Gönna, G. Electrochemical series of elements in the $Na_2O{\cdot}2SiO_2$ glass melt. *J. Non-Cryst. Solids* **260,** 147–154 (1999).

71. Di Martino, J., Rapin, C., Berthod, P., Podor, R. & Steinmetz, P. Corrosion of metals and alloys in molten glasses. Part 1: glass electrochemical properties and pure metal (Fe, Co, Ni, Cr) behaviours. *Corros. Sci.* **46,** 1849–1864 (2004).

72. Rapin, C., Vilasi, M., Podor, R., Carton, A., Gaillard-Allemand, B., Berthod, P. & Steinmetz, P. Three Examples of high-temperature corrosion of metals by molten glasses. *Mater. Sci. Forum* **461-464,** 1125–1132 (2004).

73. Fischer, B. Reduction of platinum corrosion in Molten glass. *Platin. Met. Rev* **36,** (1992).

74. Brandes, E. A., Brook, G. B. & Smithells, C. J. *Smithells metals reference book.* (Butterworth-Heinemann, 1998).

75. Podor, R., David, N., Rapin, C. & Berthod, in *Adv. Fusion Process. Glass III* (Varner, J. R., Seward, T. P. & Schaeffer, H. A.) 207–214 (John Wiley & Sons, Inc., 2006).

76. Podor, R., Rapin, C., David, N. & Mathieu, S. Kinetics and mechanisms of tantalum corrosion in glass melts. *J. Electrochem. Soc.* **151,** B661–B668 (2004).

77. Podor, R., David, N., Rapin, C., Vilasi, M. & Berthod, P. Mechanisms of corrosion layer formation during zirconium immersion in a (Fe)-bearing glass melt. *Corros. Sci.* **49,** 3226–3240 (2007).

78. Podor, R., Rapin, C., David, N. & Berthod, P. Titanium corrosion in molten glasses. Part 1: Immersion tests and corrosion kinetics. *Glass Sci. Technol.* **77,** 36–43 (2004).

79. Rapin, C., Podor, R., Michon, S., Berthod, P. & Mathieu, S. Titanium corrosion in molten glasses. Part 2. Electrochemical study and corrosion mechanisms. *Glass Sci. Technol.* **77,** 88–94 (2004).

80. Carton, A., Rapin, C., Podor, R. & Berthod, P. Corrosion of Chromium in Glass Melts. *J. Electrochem. Soc.* **153,** B121 (2006).

81. Kofstad, P. *High Temperature Corrosion*. (Elsevier Applied Science, 1988).

82. Wallwork, G. R. & Hed, A. Z. Some limiting factors in the use of alloys at high temperatures. *Oxid. Met.* **3,** 171–184 (1971).

83. Dutta, R. S., Yusufali, C., Paul, B., Majumdar, S., Sengupta, P., Mishra, R. K., Kaushik, C. P., Kshirsagar, R. J., Kulkarni, U. D. & Dey, G. K. Formation of diffusion barrier coating on superalloy 690 substrate and its stability in borosilicate melt at elevated temperature. *J. Nucl. Mater.* **432,** 72–77 (2013).

84. Raj, K., Prasad, K. K. & Bansal, N. K. Radioactive waste management practices in India. *Nucl. Eng. Des.* **236,** 914–930 (2006).

85. Lizarazu, D. Comportement en oxydation l'air et comportement lectrochimique dans le verre fondu d'alliages nickel-chrome. PhD Thesis Université Henri Poincaré (1996).

86. Di Martino, J., Rapin, C., Berthod, P., Podor, R. & Steinmetz, P. Corrosion of metals and alloys in molten glasses. Part 2: nickel and cobalt high chromium superalloys behaviour and protection. *Corros. Sci.* **46,** 1865–1881 (2004).

87. Lizarazu, D., Steinmetz, P. & Bernard, J. L. Corrosion of nickel-chromium alloys by molten glass at 1100 °C : An electrochemical study. *Mater. Sci. Forum* 709–719 (Trans Tech) (1997).

88. Manfredo, L. J. & McNally, R. N. Solubility of refractory oxides in soda-lime glass. *J. Am. Ceram. Soc.* **67,** 155–158 (1984).

89. Luo, G., Li, J., Shen, Q., Zhang, D. & Zhang, L. Corrosion behaviour of tin dioxide based electrode material at high temperature in molten soda-lime-silicate glass. *Corros. Sci.* **50,** 591–595 (2008).

90. Pardoen, B., Duvigneaud, P. H. & Plumat, E. Effect of Sintering on the impurities on SnO_2. *Silic Ind* **43,** 73 (1978).

91. Guigonis, J. M. L. Use of sintered refractory material based on tin oxide for producing glass. U.S. Patent 6880365 (2005).

92. Gateau, P., Petitjean, C., Panteix, P. J., Rapin, C. & Vilasi, M. Solubility of tin dioxide in soda-lime silicate melts. *J. Non-Cryst. Solids* **358,** 1135–1140 (2012).

93. Young, D. J. *High Temperature Oxidation and Corrosion of Metals, Volume 1*. **1,** (Elsevier Science, 2008).

94. Chellah, N. Etude de l'interaction entre une zircone du système ZrO_2-Nd_2O_3 et un dépôt complexe à base de Ca, Al, Si Application aux barrières thermiques. PhD Thesis Université Henri Poincaré (2013).

95. Monteiro, A. Etude des mécanismes de réactivité chimique des précurseurs lors de l' laboration d'un verre de confinement de d chet de haute activit : de l'exp rimentation à la modélisation. PhD Thesis Université de Toulouse (2012).

96. Sugita, K. *Historical Overview of Refractory Technology in the Steel Industry*. 8–17 (1998).

97. Hirata, T., Morimoto, T., Deguchi, A. & Uchida, N. Corrosion resistance of alumina-ceramic materials against molten slag. *Mater. Trans.* **43,** 2561–2567 (2002).

98. Abdelouhab, S. D termination de grandeurs physico-chimiques dans les verres fondus - Relation avec le comportement en corrosion du chrome et d'alliages chromine-formeurs. PhD Thesis Université Henri Poincaré (2005)

99. Khedim, H. Etude de la limite de solubilite de la chromine (Cr_2O_3) dans les silicates fondus-determination de grandeurs thermodynamiques et physicochimiques. PhD Thesis Université Henri Poincaré (2008).

100. Claes, P., Duveiller, P., Tilquin, J. Y. & Glibert, J. In situ electrochemical and spectrophotometric investigation of the oxygen pressure dependence of the [Cr(VI)]/[Cr(III)] ratio in a borosilicate melt. *Berichte Bunsen-Ges.-Phys. Chem.* **100,** 1479–1483 (1996).

101. Graham, H. C. & Davis, H. H. Oxidation/vaporization kinetics of Cr_2O_3. *J. Am. Ceram. Soc.* **54,** 89–93 (1971).

102. Caplan, D. & Cohen, M. Cathodic reduction of oxide scales on Cr and Fe-25 Cr Alloy. *J. Electrochem. Soc.* **108,** 1005–1008 (1961).

103. Khedim, H., Abdelouhab, S., Podor, R., Rapin, C., Vilasi, M., Panteix, P.J., Toplis, M. & Faure, M. Kinetic and equilibrium factors affecting saturation of chromium oxide in soda-silicate melts. *J. Non-Cryst. Solids* **357,** 31–42 (2011).

104. Khedim, H., Podor, R., Rapin, C. & Vilasi, M. Redox-control solubility of chromium oxide in soda-silicate melts. *J. Am. Ceram. Soc.* **91,** 3571–3579 (2008).

105. Mathieu, R., Khedim, H., Libourel, G., Podor, R., Tissandier, L., Deloule, E., Faure, F., Rapin, C. & Vilasi, M. Control of alkali-metal oxide activity in molten silicates. *J. Non-Cryst. Solids* **354,** 5079–5083 (2008).

106. Ledoux, X. Contribution à la mise au point de matériaux métalliques pour les unit s de production d'hydrogène par vaporeformage du gaz naturel : 1/ Etude de l'oxydation de mat riaux de structure l'air entre 650 et 1050°C 2/ Élaboration de revêtements et tude de leur r sistance l'oxydation. PhD Thesis Université Henri Poincaré (2012).

107. Bianco, R. Pack Cementation aluminide coatings on superalloys: codeposition of Cr and reactive elements. *J. Electrochem. Soc.* **140,** 1181 (1993).

108. Levine, S. R. & Caves, R. M. Thermodynamics and kinetics of pack aluminide coating formation on IN-100. *J. Electrochem. Soc.* **121,** 1051 (1974).

109. OUTOKUMPU RESEARCH, "HSC Chemistry for Windows 5.1", (2003).

110. Di ar tino, . Oxydation haute temp rature et corrosion par le verre C3 de superalliages base cobalt. PhD Thesis Université Henri Poincaré (2002).

111. Taneichi, K., Narushima, T., Iguchi, Y. & Ouchi, C. Oxidation or nitridation behavior of pure chromium and chromium alloys containing 10 mass% Ni or Fe in atmospheric heating. *Mater. Trans.* **47,** 2540 (2006).

112. Buscail, H. *et al.* X-Ray diffraction to study the oxidation mechanism of chromium at elevated temperatures. *Mater. Sci. Forum* **461-464,** 93–100 (2004).

113. Caplan, D. & Sproule, G. I. Effect of oxide grain structure on the high-temperature oxidation of Cr. *Oxid. Met.* **9,** 459–472 (1975).

114. Hindam, H. & Whittle, D. P. Microstructure, adhesion and growth kinetics of protective scales on metals and alloys. *Oxid. Met.* **18,** 245–284 (1982).

115. Cabet Leflaive, C. Corrosion des alliages base nickel par le verre fondu et sa vapeur. PhD Thesis Université Henri Poincaré (1999).

116. Schreiber, H. D., Kozak, S. J., Fritchman, A. L., Goldman, D. S. & Schaeffer, H. A. Redox kinetics and oxygen diffusion in a borosilicate melt. *Phys. Chem. Glas.* **27,** 152–177 (1986).

117. Van Limpt, H., Beerkens, R. & Verheijen, O. Models and Experiments for Sodium Evaporation From Sodium-Containing Silicate Melts. *J. Am. Ceram. Soc.* **89,** 3446–3455 (2006).

118. Konta, J. Volatility of oxides from silicate melt and the origin of moldavites. *Miner. Mag.* **40,** 70–78 (1975).

119. Doremus, R. H. Diffusion in glasses and melts. *J. Non-Cryst. Solids* **25,** 261–292 (1977).

120. Lamkin, M. A., Riley, F. L. & Fordham, R. J. Oxygen mobility in silicon dioxide and silicate glasses: a review. *J. Eur. Ceram. Soc.* **10,** 347–367 (1992).

121. Lafroukhi, O. Affinage des Verres au Plomb de Type Crystal. Comparaison des Pouvoirs Affinants des Systemes As3+/As5+ et Sb3+/Sb5+ Corrosion des Refractaires. PhD Thesis Université de Nancy I (1990).

122. Sasabe, M. & Goto, K. S. Permeability, diffusivity, and solubility of oxygen gas in liquid slag. *Met. Trans.* **5,** 2225–2233 (1974).

123. Wendlandt, R. F. Oxygen diffusion in basalt and andesite melts: experimental results and discussion of chemical versus tracer diffusion. *Contrib. Miner. Pet.* **108,** 463–471 (1991).

124. Goldman, D. S. & Gupta, P. K. Diffusion-controlled redox kinetics in a glassmelt. *J. Am. Ceram. Soc.* **66,** 188–190 (1983).

125. May, H. B., Lauder, I. & Wollast, R. Oxygen diffusion coefficients in alkali silicates. *J. Am. Ceram. Soc.* **57,** 197–200 (1974).

126. Dunn, T. Oxygen diffusion in three silicate melts along the join diopside-anorthite. *Geochim. Cosmochim. Acta* **46,** 2293–2299 (1982).

127. Litton, D. A. & Garofalini, S. H. Vitreous silica bulk and surface self-diffusion analysis by molecular dynamics. *J. Non-Cryst. Solids* **217,** 250–263 (1997).

128. Turkdogan, E. T. & Society, M. *Physicochemical properties of molten slags and glasses*. (Metals Society, 1983).

129. Philibert, J. *Diffusion et transport de matière dans les solides*. (Les editions de physique, 1985).

130. Schaeffer, H. A., Lachenmayr, H. & Pye, L. D. Oxidation studies of amber glass. *Glas. Ber* **56K(I),** 602–607 (1983).

131. Berry, A. ., O'Neill, H. S. C., Scott, D. R., Foran, G. . & Shelley, J. M. G. The effect of composition on Cr2+/Cr3+ in silicate melts. *Am. Miner.* **91,** 1901–1908 (2006).

132. Morita, K., Tsukiashi, K., Kimura, M. & Sano, N. Activity of chromium oxide in CaO-SiO_2 based slags at 1873 K. *Steel Res. Int.* **76,** 279–283 (2005).

133. Fluegel, A., Varshneya, A. K., Earl, D. A., Seward, T. P. & Oksoy, D. *Melt Chem. Relax. Solidif. Kinet. Glas.* (Li, H., Ray, C. S., Strachan, D. M., Weber, R. & Yue, Y.) 129–143 (John Wiley & Sons, Inc., 2006).

134. Murata, T., Torisaka, M., Takebe, H. & Morinaga, K. Compositional dependence of the valency state of Cr ions in oxide glasses. *J. Non-Cryst. Solids* **220,** 139–146 (1997).

135. Huang, W. & Chang, Y. A. Thermodynamic properties of the Ni–Al–Cr system. *Intermetallics* **7,** 863–874 (1999).

136. *Binary alloy phase diagrams*. (ASM International, 1990).

137. De la Parra-Arciniega, S. M., Álvarez-Méndez, A., Torres-González, L. C. & Sánchez, E. M. Crystallization kinetics of a soda lime silica glass with TiO_2 addition. *Rev. Mex. Física* **55,** 32–37 (2009).

138. Wang, M.-T. & Cheng, J.-S. Viscosity and thermal expansion of rare earth containing soda-lime-silicate glass. *J. Alloys Compd.* **504,** 273–276 (2010).

139. Shen, J., Green, D. J., Tressler, R. E. & Shelleman, D. L. Stress relaxation of a soda lime silicate glass below the glass transition temperature. *J. Non-Cryst. Solids* **324,** 277–288 (2003).

140. Zamoum, F., Benlaharche, T., David, N., Podor, R. & Vilasi, M. Kinetics of high temperature oxidation of (Nb,Co,Cr)7Si6 and (Nb,Co,Cr)8Si7 silicide compounds. *Intermetallics* **16,** 498–507 (2008).

141. Wagner, C. Fehlordnungserscheinungen in kristallisierten polaren Verbindungen als Grundlage für Elektronen- und Ionen-Leitung. *Z. Für Elektrochem. Angew. Phys. Chem.* **39,** 543–545 (1933).

142. Berthod, P. Kinetics of High temperature oxidation and chromia volatilization for a binary Ni–Cr Alloy. *Oxid. Met.* **64,** 235–252 (2005).

APPENDICES

Appendix A: Characterisation of the alloys prepared by high frequency induction melting

The diffractograms of X-ray diffraction analysis (XRD) and the microstructures of the prepared alloys are shown in Figure A.1 and Figure A.2.

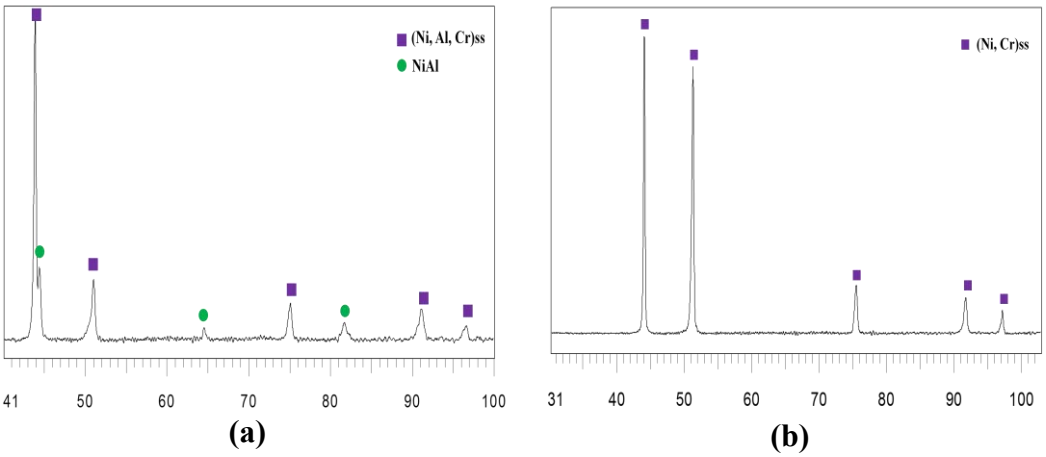

Figure A.1: Diffractograms of the obtained (a) Ni-8Al-28Cr (wt.%) and (b) Ni-30Cr (wt.%)

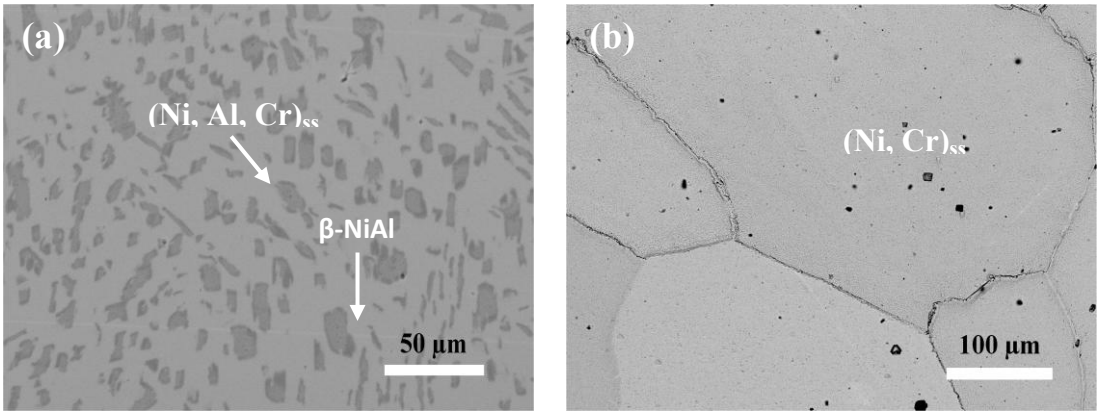

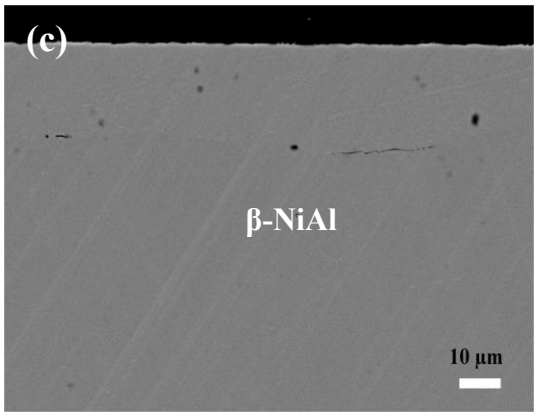

Figure A.2: Microstructures of the obtained (a) Ni-8Al-28Cr (wt.%), (b) Ni-30Cr (wt.%) and (c) NiAl (bulk)

The diffractograms of XRD (Figure A.1) and the micrographs of SEM (Figure A.2) prove that the Ni-8Al-28Cr contains β-NiAl precipitates in the matrix of (Ni, Al, Cr) solid solution. The β-NiAl precipitate contains 6.5 at.% of dissolved Cr. A homogeneous (Ni, Cr) solid solution and β-NiAl exist in Ni-30Cr and NiAl (bulk). The details of the phases measured by EPMA are listed in Table A.1:

Table A.1: The measured compositions of the alloys by EPMA

Alloys	Phases	Compositions (at.%)		
		Ni	Al	Cr
Ni-8Al-28-Cr	β-NiAl	57.51	35.77	6.48
(wt.%)	$(Ni, Al, Cr)_{ss}$	55.65	11.70	32.64
Ni-30Cr (wt.%)	$(Ni, Cr)_{ss}$	65.84	/	34.05
NiAl (bulk)	β-NiAl	48.20	51.76	/

The isothermal section of Ni-Al-Cr system at 1200^{o}C (Figure A.3) shows that the raw alloy is situated in the region where the γ-(Ni, Al, Cr) is in equilibrium with β-NiAl.

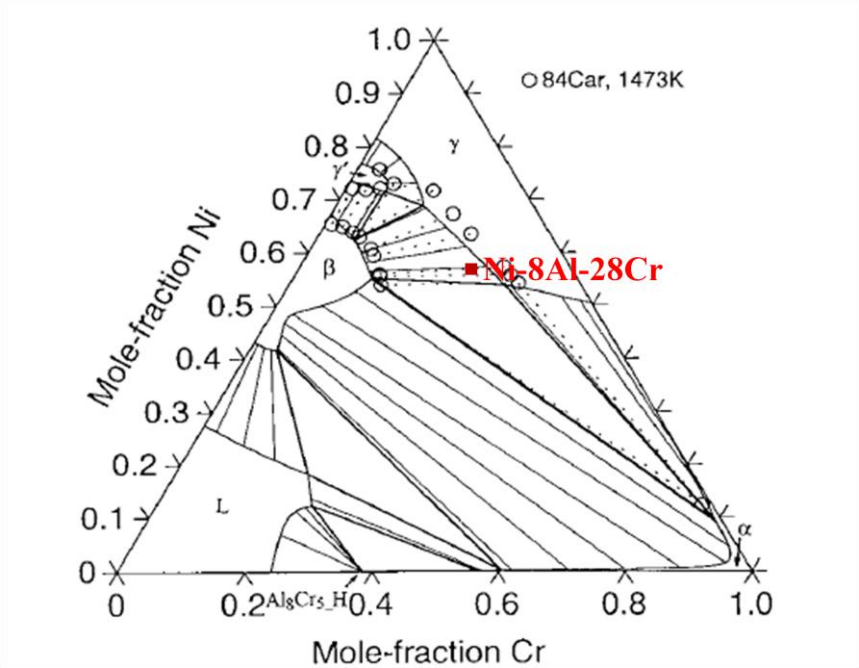

Figure A.3: The ternary phase diagram of Ni-Al-Cr system at T = 1200°C[135]

Appendix B: Characterisation of the alloy prepared by pack cementation technique

The diffractogram of X-ray diffraction analysis (XRD), the microstructures and the concentration profile of the obtained alloy are shown in Figure B.1 and Figure B.2.

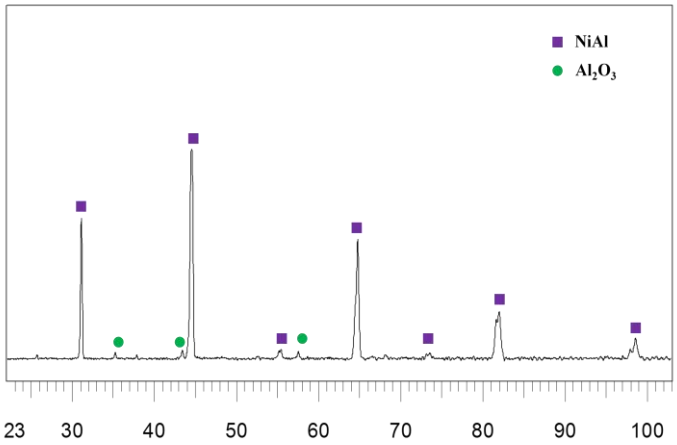

Figure B.1: Diffractogram of the coating obtained by pack cementation technique

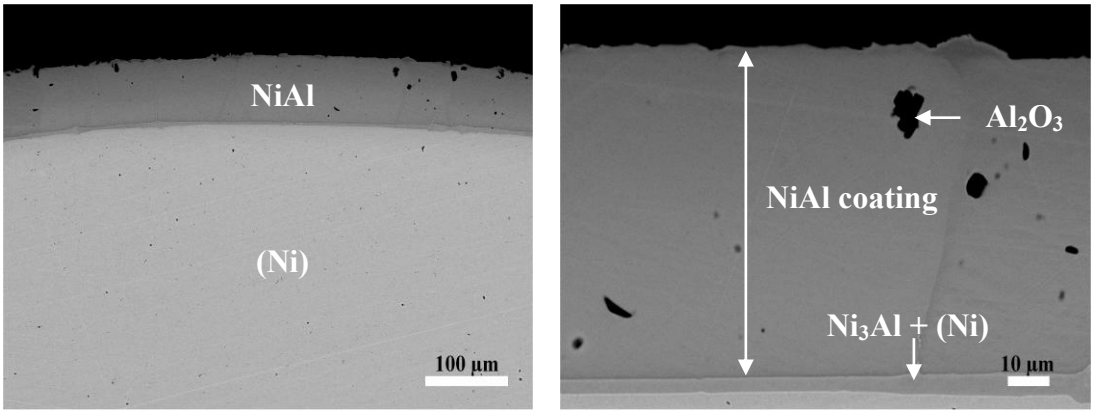

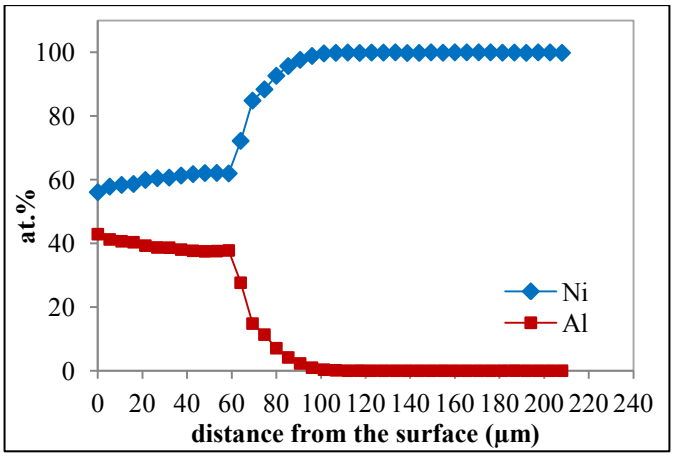

Figure B.2: The micrographs and the composition of the coating obtained by pack cementation technique

The characterisation of the obtained alloy with the support from the phase diagram in Figure B.3 confirms the existence of NiAl layer with the thickness of ~ 60 µm. The interdiffusion layer takes place at ~ 40 µm of the thickness above the Ni substrate. The diffractogram and micrographs in Figures B.1 and B.2 verify the existence of inert filler Al_2O_3 which was embedded within the NiAl coating. Since the coating grows outward, the aluminide coating envelops or entrapes particles during growth.

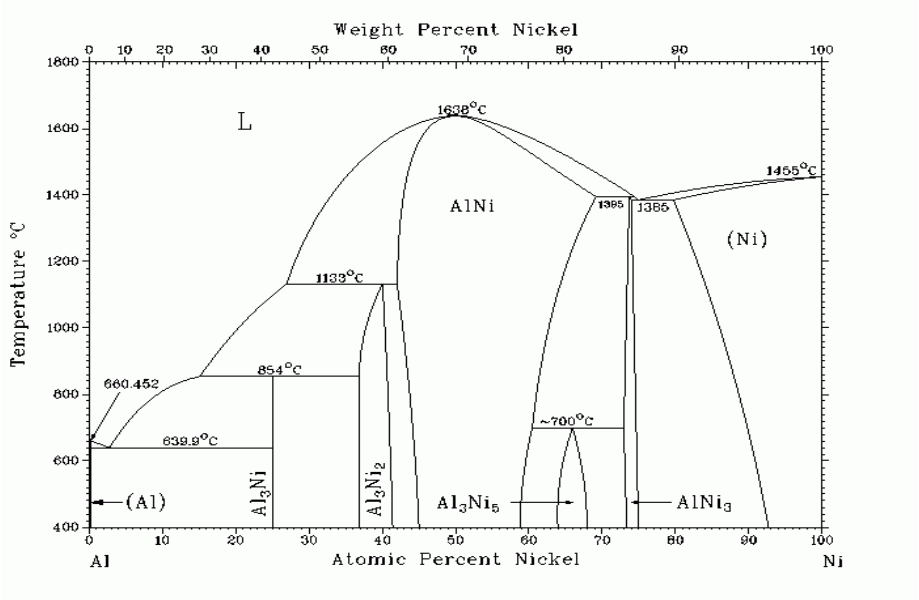

Figure B.3: Binary phase diagram of Ni-Al[136]

Appendix C: Characterisation of glass precipitates by differential thermal analysis (DTA)

The glasses were analysed by differential thermal analysis (DTA) with heating rate of 10°C per minute up to 1300°C (where all of the glasses is in liquid state, as illustrated in Figure C.1). The data were recorded during the heating and cooling steps of the melts.

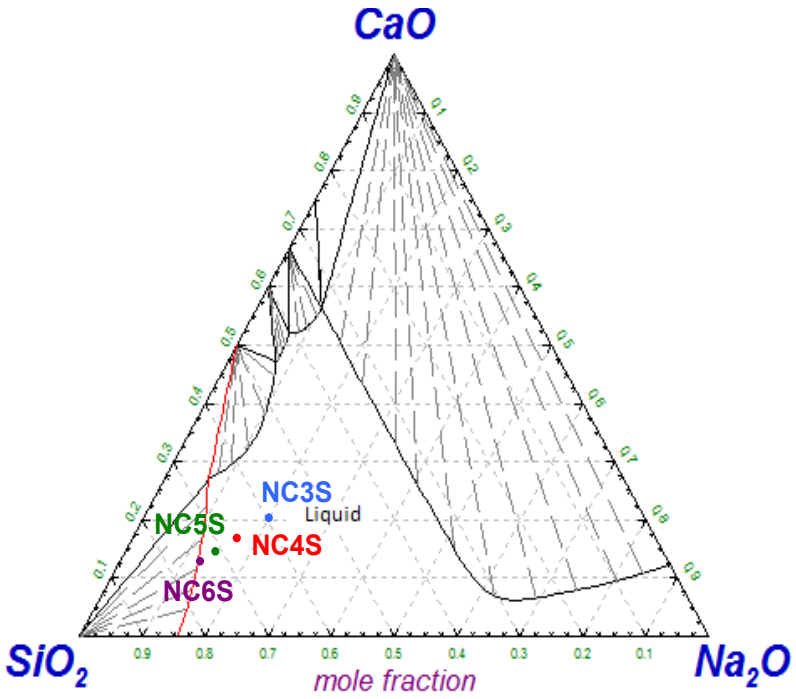

Figure C.1: Ternary phase diagram of Na_2O-CaO-SiO_2 system at 1300°C

On the DTA plots (Figure C.2), the endothermic peaks which represent the glass transition temperature appear in the 570°C - 600°C range for the four glasses, which is coherent with the range usually observed for soda-lime silicates[137–139]. The exothermic peaks observed at 800°C for NC3S, 850°C for NC4S and ~ 950°C for NC5S and NC6S correspond to a crystallisation phase. The melting of these precipitates is observed through the endothermic peaks at 1150°C for NC3S, and

below 1050°C for the three other glasses. During the cooling process, only NC3S presents an exothermic peak at ~ 1020°C. Since the temperatures observed for the precipitation and the melting in the case of NC5S and NC6S are very close, one may conclude that the same phases have been observed in both glasses. Nevertheless, these temperatures are very different from the ones measured in the case of NC3S, which suggests that another different phase is involved for this glass.

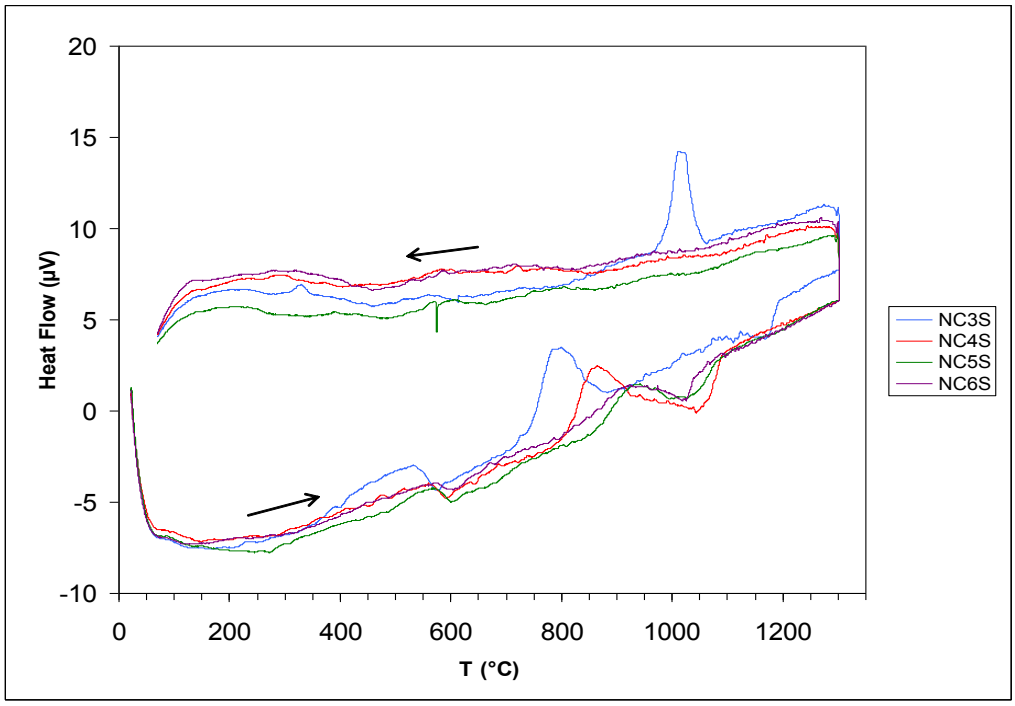

Figure C.2: DTA analysis of NC3S, NC4S, NC5S and NC6S with the scan rate of 10°C/min

In order to characterise these precipitates, the heat treatments at different temperatures, followed by air quenching, were performed on NC3S and NC6S. The obtained glasses after the heat treatments were not transparent which proved the presence of precipitates in the glass matrix. The samples were then characterised by SEM and XRD analyses. The details of the experiments and the obtained results are discussed in the following paragraphs.

(a) NC3S

The precipitates formed in NC3S were characterised by quenching the samples after two series of heat treatments. A first heat treatment was conducted at a temperature between the precipitation and melting temperatures during the heating process as has been observed in the DTA analysis. The quenching was performed after 2 h of heat treatment at this temperature. A second heat treatment was performed at a temperature which lies just after the occurrance of the precipitation peak when the melt was cooling down. The sample was held at this temperature for 2 h before quenching. The XRD diffractograms of the obtained glasses after these two heat treatments are reported in Figure C.3. The identical diffractograms prove that the same phase has been formed during the heating and cooling processes. The phase has been identified as a solid solution $(Na_2,Ca)Na_2CaSi_3O_9$, containing 50 mol.% of SiO_2 and exhibiting hexagonal symmetry.

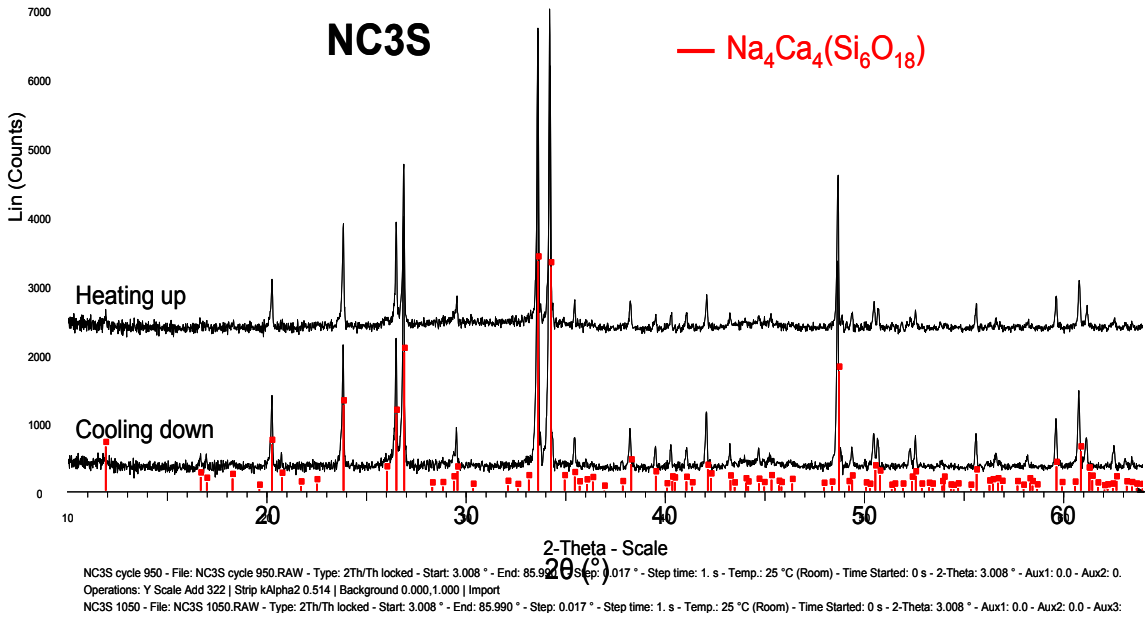

Figure C.3: Diffractograms of quenched NC3S for precipitated phase identification after heating and cooling processes

SEM observation (Figure C.4(a)) of the quenched sample during the cooling process reveals the presence of precipitates with hexagonal shapes homogeneously dispersed in the glass matrix. The grain shape can be directly correlated to the symmetry of the phase determined by XRD. The phase composition was measured by EDS analysis, leading to the solid solution $(Na_2,Ca)Na_2CaSi_3O_9$ which was already identified by XRD analysis. The X-ray mapping of sodium, calcium and silicon was performed by Back-scattered electron (BSE) and reported in Figure C.4(b), (c) and (d) respectively.

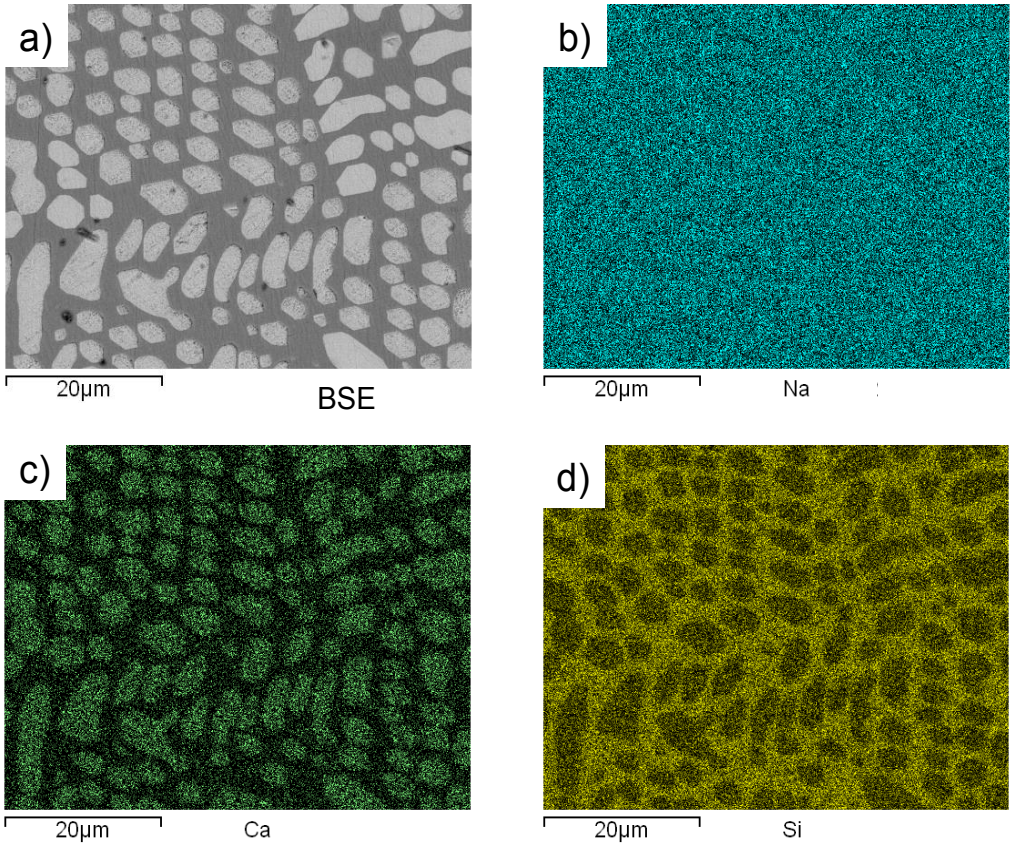

Figure C.4: Micrograph of quenched NC3S during cooling process (a) X-ray mapping of Na (b), Ca (c) and Si (d)

The molar oxides proportions in NC3S and in the precipitated grains (proportions measured through EDS analysis) reported in Table C.1 can be directly correlated to the X-ray mapping observations.

Table C.1: Molar proportions of Na_2O, CaO and SiO_2 in NC3S and in the precipitated phase

Molar proportions	**Na_2O**	**CaO**	**SiO_2**
NC3S	20%	20%	60%
$(Na_2,Ca)Na_2CaSi_3O_9$	~ 20%	~ 30%	~ 50%

As the sodium oxide content is identical between the glass matrix (NC3S) and the precipitates, therefore the Na mapping shows not much contrast between these phases (Figure C.4(b)). The higher content of CaO and SiO_2 in precipitated grains and glass matrix respectively can be clearly observed in the calcium and silicon mappings (Figure C.4(c) and Figure C.4(d) respectively).

(b) NC6S

According to the DTA analysis, the precipitation temperature in NC6S is ~ 950°C and the melting of the phase occurs at the temperature ~ 1020°C. As a consequence, the NC6S sample was subjected to a heat treatment at 950°C for 2 h before being quenched in air.

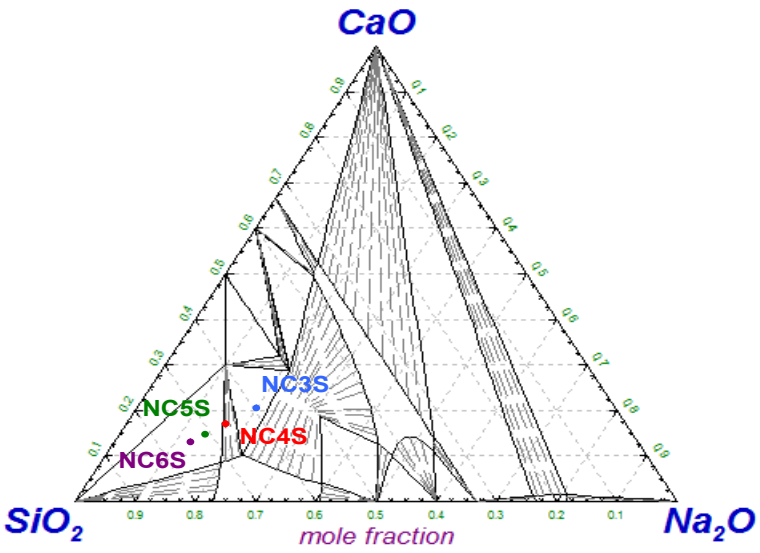

Figure C.5: Ternary phase diagram of Na_2O-CaO-SiO_2 system at 950°C

The ternary phase diagram of the glass elements at 950°C shows that at this temperature, NC6S composition is in equilibrium with three phases; pure silica SiO_2, a ternary compound $Na_2Ca_3Si_6O_{16}$ and a liquid phase.

The presence of the ternary compound $Na_2Ca_3Si_6O_{16}$ and pure silica SiO_2 is clearly confirmed in the diffractogram presented in Figure C.6(a). The two precipitated phases can be observed in the glass matrix (Figure C.6(b)), thus confirming the presence of NC6S in three phases of equilibrium as shown in the ternary phase diagram (Figure C.5).

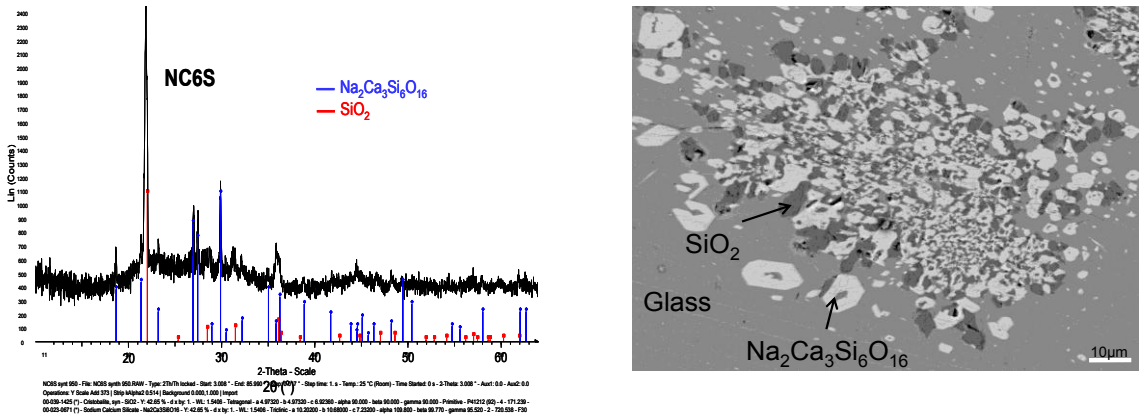

(a) (b)

Figure C.6: Diffractogram of the quenched NC6S after heat treatment at 950°C for 2 h (heating process) (a), and BSE micrograph of the same sample (b)

Appendix D: Isothermal oxidation of Ni-based alloys

The oxidation kinetics of Ni-based alloys in air was determined by an isothermal thermogravimetric analysis at 1100°C and 1150°C for 100 h. An isothermal oxidation was performed in order to evaluate the thickness of the formed oxides at a given temperature. The samples were characterised by classical methods *i.e.* XRD and SEM-EDS. The results were then treated depending on the observed phenomena.

- **Ni-30Cr alloy**

(a) Characterisation of the oxide layer

The micrographs in Figure D.1 reveal a development of ~ 8 µm - 12 µm and ~ 12 µm - 14 µm of thickness of oxide layer after 100 h of oxidation at 1100°C and 1150°C respectively. Even though the oxide is adherent to the alloy, the spallation of the layer which is due to the cooling process has been observed on some regions of the sample at both temperatures.

1100°C	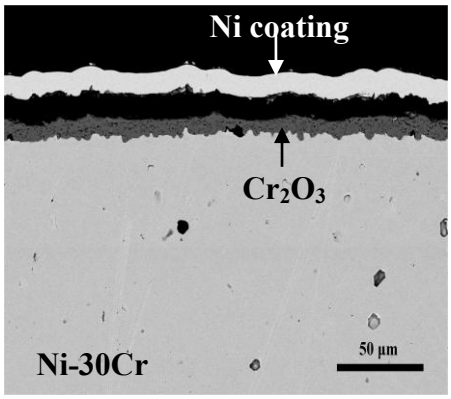	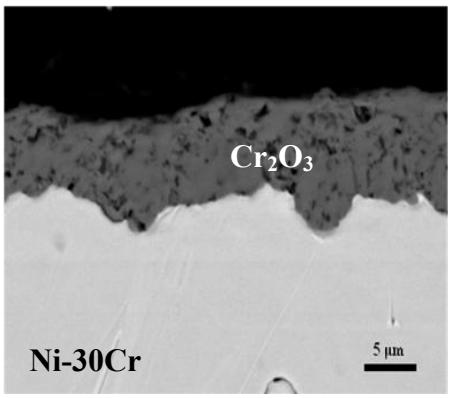

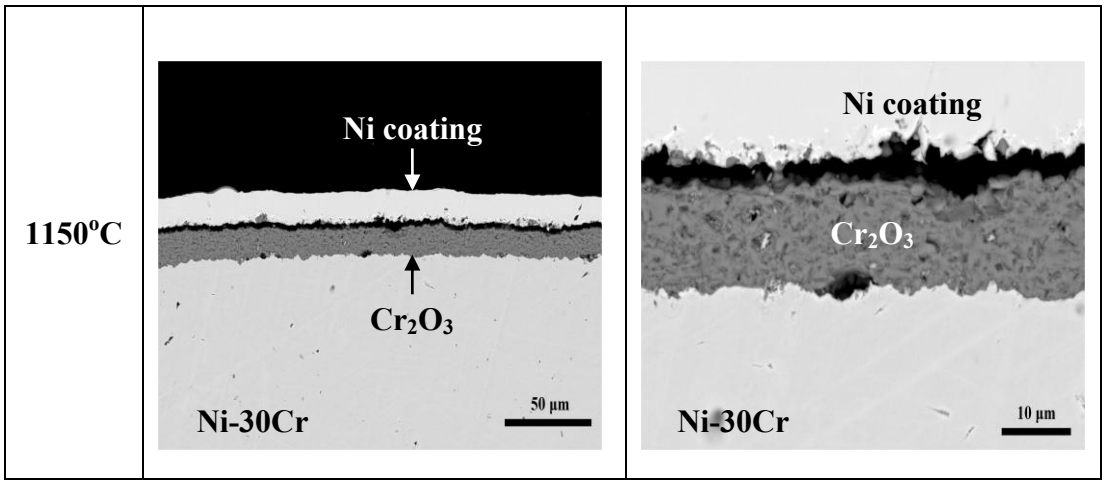

Figure D.1: The cross section of Ni-30Cr alloy after 100 h of oxidation in air at 1100°C and 1150°C

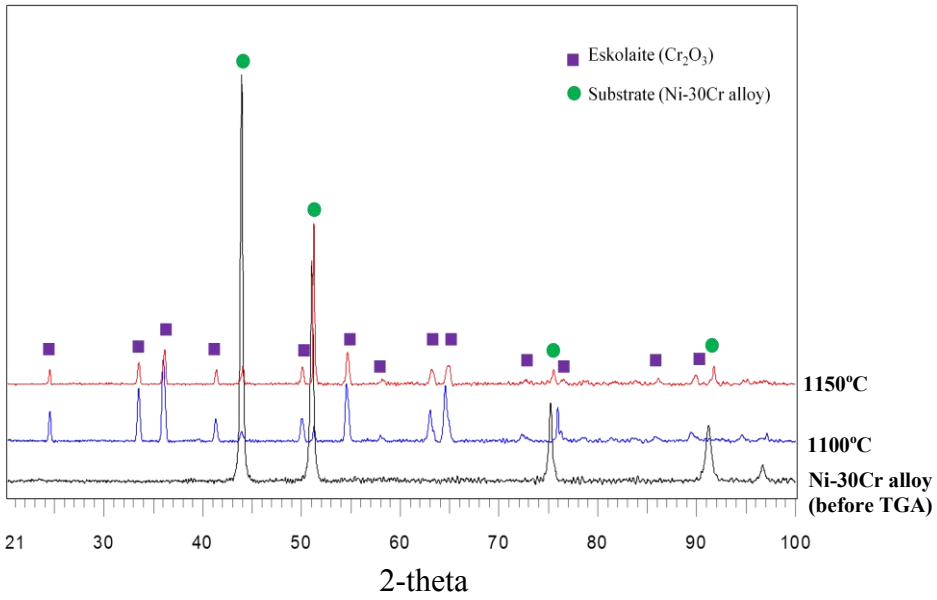

Figure D.2: XRD diffractograms of Ni-30Cr alloy after 100 h of oxidation in air at 1100°C and 1150°C

The diffractograms in Figure D.2 reveal the existence of chromia (Cr_2O_3) after 100 h of oxidation for both temperatures. The high Cr content in this alloy (30 wt.%) may lead to the selective oxidation of Cr[81]. Even though the higher weight gain has been observed by TGA for 1150°C, the Cr_2O_3 peaks are more significant at

1100°C. This phenomenon might be caused by spallation of the Cr_2O_3 layer during the cooling process which is more severe at higher temperatures.

(b) Raw thermogravimetric data

The variation of mass change (Δm/S) as a function of time (h) for Ni-30Cr alloy at two different temperatures are shown in Figure D.3.

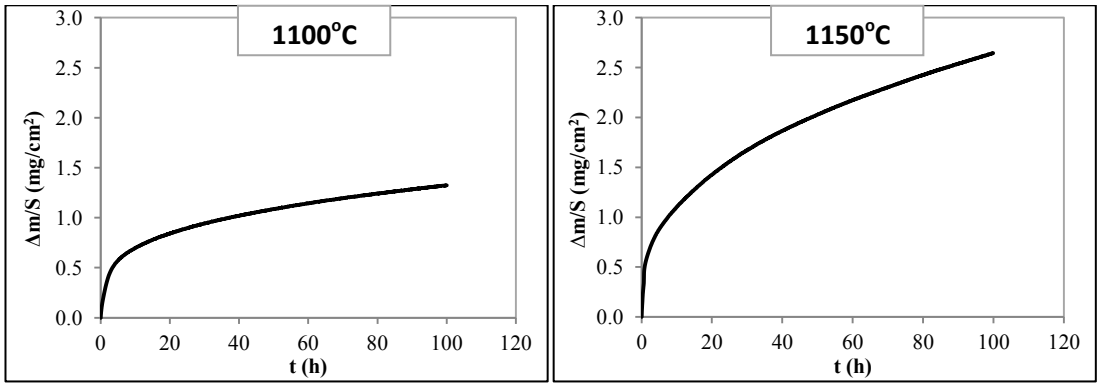

Figure D.3: Thermogravimetric analysis of Ni-30Cr alloy in air atmosphere at (a) 1100°C and (b) 1150°C

The resulting curves show a significant increase of the weight gain with the temperature for Ni-30Cr alloy. Both plots seem to follow a parabolic type which reflects an establishment of protective layer at the interface of the alloys and the limitation of the oxidation reaction by the solid state diffusion of the elements through the layer.

(c) Treatment of the thermogravimetric data

Chromium oxide (Cr_2O_3) which develops during the oxidation is not stable when exposed to a very high temperature. At temperatures higher than 1000°C, the

Cr_2O_3 suffers from a volatilisation phenomenon according to the following equation[102]:

$$Cr_2O_3 + \frac{3}{2}O_2(g) \rightarrow 2CrO_3(g) \quad (1)$$

As a consequence, the oxidation kinetics of chromia forming alloy must be described by taking into account both mass gain kinetics which is due to chromia formation and also the chromia volatilisation which is due to its oxidation into CrO_3(g). The model which has been developed by Zamoum *et al.*[140]. will be used herein in order to treat the data.

The growth rate of oxide following a parabolic oxidation can be described by Wagner's law[141] according to the following equation:

$$\frac{dx}{dt} = \frac{k_{pe}}{x} \quad (2)$$

where x is the thickness (cm), k_{pe} is the parabolic oxidation rate constant (cm^2/s) and t is the time (s). The chromia vaporisation can be described by the following equation:

$$\frac{dx}{dt} = -k_{le} \quad (3)$$

where k_{le} is the linear volatilisation rate (cm/s). The combination of Eq. 2 and 3 gives the variation of the oxide thickness with time which is given by Eq. 4.

$$\frac{dx}{dt} = \frac{k_{pe}}{x} - k_{le} \tag{4}$$

The integral form of Eq. 4 will result in the following equation:

$$t = \frac{-x}{k_{le}} - \frac{k_{pe}}{k_{le}^2} \ln(k_{pe} - k_{le}x) + C \tag{5}$$

where C is the integration constant, which can be determined by using the following condition: x = 0 at t = 0. Then Eq. 5 becomes:

$$t = \frac{k_{pe}}{k_{le}^2}\left[-\frac{k_{le}}{k_{pe}}x - \ln\left(1 - \frac{k_{le}}{k_{pe}}x\right)\right] \tag{6}$$

If the mass variation is considered due to O^{2-} fixation by the forming oxide scale, Eq. 4 can be deduced to:

$$\frac{d\frac{\Delta m_{oxide}}{S}}{dt} = \frac{k_p^{'}}{\frac{\Delta m_{oxide}}{S}} - k_l^{'} \tag{7}$$

where

$$\frac{\Delta m_{oxide}}{S} = x \times \rho_{Cr_2O_3} \times \frac{3 \times M_{O^{--}}}{M_{Cr_2O_3}} = x \times A \tag{8}$$

$$k_p^{'} = \frac{k_{pe}}{A^2} \tag{9}$$

$$k_l^{'} = k_{le} \times A \tag{10}$$

where S represents the oxidised surface area (cm^2), $\Delta m_{oxide}/S$ is the mass variation due to O^{2-} fixation (g/cm^2), k_p' is the parabolic constant (g^2/cm^4 s), k_l' is the linear volatilisation constant (g/cm^2 s), $\rho_{Cr_2O_3}$ is the density of Cr_2O_3 (g/cm^3), M_{O^-} is the atomic mass of oxygen (g/mol) and $M_{Cr_2O_3}$ is the molar mass of Cr_2O_3 (g/mol).

Therefore, the total mass variation given by thermogravimetric analysis, $\Delta m/S$ is given by the following equation:

$$\frac{\Delta m}{S} = \frac{\Delta m_{oxide}}{S} - \frac{\Delta m_{Cr}}{S} \tag{11}$$

where $\Delta m_{Cr}/S$ represents the mass variation due to Cr loss (g/cm^2) and is given by the following equation:

$$\frac{\Delta m_{Cr}}{S} = k_l^{''} t = k_l^{'} t \times \frac{2 \times M_{Cr}}{3 \times M_{O^-}} = k_l^{'} t \times B \tag{12}$$

where M_{Cr} is the atomic mass of chromium (g/mol). The combination of Eq. 7, Eq. 11 and Eq. 12 leads to the development of the following equation:

$$\frac{d\left(\frac{\Delta m}{S} + k_l^{'} t \times B\right)}{dt} = \frac{k_p^{'}}{\left(\frac{\Delta m}{S} + k_l^{'} t \times B\right)} - k_l^{'} \tag{13}$$

The partial differential of Eq. 13 leads to the following equation:

$$\frac{d\left(\frac{\Delta m}{S}\right)}{dt} = \frac{k_p^{'}}{\left(\frac{\Delta m}{S} + k_l^{'} t \times B\right)} - k_l^{'}(1+B) \tag{14}$$

The plot of d(Δm/S)/dt as a function of 1/[(Δm/S)+ k_l't x B] leads to a linear function if k_l' is correctly chosen with the slope of k_p'. The [d(Δm/S)]/dt = *f* [1/((Δm/S)+ k_l't x B] graphs for the Ni-30Cr alloys, as well as the corresponding best-fit lines are reported in Figure D.4.

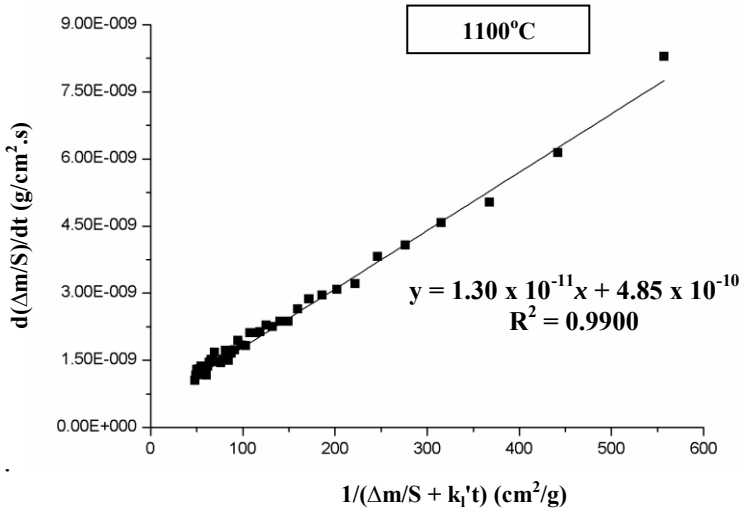

(a)

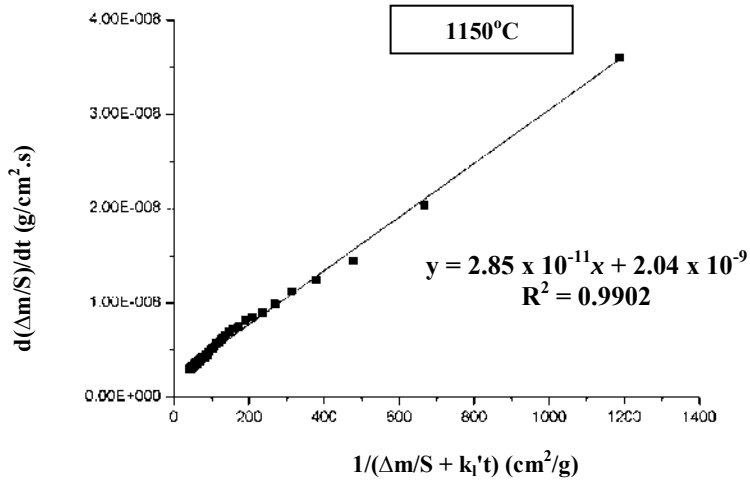

(b)

Figure D.4: The plot of d(Δm/S)/dt as a function of 1/[(Δm/S)+ k_l't x B] for Ni-30Cr at (a) 1100°C and (b) 1150°C

The oxidation and volatilisation rates for Ni-30Cr alloy at 1100°C and 1150°C are reported in Table D.1.

Table D.1: Parabolic and linear constants determined for Ni-30Cr alloy for oxidation at 1100°C and 1150°C

Ni-30Cr	$k_p^{'}(g^2/cm^4s)$		$k_l^{'}(g/cm^2s)$	
	this work	Berthod *et al.*[142]	this work	Berthod *et al.*[142]
1100°C	1.3×10^{-11}	2.3×10^{-11}	5.5×10^{-8}	8.7×10^{-9}
1150°C	2.9×10^{-11}	-	6×10^{-8}	-

The k_p' value at 1100°C is in good correlation with the one determined by Berthod *et al.*[142] for the same kind of alloys but calculated by another refinement method. By comparing the k_p' values with Hindam and Whittle diagram[114] (Figure D.5), the values are perfectly coherent with the "Cr_2O_3-forming alloys" domain for both temperatures. The k_l' value determined in this work is ~ 6 times higher than the one determined by Berthod *et al.*[142].

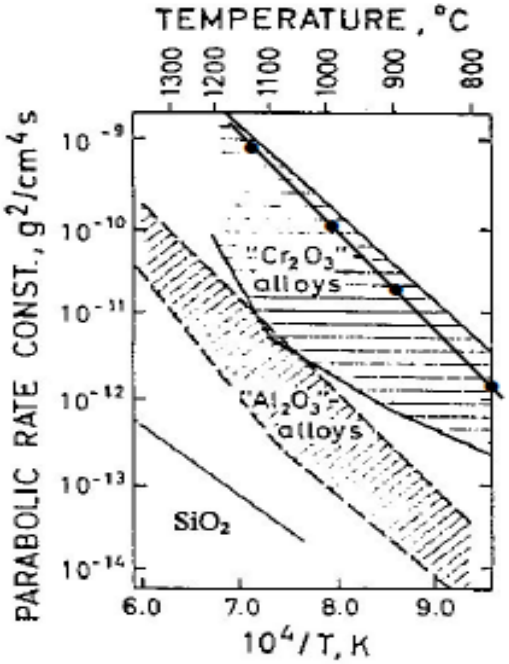

Figure D.5: A compilation domain of experimental values of k_p for chromia and alumina forming alloys[114]

- **NiAl and Ni-8Al-28Cr alloys**

The oxidation kinetics of the two materials were determined by an isothermal thermogravimetric analysis of 100 h at 1100°C for NiAl, and at 1100°C and 1150°C for Ni-8Al-28Cr.

(a) Characterisation of the oxide layer

Figure D.6 and Figure D.7 present the XRD diagram performed on the samples after TGA. In both cases, the XRD diffractograms made after the 100 h isothermal treatment are comparable to the raw alloys as they still exhibit the peaks characteristic of the substrate (NiAl, or Ni-8Al-28Cr + NiAl). Only one oxide is detected on the surface of the samples after the TGA analysis, which is alpha-alumina (corundum).

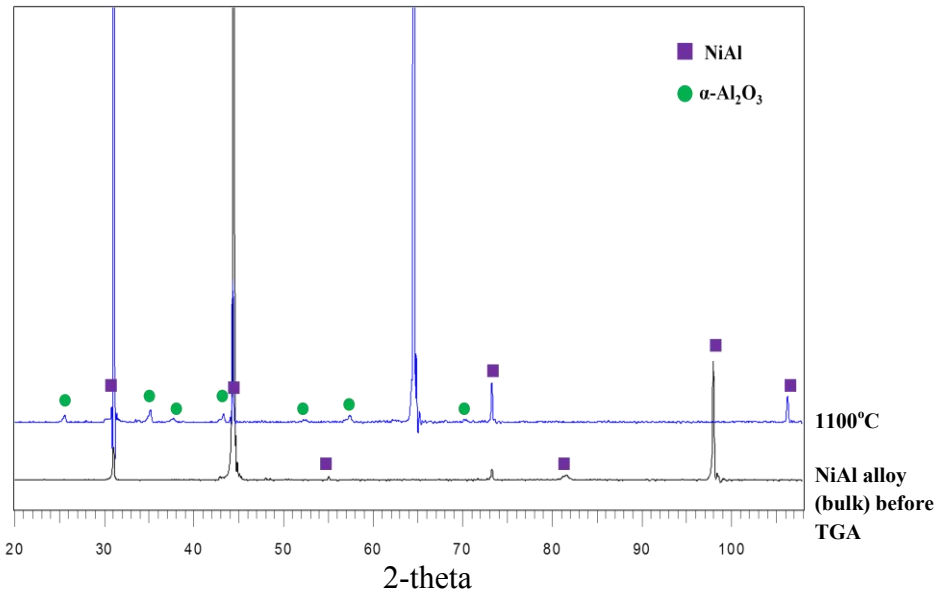

Figure D.6: XRD diffractograms of NiAl alloy (bulk) after 100 h of oxidation in air at 1100°C

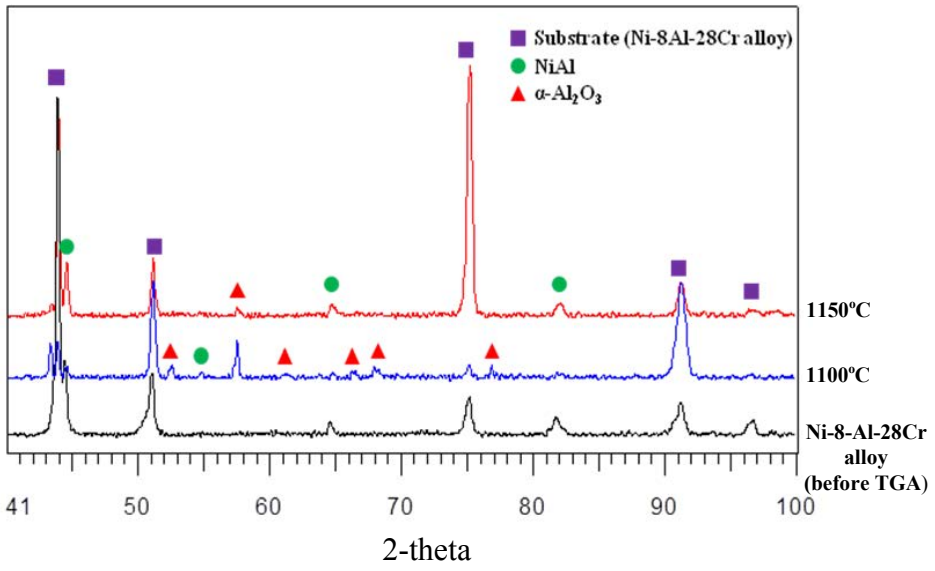

Figure D.7: XRD diffractograms of Ni-8Al-28Cr alloy after 100 h of oxidation in air at 1100°C and 1150°C

(b) Raw thermogravimetric data

The variations of mass change as a function of time for both alloys at 1100°C, and at 1150°C for Ni-8Al-28Cr are presented in Figure D.8.

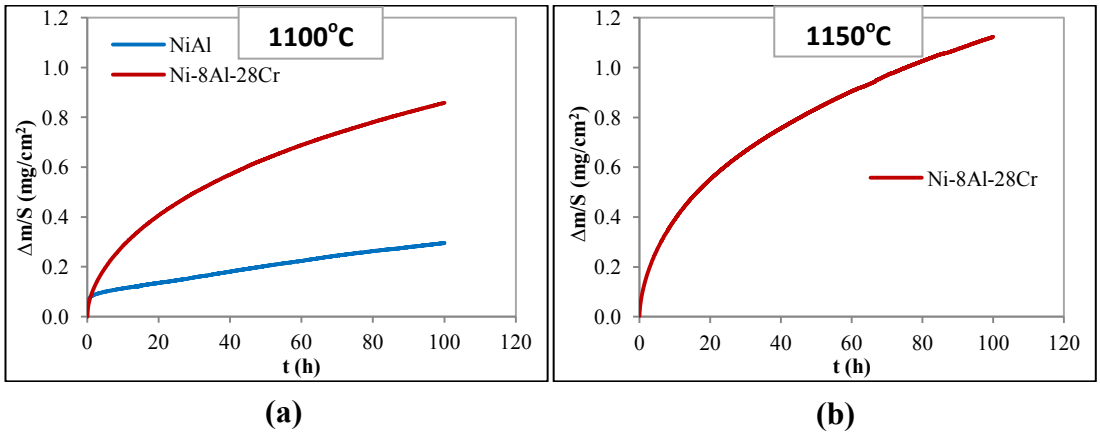

(a) **(b)**

Figure D.8: Thermogravimetric analysis of NiAl and Ni-8Al-28Cr alloy in air atmosphere at (a) 1100°C and (b) 1150°C

For both temperatures, the Ni-8Al-28Cr plots seem to exhibit parabolic type reflecting a diffusion limited kinetics possibly due to the existence of a protective

oxide layer. The weight gain is much lower in the case of the NiAl sample at 1100°C.

(c) Treatment of the thermogravimetric data

Contrary to Cr_2O_3, Al_2O_3 does not suffer from oxidative evaporation, thus making it more stable in the air at high temperatures as compared to the chromia. As a consequence, the treatment of the thermogravimetric data is much easier than the treatment for chromia-forming alloys. Figure D.9 reports the evolution of the weight gain as a function the square root of time at 1100°C for NiAl, and at 1100°C and 1150°C for Ni-8Al-28Cr. The representation using the square root of time gives a very good linearity in the case Ni-8Al-28Cr for both temperatures. Thus the growth kinetics of the Al_2O_3 layer corresponds to Wagner's law:

$$\left(\frac{\Delta m}{S}\right)^2 = k_p \times t \tag{15}$$

The slopes of the plots of Ni-8Al-28Cr in Figure D.9 give the k_p values for the two studied temperatures, which are reported in Table D.2.

Table D.2: Parabolic constants of Ni-8Al-28Cr alloy for oxidation at 1100°C and 1150°C

Ni-8Al-28Cr	1100°C	1150°C
k_p ($g^2/cm^4.s$)	1×10^{-12}	4×10^{-12}

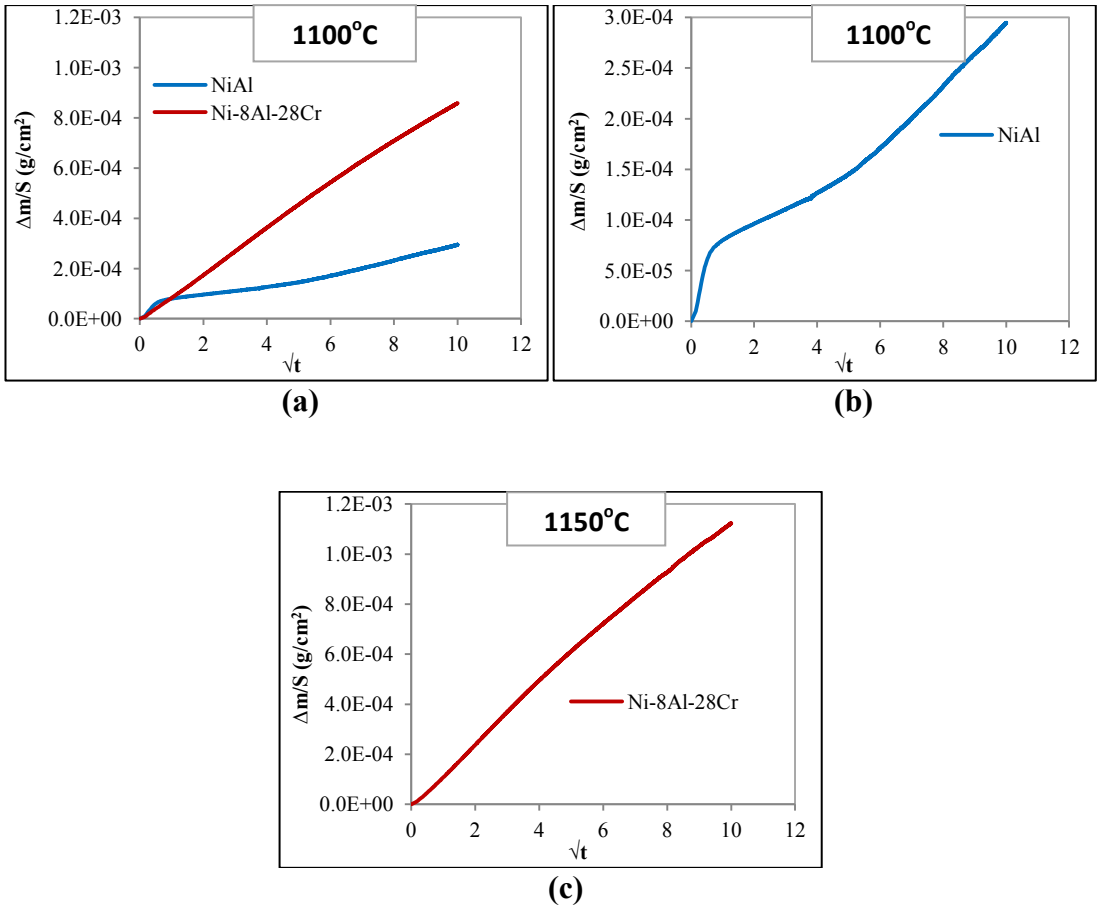

Figure D.9: Weight gain as a function of square root of time of (a) NiAl and Ni-8Al-28Cr at 1100°C, (b) NiAl at 1100°C (enlargement of the plot in (a)) and (c) Ni-8Al-28Cr at 1150°C

The case of NiAl seems to be more complex, as no linearity is observed in the plot of Figure D.9(b). Further investigation would be required in order to have an access to the accurate value of the kinetic constant. However, the XRD diffractogram in Figure D.6 clearly shows that the material is an alumina-forming alloy. The growth kinetic is difficult to be evaluated, but it seems to be lower than that of Ni-8Al-28Cr alloy.

As the measured k_p values are one order of magnitude lower than for the chromia forming alloys, the time required to form an oxide scale on this kind of alloys will be much longer.

LIST OF PUBLICATIONS

Journals

1. Abdullah, T. K., Petitjean, C., Panteix, P. J., Rapin, C., Vilasi, M., Zuhailawati, H. & Rahim, A. A. Dissolution equilibrium of chromium oxide in a soda lime silicate melt exposed to oxidising and reducing atmospheres. *Journal of Materials Chemistry and Physics* (2013). http://dx.doi.org/10.1016/j.matchem phys.2013.07.055

2. Abdullah, T. K., Petitjean, C., Panteix, P. J., Rapin, C., Vilasi, M., Zuhailawati, H. & Rahim, A. A. Stability of protective oxide layer against corrosion: solubility measurements of chromium in soda lime silicate melts. *Journal of Oxidation of Metals* (2013). DOI: 10.1007/s11085-013-9400-4

Presentations

1. Abdullah, T. K., Petitjean, C., Panteix, P. J., Rapin, C., Vilasi, M., Zuhailawati, H. & Rahim, A. A. Corrosion of chromia/alumina forming alloys in molten glass: correlation with solubility of the protective oxide in the melt. Colloquium - IJL-USM, Vandoeuvre-les-Nancy, 13 - 15 November 2012. Oral presentation.

2. Abdullah, T. K., Petitjean, C., Panteix, P. J., Rapin, C., Vilasi, M., Zuhailawati, H. & Rahim, A. A. Corrosion of superalloys by molten glass: behaviour of chromia in soda lime silicate melts. The European Corrosion Congress (EUROCORR), Istanbul, Turkey, 9 - 13 September 2012. Poster presentation.

3. Abdullah, T. K., Petitjean, C., Panteix, P. J., Rapin, C., Vilasi, M., Zuhailawati, H. & Rahim, A. A. Stability of protective oxide layer against corrosion: solubility measurements of chromium in soda lime silicate melts. 8th International Symposium on High-Temperature Corrosion and Protection of Materials, Les Embiez, France, 20 - 25 May 2012. Oral presentation.

4. Abdullah, T. K., Petitjean, C., Panteix, P. J., Rapin, C., Vilasi, M., Zuhailawati, H. & Rahim, A. A. Solubility of chromium oxide in soda lime silicate melts: a kinetic point of view. 43ièmes Journées d'Etude sur la Cinétique hétérogène (JECH43), Vandoeuvre-les-Nancy, France, 29 - 30 March 2012. Oral presentation.

5. Abdullah, T. K., Petitjean, C., Panteix, P. J., Rapin, C. & Vilasi, M.. Corrosion of superalloys in molten glasses: study of chromia solubility in soda lime silicate melts. The European Corrosion Congress (EUROCORR), Stockholm, Sweden, 5 - 8 September 2011. Poster presentation.

6. Abdullah, T. K., Petitjean, C., Panteix, P. J., Rapin, C. & Vilasi, M.. Corrosion of superalloys in molten glasses: study of chromia solubility in soda lime silicate melts. Jounee L'Ecole Doctorale Lorraine, Vandoeuvre-les-Nancy, France, 25 May 2011. Oral presentation.